

Modeling the Interaction between Cardiac Assist Devices and the Left Ventricle

Modellering van de Interactie tussen Hartondersteunende Pompen en het Linkerventrikel

Stijn Vandenberghe

Promoters:

Prof. dr. ir. Pascal Verdonck

Prof. dr. ir. Patrick Segers



Dissertation submitted in partial fulfillment of the requirements for the degree of “Doctor in de Toegepaste Wetenschappen”.

The research reported in this dissertation was performed with the financial support of the Institute for the Promotion of Innovation by Science and Technology in Flanders, IWT-993171.

This dissertation was printed with the financial support of the Arrow International Cardiac Assist Division, Weesp, The Netherlands.



© 2004 Parts of this book may only be reproduced if accompanied by clear reference to the source.

Suggested citation: Vandenberghe S. Modeling the Interaction between Cardiac Assist Devices and the Left Ventricle. PhD dissertation. Ghent: Ghent University; 2004.

cover drawing by Esther Feagan

Promoters:

Prof. dr. ir. P. Verdonck

Prof. dr. ir. P. Segers

Hydraulics Laboratory

Civil Engineering Department (TW15)

Faculty of Engineering

Ghent University

St.-Pietersnieuwstraat 41

B-9000 Gent

hydraulica@navier.ugent.be

Members of the exam committee:

Prof. R. Verhoeven (president, Faculty of Engineering, UGent)

Prof. J. Vierendeels* (secretary, Faculty of Engineering, UGent)

Dr. D. De Wachter (Faculty of Engineering, UGent)

Prof. B. Meyns* (Faculty of Medicine and Health Sciences, KULeuven)

Dr. G. Rakhorst (Faculty of Medicine, RUGroningen)

Prof. H. Reul (Institute for Biomedical Technology, RWTH-Aachen)

Prof. H. Schima* (Center for Biomedical Research, Universität Wien)

Prof. P. Segers* (promoter, Faculty of Engineering, UGent)

Prof. G. Van Nooten (Faculty of Medicine and Health Sciences, UGent)

Prof. P. Verdonck* (promoter, Faculty of Engineering, UGent)

* also member of the reading committee

Hearts will never be practical
until they can be made unbreakable

Wizard of Oz.

Abstract

Ventricular assist devices (VADs) basically are blood pumps that are used routinely in clinical practice for the support of end-stage heart failure patients. They are mostly used until the patient's native heart is replaced with a transplant, but in select cases they can heal a patient's heart and subsequently be removed. Especially in the latter case it is important to have a detailed knowledge of the effect of the device on the native heart. In this dissertation, the interaction between a VAD and the heart's left ventricle is studied on hydrodynamic level with an in vitro and a mathematical model. The results are further compared to data obtained from animal studies.

First, a summary is given of the cardiovascular system, heart failure, and available therapies. Especially the different applications of VADs are highlighted. Next, the newly developed in vitro and mathematical models used for the subsequent studies are presented.

These models are used to study the interaction between the left ventricle and a rotary blood pump (Medos Deltastream / Medos-HIA microdiagonal pump), where aside from a stationary impeller speed (normal use), also pump failure and varying impeller speed (pulsatile use) are simulated. The normal use of a rotary pump as VAD is also studied in sheep. It can be concluded that pump failure does not bring about an acute threat if the VAD has a sufficiently high hydraulic resistance. The normal use of such a VAD leads effectively to unloading of the left ventricle, and this can be improved by using the device in a pulsatile mode.

Next, a minimally invasive VAD (PUCA II) consisting of a valved catheter and positive-displacement pump is studied in an in vitro model, where it can be concluded that the device can effectively augment aortic pressure and flow, but is less suitable to unload the left ventricle. Effective unloading can be obtained by using this device in the (abdominal) aorta.

Finally, the lessons learned from these studies are summarized, and it is demonstrated from sheep and calve data that the use of a VAD alters native heart function in such a way that the most common modeling method for left ventricular function becomes inadequate.

Preface

The contents of this book is based on the research I have performed in the last four years at the Hydraulics Laboratory in Gent. However, I did not do this on my own and there are many people that contributed to my work over the years. I am grateful to all of them for consciously or unconsciously educating me as a researcher. I especially would like to thank the people I know in Leuven, particularly Bart Meyns. However, there is no doubt that I am most in debt with the folks of that small world covered by the penthouse and governed by prof. Verhoeven (i.e., the Hydraulics Laboratory).

I owe my first words of gratitude to Pascal Verdonck, who first introduced me to biomedical engineering and later tempted me to do research and start a PhD. Looking back at the past years, I can safely state that his primary role was to manage and promote me and my work. When it comes to research and my skills as a researcher, I have to give most credit to Patrick Segers. He taught me the basics, always came up with new ideas and perspectives and, together with Pascal, guarded the quality of my output. Patrick and Dirk will always be remembered as ‘the post-docs’ - experts in their field who actually seemed to know what they were doing and did it twice as fast as me.

Apart from these people, I also waved goodbye to or welcomed several PhD students in the lab. First I intruded into Peter and Stefaan’s office and later I saw how they were gradually replaced by new troops. I think I spent most of my time in the company of Kris and Sunny, but I can honestly state that I have learned from each of the others too. I’d like to thank them all for their companionship, their advice, and their support and I hope that I have contributed positively to their lives and/or careers. I am also grateful to Manuella and Kristien for helping me out with administrative labyrinths and to Chris, Marcel, Martin, and Stefaan for the constructions that made experiments possible. I should also mention some temporary pupils that helped with the experiments and I sincerely hope that they learned something from me. The results of their work are also blended in this dissertation, so thank you Jan, Jeroen, Rana, and Marina. Wasn’t it fun to play with fluids?

While spending time in the lab, I neglected some other aspects of life. I probably didn't make as much time for my family and friends as I should have. I would like to apologize for this and thank you all for your understanding and support. I am especially grateful to my parents for their continuing support and care taking.

Although winding up this book means that a goal is reached, I do not experience this as a decisive moment in my life. It is certainly special and in a way a relief, but I already experienced a major turning point when I managed to set myself free and move to Pittsburgh. I wish to express my gratitude to Jim Antaki, Harvey Borovetz, and Sanjeev Shroff for sharing their wisdom with me and for showing respect for my knowledge and skills. This book is now to me a tool to pursue on the path to other research groups, and I hope I can be a bridge between all the researchers that share my interests and that I will run into on my journey.

Finally I would like to express how much I appreciate the help of the people that reviewed parts of this book. They wrestled through the extended texts that I handed over to them and helped me to improve the quality of this dissertation. All together they read over 3 kg of paperwork in the last few weeks. Thanks Patrick, Pascal, Tom, Guy, Sunny, Gerhard, Bart, Esther, and Jim. I hope you can also enjoy the full version.

Now it is my time to make space for the following generation in the Hydraulics Laboratory. I hope I left a mark there and that this dissertation will be read from time to time. Doing the research was often stressful and sometimes fun, but I hope there is more to it. This work is only valuable if it can somehow contribute to the improvement of the treatment of heart failure patients.

Stijn,

Gent, February 2004

Table of Contents

Abstract	i
Preface	iii
Table of Contents	v
Overview and rationale	1
CHAPTER I - Introduction	3
A. Anatomy and physiology of heart and circulation	4
1. Introduction	4
2. The circulation	5
3. Blood vessels	7
4. The heart	9
5. The conduction and contraction system of the heart	11
6. The cardiac cycle	14
7. Assessment of cardiac function	18
8. Wall stress.....	26
9. Blood pressure regulation	28
B. Heart Failure.....	30
1. Introduction	30
2. Congenital heart disease	31
3. Low Output Syndrome	31
4. Congestive Heart Failure	32
C. Therapies for CHF.....	36
1. Introduction	36
2. Pharmacological treatment	37
3. Surgical reshaping	38
4. Dynamic cardiomyoplasty	41
5. Cardiac containment	42
6. Heart Transplant	43
7. Artificial heart.....	45
8. Cardiac assist	48
D. Classification of ventricular assist devices	53
1. Introduction	53
2. Duration of support.....	53
3. Position of the device	54
4. Pumping principle.....	57
E. Application of ventricular assist devices	64
1. Introduction	64
2. Post-cardiotomy failure and acute cardiogenic shock	64
3. Bridge to transplantation	65
4. Permanent cardiac assist.....	66

5. Bridge to recovery	67
6. Other applications	69
F. Physiological impact of continuous and pulsatile blood flow	71
1. Introduction	71
2. Reasons of controversy	72
3. Insights from animal studies	74
4. Clinical experience	78
5. Pulsatile alternatives	79
6. Conclusion	80
CHAPTER II - In vitro Modeling of Ventricular Assist	81
A. Introduction	82
B. Afterload models	84
1. Characterization of afterload	84
2. Lumped <i>in vitro</i> afterload models	85
3. Distributed <i>in vitro</i> afterload models	92
C. Preload models	95
1. Static preload models	95
2. Dynamic preload models (heart simulators)	96
CHAPTER III - Mathematical Modeling of Ventricular Assist	99
A. Overview of mathematical cardiovascular modeling	100
1. Introduction	100
2. Cardiac models	101
3. Afterload models	112
4. Assist device models	116
B. The Hydraulics Laboratory mathematical model	122
1. Introduction	122
2. Cardiac model	123
3. Afterload model	129
4. Assist device model	130
5. Program setup	135
CHAPTER IV	
Hydrodynamic Analysis of Heart - Rotary Blood Pump Interaction	143
A. Introduction	144
1. Overview of the chapter	144
2. The Medos Deltastream pump	145
3. The Medos-HIA microdiagonal pump	147
4. Characterization of the Medos pumps	148
B. Mathematical model study of rotary blood pump failure [†]	155
1. Abstract	155
2. Introduction	155
3. Materials and methods	156
4. Results	160

[†] The contents of this section was published in an international journal

5. Discussion.....	164
6. Conclusions	168
7. Acknowledgements	168
C. Mathematical model study of ventricular assist with a rotary blood pump in continuous and pulsatile mode [†]	169
1. Abstract.....	169
2. Introduction	170
3. Materials and methods.....	171
4. Results	175
5. Discussion.....	181
6. Conclusions	184
7. Acknowledgements	184
D. In vitro model study of rotary blood pump failure and ventricular assist with a rotary blood pump in continuous and pulsatile mode	185
1. Introduction	185
2. Materials	185
3. Methods	188
4. Results	191
5. Discussion.....	197
6. Study limitations.....	200
7. Conclusions	201
E. In vivo study of ventricular assist with a rotary blood pump in continuous mode: impact of cannulation site [†]	202
1. Abstract.....	202
2. Introduction	202
3. Methods	204
4. Results	207
5. Discussion.....	212
6. Study limitations.....	215
7. Conclusion	215
8. Acknowledgements	216
CHAPTER V	
Hydrodynamic Analysis of Heart - Pulsatile Catheter Pump Interaction... 217	
A. Introduction.....	218
1. Overview and rationale of the chapter.....	218
2. The PUCA II pump.....	219
B. Hydrodynamic characterization of ventricular assist devices [†]	221
1. Abstract.....	221
2. Introduction	221
3. Materials and methods.....	222
4. Results	225
5. Discussion.....	230
6. Acknowledgements	233
C. PUCA II pumping capacities versus high-flow volumetric devices	234
1. Introduction	234

[†] The contents of this section was published or accepted for publication in an international journal

2. Methods.....	234
3. Results and discussion	235
4. Conclusions	240
D. In vitro evaluation of the PUCA II intra-arterial LVAD [†]	241
1. Abstract	241
2. Introduction	241
3. Materials and Methods	243
4. Protocol	245
5. Results	247
6. Discussion	251
7. Conclusion	257
8. Acknowledgements	257
E. In vitro assessment of the unloading and perfusion capacities of the PUCA II and the IABP [†]	258
1. Abstract	258
2. Introduction	258
3. Materials.....	259
4. Results	263
5. Discussion	267
6. Study limitations	269
7. Conclusion	270
8. Acknowledgements	270
CHAPTER VI - Conclusions	271
A. Summary of the rotary blood pump studies	272
1. Introduction	272
2. Pump failure	273
3. Unloading with constant rotational speed	275
4. Unloading with modulated rotational speed	277
B. Summary of the PUCA II studies	278
1. Introduction	278
2. Available information on PUCA.....	279
3. PUCA II studies performed at the Hydraulics Laboratory	280
4. Conclusion	281
C. Lessons learned for future modeling of cardiac assist.....	282
1. Introduction	282
2. Resistance issues	283
3. Cardiac modeling issues.....	285
4. Conclusion	292
D. Final thoughts and comments.....	293
References	295

[†] The contents of this section was published in an international journal

Overview and rationale

Many ventricular assist devices have been developed since the 1960s and many more are currently in a development phase. The rationale for this work was therefore not the design of a new device or a contribution to the development of a particular device. Nor was it the goal to demonstrate the safety and efficacy of a device as it is required by institutions such as the US Food and Drug Administration (FDA) or the CE directives. The primary goal of the project summarized in this dissertation was to investigate the interaction between ventricular assist devices and the native (failing) heart, and to get one step closer to the full comprehension of the intervening phenomena.

In spite of two decades of extensive experience with implantable ventricular assist devices, it is still not clear how the heart experiences the assistance and what the ideal device or operation mode would be. The fact that these devices have been used as a therapeutic instrument (“bridge to recovery”) in select cases in recent years, further urges the need to understand the heart-device interaction. The main component of such a device is a blood pump, and its interaction with the heart takes place on several levels, e.g., purely mechanical interaction, biochemical reaction, response on the nervous control of the heart. The heart-device interaction is further complicated by the combination of ventricular assist devices with pharmacological therapy. In this work, the intention was to focus on the mechanical heart-device interaction of two types of devices that are fairly new and with which the experience is very limited: the (rotary) diagonal pump (in standard and miniaturized version) and the PUCA II volumetric pump.

The first chapter of this dissertation is intended for readers without medical background and it therefore introduces the basic function of the heart and various forms of heart failure. Methods for treatment of heart failure are briefly explained, with special attention to ventricular assist devices and their various forms and applications. There are basically two types of devices: the ones that generate a continuous blood flow (with a rotary pump) and those generating a pulsatile flow (with a positive-displacement (volumetric) pump). Each type has specific advantages and disadvantages and assist device investigators are basically split in proponents for either type. Therefore the physiological effect of

these two types of generated flow is discussed in detail at the end of the first chapter.

The following two chapters (II and III) present the tools available for the study of the heart-device interaction. First, there are the *in vitro* models that are a hydraulic simulation of the (systemic) cardiovascular system. Apart from the complete cardiovascular model that is used for ‘dynamic’ interaction studies, also a model of the vascular system without the heart can be used for ‘static’ studies; to assess information on the basic function of the device under test. Besides *in vitro* models, also mathematical models are useful tools to study the heart-device interaction. Chapter III gives an overview of methods to model the cardiovascular system in mathematical terms, where the function of the heart, the vessels, and the ventricular assist device is simulated with functions and equations, which can be solved by computer programs. A detailed description of the model that has been developed in the course of this project is given at the end of that chapter.

Chapters IV and V consider the interaction studies itself. Extensive studies with the rotary (diagonal) pumps are described in chapter IV, where the load on the heart is investigated for three scenarios of pump use. First, there is the case of sudden pump failure, followed by regular unloading of the heart with a continuously running rotary pump. The final highlighted scenario is the use of a rotary pump with a modulated rotational speed, in such a way that a pulsatile flow is generated. These three scenarios are investigated with the mathematical model and an *in vitro* model, further supported with unloading studies in real sheep (*in vivo*). Chapter V concerns volumetric pumps, with a main focus on a catheter-based device that is intended for short-term support: the PUCA II pump. This device is characterized in the static *in vitro* model, followed by a dynamic interaction study. The heart-device interaction is further compared to the effect of an intra-aortic balloon pump.

Finally, chapter VI summarizes the conclusions drawn from the previous chapters, and it highlights some drawbacks of the *in vitro* and mathematical models that are used for heart-device interaction. These remarks are generally valid for models currently used throughout the world. Consequently, suggestions are given for further improvement of ventricular assist models to study the heart-device interaction.

CHAPTER I

Introduction

A. ANATOMY AND PHYSIOLOGY OF HEART AND CIRCULATION

1. Introduction

In the second century, the famous anatomist Claudius Galenus, or Galen, performed animal experiments and produced many manuscripts in which he revealed the secrets of circulation in the human body. Although according to his theory, there wasn't much circulating (see Fig. I-1). He believed that food was directly converted into blood in the liver. Blood was needed for nutrition of the body and moved back and forth like tides in two completely separated systems: arteries and veins. In the heart, he claimed, blood was mixed with air (pneuma) to add spirit to the arterial system. This theory was readily accepted and taught by physicians for the following 15 centuries.

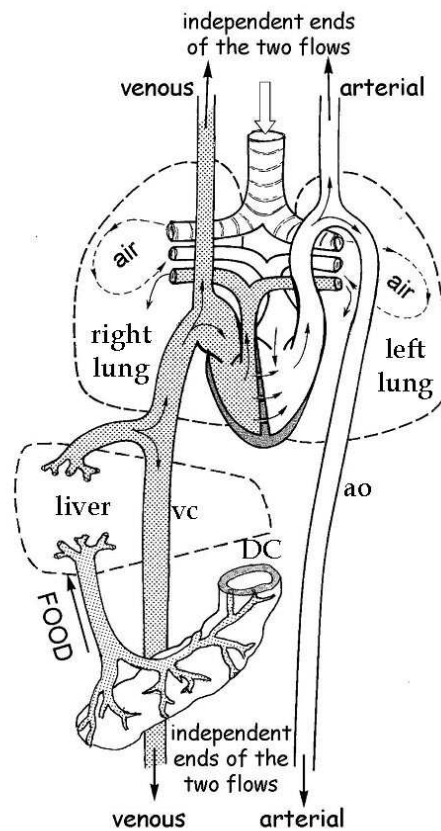


Fig. I-1: Illustration of Galen's view on circulation.
DC: digestive channel. ao: aorta. vc: vena cava.

Throughout his versatile career as a botanist and anatomist, William Harvey has always criticized Galen's theory. His own experiments in the 17th century revealed that there is a continuous movement of blood in a closed system in the body of mammals, and that the heart is the pump that maintains this circulation. He hereby laid the foundations for our current insights in the mammalian circulatory system.

2. The circulation

The circulatory system is composed of a pump and conduits (blood vessels) that lead to organs where exchange processes occur. The transport medium is blood, composed of plasma, red and white blood cells, and platelets. The blood is responsible for transporting heat and oxygen and supplying this to muscles and end organs. The organs in turn release waste products (lactic acid, ureum, ...) or functional substances such as hormones which are then transported and exchanged again in other organs. In the lungs, fresh oxygen is supplied to the blood.

To provide an efficient circulatory system that allows sufficient gas exchange through the lungs, the mammalian circulatory system is actually composed of two circuits that are connected in series (see Fig. I-2). Blood runs through these circuits at the same flow rate, which is about 5.5 l/min at rest. The largest loop is the systemic circulation that is maintained by the left side of the heart and provides oxygen rich blood to all the major organs except for the lungs. This part of the circulatory system starts in the aorta, an elastic artery with a diameter of about 2.5 cm that originates directly from the heart. After the blood has passed the organs, it flows into the right side of the heart via the caval veins (inferior and superior). The 'right heart' subsequently pumps the blood through the pulmonary circulation, beginning with the pulmonary artery. The main function of this circulation is to pass blood through the lungs for gas exchange. The pulmonary circulation ends in the left side of the heart via four pulmonary veins, and from there the oxygenated blood is again ejected in the systemic loop.

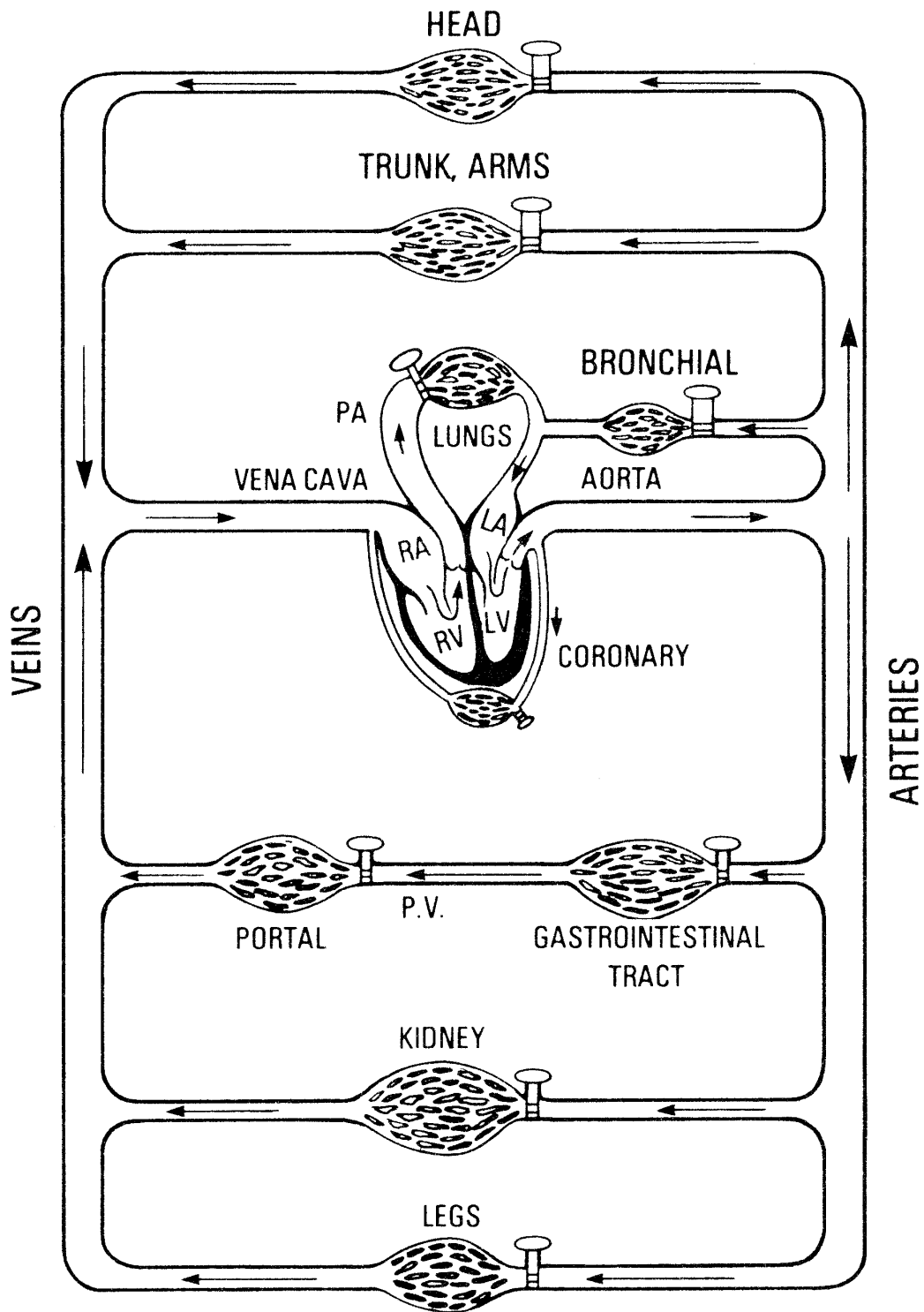


Fig. I-2: Schematic overview of systemic and pulmonary circulation ^[1]. PA: pulmonary artery. RA: right atrium. RV: right ventricle. LA: left atrium. LV: left ventricle. PV: portal vein.

3. Blood vessels

Blood needs to be transported fast and efficiently between the organs, yet allowing enough time for the exchange of substances with the organs. Therefore, different types of blood vessels are present in the circulatory system. The large arteries split into smaller arteries, which branch progressively and form narrow vessels that are called arterioles (see Fig. I-4). The arterioles branch further into innumerable capillaries with a very small cross section (diameter below 10 μm). Because there are so many capillaries, the total cross section of the vascular system actually increases as a result of the branching. Consequently, the blood will slow down (200 times slower at capillary level than in the aorta) and allow an efficient exchange. The capillaries will eventually converge again in venules and further into veins. In general, arteries are vessels that transport blood away from the heart while veins transport it towards the heart.

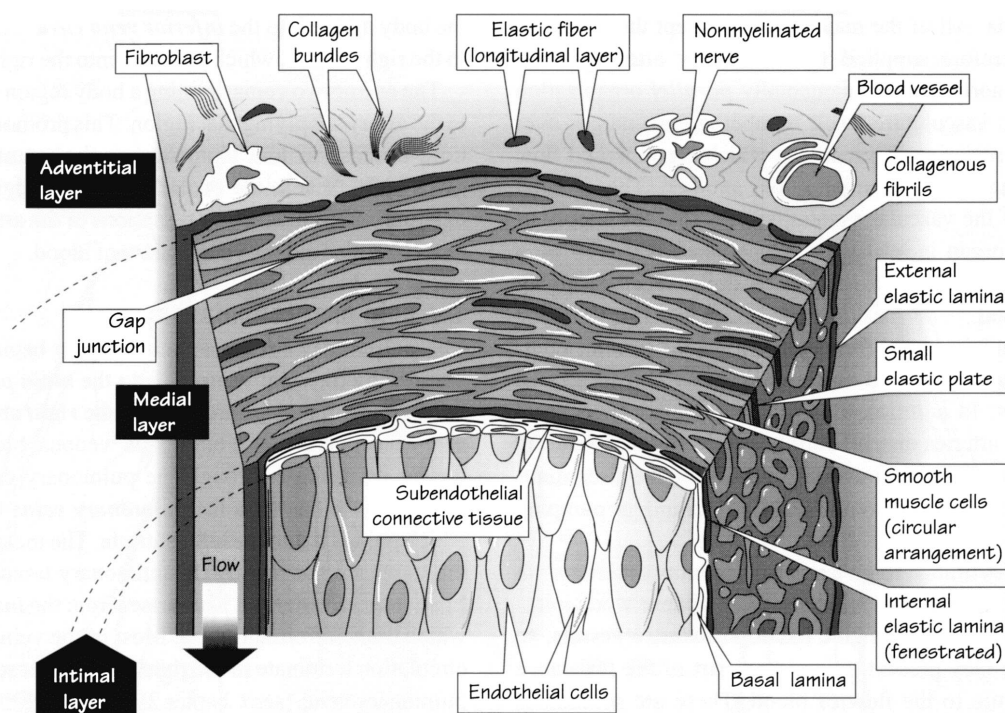


Fig. I-3: Detailed sketch of the general structure of a blood vessel.

In spite of all these different types, all blood vessels are composed of the same three layers, albeit in different proportions (see Fig. I-3). The inner layer is called the intimal layer, which consists of a flat sheet of endothelial cells, resting on a thin sheet of connective tissue. This layer is necessary for blood contact because it releases products that prevent blood clotting. The middle layer is called the medial layer and provides strength and constrictive power to the blood vessels. It

is constructed of smooth muscle cells embedded in a matrix of elastin (~ elasticity) and collagen (~ strength) fibers. The outer layer is called the adventitia layer, made of connective tissue that binds the vessel to surrounding structures to hold it in place. The only exception to this three-layer system are the capillaries, that only consist of a single layer of endothelial cells to allow rapid exchange of substances between blood and surrounding tissue.

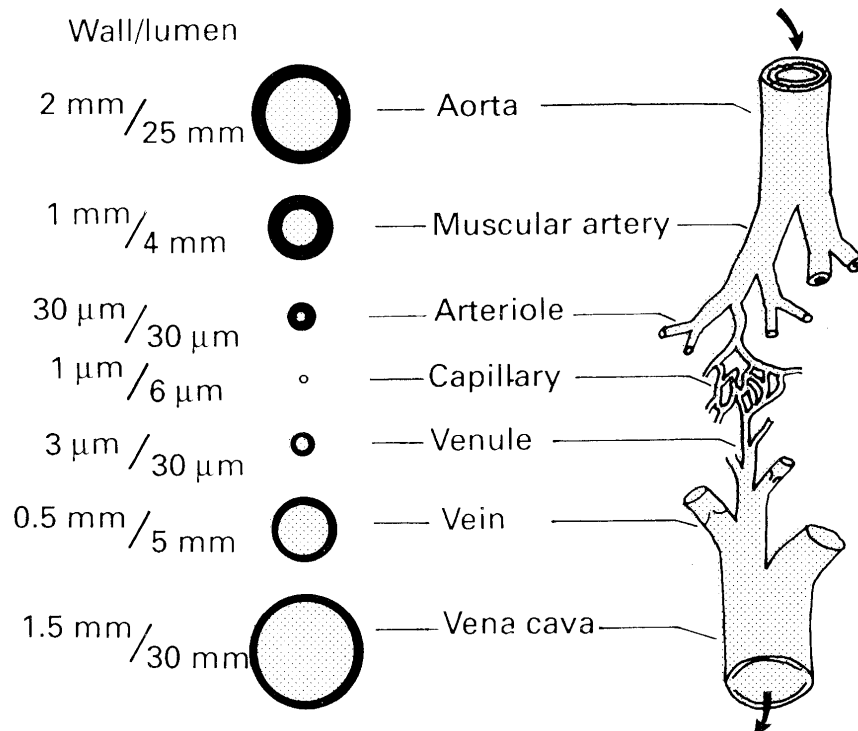


Fig. I-4: Wall thickness and inner diameters of different types of blood vessels ^[2].

From functional perspective, the large vessels such as the aorta and the pulmonary artery act as dampers that convert the pulsating flow from the heart to a more continuous flow. For this, they are very elastic by their high content of elastin fibers in the medial layer. Smaller arteries are more muscular and have a relatively higher wall thickness (see Fig. I-4) and they only exert a low resistance on the blood flow, making them function as regular conduits. The arterioles, on the other hand, are true resistance vessels. They are smaller than regular arteries and have a wall thickness equal to their own internal diameter. A high pressure drop is present over these vessels, and the actual total vascular resistance is mainly regulated by the dilation and constriction of these vessels. The capillaries then act as exchange vessels and cause very little pressure drop because of the

many parallel circuits. Venules and veins have the same wall structure and differ mainly in size. They all have a thin media layer that allows them to distend or collapse and thus act as a variable volume reservoir. The veins in the limbs are also equipped with valves to prevent backflow. Veins are relatively larger and more numerous than arteries and as a consequence they contain about two-thirds of the circulating blood. Their innervation allows for active control of the stored volume.

4. The heart

The human heart is located in the mediastinum, the space between the lungs in the thoracic cavity. A normal heart has the size of a person's fist and weighs about 300 grams. It consists mainly of muscle cells (myocytes) that form the myocardium, the muscle wall of the heart. On the inside, the heart is covered with a layer of endothelial cells that is called the endocardium. The outer layer is the epicardium. The heart is further embedded in the pericardium to prevent friction injuries as a result of the continuous pumping action of the heart and the tidal moving of the lungs. This pericardium is in fact a flat double layered membrane that contains 20 to 30 ml of lubricating fluid to fulfill its cushioning function.

To execute its pumping function and maintain the pulmonary and systemic circulation, the heart is divided into four chambers (see Fig. I-5). The two top chambers are called the atria (sing.: atrium) and their main function is to provide sufficient and well-timed filling of the chambers below. For this, the atria can function as a blood collecting reservoir, as a conduit, and as a pump, and alternate between these functions during the cardiac cycle. The atria, however, are only faintly muscled and thus have only limited pumping power. The real pumping action of the heart is performed by the lower chambers, the ventricles. These have a thick myocardial wall, which is needed to create the pressures necessary to eject the blood against the resistance of the blood vessels. To direct the flow, the ventricles have an inflow and outflow valve, which are embedded in a fibrous disc (annulus fibrosus), which separates the ventricles from the atria.

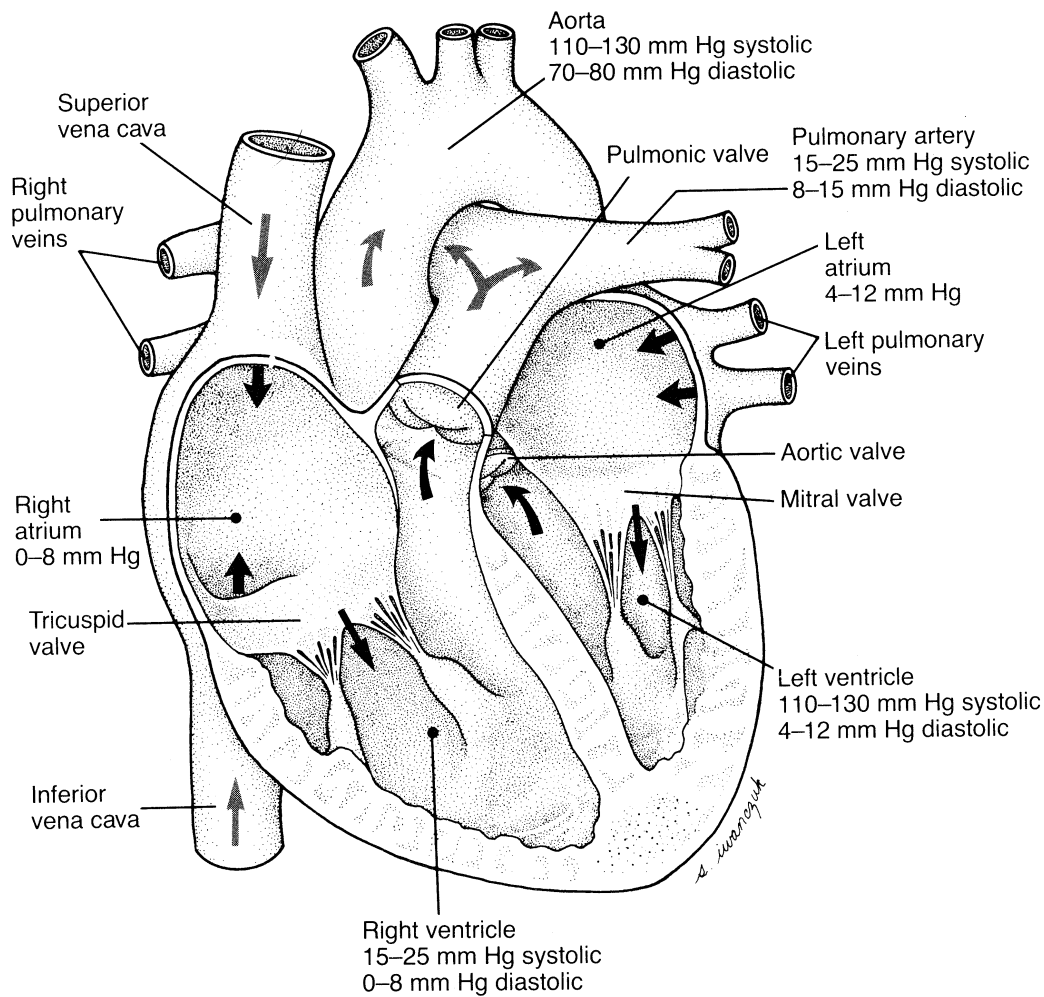


Fig. I-5: Anatomy of the heart and the governing pressures ^[3].

The atria and ventricles are divided in a left and a right part by the septum. From functional perspective, the left atrium and ventricle ('the left heart') provide blood flow into the systemic circulation and the right atrium and ventricle maintain the pulmonary circulation. Sequentially, the blood that comes from the lungs flows through the pulmonary veins, the left atrium, the left ventricle, and via the aorta into the systemic circulation. There it is collected again in the vena cava and flows further through the right atrium, right ventricle, pulmonary artery, and back to the lungs. The left ventricle has the mitral valve to prevent backflow to the atrium and the aortic valve as an outflow valve, to prevent regurgitation from the aorta into the ventricle. The right ventricle has the tricuspid valve and the pulmonary valve for the same purposes.

Since the heart is an organ in itself, it also requires supply of oxygenated blood. Therefore the left and right coronary arteries originate directly downstream from

the aortic valve and form a network of arteries on the epicardium (see Fig. I-6). The main arteries on the left heart are the left anterior descending (LAD) and the circumflex (LCx) coronary arteries. Through these arteries and capillaries, blood is supplied to the myocardium. The arteries go over into veins that gather in the coronary sinus in the right atrium, where the oxygen deficient blood is collected and directed to the pulmonary circulation.

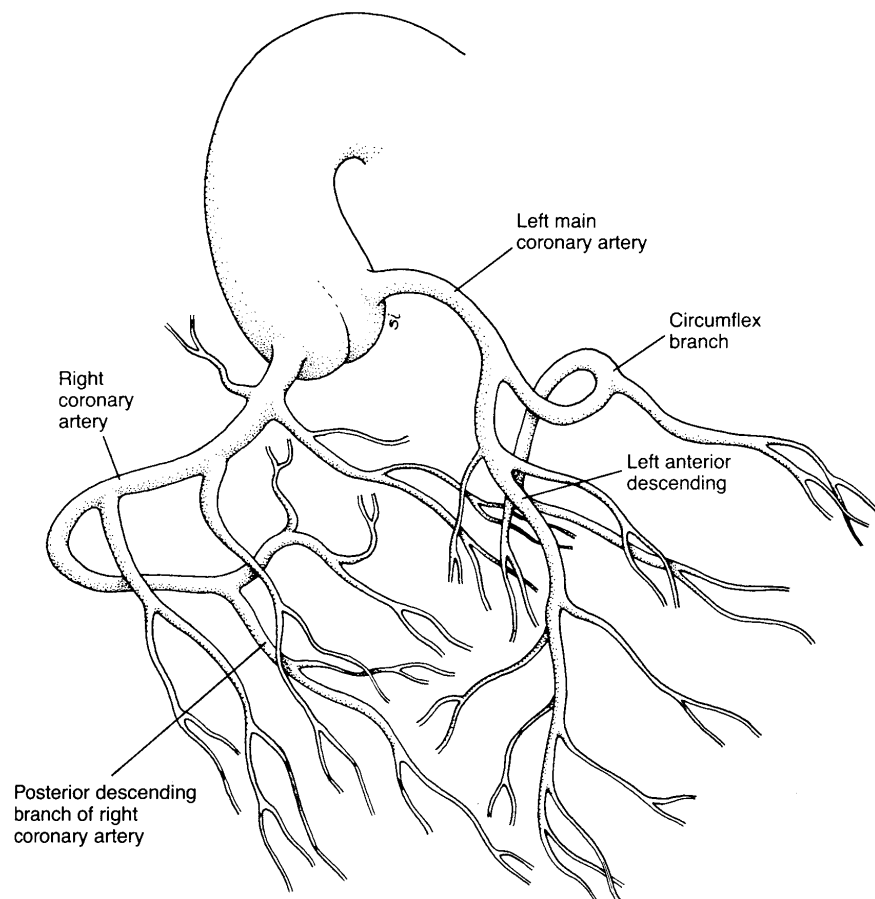


Fig. I-6: Sketch of the coronaries as they lay upon the heart ^[3].

5. The conduction and contraction system of the heart

5.1. Electrical conduction

The contraction of the heart muscle is initiated by an electrical pulse, stimulating every muscle fiber that contributes to the contraction. This electrical pulse is in fact generated within the heart itself and propagated by a special conduction system, so there is no need for external innervation to initiate contraction. As a result, the heart will keep beating at its basal rate when it is excised from the body. The intact *in situ* heart, however, has external innervation to regulate the heart rate.

The sino-atrial (SA) node in the right atrium is the actual pacemaker that discharges pulses at regular intervals. The pulse (or action potential) is passed on through modified muscle cells over both atria, resulting in atrial contraction. Because the fibrous plate between the atria and ventricles is electrically isolating, that action potential is not passed on to the ventricle. Instead, the atrioventricular (AV) node that is located just above that plate is activated and from there the action potential is spread over the ventricles through bundles of long conductive fibers. The action potential is then passed on from cell to cell at high speed, making the ventricles contract (and generate pumping power) virtually as one entity. The AV node causes a delay in the pulse transmission that is important for the harmonization of atrial and ventricular pumping action.

5.2. The electrocardiogram

The collective electrical activity of all the heart muscle cells is reflected in the electrocardiogram (ECG) that can be measured at the body surface with an ECG monitor. The resulting waveform has a typical morphology (see Fig. I-7, bottom graph). The first bump is referred to as the P wave and it corresponds to the electrical activity of the SA node, which indicates the start of atrial contraction. It is followed by a plateau that is referred to as the PR interval and that indicates the delay in the AV node. The following high-amplitude peak is the QRS complex that indicates the electrical activity of the ventricles, and thus the onset of ventricular contraction. Because of the numerous muscle cells that are activated almost simultaneously, this part of the signal reflects the highest electrical activity and it can be used for triggering of cardiovascular devices. Finally, the asymmetrical T wave reflects the repolarization of the ventricular muscle mass.

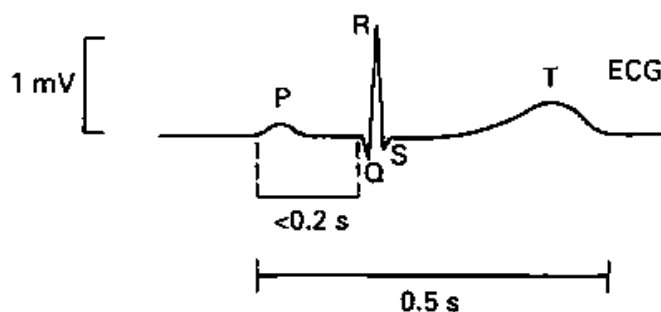


Fig. I-7: The ECG: electrical activity of the heart as it can be measured at the body surface ^[2].

5.3. Contraction of muscle fibers

On microscopic level the myocardium consists of a structured bundling of muscle fibers with various orientations (see Fig. I-8). They act together as one functioning entity that makes complex motions during the cardiac cycle. Each ventricular fiber is actually a cell (myocyte), that is constructed of a bundle of myofibrils which in turn contain sarcomeres. These are the actual contracting elements, consisting of several thick myosin filaments surrounded by six thin actin filaments (see Fig. I-8). These filaments are connected via crossbridges, and they can slide over one another by repositioning the crossbridges. This is called the sliding filament principle and it results in shortening of the sarcomere (and myofibril, and muscle fiber) and the development of force. Such a contraction consumes a lot of energy and oxygen, while also a high quantity of calcium ions (Ca^{2+}) is mandatory for the activation and deactivation of the sliding mechanism.

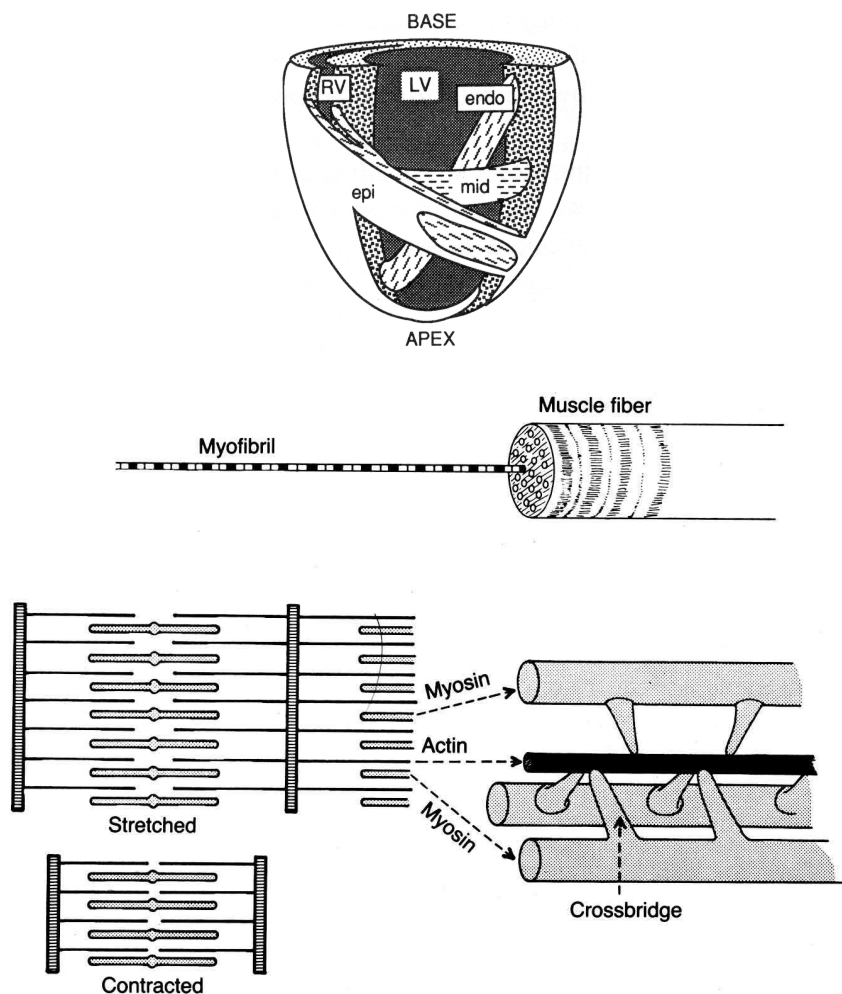


Fig. I-8: Top: Sketch of the (simplified) orientation of the muscle fibers in the left ventricle^[4].
Bottom: composition of a muscle fiber^[3].

6. The cardiac cycle

In order to pump blood through the circulatory system, the heart goes through alternating phases of filling and ejection. Before describing these phases in detail, it has to be clear that both atria and both ventricles work synchronously, but that atria and ventricles go through different phases. Consequently, there are two pumping cycles going on in the heart, where the ventricles lag behind the atria. Because the atria, just as the ventricles, can be seen as one muscle, only the (normal) function of the left side of the heart will be discussed. On the right side, the exact same phases occur but at lower pressure levels.

At a certain time in the cardiac cycle, the ventricle will start to relax and the pressure inside will drop rapidly while the volume stays constant (isovolumic relaxation, see below). Both the atrium and the ventricle will then be relaxed (in 'diastole') and the mitral valve will open as a result of the governing gradient (see 'start' in Fig. I-9, (a)). The atrium has been functioning as a reservoir up to then and the collected blood can now flow to the ventricle to ensure rapid filling (see Fig. I-10, 'mitral inflow'). This filling phase is actually managed by sucking action of the ventricle that recoils to its natural shape. Once the collected blood is transferred to the ventricle, the atrium will function as a conduit and blood from the pulmonary veins will be channeled directly into the ventricle. This phase (diastasis) is marked by slow filling of the ventricle. The final phase of ventricular diastole is actually the atrial systole (A-wave): the atrium contracts and functions as a pump to fill the ventricle with extra blood (see Fig. I-9, (b)). This 'atrial kick' only contributes for 20% to the ventricular filling, which can be seen in the small bump in the volume curve of Fig. I-10. If the heart would beat 65 times per minute, which is a normal heart rate at rest, then a whole heart cycle would last 0.92 seconds. The ventricular diastole (isovolumic relaxation + rapid filling + diastasis + atrial kick) would last almost two-thirds of the beat (0.57 seconds).

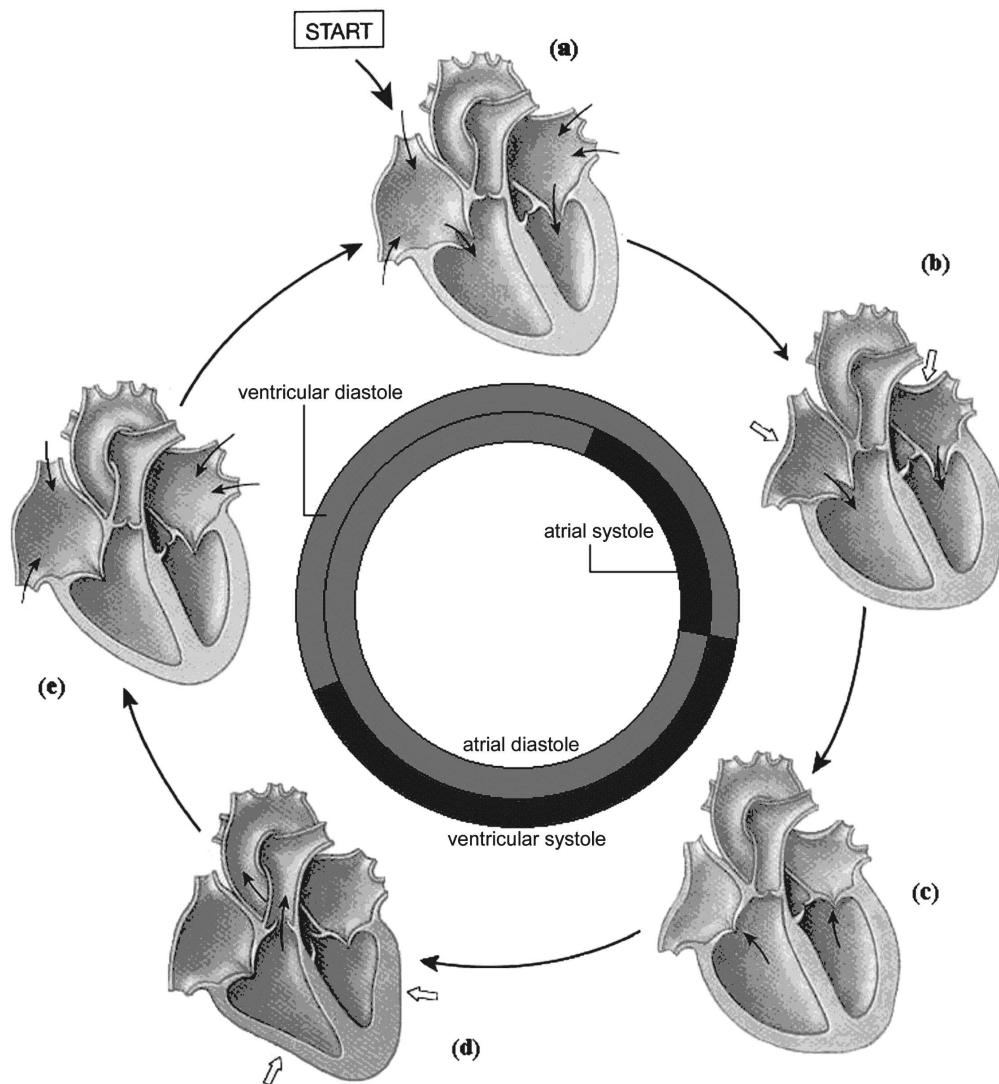


Fig. I-9: Different phases in the pumping cycle of the heart. a. early ventricular diastole; b. atrial contraction and late ventricular diastole; c. ventricular isovolumic contraction; d. ventricular ejection; e. ventricular isovolumic relaxation.

The volume contained in the ventricle at the end of the ventricular filling phase is appropriately called the end-diastolic volume (EDV) and is typically around 120 ml in an adult human. Because there are different ways to define and determine the end of diastole (e.g., by pressure, ECG, etc.), this is not always equal to the maximal ventricular volume, but EDV is at least an approximation of maximal volume. The corresponding pressure is the end-diastolic pressure (EDP). These values are often used as an indication of the preload that the ventricle is subjected to (i.e., to what level the heart is loaded and stretched at the start of contraction).

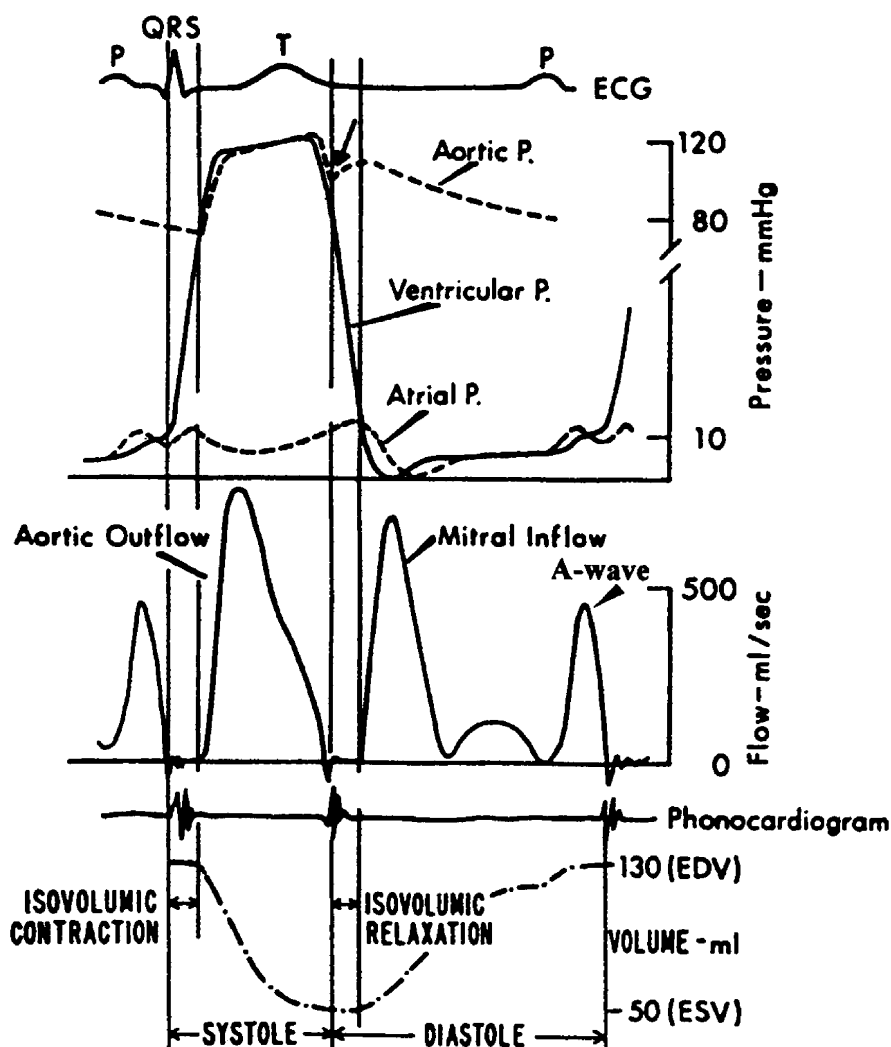


Fig. I-10: Overview of ECG, aortic, atrial, and ventricular pressure (P.), aortic and mitral flow, heart sounds, and ventricular volume and their respective timing. Adapted from Yellin ^[5].

Following diastole, the ventricular systole or contraction commences. It lasts 0.35 s and is divided in an isovolumic contraction phase and an ejection phase. During the short isovolumic contraction (0.05 s), the ventricular muscle gets tensed and builds up pressure. Consequently, the pressure gradient over the mitral valve is reversed and the valve will close. The ventricular pressure will then be in a range where the governing pressure heads keep both valves closed, preventing ventricular volume variation (Fig. I-9, (c)).

At the end of the isovolumic contraction, the intraventricular pressure will exceed aortic pressure and consequently the aortic valve will open. Rapid ejection of blood through this valve will follow (Fig. I-9, (d)). The arterial system cannot drain at the same rate and as a result there will be storage of blood in the compliant large arteries where the arterial pressure will rise to its maximum

(systolic blood pressure). After approximately 0.15 s, the ejection slows down and the drainage rate of the arterial system will exceed the ejection rate of the heart, resulting in a gradually decaying arterial blood pressure. Ejection continues when the ventricular muscle has started to relax as a result of the momentum of the outward flow. The rapidly decreasing ventricular pressure will impose an inverse pressure gradient over the aortic valve and this will slow down the outflow. Eventually, a short backflow will cause the aortic valve to close and end the ejection. This can be seen as a disturbance in the aortic pressure that is referred to as the dicrotic notch. Because of the continuing outflow as a result of momentum, and because of the different definitions of systole, there is a disparity between end-systolic pressure and end-ejection pressure. By the end of ejection, a healthy left ventricle will have ejected about 80 ml of blood in one stroke. This is called the stroke volume (SV) and it is on average 67% of the end-diastolic volume. This value is called the ejection fraction (EF) and is defined as: $EF = SV/EDV \cdot 100$.

The ventricular diastole of the next cycle will then start again with a phase of rapid relaxation that is translated in an isovolumic pressure drop: the tension in the muscle suddenly falls, resulting in pressure gradients that keep both valves closed and preclude ventricular volume variation (Fig. I-9, (e)). This phase lasts 0.08 s, followed by a new rapid filling phase of approximately 0.15 s. All throughout ventricular systole and isovolumic relaxation, the atrium was relaxed and the mitral valve was closed. Blood coming from the pulmonary veins was then stored in the compliant atrium that thus functioned as a reservoir. During the ventricular diastole, when the aortic valve is closed, the arterial blood pressure decays to a minimum value (diastolic blood pressure) and the large arteries return to their natural volume.

In total, the ventricular diastole lasted 0.57 s and the systole 0.35 s for a resting heart rate of 65 beats per minute (BPM). During exercise, the metabolic demand of the body will increase and thus a higher blood flow is required. This is mainly achieved by increasing the heart rate. The higher the heart rate, the shorter the cycle time will be, and it is especially the diastole that is shortened (see Fig. I-11). Since this is the phase during which the myocardium is supplied with oxygenated blood, it means that the heart can only function properly up to a certain heart rate. At high heart rates, the 'atrial kick' gains importance because it compensates for the lack of time to fill the ventricle passively.

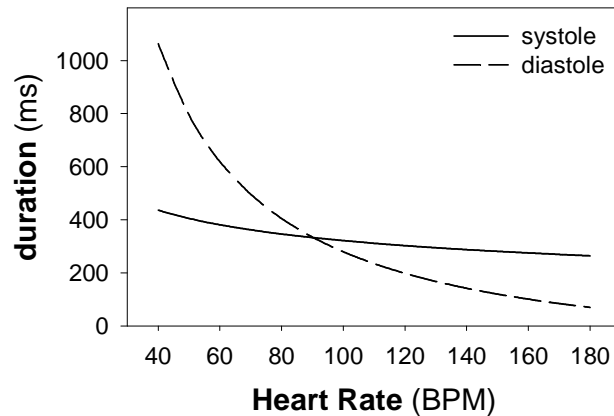


Fig. I-11: Duration of systole and diastole as a function of heart rate. Systole was defined as the QT interval of the ECG and diastole as the remainder of the heart period.

7. Assessment of cardiac function

7.1. Cardiac pump function

The heart in its natural environment is subject to numerous regulation mechanisms that adjust the function of the heart to the demand of the body. The vasomotor center from the brain regulates the inotropic state (contractility) and the heart rate based on information it gets from various ‘pressure gauges’ (baroreceptors) and chemical sensors (chemoreceptors). To quantify the function of the heart, the main interest goes to the pressures and the flows it can generate, just as with a regular water pump. The function of these pumps (e.g., a central heating pump) is usually visualized in a graph that covers a broad range of pressures and flows and from which the desired working point can be assessed. A similar approach can be adopted for the heart. In the following discussion, the focus will be on the left ventricle (LV) as it is the most powerful pump chamber of the heart.

The pressures necessary to determine the function are measured inside the LV, and averaged over the course of a heart beat in order to obtain one pressure value (mean pressure) for a certain working point at a certain functional state. The same is done with the flow generated by the heart (mean flow or cardiac output), but this is measured at its output, i.e., in the aortic arch. Several different working points can be obtained, for example by changing the pressure that the heart has to eject against (afterload). This will result in a number of pressure-flow data pairs that will together form a parabolic pump graph as seen in Fig. I-13 and Fig. I-14.

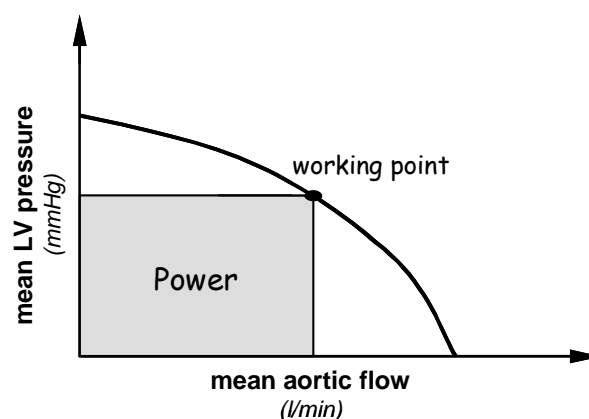


Fig. I-12: Schematic drawing of a cardiac pump characteristic.

The extreme points of the graph can be interpreted as follows: if the aorta is clamped, no flow will be generated but a high pressure will form in the LV, while if the aorta is completely open without afterload, a high flow can be generated, but no build up of pressure will be realized. The shape of the graph in between these points seems characteristic for each individual heart, although its position can change with functional state. Just as with water pump graphs, the rectangular surface under a working point is the mean power generated by the left ventricle since it is the product of the governing pressure and flow.

In experimental setups it is further possible to change the functional state of the heart. Electrical pacing or chronotropic drugs change the heart rate, while inotropic drugs like dobutamine and epinephrine can change the contractile state (inotropy) of the heart. The effect of these alterations is seen in Fig. I-13. The left panel of this figure also shows how the volume in the LV at end-diastole ('filling') alters the position of the pump graph, where increased filling yields a higher, and thus more powerful pump graph. This effect is known as the Frank-Starling mechanism, which states that the pre-stretch of the cardiac muscle fibers – as a result of increased filling – is a determinant for the generated power (Fig. I-14). This is in fact a simple consequence of the sliding filament arrangement and the initial overlap between actin and myosin in cardiac muscle, which is determined by filling.

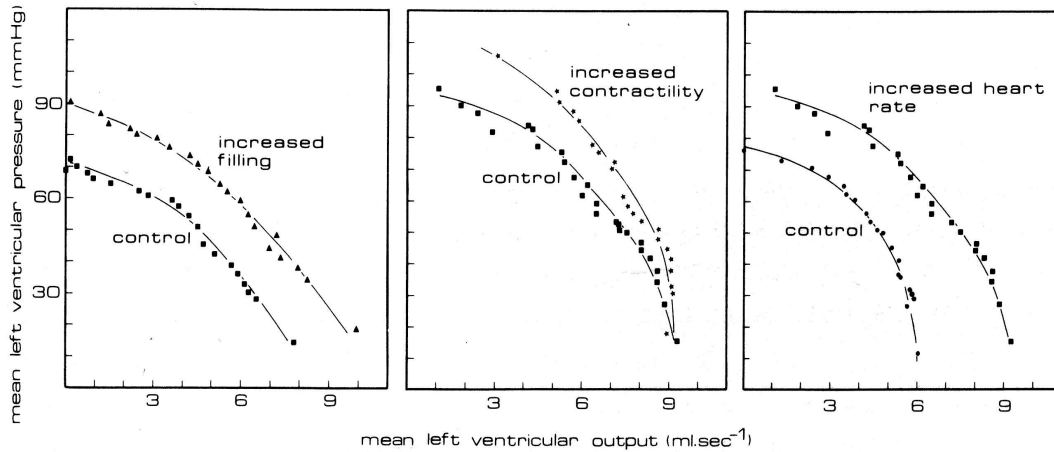


Fig. I-13: LV pump function graphs of an isolated cat heart ^[4].

Although the effect was already known and reported decades before ^[6], Otto Frank linked his name to this mechanism in the 1890s when he reported that increased filling results in increased isovolumic[†] pressure in frog ventricles. Two decades later, Ernest Starling was able to produce isobaric[‡] heart beats with his ‘Starling resistor’ and found that increased filling leads to higher cardiac output (CO).

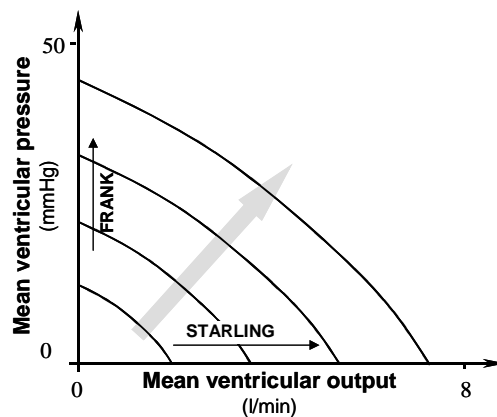


Fig. I-14: Sketch of LV pump function graphs. The gray arrow indicates the influence of increased filling, while the black arrows indicate the findings of Frank and Starling.

[†] In an isovolumic heartbeat the LV volume stays constant over the whole heart cycle. This can be obtained by clamping the aorta.

[‡] In an isobaric heartbeat the pressure in the LV stays constant over the whole heart cycle.

7.2. Pressure-volume loops and elastance

Another method of visualizing and quantifying cardiac function is plotting the instantaneous LV volume versus the instantaneous LV pressure. The resulting pressure-volume diagram is typical for a given heart in a specific functional state and at a specific working point. Consequently, many pressure-volume diagrams (or PV-loops) can be obtained from one heart. Where in the previous method the oscillatory effects of the heart were neglected by averaging over the cardiac cycle (mean values), here they are taken into account and thus a more detailed evaluation can be performed. As depicted in Fig. I-15, the pressure volume diagram, which is run through counterclockwise, can be split up in four phases that are representative for ventricular function: isovolumic relaxation, filling, isovolumic contraction, and ejection.

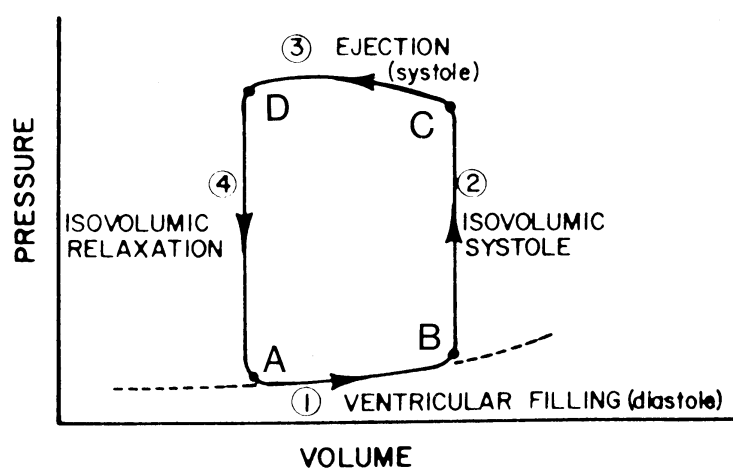


Fig. I-15: Sketch of a pressure-volume diagram of the left ventricle. The letters indicate valve action: A. mitral valve opens; B. mitral valve closes; C. aortic valve opens; D. aortic valve closes.

Suga and Sagawa further elaborated on the pressure-volume diagram^[7,8]. One of their important findings is that with different loading conditions the position and shape of this loop changes, but that the end-systolic points (approx. point D in Fig. I-15) always stay on the same line if the contractility is not altered (see Fig. I-16). This line is referred to as the end-systolic pressure-volume relation (ESPVR). Altering the functional state of the ventricle with inotropic drugs results in a rotation of the line around its volume intercept (V_0). Consequently, the slope of the ESPVR is correlated to the contractility and it would be of great clinical importance if only it could be measured easily in patients. The slope is referred to as end-systolic elastance (E_{es}), since it is an indicator of the elasticity

of the heart (elastance is the reciprocal of compliance) at end-systole, which is approximately the maximal elastance that can be obtained by the ventricle when in the same contractile state. Similarly, the end-diastolic elastance (E_{ed}) can be found as the slope of a line that connects the end-diastolic points of different PV-loops. Such a line (or curve) is known as the end-diastolic pressure-volume relationship (EDPVR, see Fig. I-16).

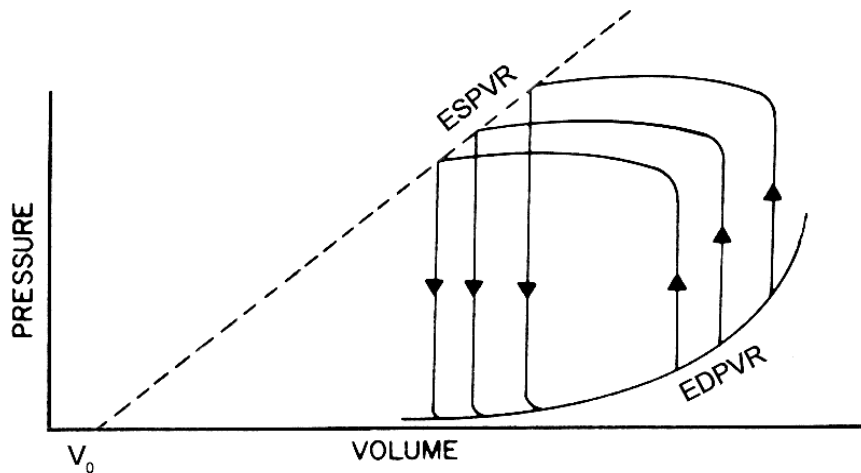


Fig. I-16: The end-systolic pressure volume relationship (dashed line) and its volume intercept (V_0) derived from differently loaded heart beat data ^[9].

Suga and Sagawa further defined the time-varying elastance theory: from the volume intercept of the ESPVR, a line can be drawn to each point of the PV-loop and thus a slope or elastance can be calculated for each time point of the heart cycle. Time-varying elastance is therefore defined as:

$$E(t) = \frac{p(t)}{[V(t) - V_0]} \quad [\text{Eq. I-1}]$$

with:

- $E(t)$: time-varying elastance (mmHg/ml)
- $p(t)$: time-varying LV pressure (mmHg)
- $V(t)$: time-varying LV volume (ml)
- V_0 : the volume intercept of the ESPVR (ml)

The elastance curve has a typical shape and its maximum is thus equal to E_{es} (see Fig. I-17). In spite the fact that the PV-loop varies in shape and position as a result of different loading conditions, the elastance curve itself is independent of preload (filling of the LV) or afterload (aortic pressure) ^[7]. Therefore the curve is characteristic for a given heart in a specific functional state and valid for all working points.

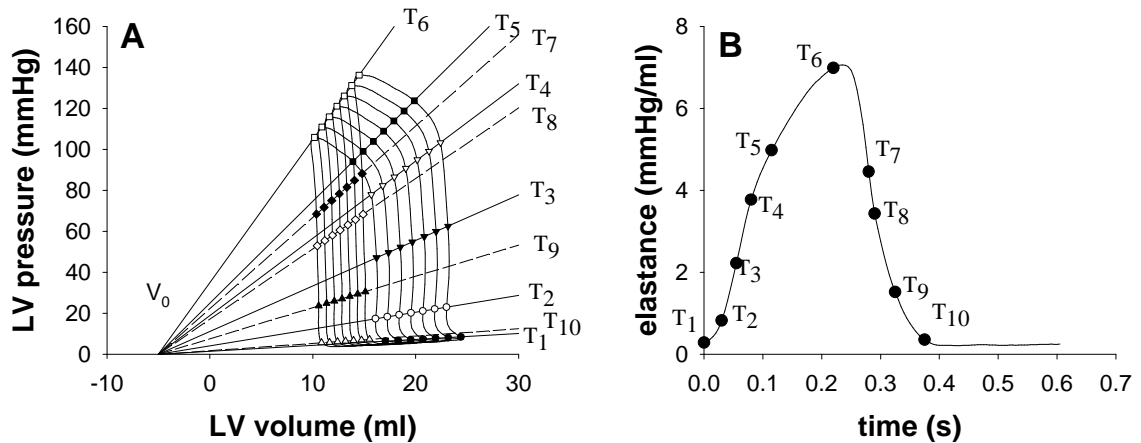


Fig. I-17: PV-loops under different preload conditions (panel A) and the related LV elastance curve (panel B). T1-T10: Various time points throughout the cardiac cycle.

Suga and Sagawa additionally found that normalization of this curve with respect to amplitude and time results in a general elastance curve that is typical for the species. Irrespective of loading conditions, heart rates, sickness, drug administration or subject, each normalized elastance curve is approximately identical. This was later confirmed by Senzaki et al. ^[10].

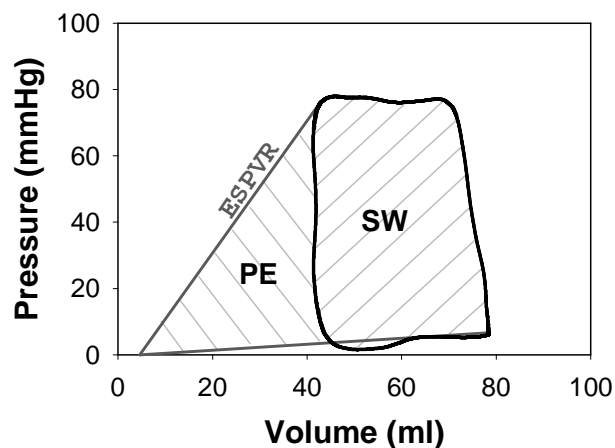


Fig. I-18: Energetic parameters in a PV-loop. PE: potential energy; SW: stroke work; ESPVR: end-systolic pressure-volume relationship.

Other interesting information can be derived from the pressure-volume diagram by quantifying areas. This results in parameters that each correlate to a specific type of energy consumption of the heart (see Fig. I-18). The surface within the PV-loop, for instance, is referred to as the stroke work (SW) or the external work, and it is a measure of the amount of energy that is transferred from the heart to the blood. In other words, this is the amount of energy that is used to

eject blood from the heart. The potential energy (PE) can be determined from the surface between the ESPVR, the EDPVR and the PV-loop and it relates to the energy that is necessary to contract the heart. Even if there were no ejection of blood (isovolumic beat), the heart muscle would still consume energy simply to build up pressure. This pressure is of course a consequence of the stress that is formed in the separate muscle fibers, which are the real consumers of the energy. The sum of the stroke work and potential energy surfaces is called the pressure-volume area ($PVA = SW + PE$). It is a measure of the total energy consumption of the ventricle and it appears to be linearly related to the oxygen consumption of the muscle ^[11]. Another index that is often used is the mechanical efficiency (Meff) of the LV, which can be defined as the ratio of the stroke work to the total oxygen consumption, or alternatively as the ratio of the stroke work to the pressure-volume area.

Further investigation and validation of the time-varying elastance theory has revealed that the ESPVR and EDPVR are in fact curvilinear and that the volume intercept actually varies during the cardiac cycle ^[12]. Nevertheless, the linear approximation as it was originally elaborated by Suga and Sagawa is still meaningful and much easier to use.

7.3. Other indices of cardiac function

To quantify cardiac function or contractility in a clinical setting, it is preferred that indices can be calculated from less invasive data or from parameters that are used for standard monitoring of patients. Also, indices that are not prone to errors due to linearization would be of interest. Therefore a number of alternatives have been applied.

7.3.1. Maximum pressure derivative

One easy to obtain measure is the so called dp/dt_{max} , which is the maximum of the LV pressure derivative (dp/dt). This maximum is normally present in early systole, at the end of the isovolumic contraction phase, and a higher value indicates a 'stronger' heart.

7.3.2. Preload recruitable stroke work

Another alternative is the preload recruitable stroke work (PRSW). Since Frank and Starling had already demonstrated the impact of the filling of the heart on the generated energy, it is logical that cardiac contractility would be derived from

measurements at different preloads. Since every different preload level yields a different PV-loop with a different stroke work, it is possible to plot the stroke work of each PV-loop as a function of preload. A line can be fitted (with good correlation) through the obtained data points and the slope is the PRSW, which is again a measure of contractility ^[13]. A disadvantage of this method is the necessity of simultaneous LV pressure and volume measurement, which is relatively unreliable with contemporary clinically available techniques.

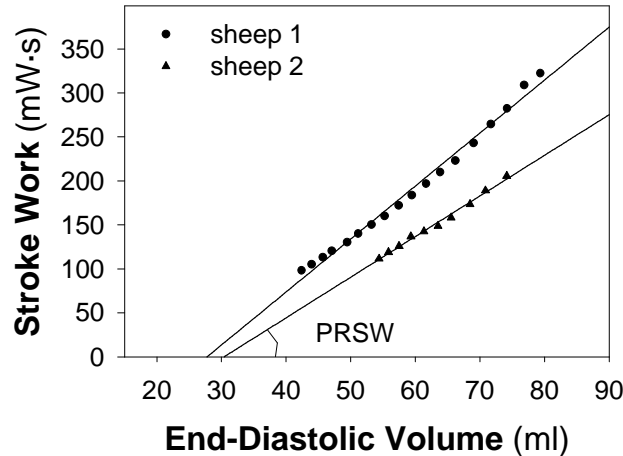


Fig. I-19: Example of the preload recruitable stroke work (PRSW) determination for 2 sheep.

7.3.3. Preload adjusted maximal power

This method is based on the power generated by the LV. As discussed with the pump function graphs, the power can be calculated as the product of LV pressure and aortic flow. This can be done for every time point of the cardiac cycle, thus yielding a power curve. The maximum of this curve is another measure of contractility, which is again highly dependent on preload. Therefore an adaptation of the power calculation can be applied by normalizing the power with respect to the end-diastolic volume. A popular way of calculating the preload adjusted maximal power (PAMP) is then ^[14-16]:

$$\text{PAMP} = \max \left(\frac{p(t) \cdot Q_{ao}(t)}{\text{EDV}^a} \right) \quad [\text{Eq. I-2}]$$

with:

PAMP: preload adjusted maximum power (mmHg·ml^(1-a)/s)

p(t): LV pressure (mmHg)

Q_{ao}(t): aortic flow (ml/s)

EDV: end-diastolic LV volume (ml)

a: constant (-)

The constant ‘a’ is experimentally determined and it is necessary to make sure that identical PAMP values are obtained for heartbeats at different preloads. Without that correction, one particular heart in a constant functional state but at different working points would yield different values and thus it would be impossible to quantify the actual contractility. Therefore, a more accurate way that also relates better to the time-varying elastance theory, is to include the volume intercept V_0 in the calculation (see [Eq. I-3]). This, however, has the disadvantage that for each PAMP calculation there is need for multiple beats at various loading conditions to allow estimation of V_0 (see Fig. I-16).

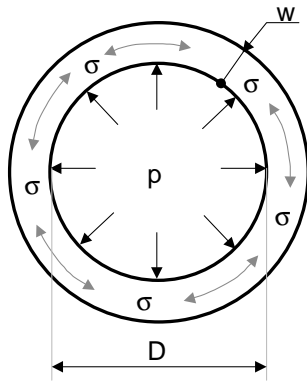
$$\text{PAMP} = \max \left(\frac{p(t) \cdot Q_{ao}(t)}{(EDV - V_0)^2} \right) \quad [\text{Eq. I-3}]$$

8. Wall stress

In 1958, Sarnoff demonstrated that one of the primary determinants of myocardial oxygen consumption is the stress in the myocardium ^[17]. It is also accepted that ventricular geometry adaptations as a result of cardiac disease and abnormal loading conditions, are a means to normalize altered ventricular wall stress ^[18,19]. It is therefore of interest for the understanding of heart disease and possible therapies to calculate the ventricular wall stress.

The ventricular wall is a non-homogeneous, anisotropic material with nonlinear elasticity that is composed of layers of fibers with different orientations embedded in connective tissue (see Fig. I-8). A complex stress distribution can thus be expected. However, it has been demonstrated experimentally that LV wall stress is distributed homogeneously and that a single value can be used to indicate the wall stress for the whole wall ^[20].

In the simplest model for wall stress calculation, the ventricle is approximated as a spherical shell. Laplace’s law [Eq. I-4] can then be applied to relate ventricular wall stress to the pressure, the inner diameter, and the (inverse of) wall thickness.



$$\sigma = \frac{p \cdot D}{4 \cdot w} \quad [\text{Eq. I-4}]$$

with:

σ : wall stress (N/m^2)
 p : pressure (N/m^2)
 D : inner diameter (m)
 w : wall thickness (m)

More geometrically realistic is to approximate the ventricle as an isotropic, homogeneous (thick-walled) ellipsoid (Fig. I-20). Two types of stresses can then be defined: meridional (longitudinal) and circumferential wall stress, which can be calculated with modified Laplace equations specifically intended for the assumed geometry ([Eq. I-5] and [Eq. I-6], respectively) ^[21].

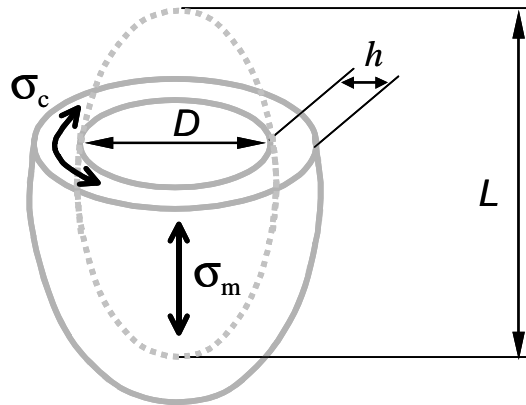


Fig. I-20: Illustration of the parameters used for the wall stress calculation. D : internal diameter. L : internal length. h : wall thickness. σ_c : circumferential wall stress. σ_m : meridional wall stress.

$$\sigma_m = \frac{p_{LV} \cdot D^2}{4 \cdot h \cdot (D + h)} \quad [\text{Eq. I-5}]$$

$$\sigma_c = \frac{p_{LV} \cdot D \cdot (2 \cdot L^2 - D^2)}{4 \cdot h \cdot (L^2 + D \cdot h)} \quad [\text{Eq. I-6}]$$

with:

σ_m : meridional wall stress at the equator (mmHg)
 σ_c : circumferential wall stress at the equator (mmHg)
 p_{LV} : left ventricular pressure (mmHg)
 D : internal ventricular diameter (cm)
 L : long axis dimension (cm)
 h : wall thickness (cm)

Apart from wall stress, it is also possible to calculate the stress in the individual muscle fibers that form the ventricular wall. Remarkably, material properties or geometry are not the major determinants for this type of stress. Arts et al. demonstrated that fiber stress is governed by ventricular pressure and the ratio of internal volume to wall volume as given in [Eq. I-7] ^[20].

$$\sigma_f = \left(1 + 3 \cdot \frac{V_{LV}}{V_{wall}} \right) \cdot p_{LV} \quad [\text{Eq. I-7}]$$

with:

- σ_f : fiber stress (mmHg)
- V_{LV} : LV internal volume (ml)
- V_{wall} : myocardial volume (ml)
- p_{LV} : LV internal pressure (mmHg)

9. Blood pressure regulation

In normal conditions, mean arterial blood pressure is maintained at physiological values by the negative feedback mechanism of the nervous system, which is controlled by the vasomotor center in the brain. If a too low arterial pressure is present, the vasomotor center will decrease the parasympathetic and increase the sympathetic activity to normalize the pressure. This works via 2 pathways: a vascular pathway (influencing peripheral resistance and volume distribution) and a cardiac pathway (influences CO).

The peripheral resistance mainly depends on the arteriolar tone. Arterioles only have sympathetic innervation, which maintains a continuous vasoconstrictor tone via the thick layer of smooth muscle cells. To regulate the necessary parasympathetic and sympathetic activity, the vasomotor center is informed of the current arterial pressure by the pressure receptors (baroreceptors) that are present in the aortic arch and in the carotid sinus. These receptors deliver electric pulses to the vasomotor center over the nerve of Hering and Cyon at a frequency that is correlated to the mean arterial pressure (MAP).

Fig. I-21 illustrates how the arterial baroreceptors influence the vascular and cardiac pathway. Next to the arterial receptors there are also cardiopulmonary baroreceptors that monitor the atrial, pulmonary and diastolic ventricular pressures. These receptors balance the effects of the arterial receptors. When for instance the arterial receptors react on increased pressure by inhibiting sympathetic activity and decreasing the heart rate, the pulmonary receptors will

in turn increase sympathetic activity to prevent a too low heart rate. In fact, the baroreceptor activity is not only dependent on the mean pressure level, but it is also influenced by the pulse pressure and the pulse rate.

Apart from the vascular pathway explained above, vascular tone is also determined by thermal and neurohormonal factors. Physiological pulsatile flow for instance, brings about systolic shear stresses that induce the secretion of different vasodilators (like NO) from the vascular walls.

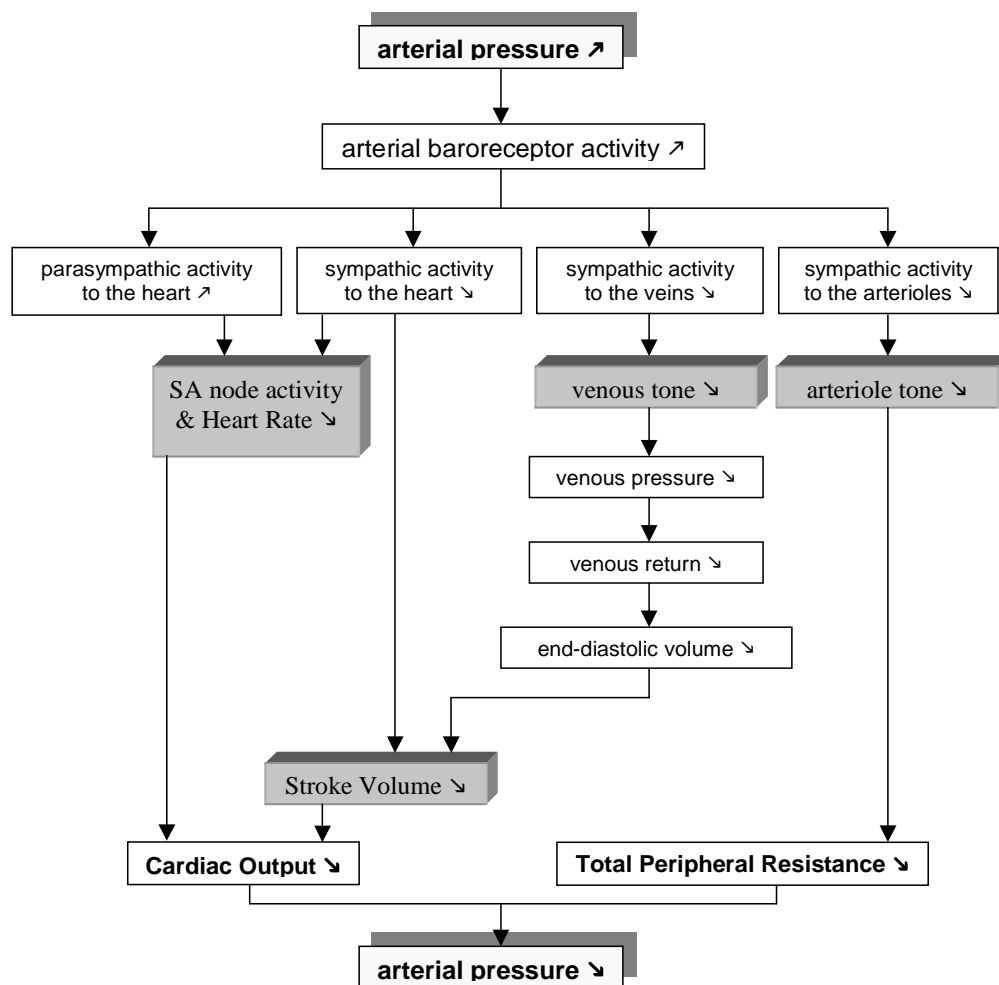


Fig. I-21: effect of baroreceptors on arterial pressure regulation.

In serious trauma, when there is great loss of blood, vasoconstriction of the blood vessels in the skin, the skeletal muscles, and the major organs will occur as a means to keep the blood in the body. However, due to a safety system of the human body (sympathetic escape) the brain and the heart escape from this vasoconstriction, since that would be more dangerous than the blood loss.

B. HEART FAILURE

1. Introduction

At present, cardiovascular diseases (CVD) are still the leading cause of death in the Western world. It has the same death rate as the following seven causes of death combined ^[22]. Worldwide, 16.7 million deaths were attributed to CVD in 2002 ^[23]. There are, however, many types of cardiovascular disease, one more lethal than the other: 32% of the 37.954 CVD deaths in Belgium was caused by diseased coronaries in 1997 ^[24]. A primary target group for treatment with cardiac assist devices are people suffering from end-stage congestive heart failure (CHF). It is estimated that there are about 5 million Americans and twice as many Europeans suffering from CHF ^[25,26]. CHF is typical for the older adult population, while new pediatric cardiac assist devices may be deployed in the treatment of congenital heart defects. Another condition where cardiac assist devices are used is the so-called “Low Output Syndrome” (LOS). These conditions are briefly discussed hereafter.

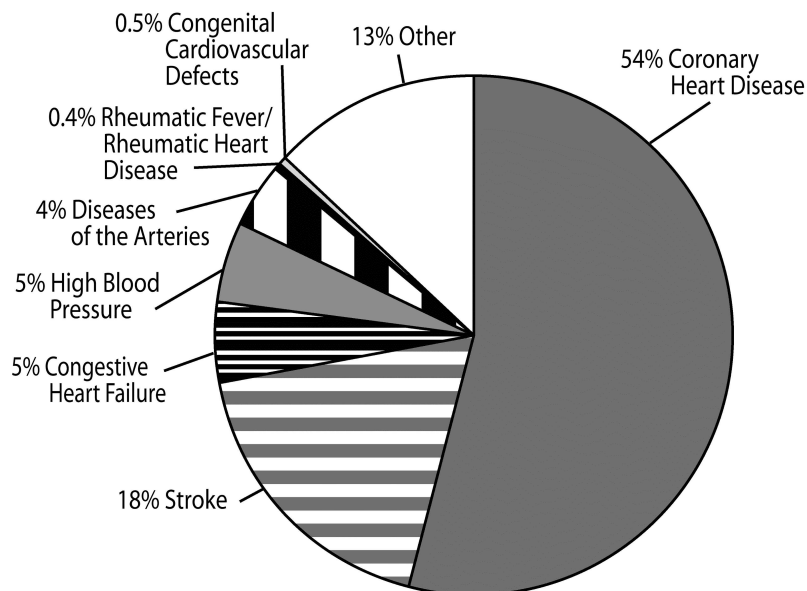


Fig. I-22: Overview of the different cardiovascular causes of death in the US in the year 2000^[22].

2. Congenital heart disease

Congenital ('existing at birth') heart defects occur in children when the heart does not develop normally during pregnancy. They are malformations of the heart that come in various forms and about 8 out of every 1,000 infants are born with them, which makes it also the type of birth defect with the highest mortality [22]. In some cases, mainly because of improved echographic technology, these defects may be detected before birth. This is not the case in all of the patients, however, and some children can live for years with a congenital defect before it is diagnosed. Some small defects may heal naturally in the infant, because the heart keeps developing after birth.

Most congenital heart defects cause blood to flow through the heart and circulation in an abnormal pattern. One of the most astonishing and fortunately rare malformations is the single ventricle, where a baby is born with only one ventricle that connects to both the pulmonary and systemic circulation. Some of the more common defects are septal defects (both atrial and ventricular) which are perforations in the septum that allow intermixing of oxygenated and deoxygenated blood and thus cause a less efficient oxygen transport. Also a transposition of the great arteries is quite common (about 10% of congenital heart disease), as is a tetralogy of Fallot. In total there are about 15 defined defects that can all occur in various combinations and in different grades of severity.

Most often, surgical treatment is required to remodel the heart and the connecting vessels. Since a number of pediatric cardiac assist devices are currently under development, congenital heart disease patients form a potential target group for application of these devices. They cannot only keep the patients longer alive and give time to the surgeons to see the natural development, but they can also provide support while the heart is recovering from reconstruction surgeries.

3. Low Output Syndrome

Open heart surgery (cardiotomy), regardless of the indication for the surgery, may result in a temporary depression of cardiac function. This post-cardiotomy heart failure is apparent when the patient cannot be weaned from the heart-lung machine that replaced the function of heart and lungs during the operation. With the low output syndrome (LOS), the heart seems incapable of producing a

sufficient cardiac output in spite of the surgery and thus it can not retake the work that it did before. One might say that the heart is in shock as a result of the operation. LOS may result from inadequate myocardial protection by the heart-lung machine or from perioperative ischemic injury.

This condition is usually temporary and can be solved by supporting the heart for a while and take over part of its load. For this, a blood pump can be used that keeps circulating the blood through the patient. Due to lack of alternatives in the past, the roller pump that was used in the heart-lung machine was also used for treatment of LOS. Biocompatibility issues prevented use of this pump for more than a couple of hours. Nowadays centrifugal pumps are more popular, also for use in the heart-lung machine. In some experienced centers it is even preferred to use a more complex blood pump that can generate a pulsatile flow, even if it is just for a short term.

Almost 1% of the patients who undergo coronary bypass surgery suffer from the low output syndrome to such an extent that they need mechanical cardiac support. Most often the patient will then recover from LOS within three days and can be weaned from the blood pump, as the heart alone pumps strong enough to maintain the circulation. However, mortality of patients after bypass surgery is significantly higher if LOS has developed.

4. Congestive Heart Failure

Congestive Heart Failure (CHF) is a term used to indicate the condition where the heart's weak pumping action leads to a buildup of fluid (congestion) in the lungs and other body tissues such as the legs, feet, ankles, and the abdomen. The 'water' in the lungs makes breathing difficult and in the legs, for instance, it causes obvious swellings (edema). A large part of the patients who suffer from congestive heart failure actually dies of the lung dysfunction that slowly suffocates them. Overall, the prognosis for CHF is poor: one out of five diagnosed patients die within the year ^[22].

CHF always results from an underlying disease that initially affected the heart function, and it is this primary heart disease that should be resolved to cure the congestion. Possible causes are heart valve disease, coronary artery disease, or cardiomyopathy.

- In heart valve disease, one or more heart valves do not function properly and surgery is required to correct or replace the valve. The valves can be either stenotic - which results in poor opening and high resistance - or regurgitant, where insufficient closure results in backflow.
- Coronary artery disease alters the supply of oxygenated blood to the myocardium by obstructed coronaries. The obstruction can be a blood clot or a plaque of fatty substances that has gradually formed inside the coronary over a long period. This can be treated by scraping or grinding the plaque away (atherectomy) or by widening the artery by shortly inflating a balloon inside (angioplasty). Other options are the placement of a stent (wire mesh tube) to keep the artery open or to bypass the blockage with an additional blood vessel.
- In case the heart muscle itself is diseased and becomes too weak to generate sufficient output, the term cardiomyopathy is used. This can for instance be caused by viral infections or alcohol or drug abuse, but most often the cause is unknown (idiopathic). Cardiomyopathy establishes itself in three forms (see Fig. I-23): dilated (large thin ventricle with little power), restrictive (stiff ventricle which impedes filling), or hypertrophic (thickened septum or myocardium that obstructs blood flow).

The lung edema that results from CHF is specifically caused by dysfunction of the left ventricle. When this ventricle is too weak to evacuate the whole blood volume coming from the lungs, a compensation mechanism tries to diminish that volume by extracting fluid from the blood and storing it in the lung tissue. If the right ventricle fails, a similar process will cause excessive fluid buildup in the veins and upstream organs, hence causing the edema in the legs. Because the kidneys are responsible for the volume regulation in the body, CHF may also put a large burden on them. The fluid buildup will affect their ability to dispose of sodium and water, and therefore they often fail as a result of CHF. If left untreated, the disease will progress and eventually other organs will weaken, resulting in a condition that is called multiple organ failure (MOF). Because of the slow but steady progression of the heart failure and its symptoms, it is also referred to as chronic heart failure.

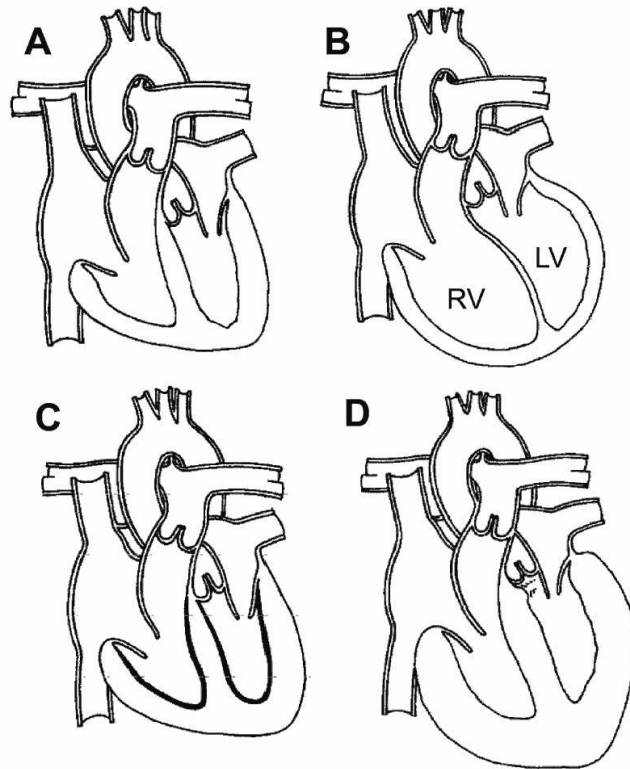


Fig. I-23: Different forms of cardiomyopathy (CMP):
A. normal heart; B. dilated CMP; C. restrictive CMP; D. hypertrophic CMP.

The severity of CHF is difficult to quantify because it has different possible causes and expresses itself in different combinations of symptoms. A classification method based on the functional status of the patient was introduced more than 30 years ago by the New York Heart Association (NYHA) and it is still popular today ^[27]. It is, however, a very rough classification that is subjective and lacks reproducibility. The NYHA scale was developed as a clinical tool, but is nowadays also often misused as a research tool in statistical analysis. Patients within the same NYHA class may show a great variability in quality of life, or a patient may show clear improvements that are not indicated by the NYHA classification and thus stay in the same class after a successful treatment. According to the NYHA classification, a patient suffering from heart failure can be divided in one of the classes below, where class I is obviously the most favorable and class IV the most severe. Patients in class IV are considered to be in an end-stage and are eligible for aggressive and invasive therapies. Typically, cardiac assist devices that are used to treat CHF can bring patients from class IV to class I.

CLASS I: This class considers patients with cardiac disease but without resulting limitations of physical activity. Ordinary physical activity does not cause undue fatigue, palpitation, dyspnea, or anginal pain.

CLASS II: Patients with cardiac disease resulting in slight limitation of physical activity are contained in this class. They are comfortable at rest. Ordinary physical activity results in fatigue, palpitation, dyspnea or anginal pain.

CLASS III: This class holds patients with cardiac disease resulting in marked limitation of physical activity. They are only comfortable at rest. Less than ordinary physical activity results in fatigue, palpitation, dyspnea or anginal pain.

CLASS IV: This class contains patients with cardiac disease resulting in inability to carry on any physical activity without discomfort. They are therefore confined to bed or chair. Symptoms of the anginal syndrome or cardiac insufficiency may be present even at rest. If any physical activity is undertaken, discomfort is increased.

C. THERAPIES FOR CHF

1. Introduction

For the fifteen centuries after Galen had spread his theory on the physiology of the human body (see section A.1), it was believed that heart failure should be treated with methods to bring balance between the four humors (black bile, yellow bile, phlegm, and blood). In 1683, up to date methods were reported by Thomas Sydenham who promoted bleeding, purges, blistering, garlic and wine. In the 20th century, the pharmacological treatment of congestive heart failure slowly evolved from mercury therapies to the actual pharmacological therapies, but large randomized clinical trials of contemporary medicines did not take place until 1986 ^[28].

Better understanding of the causes of heart failure has also led to the development of surgical approaches, e.g., to treat coronary disease or valve failure. Current technology and medical experience also allows to replace the heart when its salvation has become impossible.

It was already believed through the centuries that rest could promote the healing of heart failure, and prolonged bed rest was therefore a popular treatment method. In the 1950s, Burch even received a grant to study the healing effects of bed rest, and he reported recovery of ten out of 31 idiopathic cardiomyopathy patients ^[29]. Apart from allowing the heart to rest and ‘unloading’ it with various methods, a change in lifestyle is usually also part of therapy. Special diets are prescribed to reduce the intake of sodium and cholesterol, alcohol and smoking become taboo and, when possible, exercise is recommended.

In summary, there are various therapies for congestive heart failure that are often combined with the traditional pharmacological treatment. There are, for instance, surgical interventions that attempt to reduce the wall stress in the heart by changing its shape, or by limiting further dilatation. There are also methods and devices that assist the heart in performing its pump function, and there is the option to replace the diseased heart by a donor heart or by a device.

2. Pharmacological treatment

Drugs are always part of the treatment of heart failure, because they can unload the heart by controlling its activity or by diminishing the afterload that the arterial system bears upon it. It is, however, only in the early stages of heart failure that pharmacological support is the only therapy provided. Drugs prescribed for CHF are dependent on the condition of the patient. Sometimes the priority is to increase the blood pressure and flow, but in other cases it can be to normalize the heart rate and counter arrhythmias or tachycardia.

Diuretics are often administered to relieve the patients from edema and to extract the fluid from the lungs. Digitalis or other inotropic drugs are given to increase the power generated in the heart by increasing the amount of calcium in the muscle cells. The load of the heart is diminished by reduction of the arterial resistance, and therefore vasodilators can be administered. These also have the advantage that the blood flow through the coronaries and thus the oxygen supply to the heart improves. ACE (angiotensin-converting enzyme) inhibitors are also very popular drugs for the treatment of CHF. ACE is an enzyme that is produced in the kidney and is responsible for maintaining the tone in the blood vessels. Inhibition of this enzyme results also in a relaxation of the vessels and a reduction in afterload. ACE inhibitors also lower the amount of salt and water in the body, and consequently lower the blood pressure and relieve the lung congestion. A final series of popular pharmacological agents are the beta-blockers. They block the beta receptors in the nervous system and thus affect the sympathetic regulation of the heart. As a result, the heart rate and work of the heart will decrease and lead to a lower demand of oxygen. This type of drug may initially worsen the hemodynamics, but when tolerated they are eventually beneficial^[30].

A careful determination of the drug regimen is necessary to bring the patient to an optimal hemodynamic condition. Inotropic drugs, for example, cannot sustain their benefits during chronic treatment, and therefore the drug selection and dosage must be evaluated and adapted regularly.

3. Surgical reshaping

3.1. Ventricular volume reduction

In dilated cardiomyopathy, the myocardial muscle cells reorganize themselves (remodeling), resulting in increased internal dimensions and reduced wall thickness. This leads to increased ventricular wall stress (see A.9). More power will be required from the heart to overcome these stresses and to generate a sufficient cardiac output. Consequently, more oxygen will be consumed and the demand will exceed the supply.

A possible treatment for dilated cardiomyopathy is therefore to focus on the reduction of ventricular volume so the stresses will be normalized and ventricular function can be restored. It has already been shown that left ventricular size correlates to survival in dilated cardiomyopathy patients ^[31]. Based on this observation, the Brazilian surgeon Randas Batista introduced a new surgical technique called partial left ventriculectomy, also referred to as heart reduction surgery or the Batista procedure (see Fig. I-24).

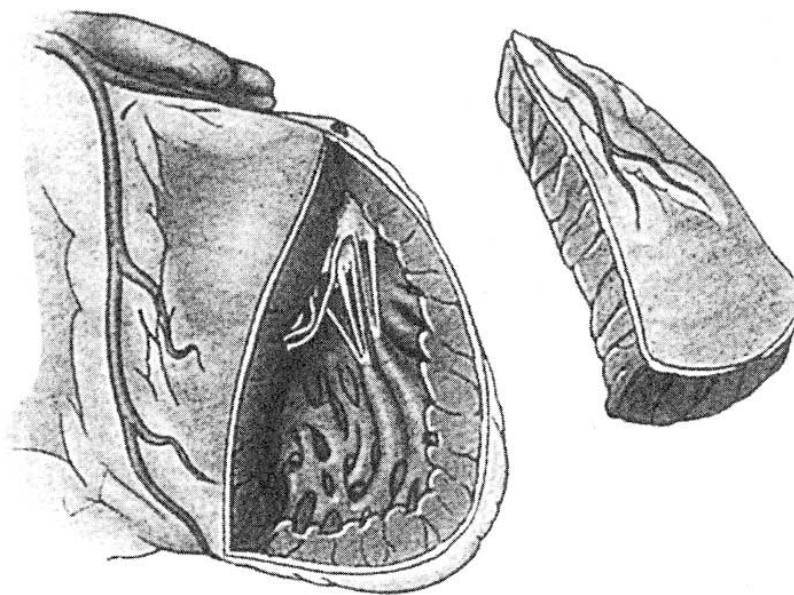


Fig. I-24: Illustration of the wedge that is excised from the left ventricle in the Batista procedure ^[32]. The exposed edges of the ventricle will be sewn together to yield a 'remodeled' ventricle.

Batista developed this technique because he lacked the technology that was available in Europe and North America to perform other treatments. After initial experiments in sheep, he first applied the technique in humans in 1994. The

controversial technique was soon adopted by other heart failure centers, although many cardiologists and surgeons were skeptical about the initial results. The heart failure population in Brazil did not have access to good pharmacological treatment, and therefore patients in an early stage of the disease were selected for the procedure, which benefited the outcome.

The original procedure prescribed to remove a wedge shaped piece of the left ventricular wall of about 100 g. After closure, the remodeled ventricle would also result in repositioning of the papillary muscles and therefore promote the mitral valve function. It is still a controversial operation nowadays which has evolved to a number of modified procedures (e.g., the Dor procedure, where mainly scar tissue is removed). The one-year survival has been reported to be 60 to 80%^[32] and more careful patient selection may improve this outcome. The remaining cardiac function should be an important factor when the procedure is contemplated: if terminal damage is present or when there is no contractile reserve, no benefits of this procedure can be expected. Some surgical centers prefer to apply this procedure only on transplant candidates, so a transplant is still possible in case the Batista procedure is ineffective. A significant number of the Batista patients also requires a cardiac assist device as a bridge to a later transplant. Consequently, the mortality resulting from this procedure can be reduced if it is only applied in hospitals that can provide transplants and assist devices as a backup.

3.2. Ventricular splinting

In a ventricular splinting procedure, the shape of the heart is changed without actually cutting into it. By permanently pushing the midlines of the posterior and anterior walls of the left ventricle towards each other with a small device, the cross section becomes bilobular, or shaped like a figure of eight (see Fig. I-25 and Fig. I-26). This changes the stress distribution in the myocardium considerably and the ventricle can roughly be approximated as two cylinders where the ratio of internal diameter to wall thickness is much more advantageous than in the original floppy dilated ventricle. Because there is no need to make incisions in the heart, it is possible to perform a ventricular splinting procedure on a beating heart without cardiopulmonary bypass (heart-lung machine), hereby seriously decreasing the peri- and postoperative risks. Two devices are currently in clinical trials: the CardioClasp and the Myosplint.

The CardioClasp (CardioEnergetics, Cincinnati, OH) basically consists of two curved pieces of polymer-coated titanium, joined with sliding cables to make an adjustable, flexible oval (see Fig. I-25). This oval is positioned around the left ventricle along the long axis and fixed with the appropriate tension to obtain the bilobular shape. The absence of blood-contacting surfaces and the fact that the tension in the device can be adjusted non-invasively are major advantages of this device. Animal experiments revealed that the device acutely changes the left ventricular shape, improves the contractility, and reduces the wall stress of failing hearts without altering ventricular pressure or cardiac output ^[33,34].

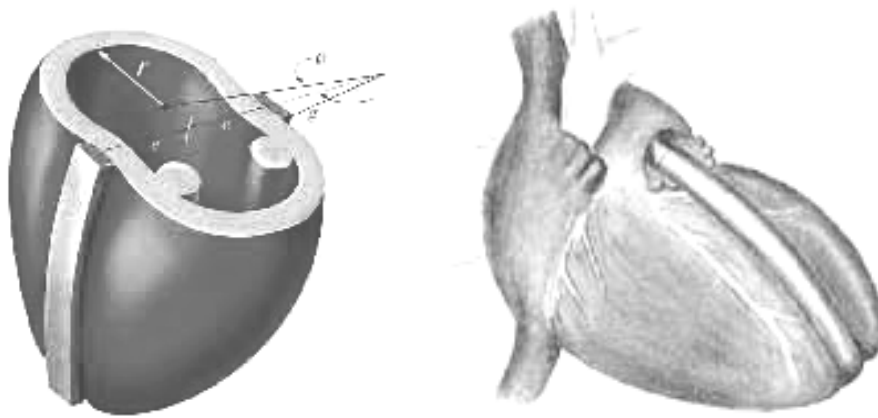


Fig. I-25: Principle and application of the CardioClasp device.

The Myosplint (MyoCor Inc., Maple Grove, MN) uses the same principle, but instead of circumventing the heart with bars, it consists of three separate splints that perforate the heart (see Fig. I-26). Each splint consists of a tension member that crosses the left ventricular cavity and the myocardium and is attached to supporting pads on the outside of the heart. A special device must be used to place the splints, but it can also be applied on a beating heart. Animal experiments showed reduced wall stress and improved systolic function while diastolic function was maintained ^[35]. Early clinical results demonstrated the safety of the device and an effective increase in ejection fraction ^[36,37].



Fig. I-26: Principle of the Myosplint device.

4. Dynamic cardiomyoplasty

In a cardiomyoplasty procedure, a skeletal muscle from the patient's own body is wrapped around a dilated heart and stimulated to contract synchronously with it. This procedure can also be performed without cardiopulmonary bypass. The muscle is usually the left latissimus dorsi, a large muscle in the back, that is dissected and rotated into the thorax cavity. A key issue in the whole concept is the training and stimulation of the muscle. Skeletal muscles normally contract intermittently and irregularly and they are subject to fatigue. By applying a proper regimen of electrical pulses, the considered muscle can be converted to a fatigue resistant muscle that keeps working continuously, although stimulation with pacemaker technology remains a requirement. Cardiomyoplasty was first used by Carpentier after years of animal experiments and now it appears that it is especially effective in patients who have mild to moderate congestive heart failure ^[32]. In those patients, it relieves the symptoms of the heart failure and it keeps the dimensions of the heart stable over a long term, thus preventing further dilation and remodeling of the heart. It is also concluded that the ventricular wall stress (and oxygen demand) are reduced as a consequence of the procedure. An alternative is the use of a mechanical device for direct mechanical compression. Several devices are available, but basically they all consist of a cup that is mounted over the whole heart and pneumatically actuated. So far, they are intended to be used acutely, as an invasive form of cardiopulmonary resuscitation (CPR). One exception is the Heart Booster (Abiomed Inc., Danvers, MA), an investigational device that is actuated with a portable fluid pump and intended for chronic support.

5. Cardiac containment

The principle of cardiomyoplasty has often been questioned, particularly the contribution to the pumping action of the heart. This is difficult to assess, but long-term echocardiographic follow up of patients clearly demonstrates that end-diastolic dimensions of the heart remain stable and that the dilatation has been halted. Kass et al. stated that the systolic contribution of the skeletal muscle is inferior to the effect during diastole, and he proposed a simple device for passive containment^[38]. A device that is focused on only supporting the end-diastolic ventricular function may be a suitable and less invasive alternative for cardiomyoplasty.

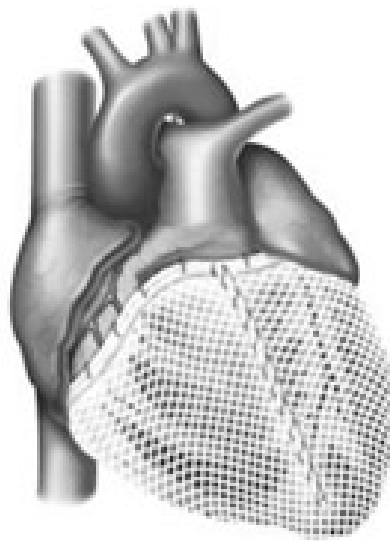


Fig. I-27: The CorCap device placed around the heart.

A device for cardiac containment is in clinical use as of 1999 under the name ‘CorCap Cardiac Support Device’ (Acorn Cardiovascular Inc., St. Paul, MN). It consists of an elastic plastic mesh or net that is slipped around both ventricles and fixed with sutures during a surgical intervention (Fig. I-27). The operation can be performed on a beating heart, but a partial sternotomy (splitting of the breastbone) may be required. The device has been tested in animals for safety and efficacy and has meanwhile been used in a few hundred patients worldwide^[39]. It was concluded that the device offers relief of the ventricular wall stress and preserves diastolic function. The net not only prevents dilatation, but it also results in improved systolic function and ejection fraction. Evidence was found that the ventricular dimensions decrease over time, which is related to a reversal

of the remodeling process and thus a healing of the diseased heart ^[40-42]. No evidence was found that the net occludes the coronaries.

6. Heart Transplant

To transplant a heart must have been the dream of many surgeons and quacks throughout history. The first successful orthotopic heart transplantation was finally performed by Christiaan Barnard in 1967 in the Groote Schuur Hospital in South-Africa (Fig. I-28). The patient only survived for 18 days. This first heart transplantation was soon followed by many others in different centers worldwide, but with an overall poor result. It was not until the availability of anti-rejection medicines (e.g., cyclosporin) in the 1980s that the procedure became an accepted standard therapy. Nowadays, 85% of the transplanted patients is still alive after one year and 71% after five years ^[22]. Today, the demand for this therapy has taken such proportions that the number of donor hearts is insufficient and people die while they are on a waiting list.



Fig. I-28: Prof. Christiaan Barnard with the first recipient of a donor heart.

Heart transplantation is still the most reliable, comfortable and durable solution for patients who have reached the end-stage of heart failure. If all other therapies are in vain, and if the function of the heart has deteriorated to the point that death is an imminent threat, then replacement of the heart should be considered. Conversely, it is required that patients who will receive a donor heart are in a suitable physical condition. Cardiac transplantation is an extremely invasive (and irreversible) procedure with a very exhausting recovery process. Patients who are

not physically fit or who have low chances of survival after the procedure will be denied the therapy in order to preserve the scarce donor hearts for patients who may have longer benefit from them. Consequently, such patients will be excluded from the transplant list, which is actually a dynamic list: depending on the evolution of their condition, patients can be signed on or drop off or change in priority status. Inclusion or exclusion is not only based on medical criteria, but also on psychological and social factors. Medical contra-indications include: severe liver, lung or kidney failure, cancer, certain infections such as tuberculosis or HIV, age, smoking habits, etc.

Patients who are accepted for heart transplantation will have to wait for a suitable donor heart. A heart will be selected on blood type and body size and patients with extreme measures therefore have little chance of quickly getting a transplant. This means that they will have to wait for a long period during which their physical condition deteriorates, along with the chance of surviving a major surgery.

Worldwide, only 3,122 cardiac transplants were performed in the year 2001, which continues the decreasing trend since 1994 (4,402 transplants reported) ^[43]. Most of the transplants in 2001 were performed in the US (2,207) where 4,096 patients were on the waiting list. The median waiting time for status 2 patients was 374 days ^[44]. As for Belgium and Luxemburg, 32 patients were on the waiting list at the end of that same year, while 80 transplants had been performed throughout 2001.

Several surgical procedures are possible for heart transplants. In most cases, part of the native heart (especially the atria) is kept in place to facilitate the connection with the new heart. There are also techniques in which the whole heart is replaced, but these require greater skill and take more time. In most cases, the operation takes about four hours, while the donor heart should be inserted within 4 to 6 hours after explantation. After the operation, the recipient needs to take anti-rejection medicine (immunosuppressants) for the rest of his life, which is 9.1 more years on average, starting with several weeks of rehabilitation ^[44].

7. Artificial heart

Before heart transplants were feasible, physicians already uttered the option of replacing a sick heart with an artificial one. The Russian Bryukhonenko already demonstrated in 1927 that it was feasible to maintain the circulation of warm-blooded animals with a device ^[45]. He developed a complex apparatus that consisted of multiple pumps, valves and tubes and was called an 'autojector'. In 1937, the first Total Artificial Heart (TAH) was implanted in a dog by the Russian team of dr. Demikhov.

The first successful mechanical support of the human circulation was performed in 1953, when Gibbon repaired an atrial septal defect and used therefore his own development: the first working heart-lung machine ^[46]. This first cardiopulmonary bypass (CPB) was maintained for 45 min. and its success led to the application of more inventions in the field of mechanical circulatory support.

In 1969, 32 years after the Russian dog experiment, dr. Denton Cooley implanted the Liotta pneumatic artificial heart (Fig. I-29) to replace a failing heart in an end-stage heart failure patient ^[47]. This is reported as the first clinical use of a total artificial heart, where the patient was supported for 64 hours before he received a donor heart.

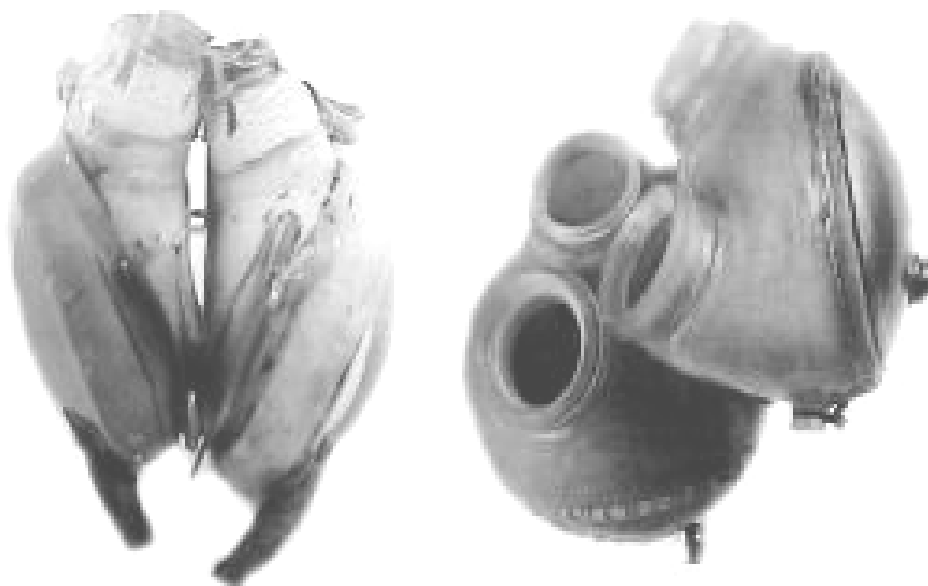


Fig. I-29: The historical Liotta (left) and Jarvik-7 (right) total artificial hearts.

After several more isolated ‘experiments’ with artificial hearts, the notorious Jarvik 7 was first implanted in December 1982. US national television turned the recipient, Barney Clark, into a movie star as they broadcasted his recovery – and subsequent death – at the University of Utah ^[48]. The Jarvik 7 was the first device that was intended to maintain the blood circulation permanently: Clark was not on the waiting list for a donor heart. He never left the hospital and died 112 days after the implantation. The device was implanted by Dr. DeVries, who treated four more patients in the following three years, one of which even survived for 620 days. The Jarvik 7 was a pneumatically actuated device developed by Robert Jarvik and Willem Kolff, the inventor of the artificial kidney. The device consists of two separate polyurethane pumping chambers that are sutured separately to the atria – after removal of the native ventricles – and are then connected to each other with Velcro. The pneumatic actuation came from a large console that tethered the patients and prevented hospital discharge. Pneumatic tubes had to be fed through the patient’s chest and increased the risk of infection.

These first trials with permanent support were very controversial since there were a lot of device-related complications: blood-clotting, valve failure, bleeding, etc. Several surgeons suggested that the device received its FDA approval for clinical trial too soon and thus trials for permanent support were cancelled. The devices were from then on solely used as a bridge to transplantation in the U.S. Parallel with the implantations by DeVries, Semb tried to discharge Jarvik 7 recipients from a hospital in Stockholm. He used a small, portable driving console, but the results were again disappointing. In 1990, the FDA even banned the further production of the Jarvik TAH because the manufacturing techniques did not meet the FDA standards ^[49].

Today, several total artificial hearts are still under investigation. They are usually very large, and even though the natural heart or part of it is taken away, pressure on the lungs is still a common problem. In most cases only the ventricles are cut away and the device is then connected with cuffs to the atria, just as with the old devices or in some heart transplant procedures. Two devices are currently in clinical use in the Western world: the CardioWest C-70 and the AbioCor.

The CardioWest device (CardioWest Technologies Inc., Tucson, AZ.) is actually an improved version of the Jarvik 7. It still consists of similar pneumatic chambers and its standard actuation is still a large, bulky console (see Fig. I-30). Five heart transplant centers in the US are allowed to implant this device in

patients who are waiting for a donor heart, and several centers in Europe can use it for the same purpose. The Heart and Diabetes Center in Bad Oeynhausen (Germany) has started trials to use the smaller pneumatic consoles of the Thoratec and Berlin Heart pneumatic ventricular assist devices on the CardioWest C-70 in order to increase the patient's mobility.

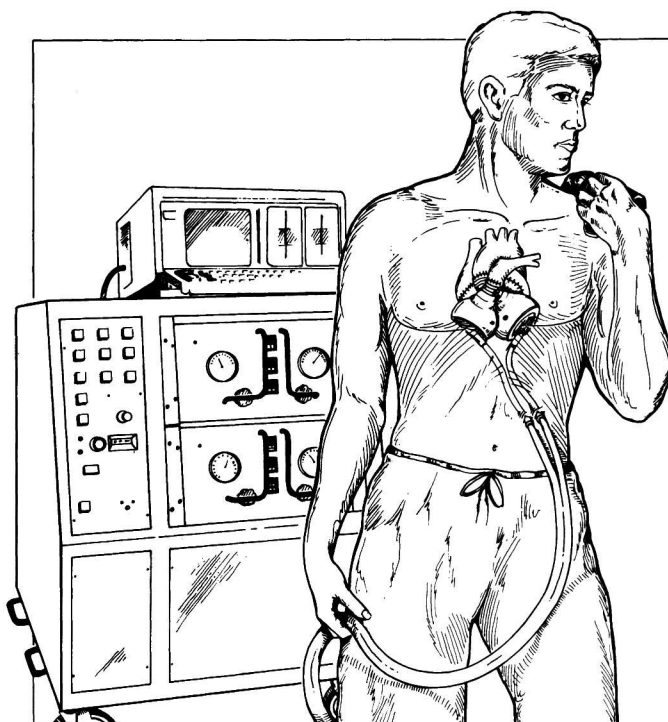


Fig. I-30: Sketch of the CardioWest TAH *in situ*, with the patient tethered to the drive console ^[50].

The more recent AbioCor (Abiomed Inc., Danvers, MA) works with a mechanical motorized system that requires electricity instead of compressed air. Consequently, a compact battery system can replace the pneumatic console, providing maximum mobility. The necessary electronics and a small battery are implanted in the body and more power is provided from larger batteries that can be worn on a belt. The energy is then transferred through the skin with a transcutaneous energy transmission system (TETS): an implanted and an external coil that work like a transformer. This means that there is absolutely no need for skin penetration for tubes or cables and that the risk of infections is drastically reduced. The use of this system even allows a patient to take off all the external components for a short time and, for example, go for a swim. The flipside of the coin is that the patient may feel more uncomfortable because of all these components that are stuffed inside the body. The cumulative size of these

components also excludes many small patients from the chance of ever receiving a system like the AbioCor. The current version of the AbioCor weighs approximately 1000 g and can only fit in the chest of a male weighing more than 90 kg. The goal of the device is to permanently replace the heart of non-transplant candidates.

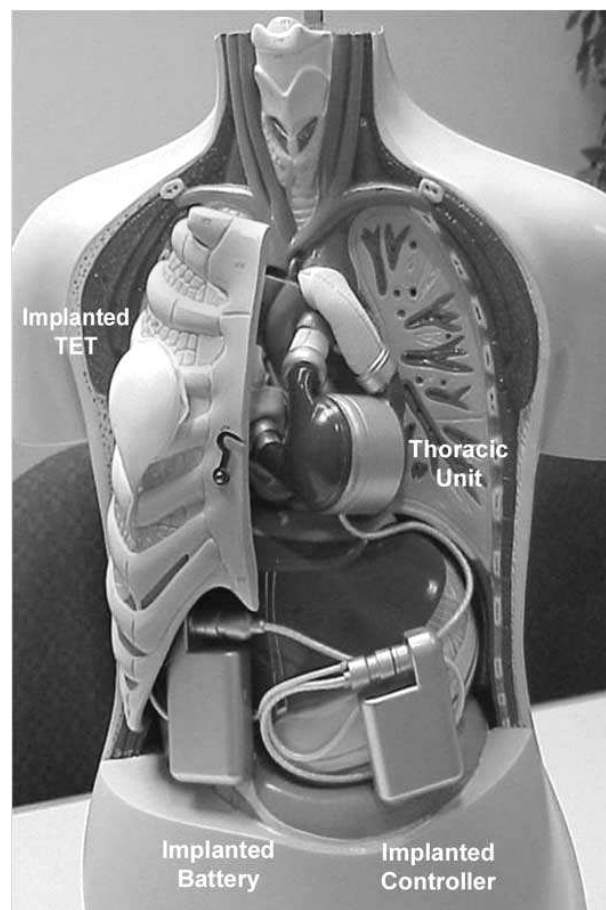


Fig. I-31: The AbioCor TAH with all the implanted components.

8. Cardiac assist

Another option for the treatment of end-stage heart failure patients is the use of a cardiac assist device (CAD). Such a device can take over the pumping function of the heart partially or fully when the heart is still in place and thus preserve its important regulatory functions (for enzymes and neurohormones, pressure, blood flow, ...). Normally, each CAD is intended to support only one ventricle and it is therefore also referred to as a ventricular assist device (VAD). Some devices allow simultaneous use of two VADs to support both ventricles and consequently there is the following nomenclature: left ventricular assist device (LVAD), right

ventricular assist device (RVAD), or bi-ventricular assist device (BVAD or BiVAD).

The clinical use of VADs started in 1961, when a simple roller pump was used by Dennis and his colleagues to support a patient in cardiogenic shock with an atrium-to-femoral artery bypass. The inflow cannula of the pump was actually inserted from the right atrium through a trans-septal puncture into the left atrium^[51]. The first implantation of a VAD that bypassed the left ventricle from the left atrium to the descending aorta was performed in 1963 by dr. Liotta et al.^[52]. A left thoracotomy was used to implant the pneumatically actuated and valved tube-like device, which supported the patient for four days. In 1966, an updated paracorporeal version of this device was used by DeBakey and resulted in the first successful use of an LVAD for post-cardiotomy recovery after 10 days of support. These successes resulted in more developments in the US under stimulation and sponsoring of the National Heart Institute. The intra-aortic balloon pump (IABP) was already invented in 1961 by Mouloupoulos, but it was not applied clinically until 1967. This device is now part of the standard treatment of end-stage heart failure patients who end up in the intensive care unit, and it is not considered a true cardiac assist device because it does not really pump blood. It does, however, support and unload the heart and it can keep patients alive while they are waiting for a donor heart.

In 1978, Golding was the first to use a rotary pump that delivers non-pulsatile flow for left ventricular assist as a bridge to transplantation, without success. The first mechanically actuated artificial left ventricle (the current Novacor) was used in 1984 to successfully support a 51-year old patient for 9 days prior to a transplantation. Soon after this event, the success of other devices followed. Of the devices that were developed in the 1970s and first used in the mid 1980s, three of them are still the most popular nowadays (Fig. I-32). They are known as the Novacor (WorldHeart, Ottawa, Canada), the HeartMate (Thoratec Corporation, Pleasanton, CA), and the Thoratec VAD (Thoratec Corporation, Pleasanton, CA). Together, they have been implanted in over 7,000 patients.

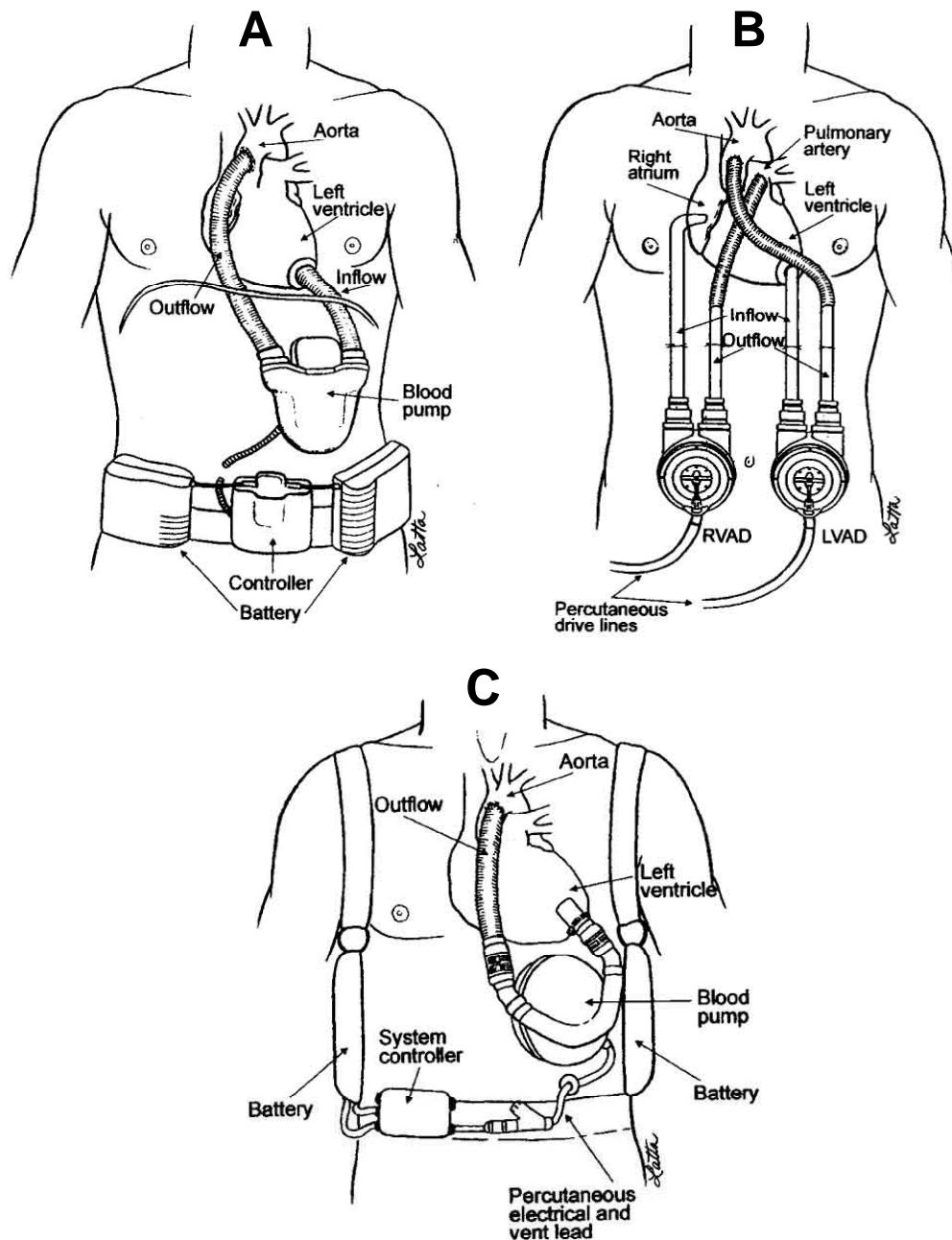


Fig. I-32: Schematic drawings of the three most used VADs: A. Novacor, B. Thoratec, C. HeartMate ^[53].

A ventricular assist device basically consists of a blood pump that is connected to a patient's native circulation with tubes called grafts or cannulas. One tube provides the inflow of blood into the pump, while the outflow tube directs blood from the pump back into the native circulatory system, preferably an artery. The device is capable of pumping blood and therefore takes over the work of the heart. There are many different pumps that function according to various engineering principles and will consequently be actuated in many different ways.

Some sort of power supply is therefore necessary, along with a controller that regulates variables such as electrical power consumption and pump output and that can communicate danger situations to the patient or surgeon via alarms.

Several options are also available for the connection to the native circulation, with similar approaches for the left and right ventricle. On the left side, for example, the inflow cannula can be fixed in the atrium, in the pulmonary veins, or in the ventricle via the atrium and mitral valve. The most popular way, however, is to excise the apex of the ventricle and insert the inflow cannula there. This provides the most direct flow path for the blood, but permanently damages the myocardium. The outflow cannula (often a flexible graft made of woven Dacron or expanded PTFE) can be sutured to the ascending or descending aorta, or in some cases even lower on the aorta. A connection with the ascending aorta provides the most natural flow path since it is closest to the aortic valve.

The main complications after the implantation of a VAD are still the same as in the early days: bleeding, infections, and thromboembolism (migrating blood clot). Hemorrhages are often the result of a high anticoagulation regime, in combination with the prolonged effects of the cardiopulmonary bypass and hypothermia applied during the implant procedure. Thromboembolism can result from an inadequate anticoagulation regime, but it is often device related: some devices provide insufficient biocompatibility of the blood-contacting surfaces, or the blood path through the device has stagnation areas as a result of incomplete ejection or kinked cannulas. Most VADs still require a median sternotomy for implantation, which leaves a large wound, prone to infection. The long hospitalization also ties the patients to a site where much infectious diseases circulate and thus increases the chance of complications. Undoubtedly, a lot of infections at and around the heart originate from the percutaneous lines that go directly from the outside into the chest and into the heart, forming a true highway for bacteria.

In 1995, 777 patients were removed from the US heart transplant waiting list because they could not survive the long waiting time. This number was gradually brought down by the increased availability of and experience with VADs. Only 571 patients died while on that waiting list in 2002. Further experience and a more aggressive approach of early implantation are likely to bring this number down even more. Studies have already shown that the survival of transplant patients is higher if they have received a VAD before the transplantation^[54]. This

is due to the better physical condition that those patients can build up while on support, in contrast with pharmacologically treated patients who are bound to their bed in the intensive care. Moreover, there are numerous patients who are not eligible for transplantation that can benefit from a VAD. These patients are often excluded from transplant because it is not ethical to ‘spill’ a good donor heart on them if there are other patients who can benefit much more of it. Since the supply of VADs can be adjusted to the demand, within logistic and financial limits, they can be used in many more patients. Their availability also allows carefully planned operations, in contrast with the hasty organization of a transplant surgery. The devices do not only prolong life, but they also improve the quality of life, and thus they can be applied in heart failure patients with a short life expectancy, such as AIDS and cancer patients. Consequently, it is estimated that by 2010, when the devices will even be more applicable due to increased safety and reduced size, there will be about 70,000 patients annually that may benefit from the implantation of a cardiac assist device ^[55].

D. CLASSIFICATION OF VENTRICULAR ASSIST DEVICES

1. Introduction

There are literally hundreds of systems for mechanical support that are either in clinical use, in a development phase, or of which the development has been halted. It is not the intention to give an overview of all these devices. Such an overview would be no more than a snapshot of the current situation, while the world of assist devices is very dynamic. It is strongly directed by the available funding (e.g., the recent NIH grants for pediatric assist devices) and as a result multiple collaborations between companies and universities were found and dismantled, companies were acquired and device names changed more rapidly than their designs. Consequently it is not useful to give an overview of all the ventricular assist devices that once upon a time have pumped fluid through an *in vitro* setup or supported an animal for a number of hours/days/months. Detailed overviews and descriptions of currently available devices can be found in other literature ^[50,56-58].

The following synopsis of assist devices presents a classification based on the duration of support, the position of the device in relation to the patient, and the most popular pumping principles. Section E gives a more elaborate discussion of the different applications of ventricular assist devices. Detailed descriptions of the devices used in the studies reported in this dissertation will be provided in the respective chapters.

2. Duration of support

To indicate the estimated duration that a patient will require mechanical cardiac support, a rough (subjective) classification results in four groups (see below). This classification can be mirrored to the different available devices, starting from cheap, simple, and easy-to-use short-term devices to complex and long-lasting devices. The first choice for patients suffering from LOS is often a short-term device, that is easier to implant and to remove, to see whether the patient's

condition improves. If this is not the case, the device can still be replaced by a long-term alternative. In general, short-term devices limit the mobility of the patient and wear out faster or cause complications and biocompatibility issues if used too long.

The four categories of support duration are ^[59]:

Short-term: ranges from a couple of hours to a number of days

Medium-term: at least a couple of days, up to several weeks

Long-term: from several weeks to months or years. Several patients have already been supported for over three years

Permanent: Although this would seem the most obvious definition, it is rather vague. It is sometimes defined as a five year period, but it may be clearer to define it as support until the patient dies of a cause that is not related to the heart failure. The first patient that survived five years on support was reported in Februari 2003 ^[60].

3. Position of the device

Ventricular assist devices can also be classified according to the way they are connected to and positioned on or inside the patient. This brings along different levels of comfort and quality of life and it is therefore also related to the duration of the support (see Fig. I-33).

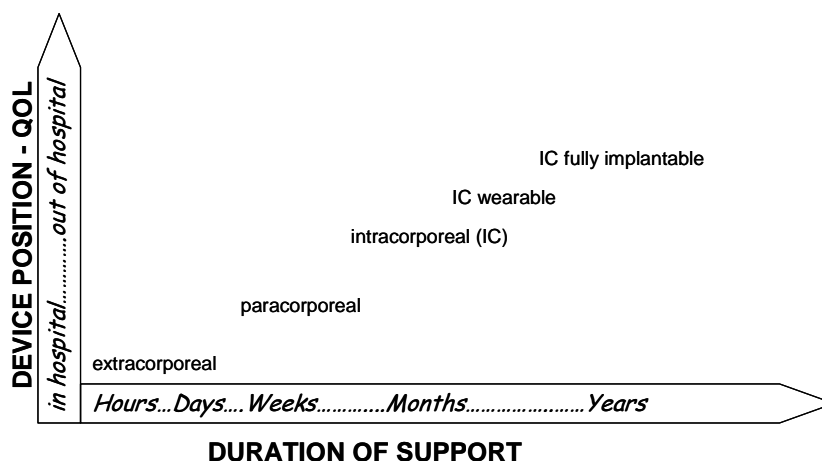


Fig. I-33: Relation between the duration of support and the position of a device with its according quality of life (QOL).

The position of the device also determines the mobility of the patient and it will depend on the adjuvant technology of the controller and power source whether the patient is allowed to get out of bed or even out of the hospital. A basic distinction can be made between VAD systems where the blood pump is inside the body of the patient (intracorporeal) or outside the body (extracorporeal). Although it may seem very uncomfortable to have a pump stuck inside your body, this approach is actually safer with respect to infections and it also allows the patient to move around more easily. An external pump is more vulnerable to mechanical impact or to temperature changes that may result in hypothermia. On the other hand, an external pump is easier to implant (only cannulas need to fit inside the body) and it allows regular inspection of the pump itself. In the extracorporeal pumps, a further distinction can be made between pumps that are away from the body, often referred to as 'bedside', and pumps that are directly on the body of the patient. The latter are called paracorporeal (example: the Thoratec VAD, see Fig. I-32, B). They have the advantage that cannulas can be made much shorter, which is mechanically safer and also prevents massive heat loss.

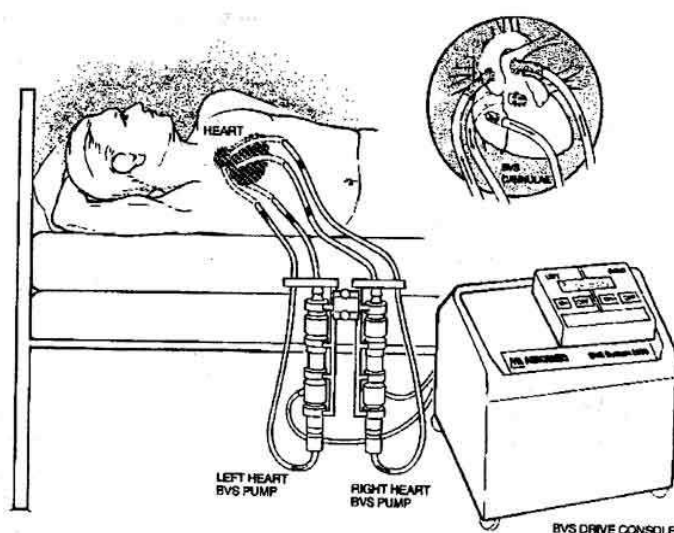


Fig. I-34: Schematic drawing of a bedside extracorporeal device: the Abiomed BVS 5000.

Most extracorporeal devices are pneumatically actuated and they were originally powered with large consoles that contained an air compressor and pressure chambers. The consoles were so large that even with the paracorporeal devices,

the patient could do no more than stumble around through the hallways of the hospital even though his physical condition was improving. Nowadays, most manufacturers provide smaller alternatives (briefcase size) that work with piston pumps and that can be carried by hand or on a small trolley. Consequently, patients with paracorporeal devices can and have been discharged from the hospital.

Intracorporeal devices can also be subdivided, in partially and fully (or totally) implantable devices. Partially implantable devices have all the hydraulic components (pump and cannulas) inside the body, but the controller and power source are still outside the body. Ventricular assist devices that are composed according to this system still require a perforation of the skin to feed through electrical lines, an air channel for compressed air, or both. This line is traditionally fed through the skin of the lower abdomen, but electrical lines can also run via the shoulder or a pedestal on the skull behind the ear. Since the pump is out of the patient's way, it is easier to manage the surgical site and these patients are routinely sent home after a recovery period in which the patient and a caregiver (partner or next of kin) learn to handle the system. An example of a partially implantable pump is the HeartMate (Fig. I-32, C). This VAD system exists in a pneumatic and an 'electric' version. The pneumatic version still requires a small console for control and supply of compressed air, and hence limits the mobility of the patient. The electric version has an external controller and two rechargeable batteries that can all be worn on a belt or holster around the shoulders. In this way, the patient has both hands free at all times and he has optimal mobility. Many other systems have adopted this approach, which can also be referred to as 'wearable' because the patient wears the system as if it were a piece of clothing.

Fully implantable systems also incorporate an electronic controller and a small implantable battery in the patient's body. They have no skin perforations, which significantly reduces the risk of infections. Because the internal battery only has limited capacity, it is continuously recharged by an external electrical power source (usually a larger rechargeable battery) through a transcutaneous energy transmission system (TETS, see C.7). Telemetry at radio frequency is normally used for adjusting the settings of the internal controller or for retrieving data that has been logged on the controller. Such a fully implantable system with an internal battery allows the patient to take off the external components for a while

(usually about 40 min.) and perform activities that are impossible for other VAD patients, such as bathing.

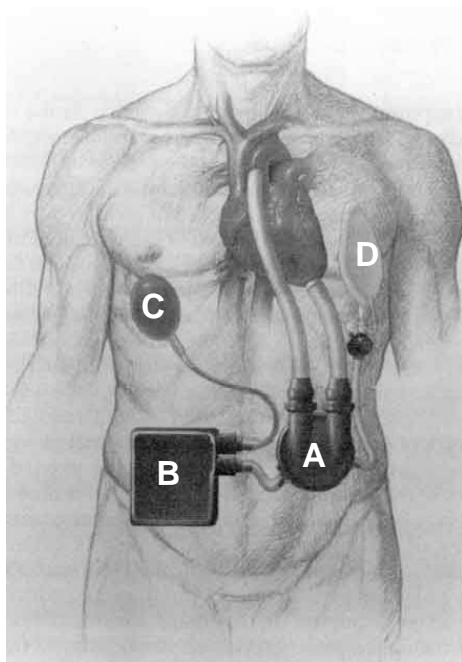


Fig. I-35: Schematic drawing of the internal components of the LionHeart fully implantable VAD (Arrow Int. Reading, PA)

- A. Blood pump
- B. Controller
- C. TETS coil
- D. Volume compensator

4. Pumping principle

When considering the pumping principle according to which the VADs generate blood flow, two major classes can be distinguished: rotary pumps and positive-displacement pumps (see Table I-1). Rotary pumps have an impeller that spins around at high speed and transfers energy to the blood by velocity changes along the impeller radius. Positive-displacement (or volumetric) pumps transfer energy to the blood by periodic dimension changes in a working space. In other words, they have a blood chamber that fills with blood during one part of the working cycle and ejects the blood during the other part, very similar to the function of the native heart. Displacement pumps thus deliver a pulsatile flow and are often referred to as ‘pulsatile pumps’, while rotary pumps traditionally deliver a constant flow and are therefore also called ‘continuous flow pumps’. There are, however, innovative designs where it is hard to tell what kind of pump it is or what kind of flow is generated. More on the difference between pulsatile and non-pulsatile flow can be found in section F.

Table I-1: Advantages and disadvantages of rotary and displacement pumps.

	DISPLACEMENT PUMPS	ROTARY PUMPS
ADVANTAGES	<ul style="list-style-type: none"> ▪ generate pulsatile flow 	<ul style="list-style-type: none"> ▪ only one moving part ▪ very compact ▪ silent ▪ highly efficient ▪ suited for mass production at low cost
DISADVANTAGES	<ul style="list-style-type: none"> ▪ require valves ▪ used membranes have a limited life-span ▪ often complex driving mechanism ▪ generally large because of the necessary dead volume ▪ not energy-efficient ▪ very expensive 	<ul style="list-style-type: none"> ▪ non-pulsatile flow ▪ difficult sealing ▪ complex physiologic control ▪ heating ▪ bearing problems: wear and thrombus formation

4.1. Rotary pumps

The impeller of rotary pumps is usually composed of a disc or cone with vanes, but there are also vaneless alternatives. The design of some main components determines the efficiency and biocompatibility of the pump. The shape and number of vanes are extremely important, as is the housing geometry and the clearance between housing and vanes. The performance and position of the motor are also determinants for biocompatibility and efficiency because the motor heat may destroy blood proteins and it therefore needs to be drained.

The rotary pumps can further be divided into radial (centrifugal), axial and diagonal rotary pumps. Centrifugal pumps have been used clinically since the late 1970s. They are characterized by their flat and wide appearance and an inflow blood path that is parallel to the rotation axis while the outflow path is orthogonal to it. Consequently, most of the centrifugal pumps have a tubular outflow connector that is tangent to the pump housing (Fig. I-36). Diagonal pumps also have an inflow parallel to the rotational axis, but the outflow is diagonal to that axis. For axial pumps, both inflow and outflow are parallel to the rotational axis. Axial pumps often also have stator vanes and flow diffuser vanes in front of and after the impeller to better guide the flow and to improve efficiency. Each design results in a different pump characteristic and, generally speaking, centrifugal pumps are more suitable to build up pressure while axial

pumps are best to generate high flows. As a result, the axial pumps used in ventricular assist devices are smaller and run at much higher rotational speeds than centrifugal pumps. Some small axial blood pumps even run at speeds of 25,000 rpm and above^[61]. In the end, all rotary pumps aim at optimal efficiency at a design point that reflects the hemodynamic needs, which is often a flow of 5 l/min at a pressure head of 100 mmHg.

Typical example of

a centrifugal pump: CorAide (Arrow Int., Reading, PA)

a diagonal pump: DeltaStream (Medos Med. GmbH, Stolberg, Germany)

an axial pump: Jarvik 2000 (Jarvik Heart Inc., New York, NY)

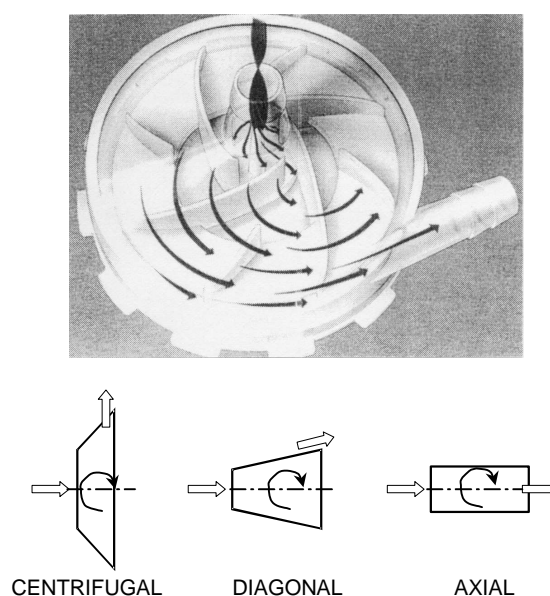


Fig. I-36: Drawing of the flow path through a centrifugal pump (top) and a sketch of the three rotary pump types (bottom).

Impeller and housing geometry and vane shapes for rotary blood pumps are nowadays mostly computer designed, where the flow path and even the pump characteristics are simulated with computational fluid dynamics. This results in highly efficient designs where the high shear stress zones and stagnation areas are limited and improved biocompatibility can be expected. Other design issues are the design of seals and bearings. In earlier rotary blood pumps the impeller was directly attached to the shaft of the electric motor and thus sealing was required to prevent blood from entering the motor. This often led to high heat generation or thromboemboli that originated from the seal: blood could not be washed away sufficiently and started clotting at the seal. Newer designs use

magnetic couplings between the motor and the impeller, so the impeller can be captured completely in the housing and a seal becomes superfluous. It is, however, necessary to support the impeller to prevent impact with the housing. The bearings used for that have the same problems as the seal: heat generation and thrombus formation. The most recent designs apply a non-contacting support of the impeller: it floats in the housing in a controlled way. This is either achieved with magnetic suspension or with a hydrodynamic bearing. Either way has the advantage that there is no longer any friction and that the blood can flow around the impeller unhindered, thus providing good washout and preventing blood clot formation. In a magnetic bearing, permanent magnets are embedded in the impeller while electro-magnets in the housing control the position and rotation of the impeller. This technology has already been applied on centrifugal and axial pumps. In a hydrodynamic bearing, the impeller is designed so it is forced to the desired (central) position by the pressure distribution between the impeller and the housing, eliminating the need for active position control. This principle has so far only been used in centrifugal pumps.

4.2. Displacement pumps

To mimic the filling and emptying function of the heart, a blood chamber with variable dimensions is necessary to collect the blood intermittently. Most displacement type blood pumps use a plastic sac as blood chamber, or a rigid shell on one side and a membrane (diaphragm) on the other. The membrane thus forms a barrier between the blood and the other pump components. These membranes are usually made out of polyurethane for its biocompatible properties and durability. Coatings are often applied on the blood contacting surfaces in order to prevent thrombus formation and to spare the patient a heavy anticoagulantia regime. Still, thrombus formation is often a problem, usually at the seams of the membranes or at grooves and microscopic cracks in other components. A sac can be formed of two halves that are glued together, or it can be seamless, but then there are still connection sites with the other blood contacting components of the pumps, such as the inflow and outflow connectors. These connectors have to contain valves to direct the blood from the heart to the pump and further to the aorta. All types of valves that are available for heart valve replacement are used in VADs. In addition, a number of new designs are used, for example polyurethane trileaflet valves that look like aortic valves but are more durable and easier to work with. Nonetheless, valves form an extra risk

in blood pumps because of the extra biocompatibility issues and because they are vulnerable and their failure has disastrous impact on pump function.

Apart from space for the ‘end-diastolic’ blood volume, the housing of a displacement pump also needs to incorporate the actuation mechanism. This ‘dead volume’ results in relatively large pumps (with the exception of pneumatic actuated ones). An actuator is necessary to compress the sac or push the membrane towards the housing and thus achieve a powerful ejection. Several mechanisms have been invented to actuate displacement type blood pumps and they will be briefly summarized below, based on the energy conversion that they apply.

4.2.1. Pneumatic actuation

Pneumatic actuation is the simplest mechanism: the sac or membrane is compressed by pressurized air during ejection. The air will flow back out of the pump during the filling phase, where a slight vacuum can be applied to improve pump filling and unloading of the native heart. Since this actuation mechanism requires a compressor of some sort, the true actuator is always outside the body on a console and connected to the pump with tubes. The advantage is that the pump can be smaller since it only needs the size of the maximum stroke volume. The disadvantage is that it limits the mobility of the patient and it cannot be implemented in a fully implantable version. Membranes also have the tendency to leak over time: as a result of diffusion, fluid from the blood will enter the actuator side of the membrane. Air, on the other hand, will also diffuse to the blood side and the use of pressurized air will promote this process.

Typical example: Thoratec VAD (Thoratec Corp., Pleasanton, CA), see Fig. I-32

4.2.2. Electromechanical actuation

This type of actuation mechanism is usually built around a (brushless) DC motor. The rotational movement of the motor is mechanically transformed into a linear movement that actuates a pusher plate (a plate that pushes on the sac or membrane). Gear systems, nut and screw combinations and other kinds of mechanical conversion systems are used to achieve the pusher plate motion. The required power form is electricity, which allows to incorporate such pumps in fully implantable systems, or as a wearable device with small portable batteries.

Typical example: HeartMate VE (Thoratec Corp., Pleasanton, CA) see Fig. I-32

4.2.3. Electromagnetic actuation

There are two types of electromagnetic actuators. The first type uses magnetic fields to move mechanical components. This can be a pusher plate or even a valved tube. In the second type, electromagnetic fields are used to create a pressure in a ferrofluid. Ferrofluids consist of a fluid (e.g., kerosene) in which magnetic particles are suspended. Such a fluid can be moved by a magnetic field. The power form for inducing magnetic fields is also electricity and consequently the same advantages as for the previous type can be assumed. Moreover, this type of actuation has fewer moving parts and is therefore less prone to friction and heating problems.

Typical example: (first type) Novacor (WorldHeart, Ottawa, Canada) see Fig. I-32

4.2.4. Indirect electro-hydraulic actuation

Instead of using gas (air) as a fluidum to compress a sac or membrane, also liquids can be used. Indirect electro-hydraulic actuators use oil because of its lubricating properties and its lower density. In contrast with pneumatic actuation, these devices do not make use of an external compressor, but they have an internal hydraulic pump (actuated itself with an electric motor) and also an internal oil reservoir. To achieve ejection, the pump moves fluid from the reservoir towards the sac or diaphragm, which is consequently pressurized and compressed. For filling of the pump, fluid is pumped back to the reservoir. The reservoir and fluid pump obviously make these devices relatively space consuming, but they have the advantage of electrical power supply and can be made fully implantable. This principle is in fact popular for total artificial hearts, where the fluid can be pumped from the left to the right side, thus eliminating the need for an extra reservoir.

Typical example: HeartSaver (WorldHeart, Ottawa, Canada)

4.2.5. Thermo-mechanical actuation

There were two systems under development where heat was converted into mechanical forces. The two systems were both based on a Stirling engine. The energy was stored in form of electrically heated salt, which was encapsulated in highly isolated containers. The development of these systems was stopped due to unsolvable problems concerning efficiency and durability of the materials. These

programs were started with the intention of using nuclear power sources for VADs in the future, and initial experiments were even performed by dr. Kolff in the 1960s. It is however doubtful that the public will ever accept the implantation of plutonium capsules as an energy source. The US government even prohibited further development of this technique that may be used in terrorist actions.

Typical example: n/a

4.2.6. Biological-mechanical actuation

There have been experiments with skeletal muscles as Cardiac Assist Devices ever since 1931. There are two types: hybrid devices (pumps that use a muscle as actuator) and strictly biological pumps.

A biological pump is different from dynamic cardiomyoplasty (see C.4) in that it actually uses grafts and valves to attach a blood pump to the heart. The pump itself is made of skeletal muscle that is sewn in a cup-form, lined with pericard, and electrically stimulated, similar to cardiomyoplasty. This kind of 'device' is referred to as a skeletal muscle ventricle (SMV). Most complications are related to thrombosis and rupture of the SMV. However, they have already been used in animal experiments for periods of more than two years .

The hybrid devices are actually mechanical pumps that use an electrically stimulated skeletal muscle as an actuator. These devices can again be categorized into several types: mechanical, indirect hydraulic, or even pneumatic ^[62]. Similarly to cardiomyoplasty, the latissimus dorsi is the preferred muscle. It needs to be repositioned and trained to become indefatigable. The pumps themselves are subject to the same problems as described above, but they can be made smaller than the average device because there is no motor or magnetic coil that consumes space. Their main advantage, however, would be the low power consumption: only a modified pacemaker is required for muscle stimulation, which can last years with one small battery.

Typical example: n/a

E. APPLICATION OF VENTRICULAR ASSIST DEVICES

1. Introduction

Ventricular assist devices can be used for different indications and in different situations. The end-goal of the application of the device may also differ from patient to patient, and thus the type of application will have its impact on the presumed duration of support and on the selection of the device. Possible end points of a ventricular assist treatment are recovery, transplantation, or death.

2. Post-cardiotomy failure and acute cardiogenic shock

In general, patients who are treated with a ventricular assist device for a short term period experienced one of the following indications: acute myocardial infarction, acute cardiomyopathy due to myocarditis, or cardiac failure after reparative open heart surgery (post-cardiotomy failure).

About 1.5% percent of the patients who undergo cardiac surgery in the US cannot be weaned from the heart-lung machine and require prolonged mechanical circulatory assist ^[30]. The fact that they get the VAD ‘unplanned’ after a traumatizing operation, may decrease their chances of a good outcome. Apparently, only 20 to 40% of post-cardiotomy VAD patients survives. Many complications usually appear, but they are rarely device-related. The low outcome is mainly related to the age of those patients and their condition before the initial surgery. Bleeding is the most common complication in post-cardiotomy supported patients because a lot of them are on centrifugal pump support and require an intense anti-coagulation regime. The basic goal of this treatment is to unload the heart and give it a period of ‘rest’ so it can gradually become fit enough to maintain a stable hemodynamic state. The patient can then be weaned from the device, which is subsequently removed. The average time to recover from a post-cardiotomy failure is 2 days ^[63], but several patients do not recover and are enlisted as a transplant candidate, after which the initial short-term device is usually replaced with a medium- or long-term version.

Post-myocardial infarction is the implant indication in 10% of all VAD patients. Myocardial infarction is a major cause of death, mainly in people above age 65, and the survivors are not a popular target group for cardiac assist because they show a high incidence of co-morbidities. However, the post-myocardial infarction patients who are treated with a VAD have a high survival rate: 74% is bridged to transplant or recovery^[30].

Acute cardiomyopathy, usually resulting from myocarditis, is the indication for implantation of a VAD in 15% of the VAD patients.

3. Bridge to transplantation

Although mechanical support may once become the preferred method to treat heart failure patients, so far the majority of physicians is convinced that a cardiac transplant is still the ultimate option. The key issue in transplantation is the availability of donor organs. They are scarce and their timing of presentation and size and type are dependent on chance. Therefore, ventricular assist devices are most often applied as an in between treatment to prevent the death of critically ill patients while they are on the transplant waiting list. In this sense, the devices are used as a 'bridge to transplantation' (BTT).

About 15% of the transplant candidates in the US requires VAD support to keep them alive until a donor heart becomes available. A result of the increasing experience with BTT is that the number of patients who died while on the waiting list has decreased over the recent years, but the disadvantage is that more candidates remain for the few available donor hearts. The VAD patients who are effectively bridged and receive a transplant (60 to 70%) have a better outcome than the traditional transplant candidate because they rehabilitated during the support period, making them physically fit and preventing - or possibly reversing - deterioration of lungs, liver, and kidney.

The duration of support with assist devices is still limited to a few months or (exceptionally) years and this is far less appealing than an average survival of 9.1 years with a human donor heart^[44]. The limitation for the assist devices is partially due to the durability of the device, but also to the many associated complications (bleeding, infections, and thrombosis) that form an imminent risk throughout the support period. The currently used devices are also relatively difficult in management: percutaneous lines and their exit wounds need taking

care of, batteries need to be replaced, backup systems must be checked regularly,.... This in contrast with transplant patients who only need pharmacological management. A bridge to transplant can only be applied in patients eligible for cardiac transplantation, which already excludes a high number of heart failure patients.

Even though BTT is not the definite solution for end-stage heart failure patients, its application results in the longest survival time of patients who are effectively transplanted. It is therefore together with post-cardiotomy support currently the major field of application of VADs. It is, however, clear that BTT does not eliminate the shortage of donor hearts and that a valuable alternative for transplantation is necessary.

The limited experience with ventricular assist systems in Belgium is only gained in the above-mentioned applications: treatment of acute failure and bridge to transplantation. Over the years 1999 and 2000, 73 patients received mechanical support, of which 31 received it as a BTT. The survival for that group was 64%, while in the acute failure group only 31% survived. Only displacement type pumps were used in the BTT group: the pneumatic Medos VAD and Thoratec VAD for medium-term support, and the electric HeartMate and Novacor for long-term support. For acute support, apart from extra-corporeal membrane oxygenation (ECMO) systems, both pneumatic displacement pumps and rotary pumps were used.

4. Permanent cardiac assist

To be a true alternative for cardiac transplantation and to form a complete treatment, an assist device should be used permanently, i.e., until the patient dies, without ever having the intention to transplant him. This application of VADs is therefore also referred to as 'destination therapy', because it is the final treatment for the heart failure. Ultimately, the device will last 'a lifetime' and the patients will eventually die of non-device or non-cardiac related causes.

This type of treatment would be a hope for the many patients who are now excluded from transplantation as a result of cancers, incurable infections, severe diabetes or non-cardiac organ dysfunction. Moreover, if VAD technology can result in higher longevity and safer use with fewer complications, it may become the standard treatment for any heart failure patient and transplants may be

preserved only for special strictly defined cases. This is however not to be expected in the near future, but in the US alone it would lead to the salvation of an estimated 50,000 to 100,000 patients ^[30].

5. Bridge to recovery

It was first reported in 1994 that a transplant candidate developed improved heart function by the use of a long-term VAD and it was uttered that healing and subsequent device explantation were future options ^[64]. Before, it was generally accepted that end-stage heart failure, and particularly dilated cardiomyopathy, was irreversible. Consequently, treatment was focusing more on halting the dilation rather than reversing it. The early reports of explantation of a device without implanting a donor heart were very controversial: had the heart really healed and had it sufficiently healed to prevent recurrence of the disease? Nowadays, explantation of devices for chronic support is more accepted, not in the least due to the extensive experience of the Berlin Heart Center ^[65,66]. Dr. Hetzer from Berlin reported in 2001 the explantation of VADs from 28 patients who were originally intended as a bridge to transplant, which adds up to 29% of their BTT population. Nine of those recovered patients showed recurring heart failure and needed a transplant later on, but the 19 others showed a stable recovery by keeping them on pharmacological support. Their longest recovery at that time was already 5.5 years. One of the conclusions drawn from their experience was that there is a large variation in the necessary support time to achieve satisfactory recovery: from 30 days to 794 days. According to their findings, this is related to the age of the patient and the duration of heart failure prior to the implantation. Young patients who only suffered from heart failure for a short period have the shortest recovery time. This recovery time is then also a good predictor for the stability of the recovery: the sooner recovery is achieved the longer it will stay. These findings suggest that, to become an effective therapy, assist devices need to be implanted sooner, when the heart has just started to deteriorate and the patient is not yet a transplant candidate.

The routine use of ventricular assist devices as a bridge to recovery would have a major impact on the health care industry and on the quality of life of the patients. At present, only BTT patients are considered for explantation once it has been determined that their heart has regained function. This results in only about 5% of the BTT patients who currently benefit from this new ‘therapy’, mainly

because only a few specialized centers are screening for possible recovery. More experience and insight in this application would result in a drastic decrease of the demand for donor hearts, and a large number of patients who are really cured as they are discharged from the hospital.

However, the question still remains how recovery can be predicted, promoted, and assessed. Prediction is difficult because little is known about the patient group that has the capacity to recover, except that up to now most of the recovered patients suffered from idiopathic cardiomyopathy. To assess the function of the heart and to determine whether it is recovering, several approaches are in use. The easiest and most popular way is to use serial echocardiography, whether or not combined with exercise tests. Most recovered patients had a displacement type pump, of which the pump rate was incrementally decreased during the echo protocol. If ventricular function stays stable and certain thresholds are obtained when the pump rate is lowered (e.g., ejection fraction $> 40\%$ and end-diastolic LV diameter < 55 mm), then the pump is finally switched off. This can only be performed for a short period and after administration of heparine to prevent clotting in the pump. If the ventricle also shows a hemodynamically stable condition in this final phase, then cardiac recovery is assumed and the pump will be explanted. There is however need for a weaning period before the explantation, so the heart can gradually get used to the higher load that it will endure once it has to maintain the circulation on its own. The most obvious way to wean a patient with the currently available devices is to gradually decrease the pump rate over a longer time period. It is, however, not possible to go down to extreme low pump rates over a long period because of the risk of clotting, while long term anti-coagulantia to prevent this would increase the risk of bleeding. The VAD team of the Berlin Heart Center for instance, therefore decreases the pump rate from 80 beats per minute (BPM) to 50 BPM over a 4-week period and then performs the explantation.

Better insight in the process of remodeling may also reveal how to initiate recovery (where implant timing may be a key issue) and how to promote it in an efficient way. It is now known that recovery is not only apparent as a mechanical improvement, but also neurohormonal and electrophysiological improvement of the heart has been observed. As a consequence, biochemical markers such as anti- $\beta 1$ auto-antibodies and brain natriuretic peptide have been proposed for prediction and functional assessment because they are present in high quantities

in heart failure patients and their concentration decreases in patients who recover by LVAD use ^[67,68]. No marker has so far been generally accepted, but it also brings along the question whether promotion of the recovery should be sought in the mechanical or the biochemical field, or both. Barbone et al. have partially answered that question by demonstrating that mechanical unloading of the myocardium is a key factor in reversed remodeling, and that reduction of wall stress is necessary ^[69]. This however, does not clarify whether biochemical changes are a consequence of the mechanical changes or whether they also play an active role in recovery and reorganization of myocytes. Even if mechanical load would be the only factor to consider, then it still needs to be determined whether it is best to relieve the myocardium of all of its stress or whether it is necessary to keep it under a certain amount of stress to prevent the muscle from becoming 'lazy' or atrophic. Or more generally: over what time period and in what quantity is unloading required, i.e., is there an optimal unloading protocol?

The studies presented in this thesis contribute to the research that will eventually find an answer to this question. Related to this, it also needs to be determined what type device is best for recovery, and the findings may have an impact on new designs for VAD systems. It may well be necessary to have devices that allow to accurately set the amount of unloading, to apply a protocol for promotion of recovery as well as for weaning from the device.

6. Other applications

If a ventricular assist device is not used to cure a patient, to keep him alive until his final breath or to keep him alive until he can be transplanted, then it can still be used to keep a patient alive until another event. It was mentioned before that part of the patients who get an assist device for post-cardiotomy heart failure is eventually enlisted on the transplant waiting list because they do not seem to recover. The initially implanted device is usually only intended for short-term support, and thus needs to be replaced with a device that can be used for a longer period. In that case, the original device was actually a bridge to a bridge to transplantation. This 'bridge to bridge' (BTB) is sometimes also performed deliberately, for example if a transplant candidate suffers from acute heart failure he can first be stabilized with a little invasive (and less traumatic) short-term assist device such as the Impella Recover (Impella Cardiotechnik AG, Aachen, Germany) before he gets a long-term device.

Another ‘bridge to ...’ application will likely become more popular with the current development of new pediatric ventricular assist devices: a bridge to corrective surgery. Congenital heart disease is often very complex and may involve several re-operations. New technology specifically aims at those patients and will allow corrective steps after which the heart does not necessarily need to be completely functional.

VADs have also been used as a bridge to the Batista procedure, where this procedure was an alternative to transplantation^[70]. It was elected for young adult patients who may survive for a longer period with Batista than with a transplant.

Finally, VADs have also been used experimentally in combination with adjuvant therapies such as stem cell injection or gene therapy to heal the diseased myocardium.

F. PHYSIOLOGICAL IMPACT OF CONTINUOUS AND PULSATILE BLOOD FLOW

1. Introduction

Pulsatility in the human body and its significance for survival was already studied in ancient Greece by Aristotle and Hippocrates. In the 17th century it was William Harvey who performed experiments to confirm the link between pulse and the blood circulation and he published his findings in his book "Exercitatio Anatomica de Motu Cordis et Sanguinis in Animalibus" (anatomical experiments on the motion of heart and blood in animals, 1628, see Fig. I-37). One century later, Stephen Hales succeeded in quantifying the pulse pressure in his famous experiment with the tied down mare and the glass manometer (Fig. I-38).

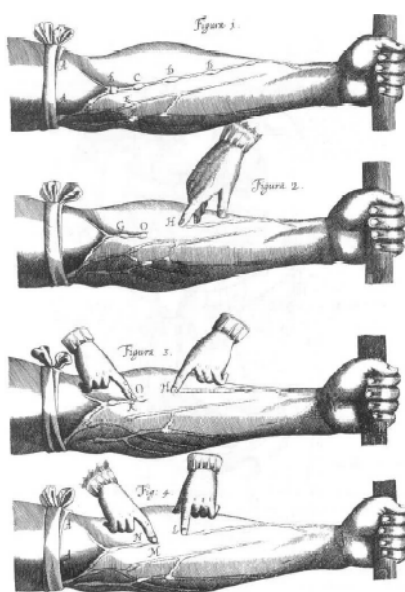


Fig. I-37: Drawing by William Harvey to illustrate palpation of pulse.

When the first cardiac assist or replacement devices were developed in the early 1960s, it was generally believed that these devices should provide flow and pressure that mimic normal physiological patterns. After the development of the first clinical rotary blood pump by Perry Blackshear, however, the issue of non-pulsatile cardiac assist became more imminent. The centrifugal pump soon became popular in CPB circuits due to its air purging capability and small size,

which would also help to overcome some of the common problems seen with cardiac assist devices. Nowadays, several rotary blood pumps are clinically available for non-pulsatile cardiac assist and many more are under development. Several new studies have been performed to assess the feasibility of long-term non-pulsatile assist or, on the contrary, as an attempt to demonstrate the superiority of pulsatile assist.

Both pulsatile and continuous flow are used in the studies discussed in this dissertation. However, the focus in these studies is mainly on the heart, which is in contrast with the many (often contradictory) studies that compared organ perfusion and related physiologic effects under pulsatile and non-pulsatile flow. As an illustration, the following section will discuss the advantages and disadvantages of the two types of flow on the perfusion of organs during long-term cardiac assist. More detailed information can be found in a recent publication by Thalmann et al. [71].



Fig. I-38: Depiction of Hales' blood pressure experiment that was published in 1733.

2. Reasons of controversy

Many studies comparing pulsatile and non-pulsatile assist have led to the conclusion that pulsatile flow and pressure patterns provide better perfusion and oxygenation of end organs. However, there are as many studies that report no

difference^[72]. An explanation for this discrepancy is that most studies investigate different parameters or give other definitions to pulsatility, and that many studies were performed without the current experience in managing rotary blood pumps.

The duration of support may be an important parameter affecting the outcome of studies. Many comparative studies focused on the effects of pulsatility during CPB or over short-term support periods, while current and future application of non-pulsatile cardiac assist devices will concentrate on long-term support. It has been reported in long-term studies^[73-76] that important changes occur in the body over time as it tries to adapt to non-pulsatile circulatory support, and thus a clear distinction must be made between acute and chronic effects.

The inflow cannulation used for the cardiac assist (atrial vs. ventricular) may also lead to different results. Also outflow cannulation is important: directing the pump outflow to the ascending aorta results in a completely different flow distribution than directing it to the descending aorta^[77,78]. In the former case, a better perfusion of the upper limbs and head is obtained.

The use of different animal species in experiments also leads to diverse conclusions, just as a mixture of healthy animals and many different heart failure models may cause confusion. Finally, one of the major problems in comparing different studies about the impact of pulsatility is the fact that different pumps with different control algorithms are used and therefore different perfusion patterns are present^[79].

Consequently there is a need for carefully defining and characterizing pulsatile and non-pulsatile assist. The problem is especially distinct in the former assist type, where apart from amplitude, frequency and waveform of the pulse, triggering is also an important determinant. The use of synchronous vs. asynchronous assist and the phase shift with the cardiac ECG will evidently influence the outcome of comparative studies with non-pulsatile assist.

One way of better characterizing the perfusion pattern that results from the cardiac assist device and the heart is to quantify the energy that it contains. Especially because the main advantage of pulsatility is not in the pressure itself but in the higher energy transfer. One suitable parameter is the so-called energy equivalent pressure (EEP), which was defined by Shepard^[80] as:

$$EEP = \frac{\int p(t) \cdot Q(t) dt}{\int Q(t) dt} \quad [\text{Eq. I-8}]$$

with:

$p(t)$: time-varying aortic pressure (mmHg)

$Q(t)$: time-varying aortic flow (l/min)

When no pulse is present, the EEP is equal to the mean arterial pressure (MAP), but pulsatility can cause a big disparity between these two parameters, depending on the morphology of the waveform. One of the requirements for the calculation of this parameter is the acquisition of instantaneous aortic pressure and flow, which is often omitted in experiments assessing the impact of pulsatility because they usually only concentrate on local perfusion of certain organs.

3. Insights from animal studies

3.1. Effect on pressure regulation

To grasp the impact of pulsatility on blood pressure regulation, it is necessary to understand the vascular and cardiac pathways for negative feedback as explained in section A.9.

If non-pulsatile cardiac assist is applied in a patient with a weak heart, then a low arterial pulse pressure may appear. It has already been reported that these patients are actually ‘pulseless’^[81,82]. The baroreceptors in the aortic arch and carotid sinus will recognize this unphysiological situation and react as if it were hypotension. Sympathetic activity will be increased by the vasomotor center, resulting in vasoconstriction and a pressure rise that actually causes hypertension.

Vasoconstriction and the resulting pressure rise have two major consequences: the peripheral circulation becomes less effective and the workload of the left ventricle is increased. Several studies have demonstrated a pressure rise, while others notice no pressure difference between pulsatile and non-pulsatile assist^[83]. A recent chronic goat study that investigated vasoconstrictive function and the baroreflex during pulsatile and non-pulsatile support could not find any difference between the two flow types^[84], while previous acute studies had demonstrated decreased constrictive function under non-pulsatile support^[85,86].

3.2. Effect on the heart and circulation

During cardiac assist, there is no significant difference between the mean arterial pressure and the cardiac output of pulsatile and non-pulsatile devices, due to the applied manual and automatic control. This is however not easy to realize because MAP and CO are linked by the peripheral resistance. There is of course a difference between the pulse pressures: non-pulsatile assist can result in a very small and undetectable pulse pressure^[82], but it can also create a pulse pressure that is approximately half of the physiological pulse pressure, depending on the residual cardiac function^[83]. Reduced pulse pressure can lead in the long run to structural changes of the aortic wall: a significantly thinner wall and higher proportion of elastin was found in chronic goat experiments^[87]. These changes did not lead to a functional change with respect to elasticity or vascular tone, while vascular contractility was significantly diminished^[88]. Other parameters such as left ventricular end-diastolic pressure, coronary artery flow, and epicardial and endocardial tissue blood flow are apparently not influenced by the type of assist.

In the limbs of a healthy person, a pumping effect similar to peristaltic compression is present: the pulses in the arteries push the blood forward in the nearby veins. Consequently, the application of a continuous non-pulsatile flow decreases venous flow. Lymph flow, which mainly depends on this 'pulse pump' may be seriously decreased as a result of chronic non-pulsatile support. It has already been demonstrated in acute animal experiments that the lymph flow is almost nil during non-pulsatile pumping^[89,90].

Another effect of chronic non-pulsatile support is the unbalance between systemic and pulmonary flow, or between left and right cardiac output^[76]. While in normal physiology the left heart output is about 1% higher than the right output as a result of bronchial and coronary flow shunting^[91], this becomes 10 to 16% in the presence of a pulsatile cardiac assist device. Non-pulsatile assist would even result in a 30% unbalance, due to increased shunting at bronchial level.

3.3. Effect on the brain

Little reliable details are known about the effect of pulsatile and non-pulsatile cardiac assist on the cerebral blood flow. Many studies demonstrated detrimental effects of non-pulsatile support on cerebral perfusion and autoregulation, but

these were all the effect of acute support (CPB) ^[92-95]. As many other studies on non-pulsatile CPB found no significant influence on cerebral metabolism ^[71,96,97]. A recent chronic goat study demonstrated that there was no significant impact on the cerebral metabolism after four weeks of non-pulsatile support, which was evidenced by a significantly lower pulse pressure ^[98]. The assessed metabolic parameters were related to the oxygen consumption and lactate and glucose differences between arterial and venous jugular blood.

3.4. Effect on kidney function

The kidneys have a very important physiological function. They do not only filtrate the blood and regulate the fluid volume in the body, but they also secrete hormones for the pressure (e.g., angiotensin converting enzyme, ACE) and hematocrit regulation (e.g., erythropoietin, EPO). Several studies have been performed on the effect of pulsatility on renal function, but there still is controversy. Some experiments show that non-pulsatile assist results in a significantly lower renal microcirculation than pulsatile assist at equal mean pressures ^[99]. Especially the perfusion of the cortex is impaired by nonpulsatile assist, while pulsatile assist imposes a redistribution of the blood flow in favor of the cortex when it tries to restore a normal physiological condition. This redistribution only appears when the renal arterial pressure is kept above 70 mmHg ^[99,100]. Impaired cortical flow can eventually result in hypertrophy of the smooth muscle cells of the renal arteries in that area ^[101], but this effect is mainly observed when low pump flows are applied. Other negative indications for non-pulsatile flow are decreased renin and sodium secretion and diminished urine output ^[90]. There can also be a pathological change of the kidneys: deformation of the arteries, expansion of Bowman's capsules and proximal tubuli,... Renal sympathetic nerve activity is apparently also influenced by the type of assist. By analyzing the frequency of action potentials, an increase in this activity was found with the use of non-pulsatile assist ^[102]. This increased sympathetic activity resulted in an increased peripheral resistance, which in turn impaired the microcirculation. In conclusion, there is overwhelming evidence that renal function is better preserved when pulsatile assist is used, and that this type of assist is the best means to restore deteriorated renal function after cardiogenic shock. There are, however, also studies that lead to the conclusion that non-pulsatile assist has no different effect on the kidneys than pulsatile assist ^[73,103,104].

3.5. Effect on splanchnic function

In case of multiple organ failure, the liver is often the most affected organ. The regional blood flows in the liver and in the mucosa of the stomach decrease significantly as a consequence of severe heart failure. By using pulsatile cardiac assist, these regional flows return to their normal values after approximately two hours, while under non-pulsatile assist these flows will only partially recover ^[95].

A question that arises for the perfusion of all major organs is to what extent the aortic flow and pressure patterns still exist at the level of the end organs. These patterns are deformed by the inertance, resistance, and compliance of the intermediate vasculature. This is especially important for the liver, since three quarters of the hepatic perfusion is maintained by the portal vein. This blood supply is collected from the veins of the intestines and is thus an indirect blood supply that already passed the microcirculation of another organ. If flow patterns are abnormal in the aorta, they will further be distorted in the intestines, and consequently the liver is very susceptible to unphysiological support. Gastric mucosal tissue is very sensitive to ischemic incidences and therefore the pH of the stomach decreases in patients with a failing heart. The use of an assist device and the associated normalization of total blood flow will augment the pH value again, but it will not recover to a normal level, nor under pulsatile nor under non-pulsatile assist.

3.6. Transition period and ideoperipheral pulsation

Since 1977, Yukihiro Nosé claims that the negative effects caused by non-pulsatile assist are only temporary and caused by adaptation phenomena ^[73]. In 1983, Leonard Golding and colleagues determined that there would be no physiological differences (arterial pressure, neural activity, urine output, end organ perfusion) between pulsatile and non-pulsatile assisted patients if the pump output of a non-pulsatile system is set 20% higher than the output of a pulsatile system ^[105]. After maintaining this higher flow for six weeks, it could be lowered to the normal range while normal body function will be preserved. Similar experiments were later performed by Taenaka et al. in an improved setting and they found no differences in hemodynamics, blood catecholamines or oxygen consumption between pulsatile and non-pulsatile support with identical flow levels ^[106].

Nonetheless, the early experiments of Golding et al. showed that, after a transition period, the circulatory system starts to generate its own pulsatility at the low rate of 40 beats per minute by varying the peripheral resistance. The pulse pressure that is initially generated is very low, but it increases with time and it reaches a value of 15 mmHg after three months of non-pulsatile pumping. This phenomenon was discovered by Dr. Tsutsui and his colleagues and was termed "ideoperipheral pulsation" ^[107]. Similar findings were reported by researchers that discovered some kind of 'auto-pulsation' generated by the circulatory system under chronic non-pulsatile assist ^[106,108,109]. This pulsation was explained by two known physiological phenomena: the Mayer wave and the Traube-Hering wave.

According to Tsutsui and Nosé, the ideoperipheral pulsation phenomenon is similar to these two waves, but it is not one of them. The fact that it only occurs after six weeks, that it generates 40 cycles per minute, and that the generated pulse pressure increases with time, suggests that it is another kind of 'auto-pulsation'. It may be an emergency backup system of the body that is activated when there is lack of natural heartbeat, as with non-pulsatile assist.

4. Clinical experience

Many studies regarding the feasibility of long-term non-pulsatile support have so far been performed in animals. The clinical experience, however is relatively limited. The effects of non-pulsatile flow on patients that have been supported for several months (with a maximum of more than two years) have recently been reported and it appears that the occurring problems are very different from the findings described above ^[110].

One of the consequences of the decreased pulsatility is more laminar flow and lower shear that can result in augmented platelet aggregation distal to already present atherosclerotic obstructions. This may eventually result in arterial occlusion. Another effect that is probably related to the altered flow is the occurrence of gastrointestinal bleeding from arterio-venous malformations as it also appears with aortic stenosis. As mentioned before, descending aortic outflow graft anastomosis causes a different (unnatural) flow pattern than ascending aortic anastomosis. In certain patients it was found that descending aorta grafting results in stasis in the aortic root, which hampers the opening of the aortic valve

and can cause occlusion of the coronary arteries. Positive clinical consequences of chronic non-pulsatile flow on end-organs is the optimization of the ratio between cardiac oxygen supply and consumption, and the maintenance or even improvement of renal and hepatic function ^[111,112]. This is in contrast with many predictions from animal experiments.

It has to be taken into account that in clinical situations, there is always some residual pulsatility due to the native heart function. In severe heart failure, the pulse pressure may be very low in the post-operative phase, but it will generally increase over time due to some degree of myocardial recovery ^[71]. Some clinical centers even select patients for non-pulsatile support in a state where there is still significant residual cardiac function, which will ensure a notable pulse pressure ^[113]. The underlying idea is to truly assist the heart rather than to take over the whole circulation. This is in contrast with many older animal studies where the heart was fibrillated to avoid pulse or any contribution of the heart ^[114,115].

Another disparity with the animal studies is the refuted idea that higher non-pulsatile flows are necessary to maintain adequate neural activity and end organ function. No extra high pump flows are used for non-pulsatile support of heart failure patients, and no adverse effects indicate that this should be the case ^[116,117].

5. Pulsatile alternatives

The most common way to provide pulsatile assist is by using positive-displacement pumps that make use of cyclic filling and emptying of a blood chamber. These devices have obvious disadvantages like size, biocompatibility issues, vulnerable valves, etc. Consequently, researchers have been investigating the feasibility of alternative methods to generate pulsatile cardiac assist.

One possible method is the use of rotary blood pumps in a pulsatile mode. This can be realized by switching between a high and a low rotational speed, or by switching off the pump intermittently. In chapter IV, it is described how the modulation of the rotational speed – i.e., superimposing a waveform on the steady rpm – results in more efficient unloading of the left ventricle. A possible problem with this kind of pulsatile alternative is the decreased efficiency and durability of the device: the current rotary blood pumps are designed to work optimally at a continuous rotational speed. Continuously varying this speed will

result in higher loads on the device components and cause a different distribution of shear stresses and stagnation and turbulence areas. Therefore, specific devices should be designed if this alternative path is to be pursued.

A different method for pulse generation with rotary blood pumps is to intermittently shift the impeller axially so it can keep rotating in the same direction and at the same speed, but generate a completely different flow path. This results in relatively low turbulence, but the two actuating systems that are required make the system more vulnerable^[118]. Alternative 'rotary blood pumps' make use of positive-displacement principles as used in the Maillard-Wankel motor or in vane pumps^[119,120].

Another way to obtain pulsatile flow is the combined use of a rotary blood pump and an intra-aortic balloon pump^[121]. The balloon pump can be triggered to the R-wave of the ECG, which can yield a pulse pressure of 40 mmHg while the rotary blood pump provides an appropriate mean flow. Although this pulse pressure is sufficient, regional blood supply to several organs is not very satisfying.

6. Conclusion

A patient who suffers from heart failure shows a deterioration in the physiological function of multiple organs. If the patient can be assisted with a cardiac assist device, this deterioration can be reversed and lead to partial or full recovery. Various studies suggest that pulsatile assist devices produce the best results when it comes to recovering and maintaining the physiological condition of various animal species. There is, however, a huge discrepancy in the many studies that have been performed on this topic. Some claim that pulsatile support provides significantly better outcome, while others demonstrate no difference and conclude that long-term assist with non-pulsatile perfusion is possible^[74,76,104,122]. At least there is agreement on one issue: no one has yet stated that non-pulsatile perfusion may be superior to pulsatile perfusion. From the limited clinical experience it can be derived that the complications arising from decreased pulsatility are limited and differ strongly from the predictions from animal studies.

CHAPTER II

In vitro Modeling of Ventricular Assist

A. INTRODUCTION

Before considering evaluation of ventricular assist devices in clinical trials, it has to be demonstrated in *in vitro* and *in vivo* tests that they are durable and that they can actually provide the required flows and pressures to sufficiently support a heart failure patient. Even though device testing and certification are beyond the scope of this dissertation, some guidelines for *in vitro* and *in vivo* testing are summarized below. These guidelines were formulated by a working group consisting of members of the American Society for Artificial Internal Organs and the American Society of Thoracic Surgeons ^[123]. The working group focused on recommendations to demonstrate the long-term reliability of mechanical circulatory support systems, but their findings are also useful for general characterization of such devices. In particular for an *in vitro* test setup that simulates the systemic circulation (a mock circulatory system or mock loop), the working group advised to consider the following variables:

- Vascular resistance
- Arterial compliance
- Venous compliance
- Left inlet or left atrial pressure
- Left outlet or aortic pressure
- Flow rates

The long-term reliability recommendations further stated that an *in vitro* setup should be able to simulate normal as well as ‘worst case’ physiological conditions. Additionally, special attention must be paid to the wear of the device and therefore it was advised to use normal saline at body temperature as a test fluid to simulate the corrosive nature of blood. The discrepancy in viscosity between blood and saline was then supposed to be eliminated by adjustments of the setup variables. For characterization of devices or interaction studies with the heart, however, there is no need to simulate corrosion or device wear.

The *in vitro* tests should allow to answer two main questions: (i) does the device produce sufficient outflow to support a patient, and (ii) does it generate appropriate pressures? Those questions are in first place important to achieve

good perfusion of the major organs and to keep the patient alive. However, with the growing interest in bridging patients to recovery, it is also interesting to find out how well the device unloads the native heart. To assess this, it is necessary to have an *in vitro* model that simulates both the heart and the blood vessels of the patient. In contrast, if the perfusion is of primary interest, then it is sufficient to simulate the ‘afterload’ that the device has to work against, i.e., the arterial circulatory system. In this setting, it is still necessary to incorporate the device as if it was filled with blood coming from the heart, but it is not mandatory to simulate the whole heart function.

In summary, each *in vitro* setup for ventricular assist studies consists of an afterload and a preload. This chapter first describes some well known afterload models, which can be lumped or distributed. Available preload models are described next, and these come in two forms: time-invariant (static) for basic characterization or time-varying (dynamic), as a simulation of heart function. Each section also describes the models fabricated at the Hydraulics Laboratory and thus presents the *in vitro* tools that were used for the studies described in chapters IV and V. More details on these models and their validation can be found in chapter V (section B).

B. AFTERLOAD MODELS

1. Characterization of afterload

The afterload of the left ventricle can be defined as the load that the heart has to eject against. Ventricular assist devices are often subjected to the same afterload (depending on the outflow cannulation site), which is formed by the systemic vascular system. The large arteries of that system have the important task to damp the pressure pulses coming from the heart (or assist device) in order to transfer a more constant pressure to the organs, which need continuous perfusion rather than intermittent. The arterioles, which have a thick muscular wall, are mainly responsible for the pressure drop and thus vascular resistance. Consequently, the main characteristics of the arterial system that need to be simulated are compliance (vessel elasticity) and resistance.

As discussed in the first chapter, the main purpose of veins besides channeling blood back to the heart, is storing blood: they can adjust the volume that they contain according to the needs of the body. They therefore act as a buffer on a low pressure level and are of lesser importance for the perfusion of the body, which mainly depends on the pressure in the arterial system. Consequently, veins are often neglected in *in vitro* tests.

To characterize the arterial system, the principle of impedance as known in electronic systems has been applied and extensively studied. The input impedance of an arterial system is defined as the ratio of time-varying pressure and flow, measured at the aortic root. As in electronics, impedance is a complex number that is calculated by decomposing the measured data in harmonic Fourier components. The impedance characteristics can then be presented in a modulus and a phase diagram as a function of the frequency, where the frequency of the first harmonic equals the heart frequency (beats per second).

Impedance matching of the native and artificial arterial systems has been performed since the 1960s. It was attempted to simulate the arterial system in as much detail as possible by breaking it up in many different components that were easy to characterize, and the preferred method was to draw the analogy with

electrical components. The functions of different branches of the arterial system are then mimicked by a combination of coils (inertance), resistors (resistance), and capacitors (compliance) of which the specific properties are known. Instead of breaking up the arterial system in distributed components, its function can also be simulated as a whole by assuming that specific properties such as compliance, resistance and inertance are not spatially distributed over the whole circulatory tree, but lumped and effective at only one site. This results in so-called ‘lumped parameter models’ as introduced in in vitro cardiovascular research by Otto Frank in 1899 ^[124]. Frank applied a model containing only two components: a compliance element and a resistor. Meanwhile it is found that at least four components are necessary to obtain impedance characteristics that sufficiently approximate the human arterial impedance: a compliance and a (peripheral) resistance component, an inertance component, and a characteristic impedance component that simulates the function of the proximal aorta ^[125].

In summary, the arterial system can be simulated with a distributed system that tries to contain as much anatomical details as possible, or it can be simulated with a lumped system that merely focuses on the main characteristics.

2. Lumped *in vitro* afterload models

2.1. Introduction

Westerhof et al. stated in 1971 that “vascular aspects, such as pressure wave travel and distributed periphery are, for studies of the heart, of no direct interest” ^[126]. This is also true for studies of ventricular assist devices, where the sole purpose of the *in vitro* setup is to create an afterload similar to the one experienced by the device *in vivo*.

The classic lumped model, consisting of a peripheral resistance in parallel with a compliance, was directly derived from Stephen Hales’ concepts elaborated in 1733. It was first routinely applied by Otto Frank, who used an air chamber (Windkessel in German) to simulate compliance, and hence all lumped arterial models are referred to as windkessel models. The concept of using trapped air proved to work well, due to the compressibility of the air, which it is not subject to fatigue as opposed to a spring system. Further advantages are the infinite supply of air and the nonlinear behavior in the same way as blood vessels: at a higher working pressure, the blood vessel will be less compliant and the air will

be less compressible. A disadvantage is that it is more sensitive to temperature changes and that a container with a relatively large diameter is required to avoid large variations in the fluid level (and the related pressure) as a result of pulsatile pumping action.

Frank's windkessel model was later (1930) extended by Broemser and Ranke who added a third (resistive) element proximal to the classic model ^[127]. They believed that this was necessary to simulate the resistance of the aortic valve, but it was Westerhof who described the real function of this element in 1968 ^[128]. This third element takes into account the high frequency properties of the proximal aorta, while the classic model is merely a bundling of the general elastic properties of the large arteries and the resistive properties of the arterioles. Hence, the classic model mainly simulates the low frequency properties of the aorta (< 4 Hz). By building a hydraulic 3-element windkessel setup (see Fig. II-1), Westerhof et al. set the trend for the following decades of mock loop studies ^[126]. Meanwhile several other, more complex models have been proposed, but it is more difficult to construct and to handle these in *in vitro* setups. Therefore complex models are mainly used in mathematical modeling.

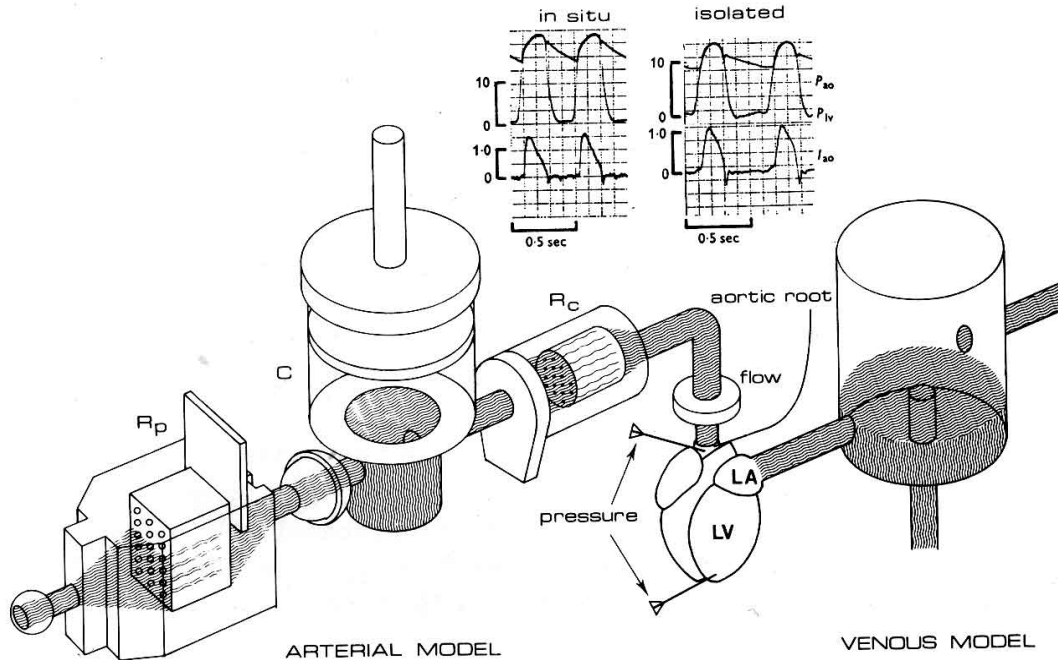


Fig. II-1: Schematic drawing of Westerhof's artificial afterload for pumping hearts.
 LV: left ventricle; LA: left atrium; R_c : characteristic resistance; C : compliance;
 R_p : peripheral resistance ^[4].

Westerhof's experiences were applied by others to design mock circulatory systems specifically for studies with ventricular assist devices. One of the first controllable mock loops was designed by Donovan for total artificial heart testing [129]. It was relatively compact and made of a transparent acrylic box (203 x 406 x 609 mm) subdivided into four chambers. It simulated both the systemic and pulmonary circulation, where the artificial heart was connected with a cannula to each chamber. An adjustable air volume was present in each chamber to simulate compliance, and a bellows-operated valve provided resistance. According to Donovan, this valve provided baroreceptor feedback by the (adjustable) spring action of the bellows. Pressure could be measured in each chamber of this mock loop, and it was even supplied with a home-made turbine flow meter to acquire aortic flow. This mock circulatory system was easy to use and very versatile, but it required a lot of fluid to obtain the desired compliances.

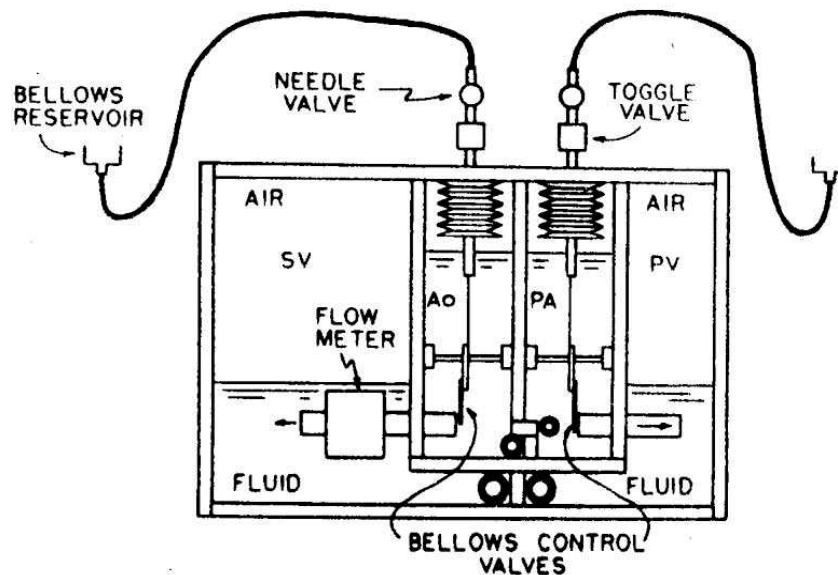


Fig. II-2: Schematic drawing of the Donovan mock loop [129].

Another historical *in vitro* setup for both artificial hearts and left ventricular assist device testing is the Pennsylvania State University mock loop, originally designed in 1971 and temporarily adopted by the National Institute of Health as the 'standard mock loop' [130]. It was updated a decade later, although the main configuration stayed the same: a systemic compliance chamber followed by a resistor, an inertance element, and a venous compliance chamber [131]. The systemic and venous compliance chambers did not contain air, but a cylinder with a piston that was sealed with a rolling diaphragm. The compliance effect

was realized with a cantilever spring that was mounted in a way that its flexing point and thus the resulting force-displacement relation at the tip (~ compliance) could be adjusted. The resistor consisted of a number of parallel flexible tubes that were mounted between two plates and thereby compressed to increase resistance.

More recent exemplary designs of mock loops are constructed by research groups in Aachen (Germany)^[132], Rome (Italy)^[133], and a collaboration between the Universities of Utah and Louisville (USA)^[134]. The group in Aachen designed a very compact and portable system that comes in a systemic and a pulmonary version. Two systems can easily be used side by side for bi-ventricular assist device or total artificial heart testing. The setup consists of three cylinders of identical dimensions, mounted adjacent to each other on a triangular plate. One of the cylinders acts as a reservoir and is not involved in the flow loop. Another cylinder is a compliance chamber in which the considered device ejects. The flow will go through the compliance chamber and pass through a vertical rotameter that indicates mean flow and through a ball valve that acts as a resistor. From there, the fluid enters the third cylinder from the top. This cylinder acts as a venous (or atrial) compliance chamber from which the device is filled. The whole system can be equipped with extra manometers and flow meters for accurate data acquisition. The compliance chamber simply uses a trapped air volume, but it is innovative in that it has an internal cylinder (open at the top) for regulation of the compliance. To decrease the compliance, air is replaced by fluid in that internal cylinder and so the fluid level in the outer cylinder - through which the flow circulates - can stay constant, thus preventing additional mass effects. The fact that a simple ball valve is used as a resistor has the disadvantage that it is highly nonlinear and that it is very difficult to regulate within the physiological range.

In contrast, mock loops designed by Sharp et al. (USA) and Ferrari et al. (Italy) use resistors comparable to the one described by Westerhof: a perforated or porous plate with a slide in front. Ferrari further automated the slide with a stepper motor. He used spring loaded compliance chambers, while Sharp used air chambers equipped with a piston to regulate the compliance. Sharp and Ferrari also included a characteristic resistance element proximal to the compliance.

All the recent designs are provided with access ports and luer-locks for instrumentation and accurate measurements. The sophisticated mock loop system of Italy even incorporates automation of the resistance elements, but apparently

not for simulation of the autonomous nervous system changes. Motorized control is used to accurately set and maintain a certain resistance value (or mean arterial pressure if desired) and thus to overcome nonlinearities and the inaccuracies of manual resistance setting ^[135].

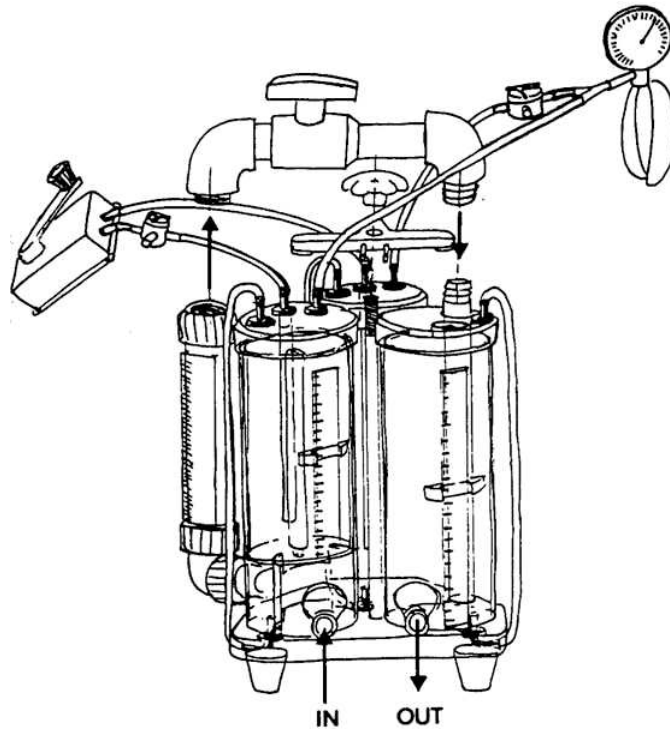


Fig. II-3: Schematic drawing of the mock loop designed at the Helmholtz Institute Aachen ^[132].

2.2. The Hydraulics Laboratory lumped afterload

2.2.1. Requirements

Apart from the vague recommendations for long-term reliability testing of mechanical circulatory support systems ^[123], further requirements were defined for the lumped afterload designed at the Hydraulics Laboratory (Ghent University, Belgium):

- modular system
- simple design of individual components that can be reproduced
- easy and accurate change of settings that simulate vascular properties
- reproducible settings
- properties adjustable during operation
- manageable: filling, emptying, and purging has to go clean and swift

- allow connection of various devices and cannulation types
- allow different test fluids
- visual control
- transportable
- easy access for instrumentation (pressure gauges, catheters, flow probes)

2.2.2. Overview

The lumped afterload model was primarily designed to mimic the systemic circulation. The main components are an air chamber (windkessel), mimicking the compliance of large blood vessels, and a resistance, mimicking the resistive action of arterioles and capillaries. The resistance is followed by an overflow reservoir that maintains a constant venous afterload pressure of 5 mmHg (with water as a test fluid) and provides an infinite venous compliance. A small (characteristic) resistance can optionally be placed proximal to the windkessel, resulting in a three-element windkessel afterload as defined by Westerhof ^[126]. An additional valve can be installed between the resistor and the venous overflow reservoir to facilitate filling, purging and component exchange. All components are connected with threaded couplings and 21 mm inner diameter PVC piping all at the same center level (60 mm above tabletop). Connections are kept as short as possible to minimize the inertia of the system, while the inevitable remaining inertia can be considered as the fourth element in the lumped windkessel model as described by Stergiopoulos et al. ^[125]. Luer-locks for pressure transducers or catheter access are present in the windkessel and before and after the resistor at the center level of the connectors. Flow rate measurement is provided proximal to the windkessel.

The compliance chamber consists of a hermetically sealed cylindrical reservoir and makes use of the elastic properties of trapped air. The compliance is adjustable with a three way valve on the lid to add or purge air. The peripheral resistor consists of a foam that is contained in a cylindrical membrane which is in turn fixed in a horizontal cylindrical housing. The membrane (and foam) can be compressed for resistance regulation by adding fluid in between the housing and the membrane. The smaller characteristic resistance is not adjustable and consists of a piece of foam that is fixed in the inflow of the air chamber. The venous overflow reservoir is a cylindrical reservoir, open to atmosphere, with a central funnel that connects to a drain pipe.

More details on the different components, their validation, and the use of the afterload in combination with a static and a dynamic preload can be found in chapter V, section B. Studies performed with this afterload model can be found in chapter IV (section D) and chapter V (sections C and D).

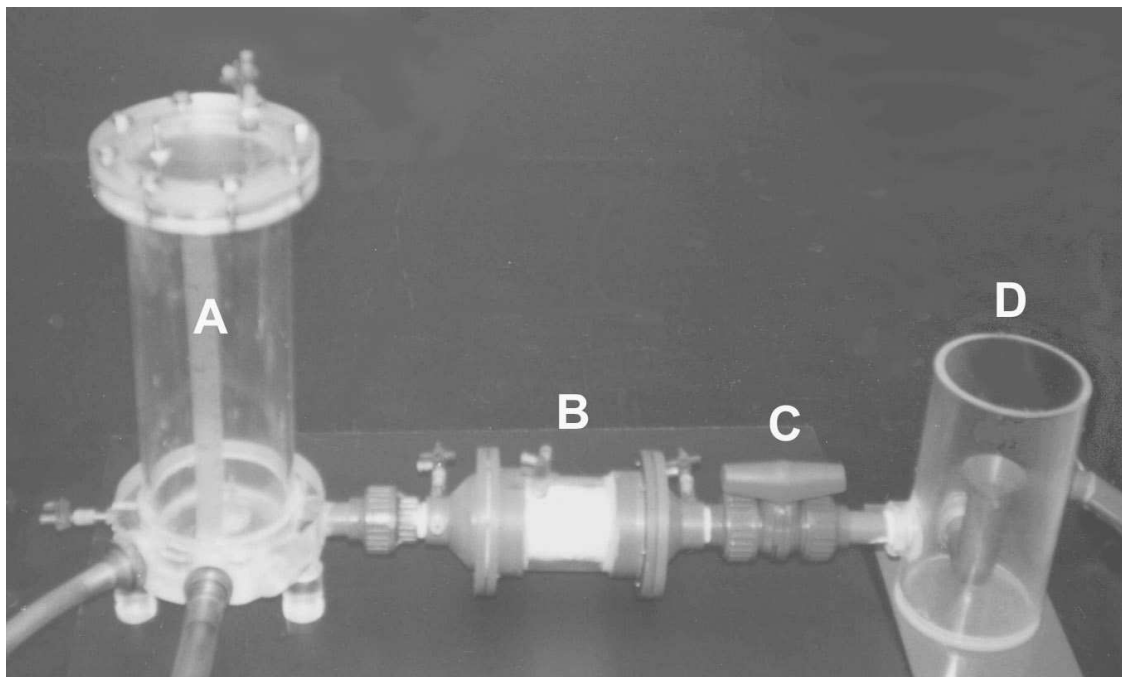


Fig. II-4: Top: overview of the lumped afterload. A: windkessel. B: resistor. C: valve. D: venous reservoir. Bottom: detailed view on the composition of the resistor, with the foam on the inside and the flanges of the membrane and the housing around it.

3. Distributed *in vitro* afterload models

3.1. Introduction

It is virtually impossible to make an exact artificial copy of the mammalian arterial system, given its vastness and complexity. Consequently, distributed arterial systems that are used as afterload in mock circulatory systems are limited to rubber versions of the large arteries. Their main benefits over lumped models are: (i) they allow realistic introduction of a device, (ii) it is possible to mimic a realistic flow distribution over different vascular regions, (iii) pressure wave propagation and reflection is more physiologic.

Besides the realistic simulation of the introduction of a device, other surgical procedures can be simulated in a distributed model, e.g., the use of vascular grafts, aneurysm treatments, and coarctation correction. Such a model allows to connect the outflow graft of a device to a rubber aorta and doing so, the effect of a compliance mismatch or the optimal insertion angle can be assessed. Most benefit, however, is achieved when studying the *in situ* performance of small, catheter-based devices such as intra-aortic balloon pumps or the Impella pumps. The fact that the flow distribution can be investigated is particularly relevant for these devices: since they are introduced through a peripheral artery and shifted retrograde through the arterial system, it is obvious that they alter the natural flow distribution and hence the perfusion of certain regions.

Distributed arterial models are more difficult to fabricate and to handle compared to lumped models, because of the multiplicity of components: each branch needs a separate end-load to provide adjustability of the flow distribution. Such an end-load consists of a resistance element and occasionally also a compliance element, each adding an extra variable to control. Due to their complexity, distributed models are rarely used for ventricular assist device studies, even though there is no doubt that these models are physiologically more correct than lumped afterload models.

3.2. The Hydraulics Laboratory distributed afterload

A detailed distributed model of the arterial tree was previously fabricated at the Hydraulics Laboratory from latex rubber for studies on cardiovascular hemodynamics in general and wave reflection in particular^[136,137]. Based on this experience, a new model from more durable silicone was developed with a dual

goal: allow introduction of a catheter-based VAD and allow assessment of the flow distribution over the arterial tree.

This afterload model consists of an aorta with eight main arterial branches, the dimensions of which were derived from literature^[138] and are representative for a human male of 85 kg (Fig. II-5). The relative portions of the total flow in each branch were also adopted from the same reference. Although the curvature of the aortic arch is neglected, the branches are connected to the aorta with respect for their anatomic location. Also the geometric tapering of the vessels is taken into account. The branches represent the carotid, the subclavian, the renal, and the femoral arteries, all for the left and right side. On the right side, the subclavian and carotid arteries are connected to the brachiocephalic trunc as in reality. The renal arteries also represent other abdominal arteries (splenic, hepatic, gastric) and hence their dimensions are rescaled with respect to the flow distribution. In reality, coronary arteries are subject to intermittent external compression from the myocardium and their correct function is therefore difficult to simulate. Nonetheless, two coronary arteries were appended to the distributed afterload because they can also serve as instrumentation sites.

The distributed afterload was fabricated with silicone rubber (Silopren LSR 2050, Artois Plastics, Ostend, Belgium) that was brushed on a slowly spinning metal mold and vulcanized in an oven at a temperature of 150 °C for 2 hours. Static and dynamic compliance measurements revealed that the final model required eight layers of silicone to obtain realistic properties (compliance = 0.5 ml/mmHg). The aorta and the arterial branches were all made separately and afterwards connected to each other. Silicone was selected for its strength and durability. Alternatives are polyurethane which is more difficult to handle, or latex, which is very cheap and manageable but less durable.

The end-loads of each branch are identical and consist of a vertical cylinder that is glued to a rectangular overflow reservoir. The cylinder is filled with foam, which can be compressed with a piston for resistance regulation. The overflow reservoir contains a vertical pipe that connects to a drainage system. The test fluid can be drained to a buffer reservoir via an open channel, or it can be collected in small reservoirs for each branch individually. These reservoirs are mounted on a slide mechanism and can be used for synchronous gravimetric flow measurements.

This distributed afterload model has been used in the studies described in chapter V, sections D and E.

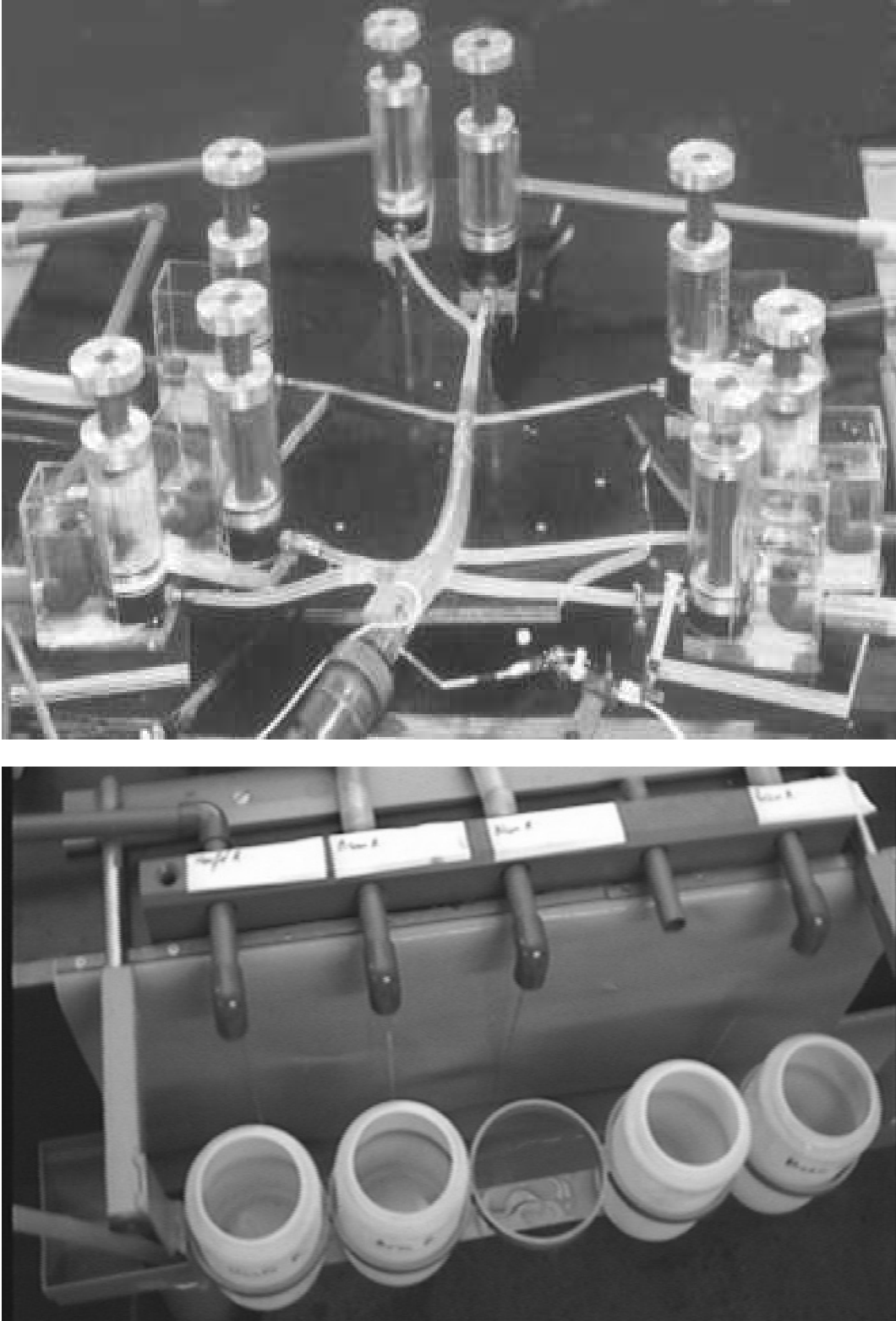


Fig. II-5: Top: overview of the distributed *in vitro* afterload with the eight branches and their individual end-loads. Bottom: view on the collection reservoirs and slide mechanism.

C. PRELOAD MODELS

1. Static preload models

Depending on the type of assist device and the preferred cannulation type, a device can be filled by the atrium or by the ventricle. In healthy subjects, the atrium would yield a relatively constant filling pressure, while high pressure variations would be present in the left ventricle. In end-stage heart failure patients, however, the ventricular function is severely compromised and the end-systolic pressure and ventricular pulse pressure are decreased. Therefore, and for practical reasons, a static preload can be used to simulate only mean ventricular pressure for validation of a ventricular assist device. A maximum mean filling pressure of 40 mmHg was deemed sufficient as a standard, which is a value that can be found in healthy subjects ^[3].

The static preload reservoir of the Hydraulics Laboratory can be used either fully independent of the afterload, or coupled to it (the afterload directly fills the preload reservoir). The latter method is most often used in other *in vitro* setups for assist device testing, possibly with an atrial compliance chamber in between. The resulting preload value is then related to the amount of fluid used in the circuit. This direct coupling is very compact, and it may seem to relate closely to the real circulation where venous pressure also forms the preload of the heart. However, this method neglects the pulmonary circulation where an additional pump and buffer vessels actually decouple preload and afterload. A direct coupling will result in fluctuation of the preload pressure due to volume variations - maximally equal to the applied stroke volume - if a displacement type device is used. To minimize these pressure variations, the dimensions of the static preload component were chosen rather large so volume variations result only in small pressure variations. With the current dimensions, a variation of 100 ml would result in a fluid level change of 6.67 mm or a pressure variation of 0.49 mmHg if water is used.

If the static preload is used in a decoupled way, the fluid from the afterload (either lumped or distributed) is drained to a buffer reservoir and subsequently pumped up with a centrifugal pump (model UPS 25-40 B, Grundfos, Aartselaar,

Belgium) to the preload reservoir, which then acts as a weir. Consequently, a constant pressure level is present at the bottom of the preload reservoir, where the connection to the device under test is located. Two additional connectors are present next to the device connector: one to pump in the fluid from the buffer reservoir and the other to drain the overflowed fluid back to that reservoir. The preload reservoir is made out of Plexiglas and measures 150 x 100 x 600 mm (w x l x h). Two vertical grooves are present on the inside between the inflow and outflow connector. Separate panes can be slid in the grooves to adjust the overflow height, and thus the preload pressure. That pressure can be varied between 5 and 40 mmHg and it can be monitored with a luer-lock on the side of the reservoir, at the center level of the connectors. All connectors are custom made and exchangeable to allow different sizes and types of devices.

The static preload model has been used for assessment of pump data to create mathematical models and for the studies described in chapter V, sections B-D.

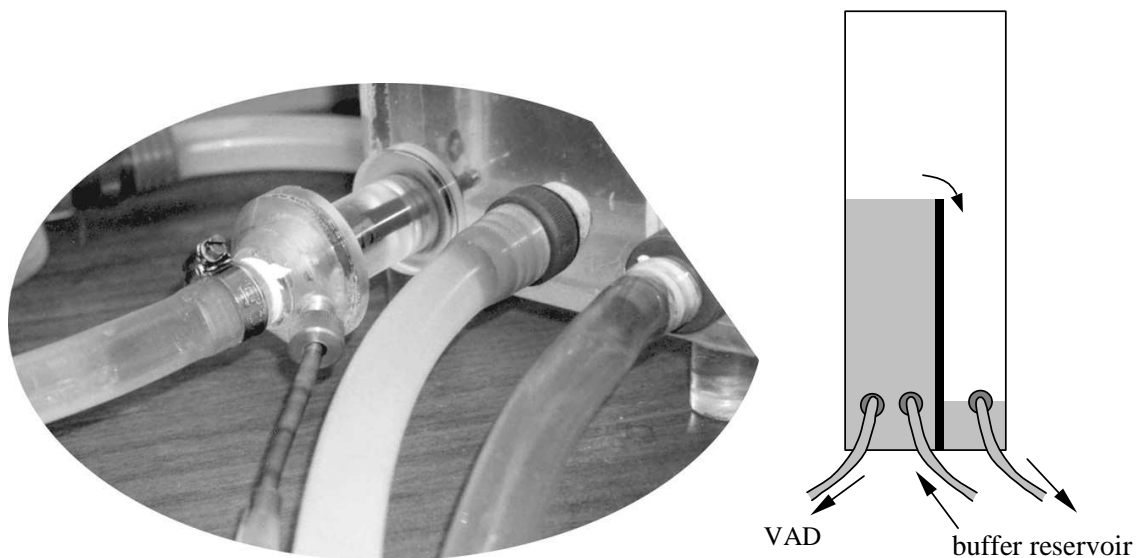


Fig. II-6: Connection of the static preload reservoir for use in a decoupled way. The most left connector in the photograph was especially designed for a catheter-based device. The middle connector serves as inflow (from the buffer reservoir) and the right connector as drain.

2. Dynamic preload models (heart simulators)

2.1. Introduction

Worldwide, there are various *in vitro* models that simulate the function of the heart (i.e., the left ventricle) and can thus be used as a dynamic preload for a ventricular assist device. Most of these ‘heart simulators’ or ‘pulse duplicators’ were custom made in cardiovascular research labs and originally intended for

artificial heart valve testing or for general simulation purposes ^[139,140]. Such systems are, to a lesser extent, also commercially available (e.g., Superdup'r, Vivitro Systems Inc., Victoria, Canada). Apart from heart simulators, it is also possible to use a displacement type ventricular assist device to create a dynamic preload ^[141].

Heart simulators mimic the hydrodynamic function of the heart, whether or not with respect to its anatomy. The most basic simulators consist of a valved container in which the volume is varied by a membrane, piston, or bellows that can be actuated with either a servo motor or a voice coil or compressed air ^[135,142,143]. If the anatomy of the heart (left ventricle) is respected, it is mimicked with a rubber sac that is suspended in water or air ^[139,140,144,145]. The actuation is then indirect, with one of the previously mentioned methods.

The simulation of heart function can be obtained by computer controlled pressure generation ^[145] or volume variation ^[135], where ventricular pressure or volume are fed back to the controller that tries to match them to a given waveform. In cardiac physiology, however, generated pressure and volume are related and therefore a more realistic simulation would be based on ventricular elastance. This can also be achieved with either pressure or volume control, but actual volume and pressure need to be fed back simultaneously and incorporated in an algorithm with a given elastance waveform ^[143].

2.2. The Hydraulics Laboratory heart simulator

This heart simulator or pulse duplicator mimics the anatomy of the left atrium (LA) and the left ventricle (LV) with two silicone rubber sacs that are suspended in a water-filled Plexiglas housing (see Fig. II-7) ^[145]. Bioprosthetic or mechanical heart valves of different sizes can be incorporated between the sacs as mitral valve and at the aortic root of the ventricle as aortic valve. The fluid flow to the atrium comes from two pulmonary veins (PVC tubing), which are connected to a static preload reservoir that simulates pulmonary pressure. The aortic root ends in an arch and a connector suitable for a lumped or distributed afterload model. A tubular extension of the ventricular apex is foreseen in the silicone sac for insertion of a cannula.

For actuation of the heart chambers, their housing communicates with an actuation column that is partially filled with water. Applying pressurized air on the water surface in such a column results in compression of the connected heart

chamber and a decrease of the water level in the column. An ultrasonic level sensor (Superprox SM606, Hyde Park Electronics LLC, Dayton, OH) is installed on top of the ventricular actuation column to measure ventricular volume changes. Ventricular and atrial pressure can be measured with catheters directly in the heart chambers or with pressure transducers on the housing. Aortic pressure can be measured at the aortic root via a luer-lock and aortic flow can be acquired with a clamp-on flow probe a few centimeters distal to the aortic valve.

The heart simulator is computer controlled with LabView software (National Instruments, Austin, TX) and pressure feedback. The error between the measured pressure and a given waveform is translated (with PI-circuitry) to the displacement of a proportional pneumatic valve that regulates the flow of pressurized air to the actuation column. During systole, the pressurized air comes from a pressurized air chamber and during diastole the actuation column is connected to atmosphere.

This dynamic preload model has been used for the validation of the lumped afterload model, which is described in section B of chapter V. This heart simulator has further been used as a dynamic preload in the in vitro studies with a rotary blood pump (chapter IV, section D) and with a catheter-based VAD (sections D and E of chapter V).

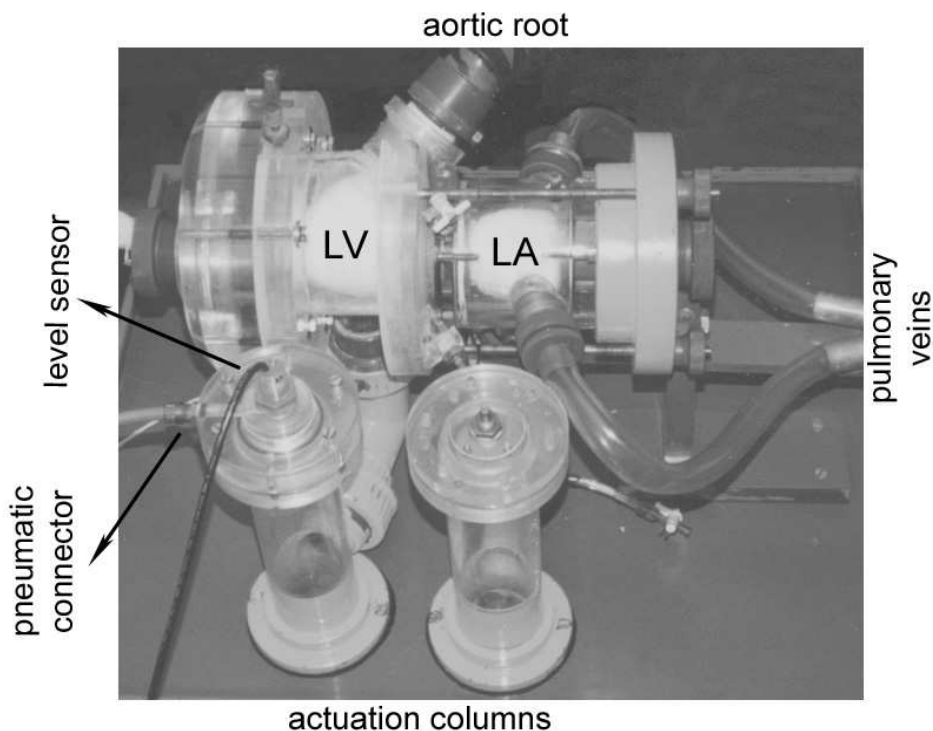


Fig. II-7: Overview of the Hydraulics Laboratory heart simulator.

CHAPTER III

Mathematical Modeling of Ventricular Assist

A. OVERVIEW OF MATHEMATICAL CARDIOVASCULAR MODELING

1. Introduction

The history of mathematical models is closely related to the evolution of mathematics. A model can be as simple as one equation, but the contemporary available computing power has opened the doors for much more complicated models. The main advantage of mathematical models over, for instance, *in vitro* models is that they are cheap and flexible. In addition, parameter values in a mathematical model can be set exactly and kept constant, while *in vitro* models are more difficult to control.

When focusing on the cardiovascular system, models of different functional levels can be created, e.g., electrophysiological models that simulate exchange of substances between cells, models that simulate the electrical conductivity of the heart, or models that simulate the mechanical behavior of valve leaflets. Models related to heart failure and ventricular unloading are mainly created in two forms: finite element models and lumped models. In this dissertation, the focus is on lumped parameter models in a mathematical form. The principle of such a model is similar as described in the previous chapter on *in vitro* models: geometrically distributed properties of the cardiovascular system are condensed in a number of discrete components. Models of cardiovascular function are often linked to electronic circuit theory and the depiction of such a model as an electrical network facilitates composition of the necessary equations. Lumped models focus on pressure (\sim voltage), volume (\sim charge), and flow (\sim current) that are generated in the cardiovascular system. To simulate the interaction between the heart and an assist device, the total model needs to combine a model of the heart, a model of the assist device, and a model of the afterload experienced by those two ‘pumps’. These three components of a total model will now be discussed in further detail.

2. Cardiac models

2.1. Time-varying elastance

The original time-varying elastance theory of Suga and Sagawa was extensively discussed in Chapter I. In short, ventricular elastance is defined as the ratio of instantaneous left ventricular pressure to left ventricular volume, corrected for a 'dead volume' (V_0), the volume in the ventricle at zero pressure ^[8].

$$E(t) = \frac{P_{LV}(t)}{[V_{LV}(t) - V_0]} \quad \text{or} \quad p_{LV}(t) = E(t) \cdot [V_{LV}(t) - V_0] \quad [\text{Eq. III-1}]$$

with:

- $E(t)$: time varying elastance (mmHg/ml)
- $p_{LV}(t)$: left ventricular pressure (mmHg)
- $V_{LV}(t)$: left ventricular volume (ml)
- V_0 : volume at zero pressure (ml)

In a pressure-volume (PV) plane, instantaneous elastance can be presented as the slope of a line connecting the V_0 intercept on the volume axis with the considered pressure-volume data point at that instant. Over the course of a heart cycle, the left ventricular pressure and volume variations will create a counterclockwise loop in the PV-plane. Consequently, the slope of the line will rise and fall, resulting in an increase and decrease of the elastance. This elastance varies according to a certain pattern that is typical for a given heart, independent of preload or afterload condition. Therefore the time-varying elastance theory is suitable for use in models of the heart where different loading conditions will be simulated.

It is assumed in the original time-varying elastance theory that the end-systolic and end-diastolic pressure-volume relations (ESPVR and EDPVR, see Fig. I-16) are linear. It has meanwhile been shown, however, that the EDPVR is best presented by an exponential or a logarithmic relation. The EDPVR in fact characterizes the passive compliance of a relaxed ventricle. It even extends to negative pressures, suggesting that the ventricle is able to suck blood during filling within a certain volume range ^[146]. It was found that the ESPVR is also curvilinear but to a much lesser extent ^[147].

Several approaches are possible to implement the elastance theory in a mathematical model. The equations used are normally set for one cardiac cycle and are solved repeatedly, where a scaling in time is applied to obtain results at the desired heart rate.

i) A first approach is based on the original elastance theory (see [Eq. III-1]), where all relations are assumed linear, including the EDPVR. If the elastance curve is plot as a function of time, then its maximum is the slope of the ESPVR in the PV-plane and its minimum relates to the slope of the EDPVR. Since diastolic pressure is always positive and non-zero - with the exception of extreme low volume conditions -, the EDPVR will have a positive value and the elastance curve as a function of time will consequently hover completely above the time axis. This first approach is the most simple one, but it has proven to be sufficiently accurate in many cases ^[148-150].

ii) Another approach is to recognize the EDPVR as the passive behavior of the left ventricle, which is always present. The pressure generated in the left ventricle can then be described as:

$$p_{LV}(t) = p_{active}(t) + p_{passive}(t) = E(t) \cdot [V_{LV}(t) - V_0] + EDPVR \quad [Eq. III-2]$$

where the active pressure (p_{active}) is generated by the contraction of the myocardium and the passive pressure ($p_{passive}$) is the result of the compliance of the myocardium. This latter part can be modeled as an exponential or logarithmic term (the mathematical description of the EDPVR), that is added to the active part. For the active part, the linear elastance theory can then be used, where minimum elastance equals zero. Thus in contrast with the previous approach, the diastolic part of the elastance curve would coincide with the time axis. In other words, the active part alone simulates a PV-loop where the diastolic filling phase (see Fig. I-15) coincides with the volume axis, while the passive part lifts the loop onto the EDPVR. Both approaches i) and ii) can obtain an increase in contractility by rescaling the elastance curve and increasing its maximum, resulting in a steeper ESPVR.

iii) A final approach to implement the time-varying elastance theory is to define the ESPVR and EDPVR as (time invariant) boundaries by a mathematical equation with a level of complexity chosen by the developer. This may be linear, but this approach easily allows to define curved boundaries. A third equation then describes a time-varying activation function ($\alpha(t)$) that determines in what proportion each boundary contributes to the instantaneous pressure and volume. In other words, it is a transition function between 0 and 1 that describes how an instantaneous data point migrates from the EDPVR to the ESPVR. Consequently,

the equation that defines the left ventricular pressure as a function of volume and time has a term for ESPVR and a term for EDPVR:

$$p(V, t) = \alpha(t) \cdot \text{ESPVR} + [1 - \alpha(t)] \cdot \text{EDPVR} \quad [\text{Eq. III-3}]$$

When the activation $\alpha(t) = 0$, the instantaneous pressure-volume data point will be on the EDPVR, while when the activation equals 1 it will be on the ESPVR. To increase the contractility of the left ventricle in this approach, it is necessary to redefine the ESPVR, while the activation function can stay the same.

A simplification adopted by all models is that the volume intercept V_0 remains constant throughout the cardiac cycle and thus acts in the PV-diagram as the pivot point for all the instantaneous pressure-volume relations. In reality, the volume intercept varies over the cardiac cycle, although within a limited range^[151]. Especially during systole the variations are very small and modeling it as a constant value is acceptable. A more realistic approach would be to use a volume value at a slightly negative pressure as a pivot point. This would reconcile with the idea of Sunagawa^[152] that ESPVR and nonlinear EDPVR cross below the volume axis.

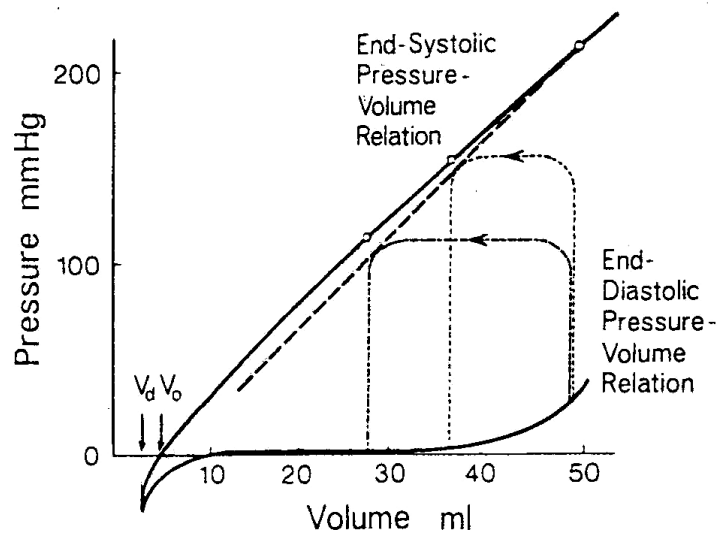


Fig. III-1: Schematic diagram to indicate the difference between V_0 (volume intercept of ESPVR) and V_d (volume at which no pressure variations can be generated).

2.2. Examples of elastance/activation curves

For modeling purposes, it is desirable to use relatively simple mathematical functions that can be created within the model, based on the time-scale and a minimum number of parameters. A commonly used activation curve consists of

the combination of a raised cosine function for activation with an exponential decaying function for deactivation ^[153]. A similar approach can be applied for elastance curves: mathematical functions can be combined in order to obtain an elastance curve that mimics patient or animal elastance functions. The simplest way is to combine linear segments, but this has the disadvantage that many parameters are required to define the total ‘curve’, and that a lot of steps are necessary to position the line segments relatively to one another ^[154]. Polynomials may be used instead, but the elastance curve is then best also split up in several parts. Splitting the curves adds one extra difficulty, especially when they have to be rescaled: the connecting points need to be continuous in value and first derivative. Below are some examples of elastance curves used in left ventricular mathematical models.

2.2.1. Sinusoidal approximation

In the normalized elastance curve that is used as an example here ^[155], the cardiac cycle is split into three parts: a rising part for contraction, a falling part for relaxation and a part where the elastance is zero for ventricular filling. This curve can be used in models according to approach ii) as described above.

$$\text{rising part:} \quad E_n(t) = \sin\left(\frac{t \cdot \pi}{2 \cdot T_{\text{rise}}}\right) \quad [\text{Eq. III-4}]$$

$$\text{falling part:} \quad E_n(t) = 1 - \left[\sin\left(\frac{(t - T_{\text{rise}}) \cdot \pi}{2 \cdot T_{\text{fall}}}\right) \right] \quad [\text{Eq. III-5}]$$

with:

- $E_n(t)$: normalized time-varying elastance (-)
- t : time (s)
- T_{rise} : 0.833 x duration of systole (s)
- T_{fall} : 0.167 x duration of systole (s)

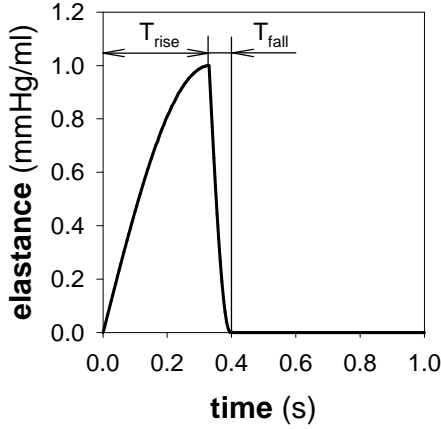


Fig. III-2: Sinusoidal model of a normalized human elastance curve.

$$T_{\text{rise}} = 0.333$$

$$T_{\text{fall}} = 0.066$$

2.2.2. Exponential approximation

This method allows to model the elastance curve with only two parts: a rising exponential and a decaying exponential with an asymptote equal to the minimum elastance. Four constant parameters plus the time indication of the maximum elastance are necessary to define the elastance curve in this way ^[156].

rising part:
$$E(t) = E_{\text{max}} \cdot (1 - e^{-\frac{t}{\tau_1}}) + E_{\text{min}} \quad [\text{Eq. III-6}]$$

falling part:
$$E(t) = E_{\text{max}} \cdot e^{-\frac{-(t-t_{\text{max}})}{\tau_2}} + E_{\text{min}} \quad [\text{Eq. III-7}]$$

with:

- E(t): time-varying elastance (mmHg/ml)
- t: time (s)
- E_{max}, E_{min}: scaling factors (mmHg/ml)
- τ₁, τ₂: time constants (s)

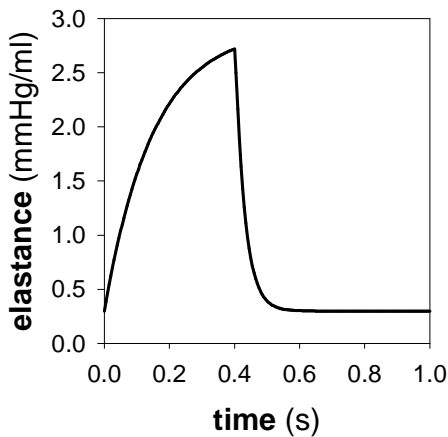


Fig. III-3: Exponential model of a human elastance curve.

$$E_{\text{max}} = 2.6 \text{ mmHg/ml}$$

$$E_{\text{min}} = 0.3 \text{ mmHg/ml}$$

$$\tau_1 = 0.15 \text{ s}$$

$$\tau_2 = 0.03 \text{ s}$$

2.2.3. Double Hill function

In contrast with the previous methods, the ‘double Hill’ function describes the elastance curve as a whole, with five parameters ^[149]. The first part of the function is an actual Hill function that determines the rising leg of the curve, while the second part is an inverted Hill function that determines the falling leg. The alpha parameters define the timing of the separate parts relative to the period T, and thus α_1 needs to be smaller than α_2 . The exponents control the steepness of the rising and falling leg, and there too n_1 will be smaller than n_2 , resulting in a much steeper falling leg.

$$E_n(t) = a \cdot \left[\frac{\left(\frac{t}{\alpha_1 \cdot T} \right)^{n_1}}{1 + \left(\frac{t}{\alpha_1 \cdot T} \right)^{n_1}} \right] \cdot \left[\frac{1}{1 + \left(\frac{t}{\alpha_2 \cdot T} \right)^{n_2}} \right] \quad [\text{Eq. III-8}]$$

with:

- $E_n(t)$: normalized time-varying elastance (mmHg/ml)
- t : time (s)
- T : period of a heart cycle (s)
- a : amplitude scaling factor (mmHg/ml)
- α_1, α_2 : shape factors (-)
- n_1, n_2 : exponential shape factors (-)

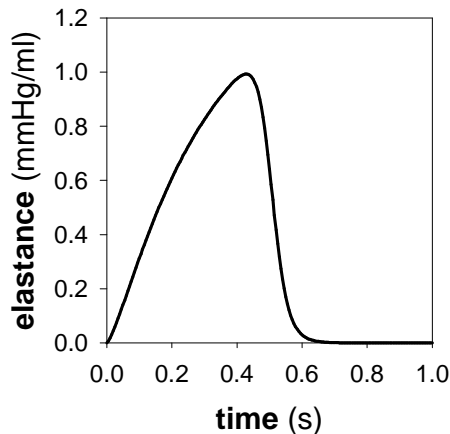


Fig. III-4: ‘Double-Hill’ model of a normalized human elastance curve.
 $a = 1.66$ mmHg/ml
 $\alpha_1 = 0.303$
 $\alpha_2 = 0.508$
 $n_1 = 1.32$
 $n_2 = 21.9$

2.3. Right ventricular and atrial modeling

Most studies and models are focusing on the left ventricle, as it is the most powerful heart chamber that provides flow to multiple organs. Pressure-volume measurements on patients have mostly been performed in the left ventricle, and data are readily available. The situation is different for the right ventricle, where only limited patient data are available. Compared to the left ventricle, right

ventricle PV-loops exhibit a more triangular shape. This is caused by a combination of a distinct right ventricular geometry and a markedly different afterload. As a consequence of the low pulmonary afterload pressures, the isovolumic contraction and relaxation phases of the right ventricle are shorter than in the left ventricle. From geometric point of view, the left ventricle can be considered as one symmetric cavity (often approximated by an ellipsoid or cone), but the right ventricle consists of two distinct parts: the sinus and the conus. These appear not to work perfectly synchronous, resulting in a two-phased contraction ^[157,158]. Therefore it is questionable whether the whole right ventricle should be modeled as one part and whether its function should be determined from one complete loop. The situation is even more confusing for models of the atria, where PV-loops show a figure of eight shape. Atria obviously have a completely different geometry compared to the left ventricle and their function and timing is also incomparable.

In summary, experience and good data are available for LV models, but to model the right ventricle and the atria, several assumptions need to be made, or conversions from animal data have to be used.

2.4. Alternative cardiac modeling methods

2.4.1. Elastance-resistance model

Although the original time-varying elastance concept of Suga and Sagawa as described above is still widely used in mathematical models, it was revised by the same authors in 1980. They suggested the following extension:

$$p(t)=E(t) \cdot [V(t)-V_0]+C_1 \cdot \left(\frac{dV(t)}{dt}\right)+C_2 \cdot \left(\frac{dV(t)}{dt}\right)_{\max}+C_3 \cdot \int_0^t V(t)dt \quad [\text{Eq. III-9}]$$

with:

C_1, C_2, C_3 : weighing factors
other variables as described above

Since ventricular volume decreases during the ejection, the three additional right hand terms are negative and result in an extra ventricular pressure drop. The second term of [Eq. III-9] represents the visco-elastic behavior of the myocardium, which originates from the extra-cellular matrix, of which collagen is an important component. The two following terms are dependent on the deactivation of the muscle fibers. Basically, the second term of [Eq. III-9] contains the ejection flow of the ventricle. It appears that higher ejection rates

result in a lower pressure generation. The third term is the peak ejection flow rate, while the last term is in fact the total volume that is ejected from the ventricle since the start of the beat. The term with the highest impact proved to be the ejection flow and as a consequence, the elastance-resistance model was created and used in different forms and variations by various researchers ^[159-161].

Ignoring the two last terms in [Eq. III-9] and reformulating the remaining extra term results in a common way of incorporating ventricular resistance in the model:

$$p(t) = E(t) \cdot [V(t) - V_0] - R_v \cdot Q(t) \quad [\text{Eq. III-10}]$$

with:

$$Q(t) = dV(t)/dt: \text{ ejection flow (ml/s)}$$

$$R_v: \text{ ventricular resistance (mmHg}\cdot\text{s/ml)}$$

The ventricular resistance is an intrinsic property of the heart and it can be quantified by creating a situation where $p(t)$ equals zero, i.e., a beat with no afterload. The generated flow will then be the maximum flow (Q_{\max}) that can be generated by the specific ventricle that is modeled.

$$R_v = \frac{E(t) \cdot [V(t) - V_0]}{Q_{\max}} \quad [\text{Eq. III-11}]$$

Consequently, the instantaneous left ventricular pressure can be modeled by substituting [Eq. III-11] in [Eq. III-10] :

$$p(t) = E(t) \cdot [V(t) - V_0] \cdot \left[1 - \frac{Q(t)}{Q_{\max}} \right] \quad [\text{Eq. III-12}]$$

This model contains three parameters that characterize a specific ventricle in a specific contractile state: $E(t)$, V_0 , and Q_{\max} . The first parameter, $E(t)$, is a waveform similar to the ones discussed before while Q_{\max} and V_0 are constants. Since it is not feasible to create a no-load condition in an *in vivo* experiment without dissecting the aorta, a method based on the combination of an ejecting beat and an isovolumic beat is usually applied to estimate the three parameters. In short, the combination of these beats allows the model to be rewritten so that only two parameters need to be determined. These can be estimated with curve fitting techniques from the pressure data of the two beats and from the flow data of the ejecting beat. An isovolumic beat has the advantage that $Q(t)$ is zero and $V(t)$ is a constant: end-diastolic volume (V_{ed}). Consequently, the isovolumic

pressure waveform ($p_{\text{iso}}(t)$) will reveal the shape of the elastance curve waveform.

$$p_{\text{iso}}(t) = E(t) \cdot [V_{\text{ed}} - V_0] = \frac{E(t)}{A} \quad [\text{Eq. III-13}]$$

The eventual equation needed for the estimation procedure is given below. Only A and Q_{max} need to be estimated and $E(t)$ can afterwards be obtained from [Eq. III-13].

$$1 - \frac{p(t)}{p_{\text{iso}}(t)} = A \cdot \left[\int_0^t Q(t) dt \right] + \frac{Q(t)}{Q_{\text{max}}} \left[1 - A \cdot \int_0^t Q(t) dt \right] \quad [\text{Eq. III-14}]$$

Depending on the available equipment, volume measurements can be performed instead of flow measurements and $Q(t)$ can be replaced with $dV(t)/dt$. This latter approach is more exact, especially in hearts where mitral regurgitation is expected. After all, the generated pressure depends on muscle fiber action and matrix interaction that results in volume variations, but the myocardium does not sense that this results in an effective ejection. A disadvantage of this method is the need for an isovolumic beat, thereby excluding human validation.

2.4.2. Isovolumic description

The elastance function obtained from ejecting beats is in fact characteristic for the combination of the ventricle with the particular arterial load that was present at the time of measurement. Grignola et al. stated that the peculiar shape of the right ventricular pressure-volume loops, for instance, is not related to different contracting mechanisms, but is due to the different load imposed by the pulmonary circulation ^[162]. Nevertheless, elastance is used in models to describe the function of the ventricle alone, regardless of the load. A more realistic model of the ventricle would be based on data acquired with the pump separated from the load. In practice, this can be achieved with isovolumic beats, where the heart always works against the same afterload, independent of the arterial system. Consequently, isovolumic beats are directly related to the ventricle's contractile state and therefore a model based on isovolumic pressure measurements was proposed by Palladino et al. ^[163]. In an isovolumic contracting ventricle, the instantaneously generated pressure is dependent on the volume contained in the ventricle and on the time point in the heart cycle. The volume stretches out the myocardium and thereby creates a passive pressure, independent of time. Active contracting mechanisms add an active pressure that is dependent on time and the

contained volume, as was already discovered by Frank in the 19th century. Isolated dog heart experiments revealed the following relationship for the passive (diastolic) pressure:

$$p_{\text{passive}} = a \cdot (V-b)^2 \quad [\text{Eq. III-15}]$$

with:

p_{passive} : passive left ventricular pressure (mmHg)
 V : left ventricular volume (ml)
 a, b : constants

This is in fact a quadratic description of the EDPVR, in contrast with the exponential or logarithmic definitions that were mentioned before. The constant b can be perceived as the volume intercept at zero pressure, while the constant a relates to the end-diastolic elastance. A description of the active pressure generation during an isovolumic beat, however, differs more from the instantaneous elastance concept. The active pressure is divided in a contraction and relaxation phase, taking the form:

$$p_{\text{active}} = A \cdot \left[\left(1 - e^{-\left(\frac{t}{\tau_1}\right)^\alpha} \right) \cdot e^{-\left(\frac{t-t_b}{\tau_2}\right)^\alpha} \right] \quad [\text{Eq. III-16}]$$

with:

p_{active} : active left ventricular pressure (mmHg)
 A : volume dependent factor (mmHg)
 α : exponential shape factor (-)
 τ_1, τ_2 : shape factors for contraction and relaxation (s)
 t_b : time delay for onset of relaxation (s)

The total description of the left ventricular pressure is given in [Eq. III-17]. Eight parameters are required for this equation, which can all be derived from experimental data with curve fitting procedures. Isovolumic beats at different volumes are therefore required and the resulting equation then characterizes a particular ventricle. The time t_p is the point at which the maximum ventricular pressure is reached, and c and d are constants that are proportional to the active pressure.

$$p(V, t) = a \cdot (V - b)^2 + (c \cdot V - d) \cdot \left[\frac{\left(1 - e^{-\left(\frac{t}{\tau_1}\right)^\alpha} \right) \cdot e^{-\left(\frac{t-t_b}{\tau_2}\right)^\alpha}}{\left(1 - e^{-\left(\frac{t_p}{\tau_1}\right)^\alpha} \right) \cdot e^{-\left(\frac{t_p-t_b}{\tau_2}\right)^\alpha}} \right] \quad [\text{Eq. III-17}]$$

The pressure in this model is instantaneous and dependent of V , which represents here the time varying left ventricular volume, and not the constant (isovolumic) volume at which the measurements were performed. Consequently, this model can be used for both ejecting beats and isovolumic beats. In the traditional time-varying elastance model – which is derived from ejecting beats – the pressure waveform of an isovolumic beat would have the same shape as the elastance curve. The factor $(V - V_0)$ will be no more than a constant, and thus a scaling factor that relates elastance to pressure. This means that that pressure waveform would be skewed to the right, while experimentally measured isovolumic pressure waveforms are symmetrical. Therefore this alternative model performs better on isovolumic beats than the traditional elastance approach (see Fig. III-5). Moreover, it can also be used on ejecting beats and it describes the function of the heart independent of the arterial load. However, this model is difficult to use because of the many required parameters and the necessary experimental data that is difficult to obtain from *in situ* hearts.

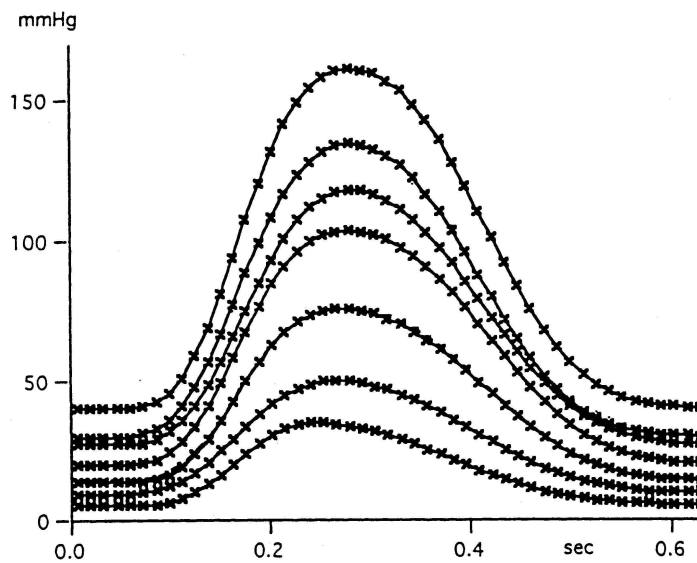


Fig. III-5: Fitting (solid lines) of [Eq. III-17] to isovolumetric pressure waveforms acquired in dogs at different volumes (crosses) ^[163].

3. Afterload models

3.1. Windkessel models

Simulating the vascular system with a mathematical model is similar to *in vitro* setups, though mathematical modeling is more flexible, and the components are ideal and really discrete. Various models with a wide range of complexity have been developed, some of which are shown in Fig. III-6. It may be desirable that the lumped afterload model is set up with components that each have a specific meaning and translate to the actual properties of the vascular system that they model. The addition of one component that does not relate to a specific property will result in a ‘meaningless model’ that may fit the vascular system input impedance well, though with meaningless values for the parameters.

Lumped afterload models that are currently in use for cardiovascular studies contain either 2, 3, 4, or 5 components and they are all based on the classic windkessel model as it was used by Frank ^[124]. The basic components are a compliance (electrical: capacitance, abbreviated as C) and a resistor (abbrev. R) that are connected in parallel. As explained in Chapter II, the former simulates the elasticity of the large arteries and the latter the resistance formed by the arterioles. This model, also referred to as an RC model, summarizes the basic functionality of the arterial system, but its impedance spectrum differs notably from measured mammalian data. The modulus tends to 0 for higher frequencies and the phase angle has an asymptote at -90° , while it should go to 0° . At high frequencies the ventricle sees an afterload that is free of reflection and is thus equal to the local high frequency behavior of the proximal aorta, as if there were no further arterial system. This observation suggested that an extra component was necessary to model the proximal aorta: the characteristic impedance (Z_c or R_c), which is mainly a resistive component. This characteristic component was added in series to the windkessel circuit by Westerhof and it was termed the modified windkessel model (RCR model) ^[128]. At high frequencies, the capacitor will behave like a bypass over R and thus R_c will be the ruling component. Hence the phase of this model in the impedance spectrum tends to 0° at high frequencies and the modulus has R_c as asymptote, which is a major improvement over the classic windkessel model.

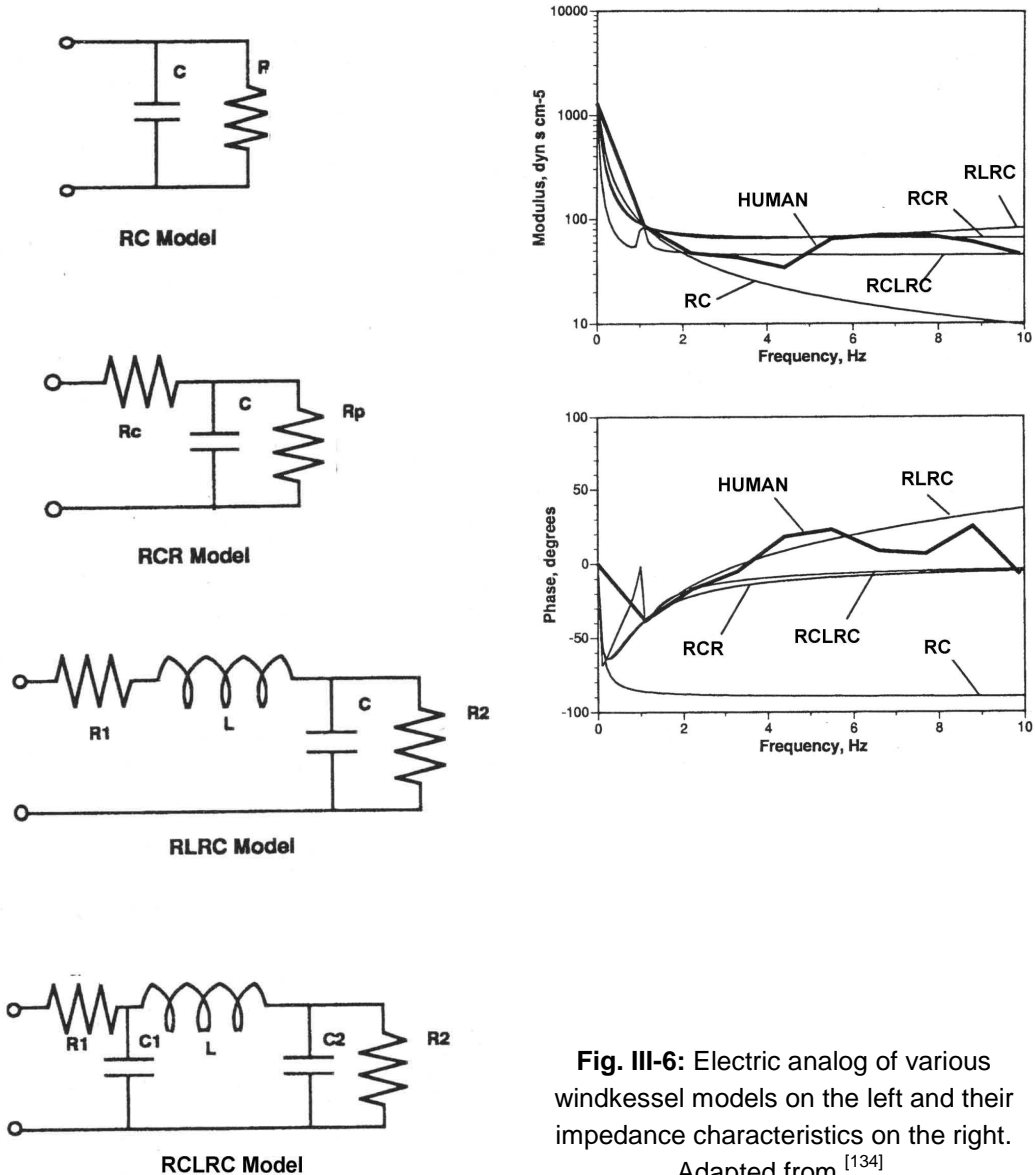


Fig. III-6: Electric analog of various windkessel models on the left and their impedance characteristics on the right. Adapted from [134].

A third model that is very popular is the four-element windkessel model, where an inductance (L) is added either in series or in parallel with the characteristic impedance [125]. This inductance represents the total inertance resulting from the mass of fluid in the arterial system. Pulsatile flow requires an acceleration (and deceleration) of this mass and thus an extra force or pressure buildup. An inductance component blocks all high frequencies and thus if it is placed in series with the characteristic impedance, it will be the only ruling component at high frequencies. Therefore it only relates to reality if it is used in parallel with the characteristic impedance, although the series composition may yield even better fitting results [164,165]. The value of the inductance in the series model will be a

magnitude lower than in the parallel model, and the value of R_c will be higher, which is out of the physiological range ^[125]. This four-element model can further be extended with another compliance element that represents the compliance of the proximal aorta. It is split off from the total arterial compliance and separated from it with an inductor. In the impedance spectrum, this fifth element seems to result only in a small improvement that does not justify the addition of the extra complexity. Comparison of the flow waveforms generated with this type of model, conversely demonstrates a superior match with human data ^[134]. The key is that the presence of two compliance elements introduces a small resonance into the model, which is not present in any of the other models presented here ^[166].

3.2. Combinations of windkessel models

Windkessel models are mainly used to mimic the systemic arterial system. The whole pulmonary circulation can in fact be neglected, when it is assumed that the blood volume ratio between pulmonary and systemic circulation stays constant (no storage) ^[167]. Nevertheless, windkessel models contain the passive properties of a branched system of elastic vessels and they even incorporate to some extent the sequence of different types of vessels with different properties (elastic vessels before resistive). The same models can also be used to simulate the pulmonary arterial system with adjustments of the resistance, inductance, and capacitance values. A meaningful model for the arterial system, however, may be meaningless for the venous circulation because of the inverted anatomical buildup: venous diameters increase downstream and junctions are present instead of bifurcations. The only model that is useful for both circulations (with adapted component values) is the classic windkessel model because it only simulates basic compliance and resistance. The modified windkessel model takes into account specific behavior at higher frequencies, which is partly due to wave propagation and reflection. This type of behavior is completely different in the venous system and consequently the meaning of R_c in the arterial system cannot be translated to the venous system. The same reasoning can be followed for the four- and five-element windkessel models.

When ventricular assist is simulated with an outflow cannulation to the ascending aorta, the afterload for both heart and pump is the same: the whole arterial system. However, it may be of interest to study the impact of an assist device and the altered flow and pressure patterns on the circulation towards, for instance, the

brain. In that case, the arterial system can be split up in an upper and a lower body part, where the former originates from the aortic arch and combines the carotid and subclavian arteries and their branches. Since that part consists of the same structure of vessel types as the whole arterial system, it can be meaningfully modeled with one of the windkessel models discussed before. This model should be used in parallel with an alike model that simulates the lower body part, with the inclusion of the proper component values. In some cases, however, the outflow graft of a ventricular assist device is anastomosed to the descending aorta because it offers an easier surgical access and for some devices also a more direct flow path (e.g., the ‘Jarvik 2000’ axial rotary blood pump). To simulate this, it is necessary to split up the arterial system in a part downstream of the cannulation site, a part for the upper body, and the part between the aortic root and the cannulation site. In this latter part, the flow generated by the pump will be retrograde, while the heart tries to force an antegrade flow. Since this part is only a piece of large artery, it needs to be modeled with an adapted windkessel, while the other parts can use traditional models.

3.3. Transmission line and T-tube model

Although windkessel models (except for the classic one) try to mimic the high frequency behavior that results from pressure wave propagation and reflection, they do not actually model pressure waves. Taylor was the first to approach arterial hemodynamics with a transmission line model that effectively simulates these pressure waves^[168]. Taylor’s first model was a single transmission line that ended in a high resistance, which can be compared to an elastic tube with a uniform diameter and a closed end. A transmission line is derived from electrical network theory and it allows to calculate the pressure and flow as a function of time and location in the tube. Consequently, the input impedance can be derived from the pressure and flow wave patterns at the inlet of the tube and it can be compared to human data. Such a model has the advantage that there is a spatial distribution of the vascular properties. Further studies with transmission line models revealed that a better approximation could be obtained by modeling the tube as geometrically and elastically tapered, and by using a modified windkessel as a terminal load^[169,170]. Experimental data also revealed that there appear to be two major reflection sites in the arterial circulation: a location near the iliac bifurcation and the head^[171]. The latter results in a faster reflection due to its location closer to the heart. To cope with this dual reflection, the concept of the

T-tube model was developed, where two parallel elastic tubes of different lengths are used that each end in their own terminal load. The short tube represents the upper body part while the long end represents the lower body. This model can accurately simulate mammalian input impedance spectra ^[172]. The basic asymmetric T-tube model is not much more complex than windkessel models: it has only 6 independent parameters if a 3-element windkessel model is used as a terminal load. Such a model may be useful in studying the impact of altered input frequency spectra as a result of the interference of the heart and a pulsatile pump. It further offers the advantage that the impact of an assist device can be studied separately for the upper and lower body part.

3.4. Arterial network models

Since the models above do not take into account the actual arterial geometry, they do not allow to predict pressure and flow at a specific location in the body. This requires mathematical arterial network models that simulate the entire geometry, just as Westerhof did in his analog model with resistors, coils, and capacitors ^[138]. Avolio et al. composed a linear transmission line model of 128 arterial segments ^[173], which is very complicated and difficult to use in simulations. Nevertheless, such complex network models are not very meaningful for ventricular assist device studies.

4. Assist device models

4.1. Cannulas

To simulate the energy losses in the inflow and outflow cannulas of an assist device, several aspects need to be taken into account. Basically, the pressure drop in the cannulas is the result of viscous losses and a resistive component is necessary to model this behavior. When pulsatile devices are used, an additional pressure drop exists due to the acceleration and deceleration of the fluid, and thus an inductance should be added. Still, this also applies to ‘continuous flow devices’, because the interaction with the heart and the varying pressure head may also result in a pulsatile pump flow. Additionally, a compliance component can be added, but this is often superfluous because the used cannulas are very stiff compared to blood vessels. Compliance elements may however be useful to simulate ventricular suction as a result of rotary blood pumps running at high

speed. Vollkron et al. mimicked ventricular suction with a pressure-dependent variable resistance in the inflow cannula ^[155].

4.2. Pumps

4.2.1. Rotary pumps

Various rotary pump models are found in literature. Some only model the hydraulic part, while others include the motor and thus the energy conversion of electrical current to fluid flow. This latter approach is especially of interest to relate the model to parameters that can actually be measured when the device is implanted: consumed power (or current) and rotational pump speed. Models can be created to validate parameter estimation methods where the current and speed are used to estimate ventricular contractility, or other parameters of the circulation that otherwise require invasive measurement techniques. The simulation of the motor is also necessary for development and validation of physiological control algorithms for rotary blood pumps. These are necessary to provide higher flows when a patient becomes more active, and also to limit the risk of ventricular suction.

An example of a purely hydraulic model of a rotary pump is the model used for numerical simulations of the current CorAide centrifugal pump (Arrow Int., Reading, PA) while it was still in a development phase ^[174]:

$$Q^2 = \pm |3.571 \cdot 10^{-5} \cdot \omega^2 - 2.838 \cdot \Delta p - 12.66| \quad [\text{Eq. III-18}]$$

with:

Q: pump flow (l/min)

ω : impeller rotational speed (rpm)

Δp : pressure head over the pump (mmHg)

Below is an example of a model including the electromechanical relations, where the current can be used as an input or controllable parameter ^[175]. [Eq. III-19] defines the hydraulic characteristics of the device (an axial rotary pump) while [Eq. III-20] defines the function of the brushless DC electromotor and relates the current to the electromagnetic force, the resulting torque, and the torque of the load in function of the flow (last term).

$$\frac{dQ}{dt} = -b_0 \cdot Q - b_1 \cdot \omega^2 + b_2 \cdot \Delta p \quad [\text{Eq. III-19}]$$

$$J \frac{d\omega}{dt} = \frac{3}{2} \cdot K \cdot I - B \cdot \omega - a_0 \cdot \omega^3 + a_1 \cdot Q \cdot \omega^2 \quad [\text{Eq. III-20}]$$

with:

- Q: pump flow (m^3/s)
- ω : impeller rotational speed (rad/s)
- Δp : pressure head over the pump (N/m^2)
- J: impeller inertia ($\text{kg}\cdot\text{m}^2$)
- K: constant of back electromagnetic force ($\text{V}\cdot\text{s}$)
- I: motor current (A)
- B: damping coefficient ($\text{kg}\cdot\text{m}^2\cdot\text{s}^{-1}$)
- a_0, a_1, b_0, b_1, b_2 : constants

4.2.2. Pneumatic displacement pumps

With the modeling of displacement pumps, more parameters need to be taken into account. Of importance are the stroke volume and the filling and ejection timing. These pumps can again be modeled only as a hydraulic component, or with inclusion of the actuation mechanism. The latter option allows to simulate control algorithms, which can be based on feedback from specific sensors. The Thoratec pneumatic VAD, for instance, has a switch to indicate when the blood chamber is completely filled. Pneumatically actuated pumps often also incorporate a means to monitor the air flow rate to and from the pump to estimate the blood flow generated by the pump. The derivative of the air flow from the pump can also be an indicator for the contractility of the ventricle.

The older driving consoles of pneumatic assist devices are based on alternate switching between pressure reservoirs (vacuum and positive pressure) with an electronically controlled valve. Simple mathematical models of the hydraulic part of pneumatic displacement pumps are based on this principle, where a positive and a negative constant voltage source in the electric analog represent the pressure reservoirs. More sophisticated models that integrate control need to use time-varying voltage sources or combine the sources with controlled resistances. The tubes between the driver and the air chamber of the pump are often modeled similar to cannulas, but a compliance component (capacitor) is mandatory in this case to simulate the compressibility of the air.

The pump chamber of a pneumatic actuated device contains a sac or a membrane to separate the air from the blood. Often, the pump housing is slightly larger than the membrane in unstressed state, leaving a gap between the two. When the pump is then actuated, the membrane's elastic properties come into play at the end of ejection and at the end of the filling. At that time, the membrane cannot

rest against the housing and will be stretched out by the pressure difference between blood and air chamber. At other times in the pump cycle, there will be a balance between the pressure in both chambers, and the membrane will be unstressed, and in reality even wrinkled. A volume dependent compliance component can be used to model this behavior of the membrane, where compliance is only present below and above certain volume thresholds. The elasticity of the membrane is not necessarily equal in both directions: stretching towards the blood side may show a different compliance than stretching towards the air side. This is due to the multi-layered composition of certain membranes and to the unstressed shape of the membrane. The compliance of the membrane can be combined with the compliance of the gas and the values can be determined experimentally.

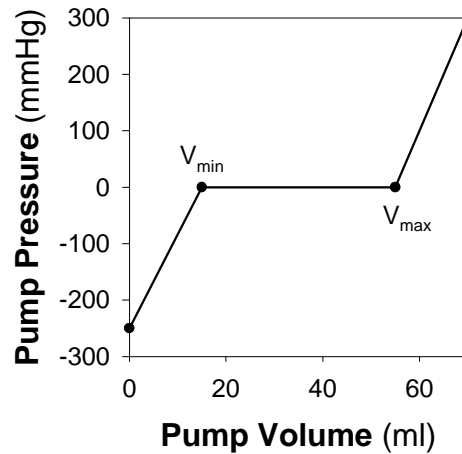


Fig. III-7: Pressure-Volume relation of a pneumatically actuated assist device with a stroke volume of 70 ml. V_{\min} : 15 ml, V_{\max} : 55 ml. Suction compliance: 0.06 ml/mmHg, Ejection compliance: 0.05 ml/mmHg.

An example of a constitutive equation for a pneumatic displacement pump can therefore be presented with the equation below, which refers to Fig. III-8.

$$\frac{a \cdot p_s + (1-a) \cdot p_d - p_p(t)}{a \cdot R_s + (1-a) \cdot R_d} = Q_i(t) - Q_o(t) + C(V) \cdot \frac{dp_p(t)}{dt} \quad [\text{Eq. III-21}]$$

The constant 'a' is a binary term that determines the activation of the pump: the pump ejects when 'a' is 1, while it fills when 'a' equals 0. So 'a' simulates the control of the electronic valves and it determines the pump rate.

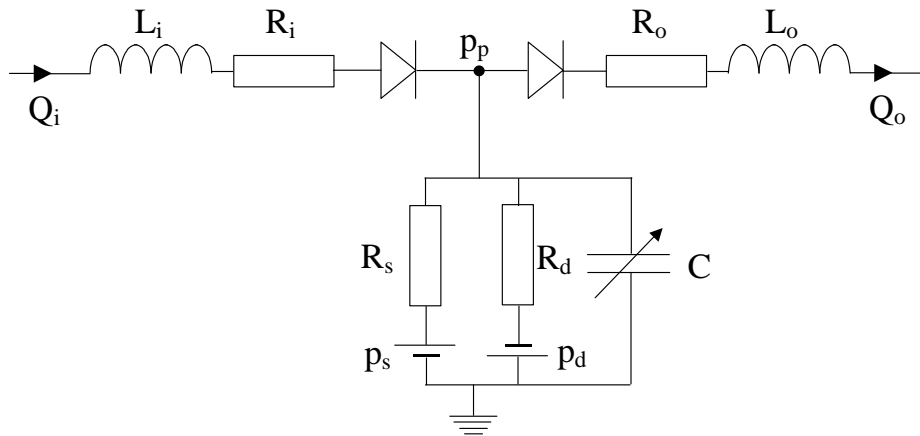


Fig. III-8: Electric analog of a pneumatic displacement pump. Q_i , Q_o : blood inflow and outflow, respectively; L_i , L_o : inductance of cannulas; R_i , R_o : resistance of cannulas and valves; p_p : pump pressure; R_s , R_d : resistance of the pneumatic tubing for pump systole and diastole, respectively; p_s , p_d : positive pressure and vacuum in the pressure reservoirs; C : pump compliance.

4.2.3. Electromechanical displacement pumps

Simulation of a mechanically actuated displacement pump can again be performed by either modeling only the hydraulic part or the hydraulic part in combination with the actuator. However, these devices are more complex than the ones described in the previous sections, and they usually incorporate more or better sensors to feed back information to the controller. Each actuation mechanism results in a specific pressure or flow waveform and therefore this type of device should be modeled with the inclusion of the actuation mechanism. If desired, the control algorithms used by the controller can also be implemented, or algorithm prototypes can be simulated. As a result of the combination of control algorithm and actuation mechanism, it is not possible to model these devices with a time-varying compliance or elastance, as is the case for the heart. More complicated experiments and fitting techniques are usually required to obtain a model that eventually gives pressure and volume as a function of time, preload, and afterload. The model discussed below simulates the function of the Novacor N100 assist device (see also Fig. I-32), which is in fact a magnetically actuated device.

In summary, the device contains a valved blood sac with a pusher plate on either side. Each pusher plate is connected to one end of a beam spring, while the other ends of the springs are fixed in a frame with a central pivot. Thus the springs can rotate towards each other and compress the sac. To actuate the springs, each

frame half contains an electromagnet, and powering the magnets results in a collapse of the frame (latching) which flexes the springs and loads them. The springs will flex back to their unloaded geometry by moving the pusher plates and squeezing the blood out of the sac.

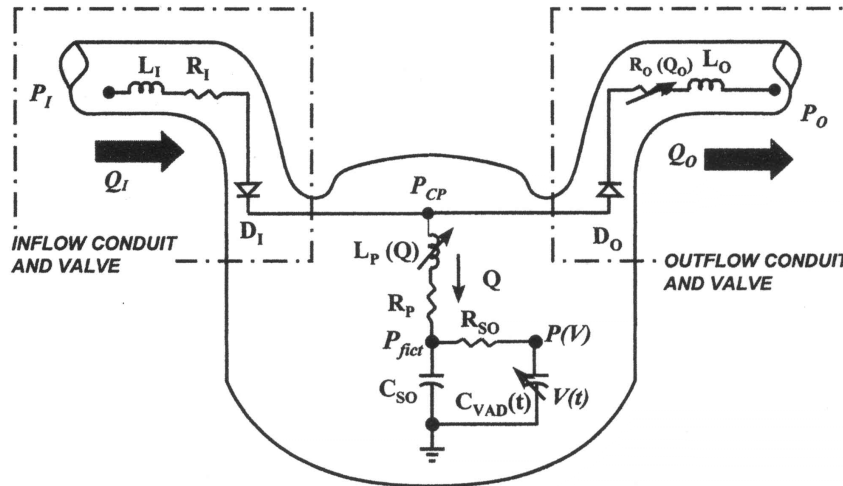


Fig. III-9: Electric analog of a mathematical model of the Novacor N100 device^[176]. See text for description of the parameters.

To model the pump function of the Novacor N100, the actuator is simulated in 2 parts: the spring and the latching system^[176]. A combination of a capacitance (C_{so}) and a resistor (R_{so}) is used to model the dynamic behavior of the latching (solenoid) system, where $R_{so} \cdot C_{so}$ forms the time constant of solenoid closure. A time varying capacitance (C_{VAD}) simulates the spring behavior. Consequently, the $P(V)$ point in the model describes the static pressure-volume relation that is only dependent on the springs. The solenoid parameters and the C_{VAD} function were derived from isovolumic beats at different volumes. Mock loop experiment data allowed to refine the model by adding a resistor (R_p) and a flow-dependent inductance ($L_p(Q)$) to simulate the dynamic fluid behavior, i.e., the viscosity and inertia effects. All together, these parameters and functions allow to compute the pump chamber pressure (P_{cp}) as a function of the instantaneous pump volume $V(t)$, and it can therefore be implemented in a model of the cardiovascular system. Yu et al. modeled the cannulas of the device as described in section 4.1, with the exception of the outflow cannula resistor: a flow dependent resistor was used to better match the experimental data. Presumably this correction is necessary because of the turbulent flow pattern at the outflow.

B. THE HYDRAULICS LABORATORY MATHEMATICAL MODEL

1. Introduction

The mathematical model developed at the Hydraulics Laboratory of Ghent University is intended for studies of heart-arterial load interaction. It is developed in Matlab 5.0 (The MathWorks Inc., Natick, MA) and makes use of the ODE45 solver for the computation of variables that are embedded in differential equations.

The mathematical model has previously been validated in several forms. In one study it was used to predict the stroke volume and aortic blood pressure in sheep, where the model generated data proved to accord well with experimental data ^[150]. In another study, normotensive and hypertensive patients were simulated to assess the concept of wall stress normalization as an initiator for left ventricular hypertrophy ^[19]. The maximum discrepancy between modeled and simulated diastolic blood pressure was 7% and for systolic pressure it measured 4.8%.

In this work, the existing basic model was extended to allow simulation of rotary blood pumps. In particular pulsatile control of these devices was studied. It has not been the intention to simulate or predict specific clinical situations, but the goal was to indicate the impact of this new concept on left ventricular load. In its current form, the model does not work with a fixed volume of blood and cannot simulate effects of bleeding or infusion. All simulations were performed with a cardiovascular model matched to sheep data to allow validation with available animal data. Yet, the model composition was chosen as basic as possible to minimize the number of assumptions and estimations and to eliminate the need for parameters from literature data. All necessary parameters for this basic model can be derived from an animal experiment where left ventricular pressure and volume and aortic pressure and flow are acquired. Even though sheep with induced heart failure were used as a reference for some studies (see chapter IV), it should be taken into account that clinical heart failure is usually more severe than it can be modeled in animals.

2. Cardiac model

2.1. Elastance

The cardiac model is restricted to the left heart, with the option to include or exclude the atrium. Both heart chambers are modeled according to the original time-varying elastance theory, where the EDPVR is assumed linear. The elastance curve can be chosen from a normalized curve that is implemented as a Fourier series, or a double Hill curve. The choice of elastance curve only determines the shape, since this curve has been normalized in time and amplitude. In a next step a rescaling is performed based on the other parameters that can be set for each heart chamber. These parameters are the maximum and minimum elastance (E_{\max} , E_{\min} , resp.), the heart rate (HR), and the time of maximal elastance (T_{\max}). Additionally, the volume intercept (V_0) needs to be set, but this is not required for the elastance curve.

A disadvantage of the linear time-varying elastance concept is that the diastolic filling in the pressure-volume plane is linear instead of curved. This is, however, only the case if a predefined elastance curve with a flat diastolic phase (e.g., the double-Hill curve) is used, as the filling of the heart chamber will then be prescribed completely by the linear EDPVR. This can be prevented by creating a custom elastance curve where the diastolic part is not flat. In this case only the minimum of the elastance curve will actually fall on the EDPVR line. The non-linearity of the real EDPVR is then in fact incorporated in the elastance curve. The remaining discrepancy with reality will be the effect of large volume shifts, where the PV-loop in this model will be trapped between linear boundaries, while in reality it are curvilinear boundaries. This will result in an underestimation of filling pressure when dilation of the heart is modeled. Conversely, the linear approach of the ESPVR may result in an overestimation of systolic LV pressure in the simulation of hearts with extremely large volumes: the ESPVR is believed to curve down towards the volume axis as of a certain volume. Different *in vivo* ESPVR characteristics can be found depending on the type of contraction (e.g., isovolumic, isotonic^[155]) and both convex and concave curvature have been reported for the lower volume range^[177,178]. Therefore, the choice for a curved ESPVR is not obvious.

In summary, the cardiac model is an approximation that is not valid for a seriously decompensated heart as seen in terminal patients, but it can be used to model heart failure as it is observed in animal models.

Table III-1: Fourier series data for human and sheep normalized elastance curve

harmonic -	HUMAN		SHEEP	
	Modulus M (mmHg/ml)	phase ϕ (rad)	Modulus M (mmHg/ml)	phase ϕ (rad)
0	0.2839	0	0.2251	0
1	0.3759	0.0837	0.2771	0.6298
2	0.2102	-1.4868	0.2227	-0.3252
3	0.0767	2.8657	0.1491	-1.3229
4	0.0481	0.1677	0.0767	3.8192
5	0.0418	4.6302	0.0326	2.0308
6	0.0194	3.0884	0.0395	0.0551
7	0.0059	-0.3054	0.0450	-1.1606
8	0.0118	4.4107	0.0355	4.0587
9	0.0084	3.1815	0.0187	2.9214
10	0.0002	1.2429	0.0067	0.9517
11	0.0031	4.1568	0.0108	-1.0987
12	0.0032	2.9462	0.0125	4.0776

$$E_n = M(0) + \sum_{h=1}^{12} [M(h) \cdot \sin(h \cdot 2\pi f \cdot t + \phi(h))]$$

E_n : normalized elastance function

h: harmonic number

f: harmonic frequency: 0.2890 Hz for human and 0.2 Hz for sheep

A means to implement a custom (normalized) elastance curve is the Fourier series description (Table III-1). This is available for humans from literature ^[10], and for sheep from own experimental data. An example of both reconstructed curves is shown in Fig. III-10, scaled for an identical contractility and heart rate. The normalized sheep elastance was constructed with pressure-volume data of four healthy sheep and 2 sheep with induced chronic heart failure by injection of microspheres ^[179]. After determination of V_0 from caval vein occlusion data, the real elastance curve for each sheep was calculated from an averaged beat. The data were then normalized with respect to time and amplitude, so the maximal elastance was 1 and it appeared at time 1, where time and elastance are both non-dimensional measures. Next, the data were consecutively resampled in order to

obtain the same time step, averaged over all the animals, and decomposed in Fourier components. A subprogram in the mathematical model recomposes the Fourier series up to the 12th harmonic with the time step that is also used in the solver of the differential equations, so no further interpolation is required. The obtained normalized curve is then rescaled according to E_{\max} , E_{\min} , HR, and T_{\max} given by the user. T_{\max} is set at 30% of the heart period by default, but it can and should be adjusted by the user. Since no control of the heart rate according to autonomous nervous activity was incorporated, an algorithm for determination of the systolic/diastolic time ratio was superfluous. In most cases, the simulations will be based on actual experimental data and thus the actual T_{\max} can be determined, without the use of an estimation algorithm.

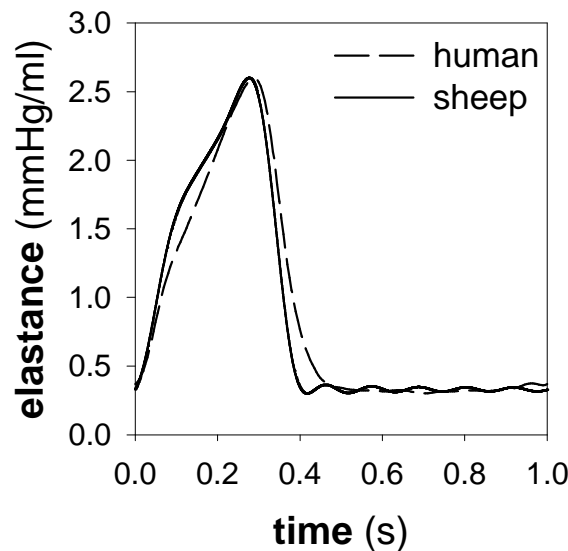


Fig. III-10: Reconstructed left ventricular elastance curves for sheep and humans at a heart rate of 60 BPM. $E_{\max} = 2.6$ mmHg/ml. $E_{\min} = 0.3$ mmHg/ml.

2.2. Preload

Since the right heart is completely neglected in this mathematical model, the preload of the left heart needs to be decoupled from the afterload in another way. A common approach is the use of a constant pressure (voltage) source between the afterload and the atrium ^[180-182]. This method simulates a constant pulmonary venous filling pressure which roughly approximates reality because the pulmonary circulation is a very compliant circuit with a low pressure source. The venous filling pressure can be set by the model user and it can be derived from animal experiments as the end-diastolic atrial pressure or pulmonary venous pressure, although these data are rarely available.

2.3. Valves

The mitral and aortic valves are basically modeled as a resistor in series with an inductor. Leakage is also included and consequently the electric analog of the valves can be seen as a parallel circuit of two resistor–inductor combinations with a diode in each branch. The diodes are opposed to each other and their purpose is to determine the flow direction through the valve in function of the pressure (voltage) difference. The practical method in the model is the comparison of downstream and upstream pressure. If upstream pressure is highest, then forward flow will open the valve and the resistor-inductance combination with the lowest values will be used so a high flow and small pressure drop will be present over the valve. In the opposite case, the combination with the highest resistance value is used which will result in a small backward (regurgitant) flow. The resistance and inductance values of the valves can be set manually for forward and backward flow. The default values are taken from literature and from fitting procedures on experimental data.

2.4. Wall stress

According to Arts et al., wall stress in the left ventricle is homogenous so it can be represented by one indicative number ^[20]. The cardiac model therefore allows to estimate the wall stress in the left ventricle as a single parameter over the time course of the cardiac cycle. For this, the ventricle is modeled as an isotropic, homogeneous thick-walled ellipsoid as depicted in Fig. I-20 and the meridional wall stress at the equator is calculated according to [Eq. III-22], which is a replicate of [Eq. I-5] in chapter I.

$$\sigma_m = \frac{p_{LV} \cdot D^2}{4 \cdot h \cdot (D + h)} \quad [\text{Eq. III-22}]$$

with:

- σ_m : meridional wall stress at the equator (mmHg)
- p_{LV} : left ventricular pressure (mmHg)
- D: internal ventricular diameter (cm)
- h: wall thickness (cm)

The internal diameter of the left ventricle is required for this calculation, just as myocardial wall thickness (h). The diameter is computed from a formula used in echocardiography ^[183], that relates the ventricular volume (V_{LV} (ml)) - which is a variable in the mathematical model - to the internal diameter.

$$V_{LV} = \frac{7 \cdot D^3}{2.4 + D} \quad [\text{Eq. III-23}]$$

Because wall thickness is rarely measured and recorded in animal experiments, an estimation of the variations in wall thickness throughout the cardiac cycle is used. It is based on the knowledge that the myocardial wall volume (V_{wall}) is constant. So, if wall volume and instantaneous internal volume are known, the outer dimensions and wall thickness of the ellipsoid can be computed. To calculate the wall volume, an arbitrary value of end-systolic wall thickness is assumed (e.g., 1) and the resulting wall stress data should be interpreted as normalized with respect to end-systole.

$$\sigma_c = \frac{p_{LV} \cdot D \cdot (2 \cdot L^2 - D^2)}{4 \cdot h \cdot (L^2 + D \cdot h)} \quad [\text{Eq. III-24}]$$

with:

σ_c : circumferential wall stress at the equator (mmHg)

L: long axis dimension (cm)

Circumferential stress can be calculated according to [Eq. III-24] (replicate of [Eq. I-6]), which additionally requires the internal long axis length (L) of the ellipsoidal model. Because the model is assumed axisymmetric, and the diameter (D) and internal volume are already known, its internal length can be calculated from the standard formula for volume calculation:

$$V_{\text{ellipsoid}} = \frac{4}{3} \cdot \pi \cdot D^2 \cdot L \quad [\text{Eq. III-25}]$$

It was found that this method yields only very little variation of the long-axis dimension L and, consequently, the circumferential wall stress calculated with this method was deemed unreliable. Furthermore, according to Arts et al., circumferential stress is very much dependent on the geometry, and an ellipsoidal approximation is not a good starting point for calculation of that type of stress^[20]. The result depends on the curvature, and thus higher stresses are found at the equator compared to the top of the ellipsoid. The circumferential stress calculated according to [Eq. III-24] is in fact the equatorial stress, which is therefore an overestimation of mean stress.

The three variables necessary for fiber stress calculation according to [Eq. III-26] (replicate of [Eq. I-7], suggested by Arts et al.) are already computed for the

meridional wall stress, and consequently a calculation of the fiber stress (σ_f) is easily implemented in the cardiac model.

$$\sigma_f = \left(1 + 3 \cdot \frac{V_{LV}}{V_{wall}} \right) \cdot p_{LV} \quad [\text{Eq. III-26}]$$

The three possible stress calculations were compared on a set of *in vivo* data, with special attention to the waveform morphology over a heart cycle. In most cases the end-systolic wall thickness will be set at 1 cm and ‘normalized stress’ will be compared between simulations, so that the amplitude of the different types of wall stress is of lesser importance. For comparison, the circumferential and meridional wall stress were scaled to match the maximum of fiber stress. It can be noted that the variation in meridional wall stress and fiber stress fit closely, while circumferential stress deviates from those two. The relatively simple approach of the thick walled ellipsoid and the resulting meridional stress calculation of Falsetti et al. was recommended previously as a parameter that suffices for clinical evaluation of myocardial wall stress^[184].

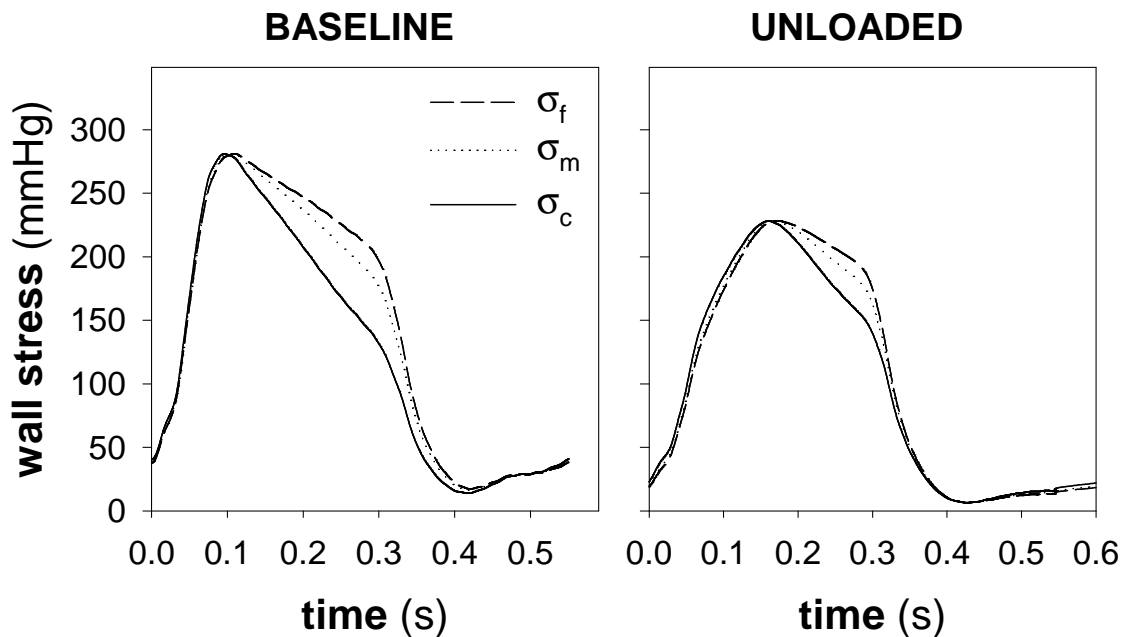


Fig. III-11: Example of different wall stress calculation methods applied on sheep data at baseline and with support of a rotary pump (unloaded) that produced 3.5 l/min. σ_f : muscle fiber stress. σ_m : meridional wall stress. σ_c : circumferential wall stress. σ_m and σ_c are rescaled to match the amplitude of σ_f . The original maxima of σ_c and σ_m were respectively 310.0 and 81.7 mmHg at baseline and 183.4 and 61.4 mmHg when unloaded.

3. Afterload model

Two options for the afterload model are programmed and can be selected: a three-element windkessel model and a four-element windkessel model, which both have been discussed before. The three-element model is the modified windkessel model consisting of a characteristic resistance in series with a parallel combination of a resistance and compliance element ^[128]. The four-element model has an additional inductance in parallel with the characteristic resistance ^[125]. Even though the series combination of the inductance and characteristic resistance tends to give better results for data fitting, the parallel combination was implemented because it relates more closely to the actual physiological afterload. This model, just as all the others, is solved in the time domain.

To obtain the parameters of the windkessel model from an animal experiment, a fitting procedure can be applied similar to the one used for the *in vitro* model validation (chapter V, section B). A separate program is available for this and it requires pressure and flow waveforms that are measured at the aortic root. In summary: aortic flow is offered as input to the afterload model and the resulting calculated aortic pressure is compared to the actual measured pressure. The values of the afterload model components are adjusted to minimize the error between measured and calculated pressure and the best fit yields parameter values that represent the real arterial system in which the data was acquired. It is important that the data are measured synchronously and at the same site, or that time delays are corrected. It is important to realize that the resulting parameters characterize the considered arterial system in a specific condition. Interventions may alter the system, e.g., by inducing vasodilation, and thus the parameters need to be adjusted or recalculated from another data set. The fitting program models the afterload in the frequency domain, which offers identical results to a time domain approach but in a more flexible way.

4. Assist device model

The mathematical model studies discussed in this dissertation (chapter IV, sections B and C) focus on a specific rotary blood pump: the Medos-HIA microdiagonal pump. More details on the device and its intended application are discussed in the following chapter. Since it is still in a development phase, all studies were performed with a prototype of the pump. The pump and the cannulas were modeled separately because the pump is only available in one size, while the cannulas can vary in size and are cut at length by the surgeon during the implantation. Only the hydraulic part of the pump is modeled and the only pump parameter that can be set by the user is the rotational speed of the impeller. The device is modeled as to simulate apical to ascending aorta cannulation, and the cannulas are assumed to be cylindrical. Consequently, the length and diameter of the inflow cannula and of the outflow cannula are the remaining four parameters that can be set.

The microdiagonal pump model was obtained from fitting procedures on experimental data acquired from the Helmholtz Institute Aachen. The basic experimental data consist of standard pressure head-flow measurements of the pump when running at different speeds. A broad range of pressure heads and according flows was obtained by varying the afterload resistance. Apart from the different speeds, data were also acquired when the pump was switched off as to simulate pump failure. These data characterize the hydraulic viscous losses over the pump and were performed with both forward and backward flow. The different flow levels through the switched off pump were achieved with an extra pump. Note that backward flow can also occur *in vivo*, even when the pump is running: in diastole aortic pressure is higher than left ventricular pressure, and thus a negative pressure head will be imposed on the pump. If it is running at a low rotational speed, the pump may not generate sufficient power to overcome this pressure head, and blood will regurgitate from the aorta to the ventricle. This situation was not mimicked in the experimental setup. To attain pump characteristics of backward flow through a running pump, the forward flow characteristics were mirrored by switching the sign of the pump resistance (see below).

In electrical network theory, a realistic voltage source can be considered as a series combination of an ideal voltage source and a resistor that models the

energy losses. Analogous, a rotary pump can be considered as the combination of an ideal pressure source and a resistive element. Consequently, the pump can be modeled as the sum of a term in function of the rotational speed (generated energy) and a term in function of the flow (energy losses). Since the flow pattern in the pump can be expected to be turbulent, the pressure loss in the pump will correlate to the square of the flow, rather than to the flow itself. The resulting pump equation, that was used to fit the data, is given below.

$$\Delta p = A \cdot \omega^2 + R_p \cdot Q_p^2 \quad [\text{Eq. III-27}]$$

with:

- Δp : pressure head over the pump (mmHg)
- A: pump constant (mmHg/rpm²)
- ω : rotational speed (rpm)
- R_p : pump resistance (mmHg·min²/l²)
- Q_p : pump flow (l/min)

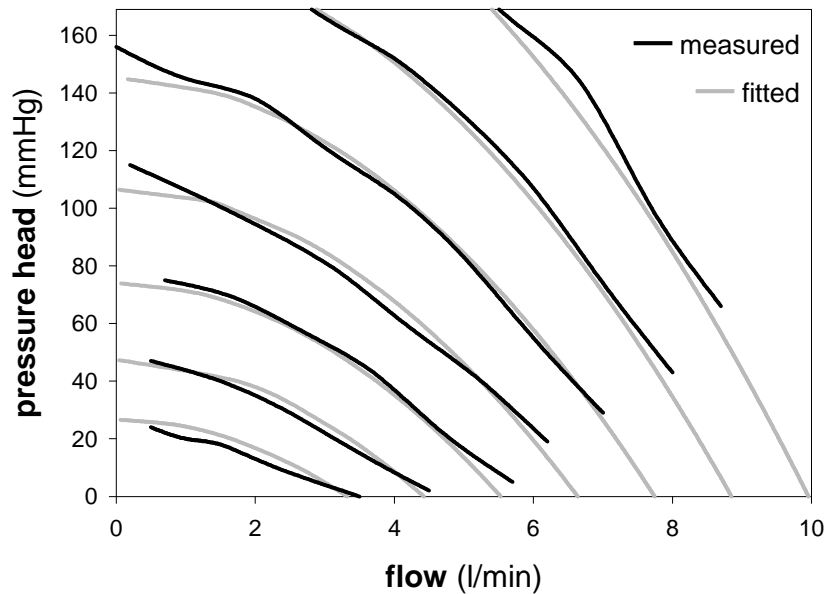


Fig. III-12: Example of the fit of [Eq. III-27] on a data set of the microdiagonal pump ($r^2 = 0.99$). The rotational speed was varied from 3000 rpm (most left plot) to 9000 rpm (most right plot) with a 1000 rpm increment. The final parameters of the fit are:
 $A=2.956 \cdot 10^{-6}$ mmHg/rpm² and $R_p=-2.415$ mmHg·min²/l².

To offer flexibility for future implementation of other devices, the pump equation is in fact rewritten in the following form:

$$Q_p^{\alpha_1} = \alpha_2 \cdot \omega^{\alpha_3} + \alpha_4 \cdot \Delta p^{\alpha_5} + \alpha_6 \quad [\text{Eq. III-28}]$$

The α parameters in this equation are constants that are stored in a separate file, containing other possible pump models in the same format. In the model of the microdiagonal pump, α_2 and α_4 represent A and R_p from [Eq. III-27], respectively, while α_3 and α_5 are 2. These parameters can be retrieved from the pump model file for combination with the cannula model.

The cannula model consists of a series combination of an inductor and a resistor for each cannula. The values of these components are calculated from the cannula dimensions as given by the user. The extra pressure drop generated by the cannulas is then:

$$\Delta p_c = \Delta p_L + \Delta p_R \quad [\text{Eq. III-29}]$$

$$\Delta p_c = (L_i + L_o) \cdot \frac{dQ_p}{dt} + (R_i + R_o) \cdot Q_p^2 \quad [\text{Eq. III-30}]$$

with:

Δp_L : pressure drop due to inertance effects (mmHg)

Δp_R : pressure drop due to viscous effects (mmHg)

Δp_c : pressure drop over the cannulas (mmHg)

L_i : inlet cannula inertance (mmHg·min²/l)

L_o : outlet cannula inertance (mmHg·min²/l)

R_i : inlet cannula resistance (mmHg·min²/l²)

R_o : outlet cannula resistance (mmHg·min²/l²)

The inertance L of a cylindrical tube is given by:

$$L = \frac{4 \cdot \rho \cdot l}{\pi \cdot D^2} \quad [\text{Eq. III-31}]$$

The flow through the cannulas is expected to be laminar, given the dominantly low Reynolds numbers ($Re < 3000$). Therefore the resistance is characterized by a linear relation between pressure drop and flow ($\Delta p \sim Q$). However, to be conform with [Eq. III-27] and to allow an easier implementation in the model, the relation was inserted in [Eq. III-30] as being quadratic ($\Delta p \sim Q^2$). To transform this back to a linear relationship, the pump flow (Q_p) was included in the denominator of the resistance calculation. The linear pressure drop due to resistance (Δp_R) is thus calculated from the Poiseulle equation for laminar flow:

$$\Delta p_R = \frac{64}{Re} \cdot \frac{1}{D} \cdot \rho \cdot \frac{u^2}{2} \cdot \frac{1}{133.33} \quad [\text{Eq. III-32}]$$

$$\Rightarrow \Delta p_R = \frac{32 \cdot v \cdot l \cdot \rho}{u \cdot D^2} \cdot \frac{Q_p^2}{A^2} \cdot \frac{60 \cdot 10^6}{133.33} \quad [\text{Eq. III-33}]$$

$$\Rightarrow \Delta p_R = \frac{32 \cdot v \cdot l \cdot \rho}{Q_p \cdot D^2 \cdot A} \cdot \frac{60 \cdot 10^3}{133.33} \cdot Q_p^2 \quad [\text{Eq. III-34}]$$

$$\Rightarrow \Delta p_R = \frac{128 \cdot \mu \cdot l}{Q_p \cdot \pi \cdot D^4} \cdot \frac{60 \cdot 10^3}{133.33} \cdot Q_p^2 = R_{i,o} \cdot Q_p^2 \quad [\text{Eq. III-35}]$$

with:

Re = u · D/v: Reynolds number (-)

u: fluid velocity (m/s)

D: cannula diameter (m)

l: cannula length (m)

ρ: fluid density (kg/m³)

v: dynamic fluid viscosity (m²/s)

μ = v · ρ: kinematic viscosity (N·s/m²)

In these equations, flow and pressure are respectively expressed in l/min and mmHg and the other variables in SI units. As a consequence of expressing the resistive behavior as a quadratic relationship, the pump flow is in the denominator of the cannula resistance ($R_{i,o}$) which makes it a flow dependent variable. The alternative is to express the resistive behavior as a linear relationship, which would give a non-flow dependent resistance. However, the dimensions of R_i and R_o would differ from the dimensions of R_p and as a consequence they would make two separate terms in the resulting differential equation. A combination of the formulas above leads to a differential equation that describes the hydraulic part of the assist device in the following form:

$$p_{ao} - p_{LV} = A \cdot \omega^2 + R_{tot}(Q_p) \cdot Q_p^2 + L_{tot} \cdot \frac{dQ_p}{dt} \quad [\text{Eq. III-36}]$$

with:

p_{ao} : aortic pressure (mmHg)

p_{LV} : left ventricular pressure (mmHg)

$R_{tot} = R_p + R_i + R_o$: flow dependent resistance (mmHg·min²/l²)

$L_{tot} = L_i + L_o$: cannula inertance (mmHg·min²/l)

Additionally, the assist device model was extended with the option to modulate the rotational speed throughout the cardiac cycle. This is a simulation of synchronous pulsatile use of rotary blood pumps. Two additional parameters need to be set: the type of modulation and the phase shift between the pump cycle and the heart cycle. This latter is set in percentage of the total cycle. There

are three types of modulation, besides the option to have a constant speed. Each type was scaled in order to have a peak to peak difference of 4000 rpm and set off to obtain a mean rotational speed equal to the speed value set by the user. The implemented modulation waveforms are: an inverted elastance curve, a negative part of a sine wave, and an inverted complete sine wave (Fig. III-13).

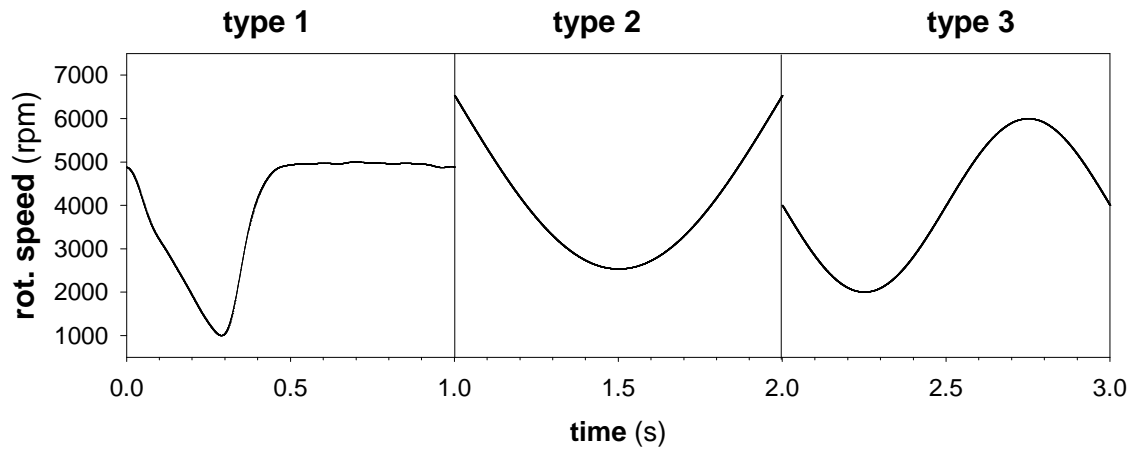
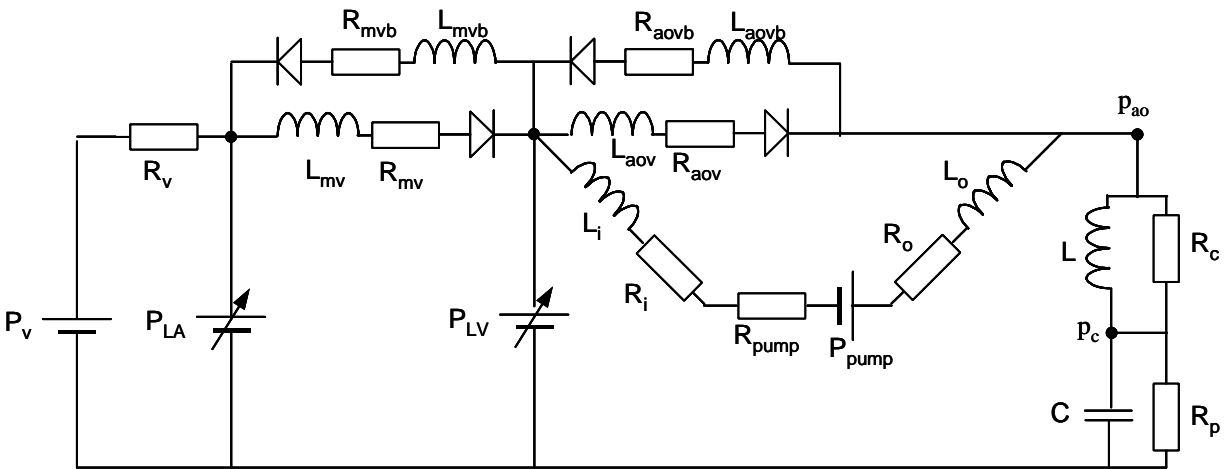


Fig. III-13: Illustration of the three rpm modulation types that are implemented in the mathematical model. All modulations have a peak to peak value of 4000 rpm and an average of 4000 rpm.

5. Program setup

5.1. Overview of all the model components



Components: L: inductor (inertance). C: capacitor (compliance). R: resistor (resistance). P: voltage (pressure) source.

Indices: v: venous. LA: left atrium. LV: left ventricle. mv: mitral valve. mvb: mitral valve backward. aov: aortic valve. aovb: aortic valve backward. i: in. o: out. c: characteristic. p: peripheral

Variables: pao: aortic pressure. pc: pressure before the peripheral resistor

Fig. III-14: Electric analog of the Hydraulics Laboratory mathematical model. Since it is possible to include or exclude certain parts, the model should be visualized with the addition of switched bypasses.

5.2. Program sequence

When all the required parameter values are inserted via the user interface and a simulation is started, the program determines the appropriate solver. Because valves can be simulated as a simple resistor or a resistor-inductor combination, and because there is a choice of pump and afterload models, several solvers were implemented. The following discussion assumes the presence of an atrium and a rotary pump in the chosen solver, relating to the whole model as depicted in Fig. III-14.

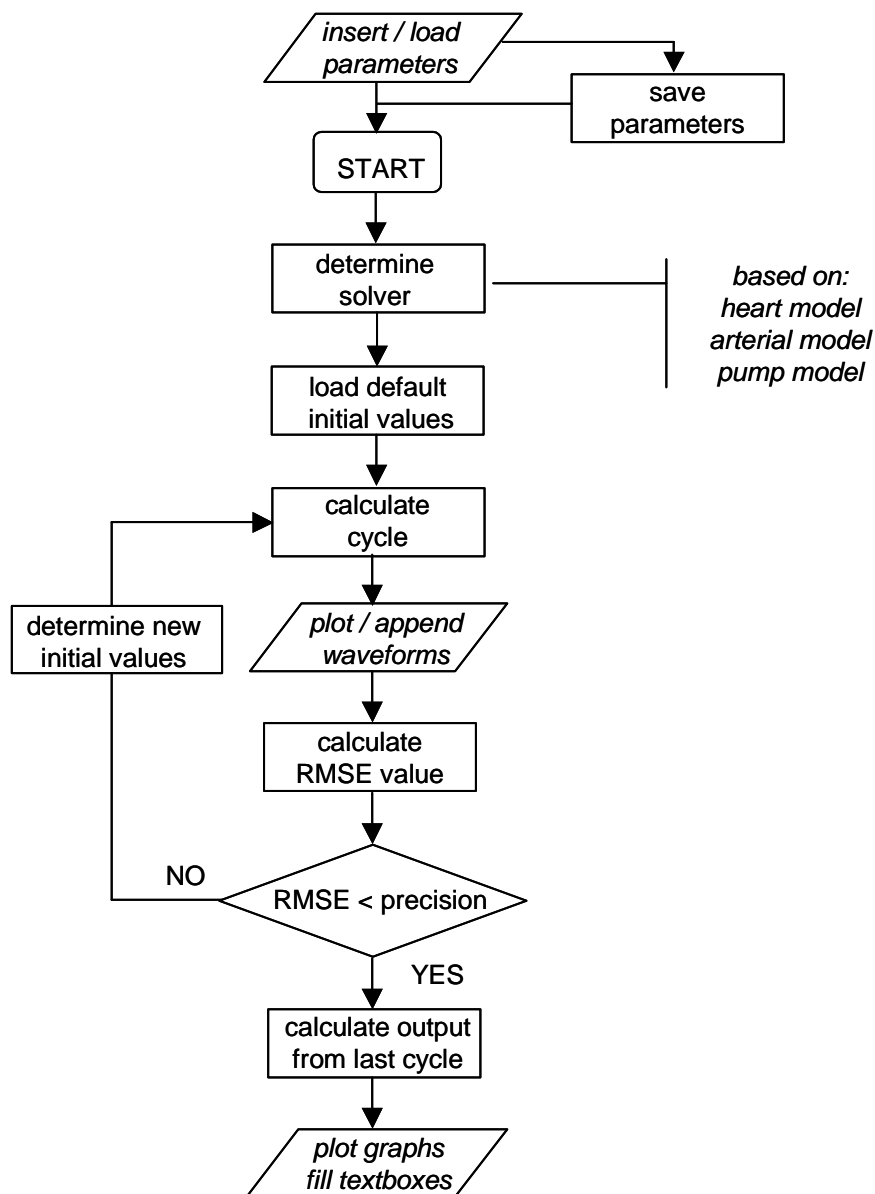


Fig. III-15: Simplified flow chart of the mathematical model simulation sequence.
RMSE: root mean squared error.

The selected solver starts with calculation of the inductance and resistance values of the pump cannulas and with determining the A and R_p values of the pump model (see [Eq. III-27] and [Eq. III-28]).

The solver will then create an empty vector for each variable, where the length is determined by the time step and the heart rate as given by the user. The rotational speed of the pump will also be calculated as a vector, as a function of the type of modulation and the phase shift that is chosen. Initial estimates for the first time point of each variable are also set by the solver before it actually solves the differential equations with Matlab's ODE45 function for every time point of one cardiac cycle. There are seven state variables in the complete model:

- flow through the mitral valve (Q_{mv})
- flow through the aortic valve (Q_{ao})
- flow through the pump (Q_p)
- the pressure proximal to the arterial compliance (p_c)
- the aortic pressure (p_{ao})
- left ventricular volume (V_{LV})
- left atrial volume (V_{LA})

Once these are solved over the heart period, further output variable vectors are derived from them: left ventricular pressure and left atrial pressure. Since the volumes of these heart chambers are known from the calculation, the pressures can be derived with the original elastance formula from Suga and Sagawa ([Eq. III-1]). A temporary output is then plotted on the user interface so the user can follow the progress of the simulation. Next, the values of the state variables at the end of the cardiac cycle are used as the initial values for the following cycle. The differential equations are then solved for a second time, the output variables are calculated once more and this second cycle is plotted adjacent to the first cycle on the user interface. Before continuing the simulation, a convergence criterion is tested: the root mean squared error (RMSE) value of the aortic pressure between the last beat and the previous beat is compared to a preset precision that is entered by the user at the start of the simulation (default: 2 mmHg). The RMSE value is defined as:

$$\text{RMSE} = \sqrt{\frac{1}{n} \cdot \sum_1^n [p_{\text{ao}}(n)_C - p_{\text{ao}}(n)_{C-1}]^2} \quad [\text{Eq. III-37}]$$

with:

- n: number of time points in a heart cycle (-)
- p_{ao} : aortic pressure (mmHg)
- C: last calculated cycle
- C-1: previous cycle

If the RMSE value is lower than this precision, convergence is assumed and the simulation is halted. Otherwise a following cycle is calculated until convergence is achieved. In case divergence is detected, the initial values for the following beat will be taken as the average of the end values of the previous two beats, instead of the values of only the last beat. Once convergence is obtained and the simulation is stopped, additional parameter calculations are performed and the output is displayed on the user interface, as explained in section 5.4.

5.3. Differential equations

The complete set of differential equations is given at page 140 for the model as depicted in Fig. III-14. The equations are given in matrix notation and the parameter and variable abbreviations relate to the ones in Fig. III-14 and above. The matrix notation should be interpreted as $\dot{x} = A \cdot x + B \cdot u$, where x is a vector with the unknown (state) variables and u the inputs. The matrix A is usually referred to as the system matrix and B is the input matrix.

Additional parameters that are not indicated in Fig. III-14 or the text are:

- E: left ventricular elastance (known vector)
- E_a : left atrial elastance (known vector)
- V_0 : volume intercept of the left ventricular ESPVR (known constant)
- V_{0a} : volume intercept of the left atrial ESPVR (known constant)

The studies that are discussed in the following chapter were based on experimental data where no atrial parameters were acquired. Consequently, a solver was chosen that did not include an atrium. The inertance of the valves was also omitted because those values could not be determined from the experimental data and estimation is unreliable. As a result, only four state variables were required: left ventricular volume (V_{LV}), aortic pressure (p_{ao}), pump flow (Q_p), and the pressure proximal to the arterial compliance (p_c). Additional outputs were then left ventricular pressure, mitral flow, and aortic flow.

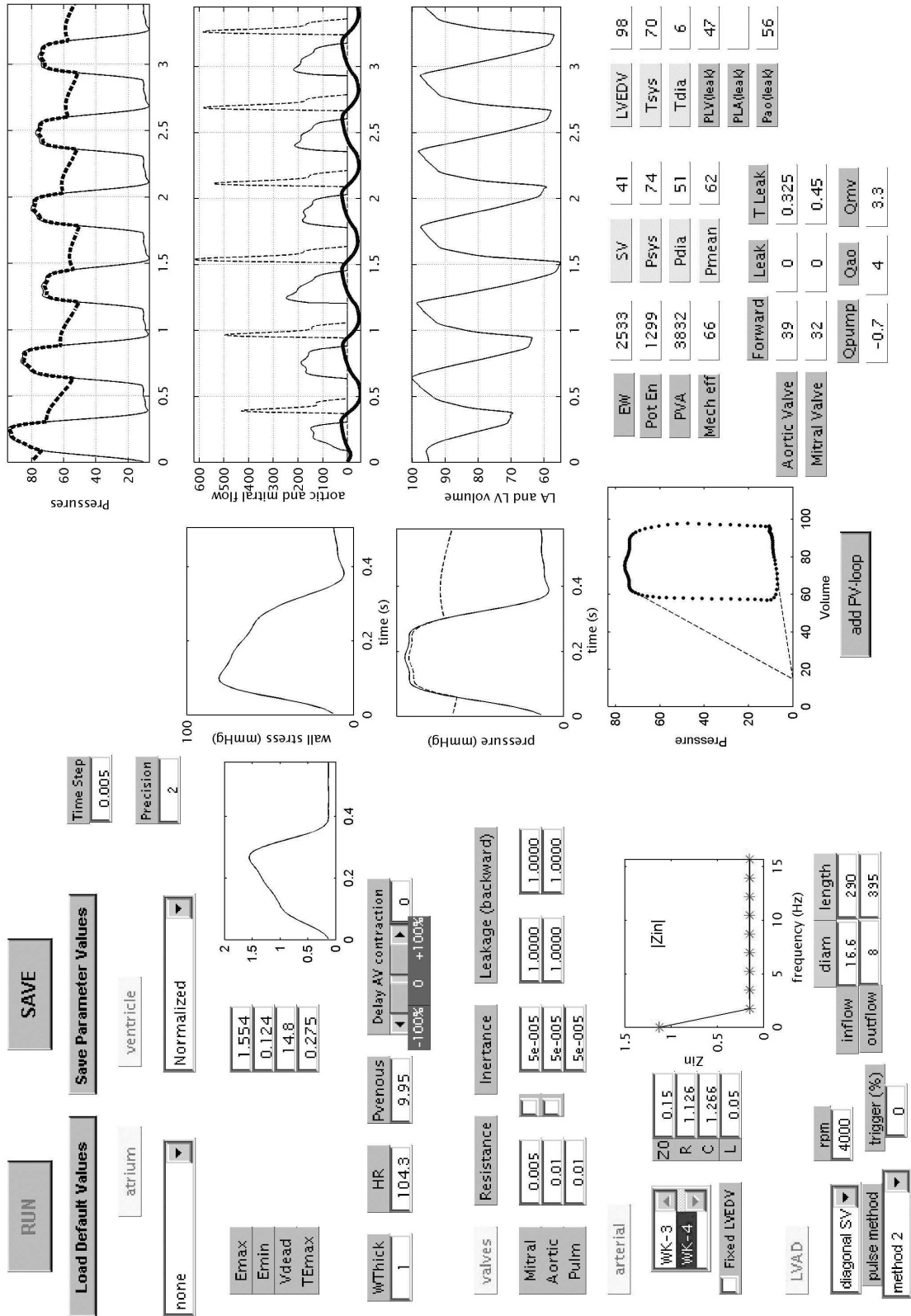


Fig. III-16: Overview of the graphical user interface of the mathematical model after a simulation where the microdiagonal pump was run at 4000 rpm, the heart was modeled only by the left ventricle, and the arterial system by a 4-element windkessel model.

$$\begin{bmatrix} \frac{dQ_{mv}}{dt} \\ \frac{dQ_{ao}}{dt} \\ \frac{dQ_p}{dt} \\ \frac{dp_c}{dt} \\ \frac{dp_{ao}}{dt} \\ \frac{dV_{LV}}{dt} \\ \frac{dV_{LA}}{dt} \end{bmatrix} = \begin{bmatrix} -\frac{R_{mv}}{L_{mv}} & 0 & 0 & 0 & 0 & 0 & 0 \\ 0 & -\frac{R_{aov}}{L_{aov}} & 0 & 0 & 0 & 0 & 0 \\ 0 & 0 & -\frac{R_{tot} \cdot Q_p}{L_{tot}} & 0 & 0 & 0 & 0 \\ 0 & 0 & \frac{1}{C} & -\frac{1}{R_p \cdot C} & 0 & 0 & 0 \\ 0 & \frac{1}{C} & \frac{1}{C} & \frac{R_c \cdot R_{tot}}{L_{tot}} \cdot Q_p & \frac{R_c}{L} - \frac{L}{R_p \cdot C} & 0 & 0 \\ 1 & -1 & -1 & 0 & 0 & 0 & 0 \\ -1 & 0 & 0 & 0 & 0 & -1 & 0 \end{bmatrix} \cdot \begin{bmatrix} -\frac{E_a}{L_{mv}} \\ 0 \\ 0 \\ 0 \\ 0 \\ 0 \\ -\frac{E_a}{R_v} \end{bmatrix} + \begin{bmatrix} \frac{Q_{mv}}{L_{mv}} \\ \frac{Q_{ao}}{L_{aov}} \\ \frac{Q_p}{L_{tot}} \\ \frac{p_c}{L_{tot}} \\ \frac{p_{ao}}{L_{tot}} \\ \frac{V_{LV}}{L_{tot}} \\ \frac{V_{LA}}{L_{tot}} \end{bmatrix} \cdot \begin{bmatrix} \frac{E \cdot V_0}{L_{mv}} & 0 & 0 & 0 & 0 & 0 & 0 \\ 0 & \frac{-E}{L_{aov}} & 0 & 0 & 0 & 0 & 0 \\ 0 & 0 & \frac{-E}{L_{tot}} & 0 & 0 & 0 & 0 \\ 0 & 0 & 0 & 0 & \frac{R_c}{L} - \frac{L}{R_p \cdot C} & 0 & 0 \\ 0 & 0 & 0 & 0 & \frac{R_c}{L} - \frac{L}{R_p \cdot C} & 0 & 0 \\ 0 & 0 & 0 & 0 & 0 & 0 & 0 \\ 0 & 0 & 0 & 0 & 0 & 0 & 0 \end{bmatrix} \cdot \begin{bmatrix} E \cdot V_0 \\ E_a \cdot V_{0a} \\ P_v \\ \omega^2 \end{bmatrix}$$

5.4. Model input and output

The possible settings and inputs for the model were described in the previous sections. Parameters are inserted in textboxes, while a listbox allows to make choices, e.g., for the different elastance curves or the pump modulation. Check boxes are further used to include or exclude components such as the inertia of the heart valves.

After a simulation has ended, output data is presented on the user interface and it can be saved to a data file. It concerns time-varying variables that are given in vector format over the whole last heartbeat and averaged and derived parameters that are given as a single value. These separate output parameters are displayed on the user interface in textboxes:

- left ventricular stroke volume and end-diastolic volume;
- mean, systolic, and diastolic aortic pressure;
- EW, PE, PVA, and mechanical efficiency of the left ventricle (see p.23);
- systolic and diastolic wall stress;
- average mitral and aortic valve flow and assist device flow;
- forward and regurgitant flow for each heart valve plus the leakage duration

The vector data contains the following variables:

- | | |
|--|--------------------------------|
| ▪ time | ▪ mitral flow |
| ▪ left atrial pressure and volume | ▪ pulmonary venous flow |
| ▪ left ventricular pressure and volume | ▪ left ventricular wall stress |
| ▪ aortic flow and pressure | ▪ assist device flow |

These data are displayed on the user interface in graphs. Three similar graphs (one for pressures, one for flows, one for volumes) show data in function of time for all the calculated beats. Other graphs display data only obtained from the last calculated heart beat: a PV-loop with indication of ESPVR and EDPVR, a plot of wall stress over time and a plot of aortic and left ventricular pressure over time.

CHAPTER IV

Hydrodynamic Analysis of Heart - Rotary Blood Pump Interaction

A. INTRODUCTION

1. Overview of the chapter

Many ventricular assist devices based on a rotary blood pump (RBP) are currently available in different forms and sizes with control algorithms of varying complexity. The goal of this chapter is not to assess the differences between these pumps or to evaluate optimal control. Instead, the studies presented in this chapter focus on the load imposed on the left ventricle by RBPs and further hemodynamic consequences in three different circumstances (scenarios).

The two pumps used have a diagonal flow path and were both developed at the Helmholtz Institute in Aachen (HIA). In the *in vitro* study (section D), the clinically available Medos Deltastream was used, while the other studies were performed with the Medos-HIA microdiagonal pump. This section further discusses the details of these pumps, while the following sections cover the individual studies.

The studies are all performed in three different models: a mathematical model (sections B and C), an *in vitro* model (section D), and an *in vivo* (sheep) model (section E).

- The first scenario that is modeled concerns sudden failure of an RBP used as assist device. This scenario is not simulated *in vivo* by the author, but reference is made to a related *in vivo* study that was previously reported by Nishida et al. ^[179].
- A second scenario is the use of an RBP running at different constant rotational speeds to provide different levels of ventricular assist.
- The third and last scenario that is simulated involves the use of an RBP running with a sine modulated rotational speed, thus providing pulsatile support. This scenario requires special attention for the effect of triggering in the case of synchronous ventricular assist. No *in vivo* simulation of this third scenario is performed, but the *in vivo* sheep model is additionally used to investigate the impact of the inlet cannulation site for ventricular assist with an RBP.

The results and conclusions of the different studies are summarized in the last chapter (section A), where the three models used (mathematical, *in vitro*, *in vivo*)

are compared and their advantages and disadvantages discussed. Even though the studies are performed with a specific type of pump, to some extent the conclusions are valid for all types of rotary blood pumps.

2. The Medos Deltastream pump

The Deltastream diagonal pump (Medos Medizintechnik GmbH, Stolberg, Germany) is a rotary blood pump intended for use in (miniaturized) cardiopulmonary bypass (CPB) circuits, which also has potential for use as an extracorporeal ventricular assist device.

The pump comes in two versions: the fully integrated DP1 that is in clinical use as of October 2000 and the more recent DP2 version. The latter has a separate pump head and pump drive that are magnetically coupled. This yields a more cost efficient operation since the drive can be re-used and only the pump head has to be disposed of. In contrast, the DP1 is one complete single-use component. However, its integrated design allows use up to 24 hours, while the DP2 can only be used for 6 hours. The *in vitro* studies described below are all performed with the DP1 pump since the DP2 was not yet available at the time of the measurements.

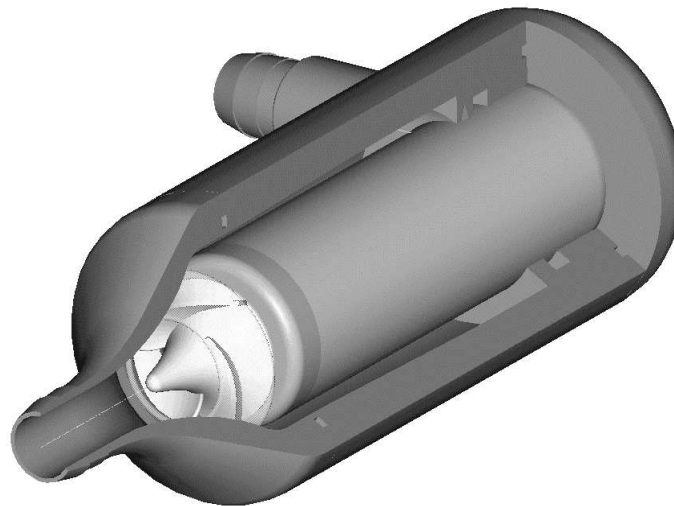


Fig. IV-1: Deltastream DP1.

The DP1 pump consists of an electric motor embedded into a stainless steel tube, which is in turn integrated into the plastic pump housing. An impeller with four straight vanes sandwiched between two conical surfaces is mounted in between the inflow connector and the motor. The outflow connector is located at the rear

of the motor, which makes the blood flowing all around the motor and thus provides cooling. The housing and impeller material is polycarbonate and the whole pump has an outer diameter of 40 mm, a length of 150 mm, and a weight of 300 g. The motor further incorporates a temperature sensor and a humidity sensor that help in predicting failure of the seal and required pump exchange. At least two and a maximum of four external pressure sensors, together with an ultrasonic flow probe, need to be connected upstream and downstream of the pump for monitoring and control.

The clinical drive console allows the pump to function in several modes:

- *Rotational speed control*, where the user can set a constant rotational speed.
- *Preload limitation*: in combination with the previous mode this will automatically reduce the rotational speed as soon as the preload pressure has fallen below a preset threshold. This to prevent suction in the venous cannula.
- *Flow control*, where the controller calculates the rotational speed in order to maintain a constant flow as set by the user.
- *Zero flow-control*, where the pump automatically maintains a rotational speed that generates a flow of 0 l/min, comparable to pump stoppage of a roller pump.

Additionally, the DP1 pump has a *pulsatile control* feature that is intended to provide a more physiological flow and pressure waveform for use as an assist device. Pulsatile perfusion is sometimes also used in CPB circuits, e.g., to improve the cerebral perfusion in patients with carotid stenosis. In this control mode, the user has to set the average flow, the desired pulse pressure and the pump frequency in beats per minute (BPM). The pump will then generate a sinusoidal varying speed of which the average and amplitude are determined with a control algorithm that evaluates these three parameters.

For the studies described below, a laboratory console intended for research purposes was used. This console served as a basic platform for development of the clinical console, which was still under development at the time. Control was provided via two LabView programs: one for rotational speed control and one for pulsatile control.

3. The Medos-HIA microdiagonal pump

The microdiagonal pump is just as the Deltastream a realization of the cooperation between Medos Medizintechnik GmbH and the cardiovascular division of the Helmholtz Institute for biomedical engineering in Aachen (HIA). The microdiagonal pump is basically a scaled down version of the Deltastream, that further underwent modifications for use as an implantable ventricular assist device. The pump has a diameter of 30 mm, a length of 80 mm and weighs 120 g. As can be derived from Fig. III-12, the device can generate a flow of 5 liters blood per minute against a pressure head of 100 mmHg at a rotational speed of 7000 rpm.

The miniaturization of the pump will allow to implant the device via a left thoracotomy (between the ribs), which is less traumatic than the traditional approach where the whole breast bone is sawn apart. Moreover, the less traumatic implantation and smaller size justifies the use of this device in an earlier stage of heart failure, where the device should only deliver part of the total blood flow. Consequently, the device is intended for use as a bridge to recovery or to transplantation and it aims at a use of two years, where apical or atrial cannulation can be applied. The pump is currently not yet available for clinical use and the studies described below were performed with data obtained from one of the prototype versions.

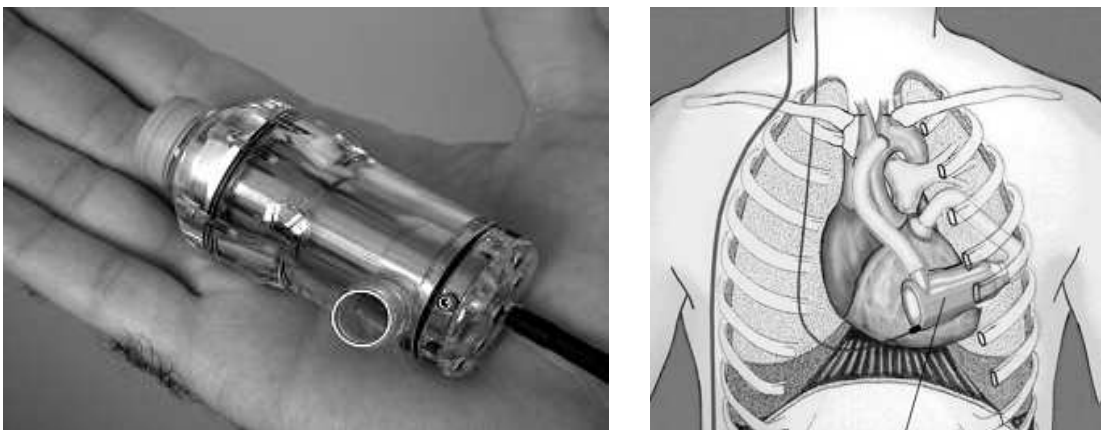


Fig. IV-2: Picture of the microdiagonal pump prototype that was used in the studies below (left) and a schematic drawing of its intended placement (right).

4. Characterization of the Medos pumps

4.1. Introduction

The flow generated by a rotary pump is dependent on the pressure head, which is in contrast with displacement pumps where preload and afterload are independent determinants. This is illustrated by the general rotary pump equation as given in chapter III and repeated below ([Eq. IV-1]). Consequently, it can be expected that the preload and afterload have an inverse effect and that the flow sensitivity to either variable is equal for a certain rotational speed. An increase in preload has the same effect on the pressure head (a decrease) as a decrease in afterload with the same increment. To characterize a rotary pump, a pump graph presenting the generated flow as a function of pressure head can be composed, and this for multiple rotational speeds.

$$\Delta p = A \cdot \omega^2 + R_p \cdot Q_p^2 \quad [\text{Eq. IV-1}]$$

with:

- Δp : pressure head over the pump (mmHg)
- A: pump constant (mmHg/rpm²)
- ω : rotational speed (rpm)
- R_p : pump resistance (mmHg·min²/l²)
- Q_p : pump flow (l/min)

Such a characterization has previously been performed at the HIA for the Medos-HIA microdiagonal pump and the resulting data was presented in chapter III, section B. The Medos Deltastream pump was characterized in the Hydraulics Laboratory with the *in vitro* model that was described earlier (chapter II), making use of the static preload reservoir that was decoupled from the afterload. The Deltastream pump was controlled by a laboratory console in both continuous mode and pulsatile mode. The experiment was performed with a water-glycerin mixture with a kinematic viscosity of $2.22 \cdot 10^{-6} \text{ m}^2/\text{s}$ at an average temperature of 29° C. Instrumentation was provided as described before.

4.2. Medos Deltastream: continuous mode

4.2.1. Methods

In continuous mode, the rotational speed was varied from 1000 to 9000 rpm with 1000 rpm increments. At each speed, the resistor was set at six different resistance values and this was combined with three different preloads (5, 20 and 35 mmHg), yielding 18 data points for each rpm. The resistances were chosen as

to obtain a broad range of afterload pressures (50, 100, 125, 150, 175, and 200 mmHg) at a flow rate of 6 l/min. A data point was obtained from acquiring the pressures and pump flow for 5 seconds at 200 Hz and averaging the resulting flow and pressure head (= windkessel pressure – preload pressure) data. The protocol for continuous mode was repeated with water as a test fluid for 2000, 4000, and 6000 rpm.

4.2.2. Results and discussion

A pump graph was composed of the continuous mode data and is shown in Fig. IV-3 for rotational speeds of 1000 to 7000 rpm. The plot of the measurements with water as a test fluid coincides with the glycerin one for a speed of 2000 rpm, while for 4000 rpm a slightly lower pressure is generated and the disparity is even larger for 6000 rpm. This is due to the higher hydraulic resistance resulting from the more viscous glycerin mixture. The pump has to generate more hydraulic power to produce a given flow compared to water experiments. For increasing pump speeds, the plots shift to the upper right and they become steeper, thus covering a larger pressure range while they all cover a similar flow range. At higher speeds, the plots are also farther apart, which relates to the general pump equation ([Eq. IV-1]) that contains a term with the square of the rotational speed.

It can be noted in Fig. IV-3 that a negative pressure head and a positive flow are measured at low rotational speeds. This is a result of the static mock loop testing with a decoupled pre- and afterload. The pressure head is defined as the pressure downstream of the pump minus the pressure upstream of the pump, and at low speeds the pump cannot generate high afterload pressure. Consequently, a negative pressure head can occur if the set preload pressure exceeds the afterload pressure. The forward flow is then generated by the pressure difference between the preload reservoir and the venous overflow reservoir, rather than by the pump itself.

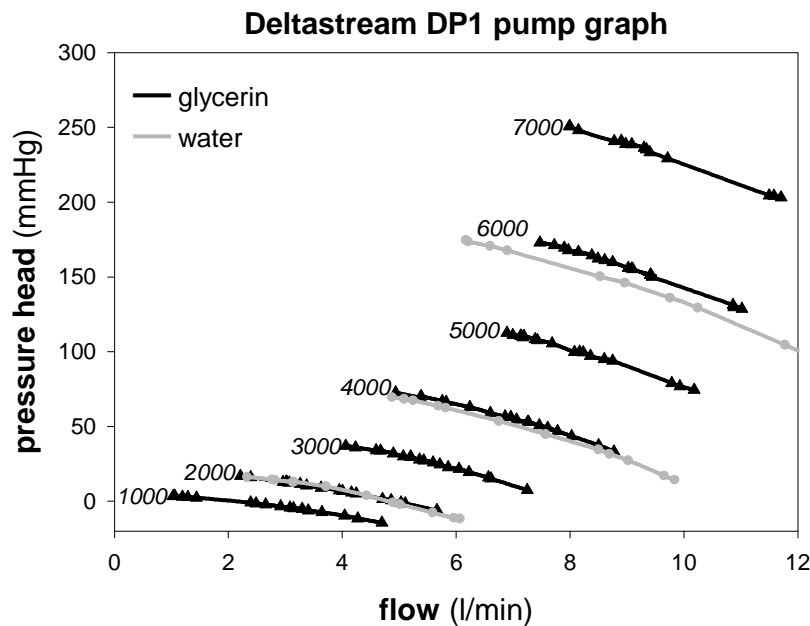


Fig. IV-3: Two-dimensional pump graph obtained from the continuous mode data. The rotational speeds (1000 to 7000 rpm) are indicated in italic.

The Deltastream pump is intended for use on CPB circuits and can therefore generate physiological flows over a large pressure range. A consequence of performing the measurements with resistances in the physiological range is that the data only cover a small part of the pump's capacity. To better characterize the pump, it is necessary to create pump flows from 0 l/min to the maximum achievable at a certain speed. For low speeds, a no-flow situation can be obtained with a relatively low resistance, while for higher and more powerful speeds a much higher resistance is required. Hence, the protocol should take into account various resistance ranges rather than being restricted to the physiological range and adopting the same resistance values for each pump speed. This is also confirmed by the fact that at higher speeds, the data points as shown in Fig. IV-3 are clustered together. This indicates that there was little effect from varying the parameters within the predetermined range.

4.3. Medos Deltastream: pulsatile mode

4.3.1. Methods

In pulsatile mode, a parameter study was performed to evaluate the response of the feedback algorithm implemented in the laboratory console. The *in vitro* model and pump were regulated to a reference setting (see Table IV-1, bold), and each of six parameters was subsequently varied over a predetermined range (see

Table IV-1), while the other parameters were kept constant at their reference value. Three settings of the pump console were varied: the pump rate, the pulse pressure, and the mean flow to be generated (set flow). The remaining three parameters were set in the *in vitro* model: the preload pressure, the resistance, and the compliance.

Table IV-1: Parameter values used in the pulsatile protocol

PR[†] (BPM)	pulse press. (mmHg)	set flow (l/min)	preload (mmHg)	resistance (mmHg·s/ml)	compliance (ml)* (ml/mmHg)
40	10	3	10	0.5	250 0.28
60	20	5	20	1	500 0.51
80	30	7	30	1.5	750 0.82
100	40	9	40	2	1000 1.05

The bold numbers indicate the reference values.

[†] PR: pump rate

* compliance expressed as the amount of air in the windkessel

4.3.2. Results and discussion

Fig. IV-4 presents pressure and flow waveforms acquired with the Deltastream DP1 functioning in pulsatile mode. The displayed data was measured with the pump console and setup regulated to the reference values. When evaluating the waveforms, it can be concluded that both ‘aortic’ pressure in the windkessel and flow deviate from physiological patterns. The Deltastream pump, however, is mainly intended for use in CPB circuits where physiological flow and pressure patterns are less important. The main goal of the pulsatility is to transfer blood with more energy to oxygen deprived body parts, e.g., through stenoses and thus the waveform shape is inferior to the contained energy. Moreover, the presence of an artificial lung and arterial filter in a CPB circuit will alter the waveforms, and when the Deltastream pump is used for ventricular assist, the remaining pumping action of the native heart will have the same effect.

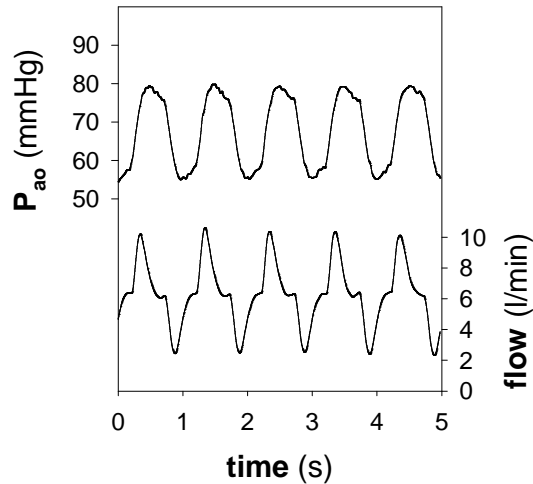


Fig. IV-4: Example of the pump flow and afterload pressure (P_{ao}) with the Deltastream DP1 working in pulsatile mode, with all parameters set at their reference values (see Table IV-1). P_{ao} is measured in the windkessel, and is therefore indicative for the aortic pressure.

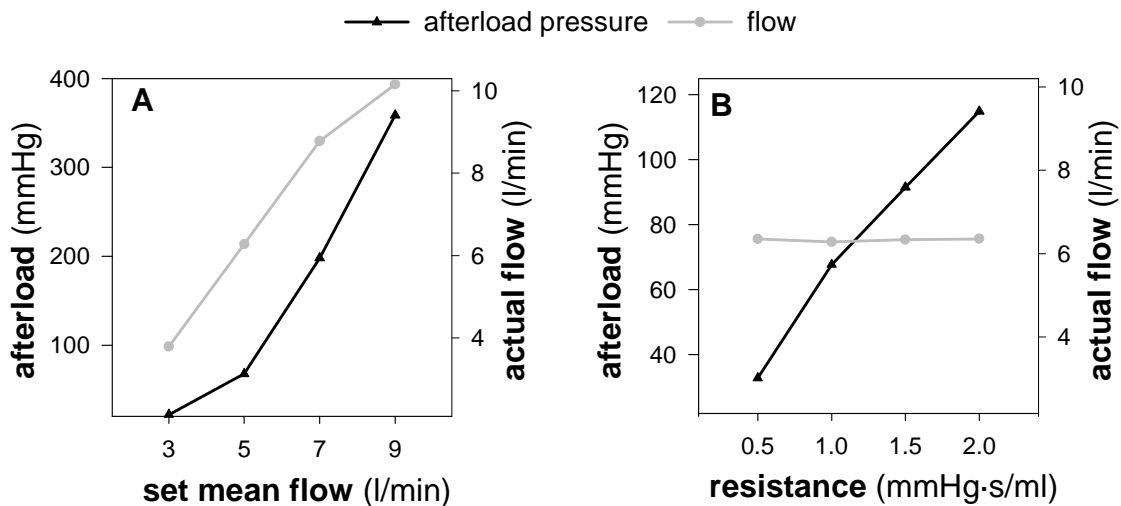


Fig. IV-5: Results of the parameter study in pulsatile mode. Panel A shows the impact of the set flow on the afterload pressure (black data, left hand side axis) and the generated flow (gray, right hand side axis). Panel B shows the impact of resistance variation in the *in vitro* setup on the same parameters.

The panels in Fig. IV-5 demonstrate the effect of the mean flow setting and the resistance on the generated pump flow and afterload pressure. Each data point was calculated as the average of pressure and flow data (as displayed in Fig. IV-4) over a number of ‘pump beats’. Although the reference value for the flow was set at 5 l/min, it can be determined from panel B that the actual flow (measured with external instrumentation, see chapter II) was a little over 6 l/min. This was confirmed with the data where the other parameters were varied: a

mean flow setting of 5 l/min results in an actual flow of 6.3 l/min. Panel A demonstrates even clearer and for other flow levels that the actual flow (gray plot) is underestimated by the control algorithm.

In spite of this discrepancy between actual flow and flow measured by the console, it can be concluded from Panel B that the flow is the main determinant for the pulsatile mode algorithm. Regardless of the resistance that it has to work against, the pump always delivers the set mean flow. From the plots in panel A, a similar conclusion can be derived: the pump generates the demanded flow and it does not take into account that this can lead to extremely high pressures if the resistance is not adjusted. The console allows to set alarms that give high pressure warnings, but there is no automated algorithm that regulates the rotational speed based on an evaluation of both pressure and flow. A control algorithm that is simply based on maintaining the required flow can apparently lead to dangerous situations and a more sophisticated control is mandatory for clinical use. The data of panel A also reveal a shortcoming of *in vitro* setups: the resistance is not adjusted as it is *in vivo*, where baroreceptor feedback helps to regulate the afterload pressure.

Variation of the remaining parameters (pump rate, pulse pressure, preload pressure, and compliance) revealed only negligible changes in afterload pressure and actual flow and are therefore not displayed. These measurements, however, revealed that there is an algorithm that determines the best amplitude and mean rotational speed required to obtain the desired pulse pressure, but this is completely secondary to the flow requirement. As a result, the pulse pressure derived from Fig. IV-4 is higher than the set reference value of 20 mmHg. A similar overestimation was noted for all pulse pressure levels.

4.4. Comparison of Deltastream and Medos-HIA microdiagonal pump

When the general pump equation is fitted to the pump graph obtained for the Deltastream pump, it yields the following equation ($r^2 = 0.99$):

$$\Delta p = 6.289 \cdot 10^{-6} \cdot \omega^2 - 0.756 \cdot Q_p^2 - 7 \quad [\text{Eq. IV-2}]$$

with:

Δp : pressure head over the pump (mmHg)

ω : rotational speed of the impeller (rpm)

Q_p : pump flow (l/min)

Previously (chapter III), [Eq. IV-3] was found for the microdiagonal pump.

$$\Delta p = 2.9 \cdot 10^{-6} \cdot \omega^2 - 2.41 \cdot Q_p^2 \quad [\text{Eq. IV-3}]$$

Consequently, the equation that characterizes the Deltastream pump can be written as:

$$\Delta p_{DS} \approx 2 \cdot A_{MDP} \cdot 10^{-6} \cdot \omega^2 + 0.3 \cdot R_{pMDP} \cdot Q_p^2 - 7 \quad [\text{Eq. IV-4}]$$

Where A_{MDP} and R_{pMDP} are the values found for the microdiagonal pump and Δp_{DS} is the pressure head generated by the Deltastream pump. This reveals that the pressure head generated by the Deltastream is approximately 2 times more sensitive to changes in rotational speed than the microdiagonal pump, while the latter is three times as sensitive to changes in pump flow. This is also derived from the graphs in Fig. IV-6, where the Deltastream plots are much higher for comparable rotational speeds and the microdiagonal plots are much steeper.

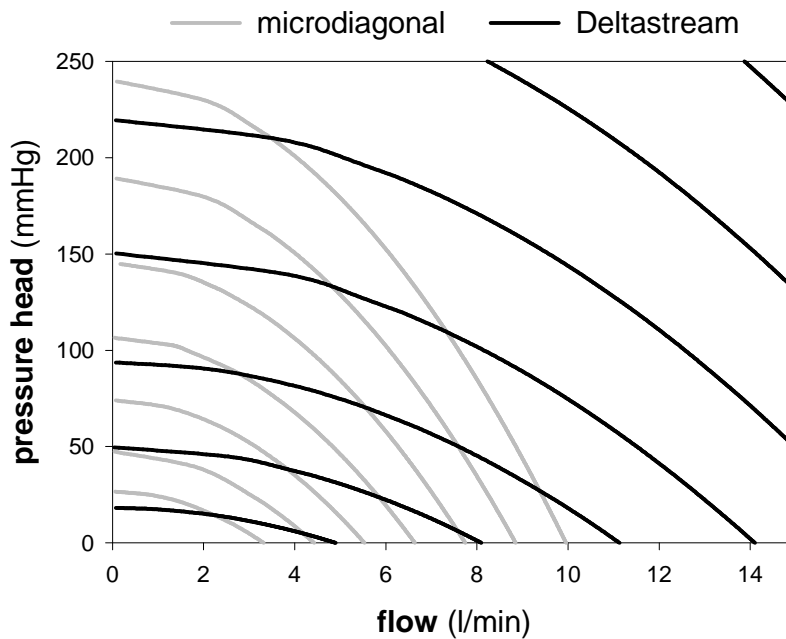


Fig. IV-6: Comparison of the pump graphs of the Deltastream pump and microdiagonal pump. The Deltastream function is displayed from 2000 rpm (lowest graph) to 8000 rpm (top right) in 1000 rpm increments and the microdiagonal pump from 3000 rpm to 9000 rpm with the same increment.

B. MATHEMATICAL MODEL STUDY OF ROTARY BLOOD PUMP FAILURE[†]

1. Abstract

In this study we used a mathematical model to study the influence of backflow through a failing rotary blood pump. We performed simulations based on animal experiments that were published earlier by Nishida et al. (Artif. Organs 2000), who used the Medos-HIA microdiagonal pump to assess the acute effect of sudden pump failure. The mathematical model consists of validated cardiac and arterial modules and a pump module. We could evaluate the influence of pump failure with mechano-energetic parameters and wall stress obtained from model output. Simulations were performed at baseline and after 15 min. of backflow in a control group and a heart failure group. Simulation results agreed well with the experiment.

Stroke volume, aortic flow and stress time integral increased significantly as a result of pump failure. However, total systemic flow and arterial pressure were not altered by backflow, and a life-threatening situation did not appear.

2. Introduction

The use of rotary blood pumps in extracorporeal circuits is an established phenomenon in perioperative cardiopulmonary bypass and post-cardiotomy support. These compact pumps can have a centrifugal, axial or diagonal concept and are easier to handle than displacement pumps. Their design is relatively simple since there is no need for valves. Most parts can be cast, which makes these pumps suitable for mass production. The last years a boost could be noticed in the research of rotary blood pumps, which are an easy target for hemolysis and anticoagulant testing, numeric flow simulations and driving algorithm

[†] The contents of this section was published in *Artif Organs* 2002;26(12):1032-1039:
Effect of rotary blood pump failure on left ventricular energetics
assessed by mathematical modeling
Vandenberghes S, Segers P, Meyns B, Verdonck P

development. Recent improvements have made these pumps more appealing and suitable for long-term or even permanent implant as a ventricular assist device [185,186].

Although reliability of all cardiac assist devices increases continuously by improved material selection, parallel electronic circuitry and extended performance testing, failure of a rotary blood pump is still a major concern. When such pumps are implanted, pump stoppage is harder to detect and emergency handling is more difficult and more invasive. Pump failure can lead to severe backflow through the pump and might end in a fatal incident as a result of the extra load imposed on the heart. Nishida et al. [179] concluded in a recent study that sudden pump failure leads to an acute depression of the hemodynamic state, which is not lethal and reversible if pump support was resumed after 15 minutes.

In our study we used a mathematical model to evaluate the effect of rotary blood pump failure on left ventricular function. Mathematical models of the cardiovascular system allow evaluation of the impact of cardiac assist while saving on the expenses of extended experimental testing and preventing the sacrifice of numerous animals. We studied hemodynamic and mechano-energetic parameters of the left ventricle (LV) in simulations based on previously performed animal experiments. This allowed us to validate the model and to generate extra information on the myocardial wall stress that could not be measured in the experiments.

3. Materials and methods

3.1. *In vivo* data

This simulation study is based on experimental data acquired by Nishida et al. [179]. Nishida et al. used 2 groups of sheep to study the effects of backflow through the Medos-HIA microdiagonal pump (Medos Medizintechnik GmbH, Stolberg, Germany). The first group (n=7) consisted of healthy control sheep while chronic heart failure was induced by coronary (LAD or LCx) embolization several weeks prior to the experiment in the second group (n=7). The data sets we selected for this study were acquired at baseline (BL) and after 15 minutes of backflow (BF), with ventriculo-arterial cannulation. Measured variables were left ventricular pressure and volume (P_{LV} and V_{LV}), mean aortic flow and pump flow

(Q_p) and carotid pressure. Volume was measured by conductance catheter (Cardio Dynamics BV, Leiden, The Netherlands) and calibrated with mean aortic flow and hypertonic saline injections for parallel conductance determination.

3.2. Computer model

The computer model used for the simulations was programmed in Matlab 5.3 (The Mathworks Inc., Natick, MA). It is a modification of an existing model that has already been used and validated for heart-arterial coupling studies ^[19,148]. The model can be divided into 3 modules, each representing a part of the simplified circulatory system proposed for this study (see Fig. IV-7): a cardiac module, an arterial module and a pump module. The complete model is programmed as a set of differential equations based on electrical analogons of the different modules.

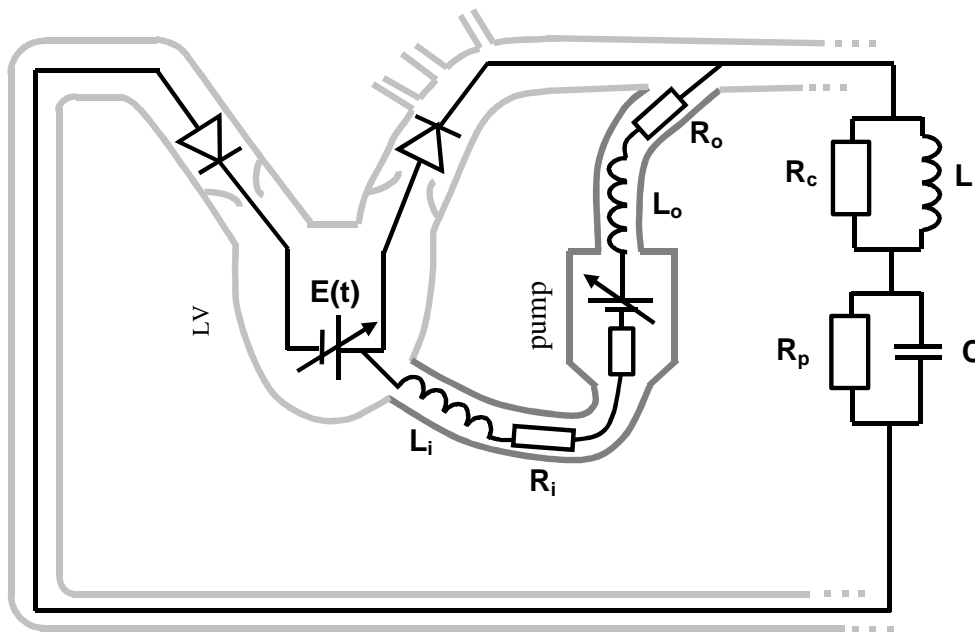


Fig. IV-7: Schematic representation of the simplified circulation model containing LV, diagonal pump and 4 element windkessel model. $E(t)$: time varying elastance; L_i and L_o : inertance of inlet and outlet cannula; R_i and R_o : resistance of inlet and outlet cannula; R_c : characteristic resistance; L : arterial inertance; R_p : peripheral resistance; C : total arterial compliance.

3.2.1. Cardiac module

This module is based on the time-varying elastance theory as elaborated by Suga and Sagawa ^[7,8]. During the experiment of Nishida et al., filling of the left ventricle (LV) was altered by inferior vena cava occlusions. This allowed us to determine the slope (E_{es}) and volume intercept (V_0) of the end-systolic pressure-volume relation and thus to calculate time-varying elastance as $E(t) = P_{LV} / (V_{LV} - V_0)$. It has been shown in dogs ^[7] and humans ^[10] that elastance curves can be

normalized in amplitude ($E_n=E/E_{es}$) and time ($t_n=t/t_{Ees}$) in order to obtain a characteristic curve ($E_n(t_n)$) for the species. The shape of this curve is similar for each subject of the species, whether healthy or with cardiovascular disease. From the pressure-volume (PV) data provided by Nishida et al., a general normalized elastance curve for sheep was derived and implemented in the cardiac model as a Fourier series. Mitral and aortic valve are modeled as linear resistors.

The experimental steady state data of Nishida et al. were averaged over a number of beats and were used to determine the input of the cardiac model for each individual sheep. With V_0 known from the vena cava occlusion measurements, end-systolic (E_{es}) and end-diastolic (E_{ed}) elastance and t_{Ees} were derived from the steady state measurements. Since $E_n(t_n)$ is known for sheep, only these parameters are needed to fully describe the time varying elastance $E(t)$ for each subject.

3.2.2. Arterial module

The arterial module is a four-element windkessel model ^[125], consisting of total peripheral resistance (R_p), total arterial compliance (C), total inertia (L) and the characteristic impedance of the aorta (R_c). The 4 parameters of this module can accurately be derived from continuous aortic pressure and flow ^[125,187]. However, only the mean of the aortic flow was known, and consequently alternative methods ^[150] had to be used based on mean carotid pressure (MCP), pulse pressure (PP), stroke volume (SV) and heart rate (HR). The peripheral resistance and compliance were calculated as

$$R_p = \frac{MCP}{SV \cdot HR} \quad (\text{mmHg} \cdot \text{s/ml}) \quad [\text{Eq. IV-5}]$$

$$C = \frac{SV}{PP \cdot 1.4} \quad (\text{ml/mmHg}) \quad [\text{Eq. IV-6}]$$

R_p and C were calculated for each sheep according to these formulas from the averaged data during baseline, while R_c and L were adjusted within limited range to improve the goodness of fit of the measured (averaged) and simulated pressure-volume loops.

3.2.3. Pump module

This module consists of an equation that was fitted ($r^2=0.99$) to pressure head-flow curves assessed from the Medos-HIA microdiagonal pump in an

experimental setup with continuous flow. Additional resistive and inertial terms are calculated in real-time, based on the cannula dimensions and added to the equation to make it valid for pulsatile flow. This results in the following equation that expresses the pressure head over the pump as a function of the pump flow:

$$P_{ao} - P_{LV} = A \cdot \omega^2 + R_{tot} (Q_p) \cdot Q_p^2 + L_{tot} \cdot \frac{dQ_p}{dt} \quad [\text{Eq. IV-7}]$$

with:

- A: pump constant (mmHg/rpm²)
- ω : rotational speed (rpm)
- R_{tot} : total resistance (mmHg·s/ml)
- L_{tot} : total inertance (mmHg·s²/ml)

3.2.4. Model output

Model output is calculated over one cardiac cycle after model convergence and consists of left ventricular pressure and volume, aortic pressure and flow (P_{ao} and Q_{ao}), mitral flow and pump flow. To calculate the wall stress, the left ventricle is approximated as a thick-walled ellipsoid in which the muscle is assumed to be isotropic and to have a constant volume. The wall thickness (w) is calculated throughout the cardiac cycle in relation to the end-systolic wall thickness. Meridional wall stress (σ_m) can be calculated as ^[21]:

$$\sigma_m = \frac{P_{LV} \cdot D^2}{4w \cdot (D + w)} \quad (\text{mmHg}) \quad [\text{Eq. IV-8}]$$

with:

- w: wall thickness (mm)
- D: inner diameter, short axis of the ellipsoid (mm)

Furthermore, a number of parameters that evaluate left ventricular function are derived from the PV-loop ^[188,189]. The external work (EW) is the area within the PV-loop and quantifies the energy that is delivered to the blood by the left ventricle. Potential energy (PE) is the triangular area between ESPVR, EDPVR and PV-loop. This area quantifies the energy that is used by the left ventricle merely to contract the muscle. The sum of these areas is known as the pressure volume area (PVA) and is closely related to the oxygen consumption of the heart ^[11,190]. The mechanical efficiency (Meff) of the LV is defined as the ratio of EW to PVA. Finally, arterial elastance (E_a) is derived as the ratio of end-systolic pressure to stroke volume. E_a is used as an indicator for the load that is placed upon the heart by the arterial system ^[191,192].

3.3. Methodology

Data from 4 sheep of each group (control and failure) were used in this simulation study. We performed 2 series of simulations with each group. In the first series we simulated the baseline conditions, where the necessary cardiac and arterial input parameters were derived from the experimental data at baseline for each sheep. The pump model was excluded for these simulations. In the second series we simulated pump failure and the resulting backflow. Here we also derived the cardiac parameters from the experimental data, but arterial parameters were copied from baseline. The pump model was included in this series, with a rotational speed of 0 rpm.

The parameters described in model output were derived from the simulation results. EW, PVA, Meff and E_a were also derived from the experimental data (averaged over a number of beats) to allow comparison between experiments and simulations. Statistics were performed on the simulation results with two-way ANOVA with repeated measures (SPSS 10.0, SPSS Inc., Chicago, IL). Significance level was $p=0.05$.

4. Results

The agreement between measured and simulated PV-loops is demonstrated in Fig. IV-8 for an animal of the control group. Especially the baseline simulation shows a good fit, while at backflow there is an overestimation of the LV end-diastolic volume (LVEDV). Comparison between measurements and simulations for each studied subject is given in Fig. IV-9. The mathematical model underestimates aortic and pump flow at backflow, while there is good agreement at baseline. The same effect is observed in the stroke volume, which is closely related to the displayed flows. Simulated mean aortic pressure (MAP) shows a very small but consistent underestimation at baseline and a very good agreement with the measurements at backflow. Measured and simulated PVA agree strongly. The simulations are thus valuable as an indication of the oxygen consumption of the left ventricle.

The effect of pump failure is noticeable on different parameters, as shown in Table IV-2. The graphs in Fig. IV-10 show a more detailed view on the effect for a sheep of the control group, while a summary of all simulations is displayed in Fig. IV-11, grouped in control and failure subjects.

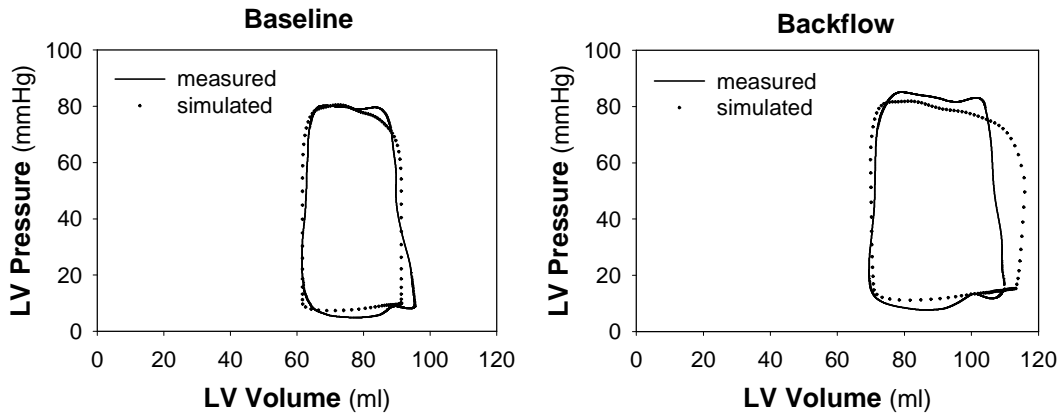


Fig. IV-8: Comparison of measured and simulated PV-loops at baseline (left) and after 15 min of backflow (right) in a sheep of the control group.

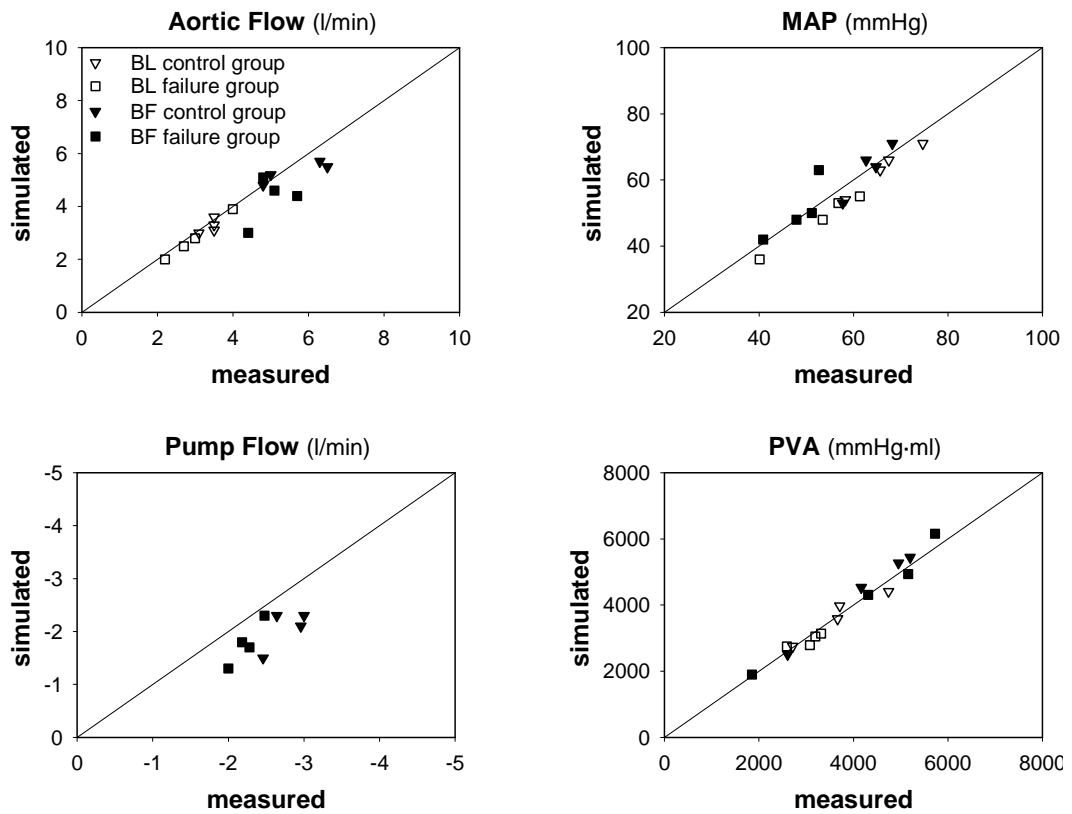


Fig. IV-9: Comparison of measured and simulated hemodynamic parameters at baseline(BL) and after 15 min of backflow (BF) in the whole studied population.

These illustrations of the simulation results show how aortic flow is significantly increased in the occurrence of pump failure. Due to the pump failure, this increase in aortic flow does not lead to a significant change in systemic flow, which is calculated at the mitral valve. Our simulations suggest that there is continuous backflow through the pump throughout the cardiac cycle, even during ventricular ejection when a negative pressure gradient appears over the pump (Fig. IV-10). The PV-loop demonstrates how LV volume is altered by this overload situation: end-diastolic volume is much higher compared to baseline, and end-systolic volume is also increased. Nevertheless, pump failure results in a significant increase in stroke volume.

Aortic pressure at backflow is almost identical to the pressure at baseline. This is the case for all simulations, giving a constant MAP for each group.

Backflow results in an (non-significant) increase in both systolic and diastolic wall stress, which is a direct consequence of the higher ventricular volume (and thus thinner wall) and the maintained pressure. The increase is most noticeable at peak ejection.

When considering PVA (Fig. IV-11), an increase is noticed at backflow for both groups, especially for the group with induced heart failure. The larger effect in the failure group can be explained by the large increase in potential energy in this group, while this energy remains constant in the control group. The external work increases equally in both groups but is higher in the control group compared to the failure group. There is no significant difference between EW, PE and PVA at baseline or at backflow, in either group.

Finally, the arterial elastance decreases significantly in all groups when backflow is induced. This could be expected since pressure is maintained while stroke volume increases.

Table IV-2: Hemodynamic and mechano-energetic parameters at baseline (BL) and during backflow (BF)

		BL	BF
SV (ml)	C	32 ± 4	44 ± 5 ^a
	F	33 ± 5	44 ± 13 ^a
LVEDV (ml)	C	82 ± 9	98 ± 18
	F	132 ± 35 ^b	161 ± 34 ^b
P_{aomax} (mmHg)	C	79 ± 7	80 ± 11
	F	65 ± 7	68 ± 9
MAP (mmHg)	C	64 ± 7	64 ± 8
	F	48 ± 9 ^b	51 ± 9 ^b
Q_{ao} (l/min)	C	3.3 ± 0.3	5.3 ± 0.4 ^a
	F	2.8 ± 0.8	4.3 ± 0.9 ^a
Q_p (l/min)	C	0 ± 0	-2.0 ± 0.4 ^a
	F	0 ± 0	-1.8 ± 0.4 ^a
EW (mmHg·ml)	C	2186 ± 370	2838 ± 764
	F	1679 ± 493	2092 ± 869
PE (mmHg·ml)	C	1494 ± 629	1602 ± 821
	F	1250 ± 345	2233 ± 1007
PVA (mmHg·ml)	C	3680 ± 706	4439 ± 1346
	F	2929 ± 192	4325 ± 1790
M_{eff} (%)	C	61 ± 11	65 ± 10
	F	57 ± 14	49 ± 8
E_a (mmHg·s/ml)	C	2.5 ± 0.4	1.8 ± 0.2 ^a
	F	2.0 ± 0.4	1.6 ± 0.3 ^a
σ_{max} (mmHg)	C	74 ± 7	87 ± 16
	F	72 ± 4	80 ± 15
STI (mmHg·s)	C	20.5 ± 2.3	24.0 ± 4.4 ^a
	F	25.3 ± 3.6	29.9 ± 5.8 ^a

^a p < 0.05 vs. baseline

^b p < 0.05 vs. control group

C: control group; F: failure group

SV: stroke volume; LVEDV: left ventricular end-diastolic volume; P_{aomax}: max. aortic pressure; MAP: mean arterial pressure; Q_{ao}: aortic flow; Q_p: pump flow; EW: external work; PE: potential energy; PVA: pressure volume area; M_{eff}: mechanical efficiency; E_a: arterial elastance; σ_{max}: max. wall stress; STI: stress time integral.

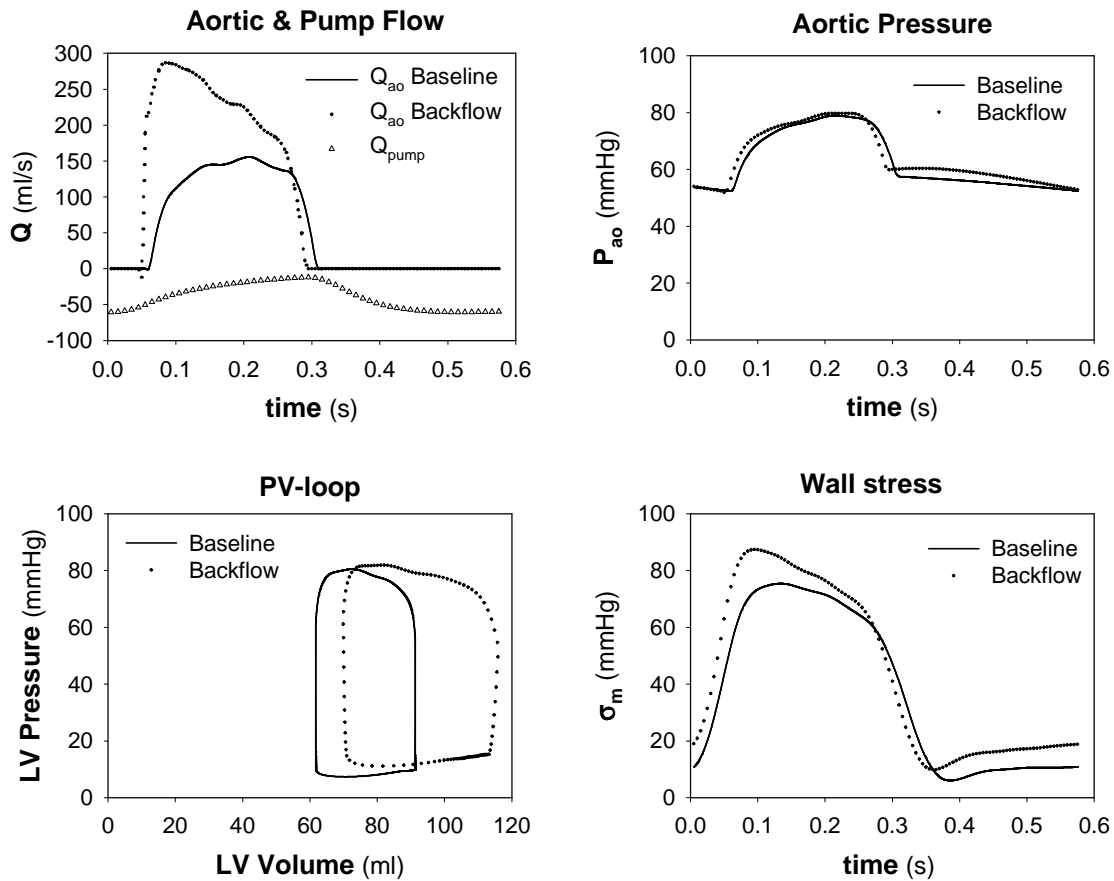


Fig. IV-10: The effect of backflow on aortic flow and pressure, PV-loop and meridional wall stress in a simulation of a sheep of the control group.

5. Discussion

It has already been verified by Nishida et al. that the end-systolic elastance, dp/dt_{max} and mean arterial pressure differ significantly between the control and the failure group, proving that coronary embolization was successful and a form of chronic heart failure was present. This result is confirmed in our simulations by significant differences in LVEDV and MAP for the control and the failure group. Still, Nishida et al. point out that conclusions must be interpreted with care since the degree of induced heart failure is less than seen in clinical implant candidates.

Since no accurate estimation of the arterial parameters from aortic pressure and flow was possible, no effort has been undertaken at this stage to quantify the error between the measured and the simulated data. Additionally, only 2 signals (LV pressure and volume) are available for comparison of model and experiment. There is good agreement between measured and simulated PV-loops

in general, especially at baseline. The arterial parameters R_c and L are adjusted to improve resemblance between the PV-loops at baseline, while these values (and R_p and C) are copied for the backflow simulations. If these parameters would be derived from the backflow experiments, the influence of backflow would be included in the parameters, thus giving a false representation of the arterial system. Therefore it is assumed that the arterial system stays constant and the parameters are copied. It is however possible that changes in the arterial system occur due to the altered circulation, explaining the inferior fit at backflow. This might also be the reason for the underestimation of aortic flow and pump flow in the backflow simulations. The underestimation of the flows indicates that a further evaluation of the model is necessary utilizing time-varying flow signals, which would also allow accurate arterial parameter determination.

Our simulations indicate a continuous negative pump flow, even during LV ejection when LV pressure is higher than aortic pressure. This is partly due to the large resistance and inertia in the long cannulas used in this experiment (inflow: 395 mm, outflow: 290 mm), which cause a low flow profile. These cannulas were used to allow visual inspection of the pump by placing it extracorporeally. Simulations with shorter cannulas (80 and 150 mm) revealed a more distinct flow profile reaching small positive flows during LV ejection. Nevertheless, the high pressure gradient during diastole causes such high backflow that it can not be compensated by the small reverse pressure gradient during systole.

We anticipated that total arterial flow would have diminished during pump failure since part of the aortic flow regurgitates into the ventricle through the failing pump. However, both the simulation results and the experimental data indicate that the backflow is compensated by an increased stroke volume and consequently a higher output through the aortic valve. Stroke volume of the left ventricle is augmented at backflow to maintain an effective stroke volume similar to the baseline condition.

The averaged results of the animal experiments show a very small, non-significant decrease in mean aortic pressure due to backflow. The simulations also show that arterial pressure is hardly altered at backflow, which is in contrast with aortic regurgitation, where a dramatic decrease in MAP appears^[193]. Again, cannula resistance and inertia may be responsible for this effect since they prevent fast pressure changes over the pump. MAP is an easy to measure non-invasive parameter that is widely used as a diagnostic tool. However, these

results show that it would be impossible to diagnose a failing rotary blood pump even by invasive arterial blood pressure measurements.

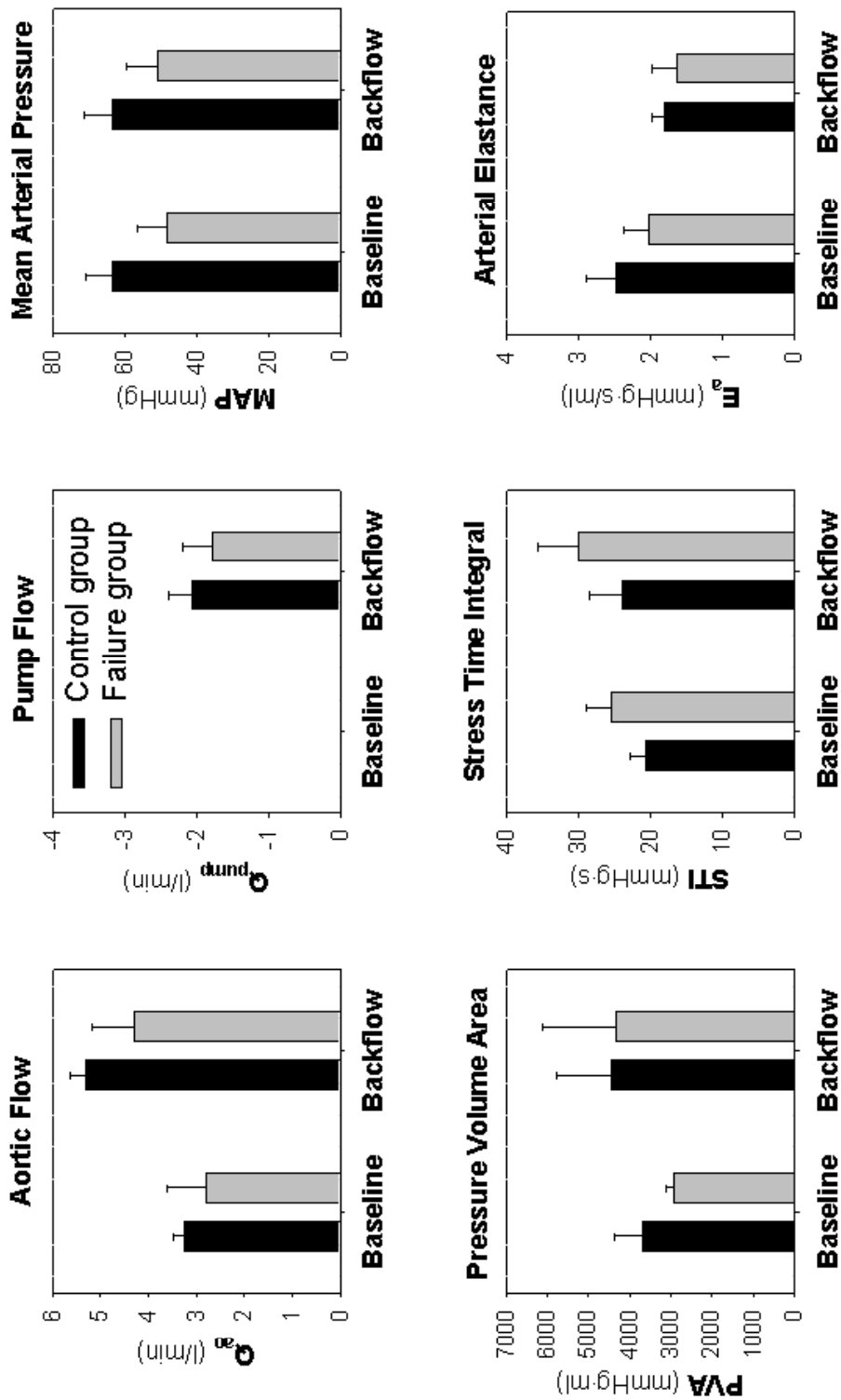


Fig. IV-11: The effect of backflow on hemodynamic and mechano-energetic parameters, derived from the simulation data for the control (grey) and the failure (black) group. Data are presented as mean and standard deviation for each group.

Ventricular wall stress cannot be measured in a simple non-destructive way. Several methods have been proposed to calculate this stress or one of its components starting from the ventricular geometry and the internal pressure, but apparently there is little difference between the models ^[20,184]. Meridional wall stress σ_m is less sensitive to geometric changes in comparison with circumferential stress and it better approximates mean fiber stress. σ_m slightly overestimates total stress ^[20], but it is a good indicator for changes in left ventricular wall tension by different loading conditions. Although the stresses resulting from these simulations are not true absolute values (a default end-systolic wall thickness of 10 mm was assumed), we consider the wall stress model as an important tool that gives valuable information of the condition of the ventricular muscle. No statistically significant change in wall stress could be demonstrated, but there is a clear trend in both groups. The simulations suggest that the high wall stress is maintained longer when backflow is present. To quantify this, we calculated the stress-time integral (STI) and found a significantly higher STI at backflow (see Table IV-2 and Fig. IV-11).

The increase in potential energy due to backflow in the failure group indicates that more energy is required to make the muscle contract in that situation (failing heart with failing pump). There is no difference in PE between the 2 groups at baseline, which shows that the failure group is more sensitive to backflow. This is also illustrated by the mechanical efficiency, which decreases due to backflow in the failure group, while it increases in the control group.

The decrease of arterial elastance should indicate that the heart is subject to a smaller arterial load, which is in contrast with the PVA and wall stress, both of which demonstrate an increased load on the heart. Since PVA and wall stress are more direct measures of the effective load on the heart, it can be concluded that E_a is a bad indicator for this load in rotary blood pump failure.

6. Conclusions

We used a mathematical model to study left ventricular mechano-energetics in the occurrence of rotary blood pump failure. Simulations were based on an experimental sheep study by Nishida et al., in which they used the Medos-HIA microdiagonal pump to assess data at baseline and during pump failure. In our model there is an underestimation of pump flow and subsequently a further evaluation is necessary with more accurate data.

Our findings confirm the conclusions of Nishida et al.: backflow through a failing pump increases stroke volume, but has little effect on aortic pressure. Aortic flow increases to compensate for the backflow. The pressure volume area (as a measure of oxygen consumption) and ventricular wall stress increase during pump failure, indicating a larger load on the heart. However, no life-threatening condition seems to appear. The arterial elastance decreases during pump failure and should not be considered as a parameter for loading of the heart.

7. Acknowledgements

The authors are grateful to Takahiro Nishida and Christoph Göbel for providing the necessary data. We also thank L. Gay for proof reading the manuscript.

This research was funded by a specialization grant of the Flemish Institute for the Promotion of Scientific-Technological Research in Industry (IWT-993171, S. Vandenberghe) and by a post-doctoral fellowship from the Fund for Scientific Research – Flanders (FWO Vlaanderen, P. Segers).

C. MATHEMATICAL MODEL STUDY OF VENTRICULAR ASSIST WITH A ROTARY BLOOD PUMP IN CONTINUOUS AND PULSATILE MODE[†]

1. Abstract

Due to the increased appeal of rotary blood pumps for long-term cardiac assist, we conducted a study of their capacity to unload the left ventricle (LV). We used a validated mathematical model of the cardiovascular system and implemented the pump characteristics of an investigational microdiagonal pump (Medos). The influence of the pump on systemic hemodynamics, LV energetic parameters and wall stress was evaluated in continuous and synchronous pulsatile mode of operation. For the continuous mode simulations, the influence of heart rate, LV contractility and pump speed was assessed in a parametric study. For the pulsatile mode, different onsets of a synchronous time-varying pump speed pattern were tested.

Our data indicate that the effectiveness of unloading in continuous mode depends on the contractility of the native ventricle. Hypocontractile ventricles are most easily unloaded, while ventricles with moderate contractility require high continuous pump speeds to achieve notable unloading. In pulsatile mode, the pump timing is an important determinant of pump/cardiovascular system interaction, with a counterpulsation setting yielding the best unloading.

[†] The contents of this section was published in *Artif Organs* 2003;27(12):1094-1101:
**Unloading effect of a rotary blood pump assessed by
mathematical modeling**
Vandenbergh S, Segers P, Meyns B, Verdonck P

2. Introduction

Cardiac assist devices of various types are widely used to keep end-stage heart failure patients alive for a limited period, to bridge them to transplantation. As opposed to that, approximately 20 years after the first experiences with the Jarvik 7, new devices have recently been introduced specifically for destination therapy or permanent support of patients. However, it is questionable whether destination therapy is the ideal alternative to cardiac transplantation, since assist devices still have a relatively short lifetime (new devices strive usually for a 5 years lifetime) and only provide approximate physiological control. Consequently, recent research efforts have focused on using assist devices as a ‘bridge to recovery’, to heal the patient’s own heart. The improved heart function following cardiac support and the possibility of subsequent device explantation was reported by Frazier in 1994 ^[64], and has since been demonstrated in clinical practice in a few hundred patients with various devices ^[66]. Unfortunately, the underlying biochemical and biomechanical processes of cardiac recovery are not yet fully understood, which makes it difficult to select patients for this new therapeutic option and to determine the optimal recovery protocol. Clinical experience indicates that ‘bridge to recovery’ can probably only be applied to a limited number of patients suffering from primary myocardial disease ^[66], where the progressive remodeling of the heart can be halted and even reversed.

Barbone et al. recently demonstrated that the load imposed on the heart is one of the major determinants of the remodeling process ^[69], but the question remains how much unloading is required in relation to the patient’s condition. To investigate recovery and eventually to apply the optimal protocol, it is necessary to have the possibility to prescribe different grades of unloading, and to assess the attendant response of the native ventricle.

In this study, we have used a computer model, previously validated for heart-arterial interaction studies ^[150] and applied to study the effect of rotary blood pump failure ^[194], to assess the unloading capacities of a rotary blood pump in different conditions. In a first series of simulations, the unloading of the left ventricle (LV) by a rotary blood pump running at constant speed is studied for different cardiac parameters and pump speeds. In a second series, the rotary blood pump is simulated in a synchronous pulsatile mode wherein the pump speed varies throughout the cardiac cycle. Variation in the trigger delay of the

pulsation pattern is performed to assess the influence upon cardiac unloading. Consequently, this study evaluates the difference between pulsatile and non-pulsatile support and their effect on cardiac function, without considering the impact on general physiology or other end-organ function.

3. Materials and methods

3.1. Computer model

The computer model used for this study is programmed in Matlab (The MathWorks Inc., Natick, MA) and consists of 3 separate modules (cardiac, arterial, and pump module) as described elsewhere ^[194]. In our model (see Fig. IV-12), we disregard the pulmonary circulation and the left atrium, which offers the advantage that all necessary input parameters for the native cardiovascular system can be derived from a standard in-vivo experiment. The cardiac module embodies the left ventricular function based on the time-varying elastance ($E(t)$) theory as presented by Suga and Sagawa ^[7], where

$$E(t) = \frac{P_{LV}(t)}{[V_{LV}(t) - V_0]} \quad [\text{Eq. IV-9}]$$

P_{LV} and V_{LV} represent LV pressure and volume, respectively, and V_0 is the volume intercept of the end-systolic pressure-volume relation. A normalized elastance curve for sheep was derived from previously acquired experimental data ^[179] and has been implemented in the program. The data of that experiment (8 sheep) were also used for calibration of the model ^[194]. When end-systolic (E_{es}) and end-diastolic (E_{ed}) elastance and the time of end-systole (t_{Ees}) of a specific sheep are known, the normalized elastance function can be scaled accordingly, and thus left ventricular function is fully characterized by E_{es} , E_{ed} , t_{Ees} , V_0 and heart rate.

The simulations in this work are based on data from one (reference) animal, of which the necessary parameters were derived from measurements (i.e., P_{LV} and V_{LV}) during vena cava occlusion and steady state. Thus cardiac reference values for the simulations are: $E_{es} = 1.55$ mmHg/ml; $E_{ed} = 0.12$ mmHg/ml, heart rate = 104 beats/min, $t_{Ees} = 0.275$ s and $V_0 = 14.8$ ml.

The systemic arterial system of a subject can be completely described by a four-element windkessel model ^[125], which is our arterial module. It consists of total

peripheral resistance (R_p), total arterial compliance (C), total inductance (L) and the characteristic impedance of the aorta (R_c). These 4 parameters can be derived via curve fitting procedures from pressure and flow continuously measured in the ascending aorta ^[187]. Due to the unavailability of continuous aortic flow, an alternative method was used to determine the systemic load of our reference animal: mean carotid pressure (MCP), pulse pressure (PP), stroke volume (SV), and heart rate (HR) were used in the following formulas:

$$R_p = \frac{MCP}{SV \cdot HR} \quad (\text{mmHg} \cdot \text{s/ml}) \quad [\text{Eq. IV-10}]$$

$$C = \frac{SV}{PP \cdot 1.4} \quad (\text{ml/mmHg}) \quad [\text{Eq. IV-11}]$$

R_c and L were adjusted within limited range to improve the agreement between measured and simulated pressure-volume loops when there was no pump present. This yielded the following arterial reference parameter set: $R_p = 1.13$ mmHg.s/ml, $C = 1.27$ ml/mmHg, $R_c = 0.15$ mmHg.s/ml and $L = 0.05$ mmHg.s²/ml.

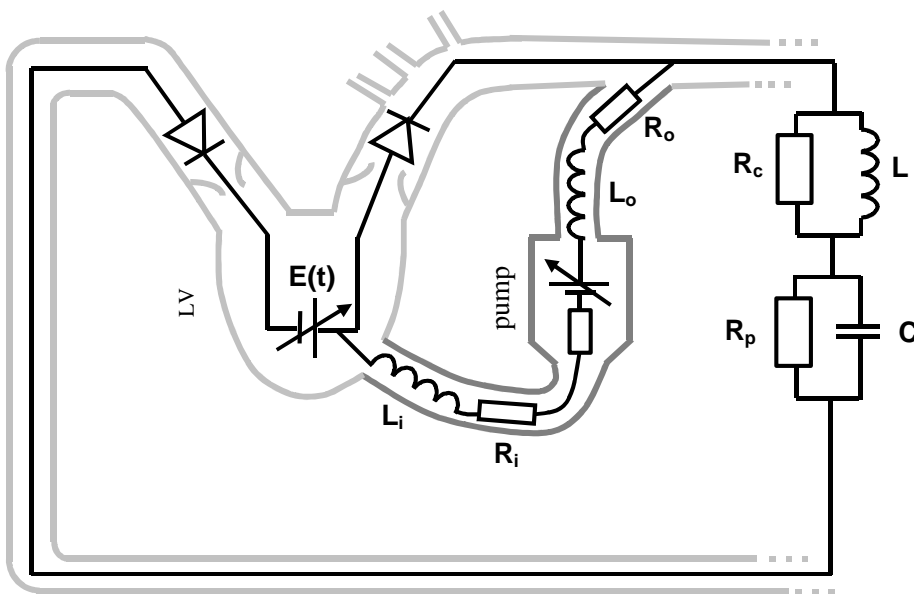


Fig. IV-12: Schematic view on the 3 modules of the mathematical model: the left ventricle (LV), the diagonal pump and the arterial 4 element windkessel module. $E(t)$: time varying elastance; L_i and L_o : inductance of inlet and outlet cannula; R_i and R_o : resistance of inlet and outlet cannula; R_c : characteristic resistance; L : arterial inductance; R_p : peripheral resistance; C : total arterial compliance.

The third (pump) module is built upon an equation that was fitted to quasi-static pressure head-flow curves assessed from the Medos-HIA microdiagonal pump in an experimental setup with continuous flow. Additional resistive (R_i , R_o) and inertial (L_i , L_o) terms are calculated in real-time, based on the inlet and outlet (index i and o , respectively) cannula dimensions and added to the equation to make it valid for pulsatile flow. This results in the following equation that expresses the pressure head over the pump in function of the pump flow, which demonstrated an excellent correlation to experimental data ($r^2=0.99$):

$$P_{ao} - P_{LV} = A \cdot \omega^2 + R_{tot}(Q_p) \cdot Q_p^2 + L_{tot} \cdot \frac{dQ_p}{dt} \quad [\text{Eq. IV-12}]$$

Where P_{ao} is the aortic pressure (mmHg), A is the pump constant (mmHg/rpm²), ω is the rotational speed (rpm), Q_p is the pump flow (l/min), $R_{tot} = R_i + R_o + R_{pump}$ is the total resistance (mmHg·s/ml), and $L_{tot} = L_i + L_o =$ total inertance (mmHg·s²/ml).

The pump module was introduced into the cardiovascular model to simulate the LV to aorta cannulation that was used in the animal experiment. The inlet cannula dimensions were 50 Fr x 290 mm (diameter x length) and the outlet cannula dimensions were 8 x 395 mm.

3.2. Model output

The output variables consisted of time-varying left ventricular pressure and volume (P_{LV} and V_{LV}), aortic pressure and flow (P_{ao} and Q_{ao}), mitral flow (Q_{tot}) and pump flow (Q_p). The term aortic flow in this context indicates in fact the flow through the aortic valve, so $\bar{Q}_{ao} + \bar{Q}_p = \bar{Q}_{tot}$. The output variables were reported for one cardiac cycle following convergence of the simulation.

To allow more detailed evaluation of left ventricular function and the interaction with the pump, additional parameters related to LV mechanical performance and energetics were derived from the pressure-volume (PV) loops^[189]. The external work (EW) was calculated as the area within the PV-loop and quantifies the energy that is delivered to the blood by the left ventricle. Potential energy (PE) was calculated as the triangular area between ESPVR, EDPVR and PV-loop. This area quantifies the energy that is consumed by the left ventricle for a single muscle contraction. The sum of these areas is known as the pressure-volume area (PVA) and is closely related to the oxygen consumption of the heart^[195].

To estimate the meridional wall stress (σ_m) imposed on the myocardium, a formula based on Laplace's law was used:

$$\sigma_m = \frac{P_{LV} \cdot D^2}{4w \cdot (D + w)} \quad (\text{mmHg}) \quad [\text{Eq. IV-13}]$$

with LV pressure (P_{LV}), inner diameter (D , short axis of the LV 'ellipsoid') and wall thickness (w) as variables ^[21]. This formula was derived assuming a thick-walled ellipsoid model for the LV. To calculate the wall thickness throughout the cardiac cycle, the muscle is assumed to be isotropic and to have a constant volume. This wall thickness is calculated relative to the end-systolic wall thickness, which was assumed to be 10 mm.

3.3. Simulations

Unless otherwise stated, all simulations were performed adopting the reference model parameters as given in the previous sections, which are derived from data measured in a healthy sheep (56 kg). The reference pump speed was chosen 4000 rpm since preliminary simulations pointed out that this is the optimal setting at which there is still cyclic flow through the aortic valve (systole), while the backflow through the pump (diastole) is minimal.

Table IV-3: Parameter values used in the first simulation series

	heart rates (BPM)	elastances (mmHg/ml)	pump speeds (rpm)
A	50	0.5	2000
B	75	1.0	4000
C	100	1.5	6000
D	125	2.0	8000
E	150	2.5	10000

One of the three variables was varied over the range A-E while the other two were kept constant at their reference value (104 BPM, 1.55 mmHg/ml and 4000 rpm, respectively).

In a first simulation series, the pump was operated in continuous mode (constant pump speed) and the following three parameters were individually varied: heart rate (HR), end-systolic elastance (E_{es}) and pump speed. Each parameter was set to 5 different values, as summarized in Table IV-3, while all other parameters were kept constant at their reference value. The time of end-systole (t_{Ees}) was adjusted in relation to the heart rate.

In a second simulation series, a sinusoidal modulation was applied to the reference pump speed, as shown in Fig. IV-13. The resulting speed pattern had the same cycle length as the cardiac cycle (synchronous support), an average of 4000 rpm and an amplitude of 2000 rpm. Only one parameter is varied in this series: the phase lag between the onset of ventricular systole and the onset of the pump speed “diastole”. The phase was varied between 0 and 100% of the full cycle in 10% increments. All other parameters were set to their reference values.

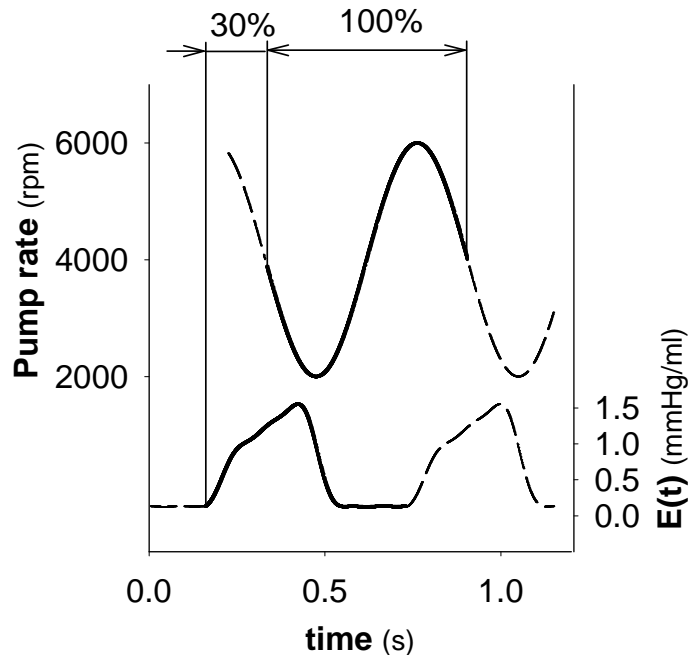


Fig. IV-13: Illustration of the pulsatile pump speed pattern, here indicating a time shift of 30% of the full cycle. The reference point is the onset of systole assessed from the time-varying elastance curve.

4. Results

4.1. Continuous mode simulations

To illustrate the effect of pump speed on the calculated variables, Fig. IV-14 shows a calculated PV-loop, LV wall stress, LV and aortic pressure and aortic flow at 2000 and 10000 rpm. The increase in speed results in a reduction of both LV volume and pressure. The combination of these effects results in a considerable decrease in maximal wall stress (31%). The peak wall stress is always reached before the end of systole. At 2000 rpm, the aortic valve opens and closes cyclically as evidenced by the partial overlap of aortic and LV pressure and the aortic flow pattern. This is in contrast with the data at 10000 rpm, where there is no aortic flow (0 l/min). This is related to the pressure head

over the aortic valve, where the aortic pressure is high and nearly constant (150 mmHg) while the LV pressure stays below 65 mmHg. When increasing the speed from 2000 to 10000 rpm, the increase in aortic pressure is much greater than the decrease in LV pressure. When comparing panels 9 and 12 from Fig. IV-15, it appears that this effect (increase in aortic and decrease in LV pressure) is most pronounced between 6000 and 10000 rpm.

Fig. IV-15 further summarizes the effects of heart rate, E_{es} and pump speed on the different mechano-energetic parameters under study. The influence of heart rate is much smaller than the influence exerted by LV contractility (E_{es}) or pump speed. All parameters - except for pump flow - rise by an increase in elastance. Panel 2 shows that at the reference pump speed of 4000 rpm, the pump provides the total blood flow in a weak heart (lowest E_{es}), resulting in cessation of mean aortic flow (continuously closed aortic valve). Improved contractility leads to increased aortic flow and decreased pump flow, although not to the same extent. Consequently, the contribution of the pump to the total mean flow is 100% for the case of minimal elastance and only 9% at maximal elastance (panels 2 and 5). Obviously, increased contractility also leads to higher pressures, LV wall stress and oxygen consumption (\sim PVA), which is demonstrated in panels 8,11,14 and 17. The major determinant of mean flow with the cardiac assist pump running at constant speed is clearly the pump speed itself, which has a much larger impact than heart rate or contractility. Aortic flow decreases steeply with increased pump rate and becomes zero from 6000 rpm on (when mean aortic pressure starts rising). Mean pump flow increases linearly with increasing pump speed, starting at a flow of -1.4 l/min at 2000 rpm (i.e., backflow through the pump) and resulting in a maximum flow of 8 l/min at 10000 rpm (not completely shown on the graph), which is rather high for sheep. The contributions of the pump to total flow are -49% and 33% for 2000 and 4000 rpm, respectively and 100% for the higher pump speeds. The increasing pump speed also results in improved unloading of the LV, which can be concluded from the decreasing wall stress and PVA (panels 15 and 18).

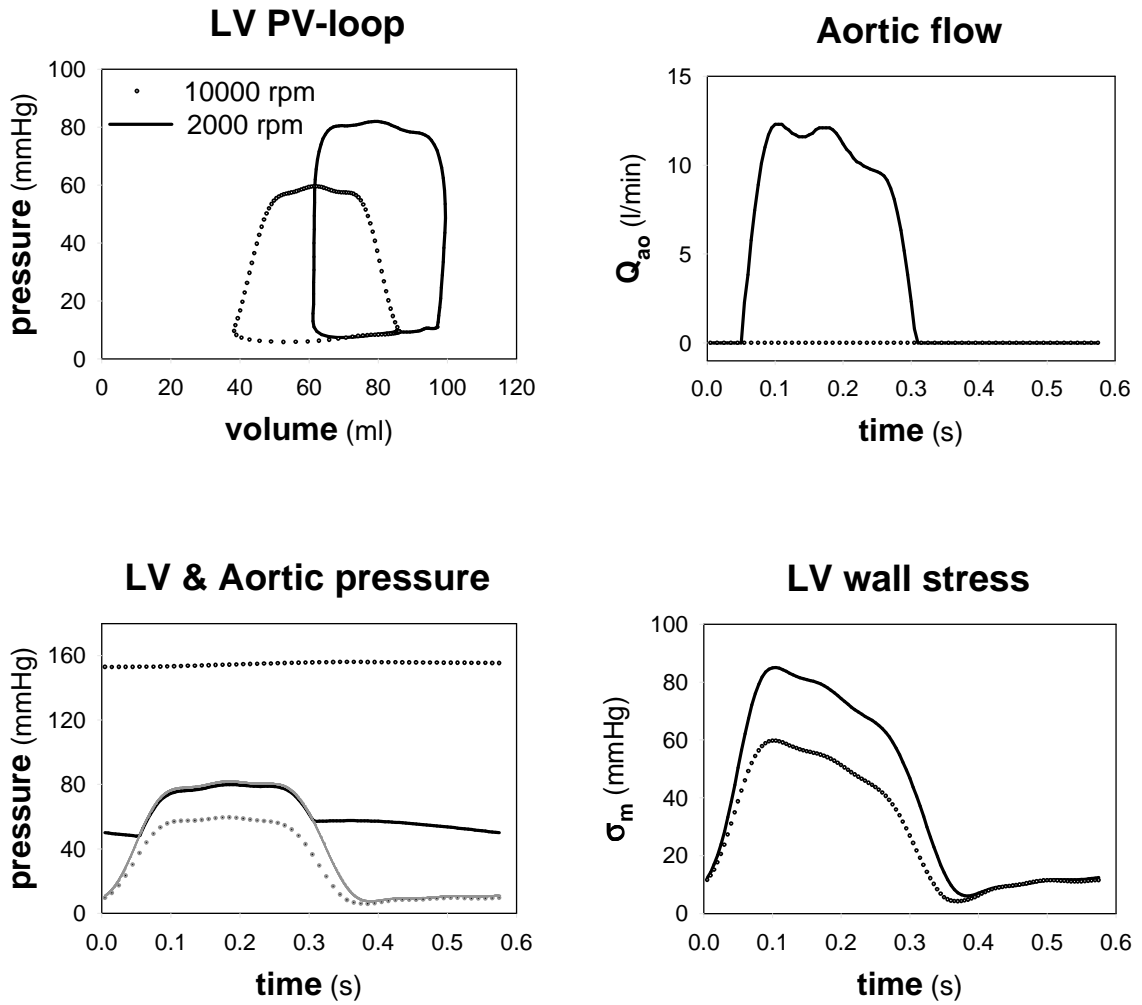


Fig. IV-14: Comparison of results obtained with a constant pump speed of 2000 (solid lines) and 10000 (dotted lines) rpm. The gray lines represent left ventricular pressure, while the black lines in the same graph show aortic pressure. Aortic flow is calculated at the aortic valve.

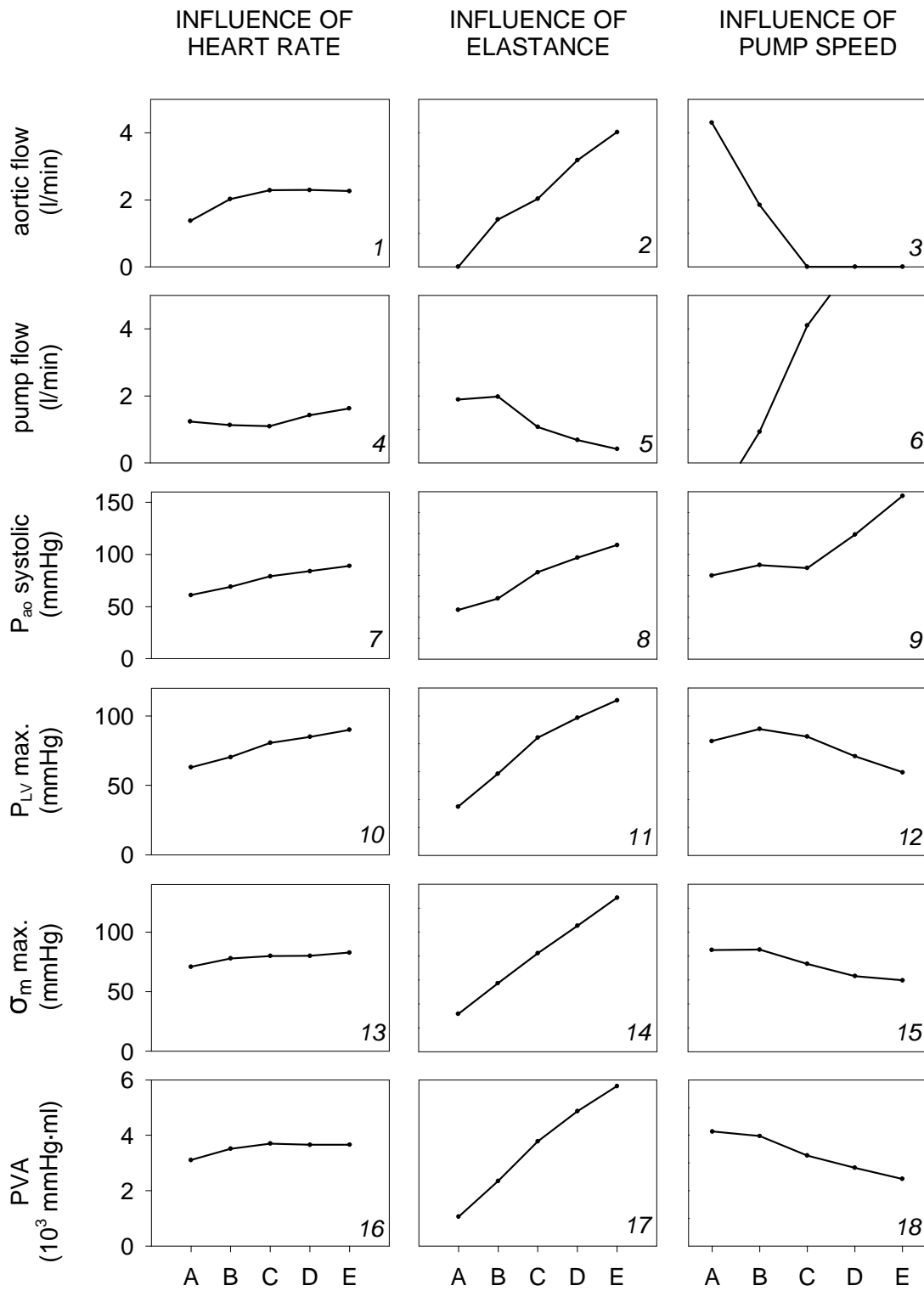


Fig. IV-15: Summary of the results of the parameter study with the pump running at a constant speed. P_{ao} systolic is the systolic aortic pressure; P_{LV} max. is the maximal left ventricular pressure; σ_m max. is the maximal calculated meridional wall stress of the left ventricle and PVA is the pressure-volume area of the calculated PV-loop. The values of A-E can be found in Table IV-3.

4.2. Pulsatile mode simulations

The simulations with the time-varying pump speed show that timing has an important effect on the hemodynamics and ventricular energetics (see Fig. IV-16). The thin horizontal lines in Fig. IV-16 represent the results from the constant speed simulations at 4000 rpm, which is our point of comparison. It can be deduced from Fig. IV-16 that a higher mean pump flow can be reached with the pulsatile pump speed pattern if the phase shift is below 40% or above 90%. The aortic flow reacts inversely to the phase shift, thus resulting in a total mean systemic flow (the sum of pump and aortic flow) that is fluctuating around the mean total flow that would be obtained if the pump were running at a constant speed of 4000 rpm.

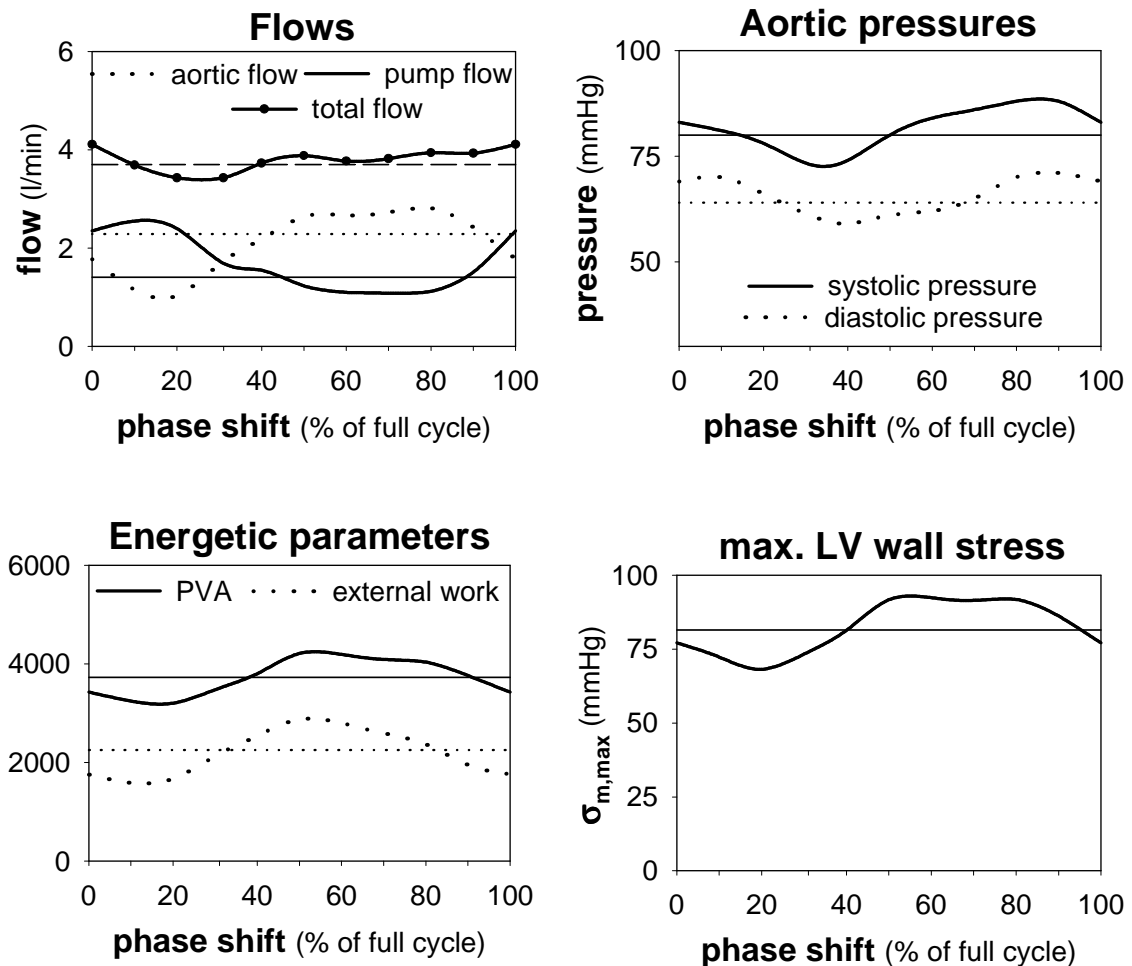


Fig. IV-16: Results of the pulsatile mode simulations as a function of the phase shift (thick lines). The thin horizontal lines represent the values calculated with a constant pump speed of 4000 rpm.

For a 0% phase shift, a mean total flow of 4.1 l/min is obtained, compared to only 3.7 l/min with the constant speed simulation. For a phase shift range of 20 to 50%, systolic and mean aortic pressure for pulsatile operation are decreased from the case of constant speed, while diastolic aortic pressure is reduced in a slightly higher range. Consequently, the pulse pressure in the pulsatile simulations is only higher than in the constant speed simulations for shifts of 50% and above. The PVA and the external work delivered by the LV are both lower than the constant speed value when considering phase shifts below 30%. Higher shifts result in external work that is markedly higher than the constant speed value. For the wall stress, 50% phase shift is the limit up to where the values obtained with the pulsatile pump speed stay noticeably lower than the constant speed value. The maximal decrease in PVA that can be obtained with a well-timed pulsatile pattern is 14% of the constant speed value. The maximum wall stress $\sigma_{m,max}$ can be reduced by 16%.

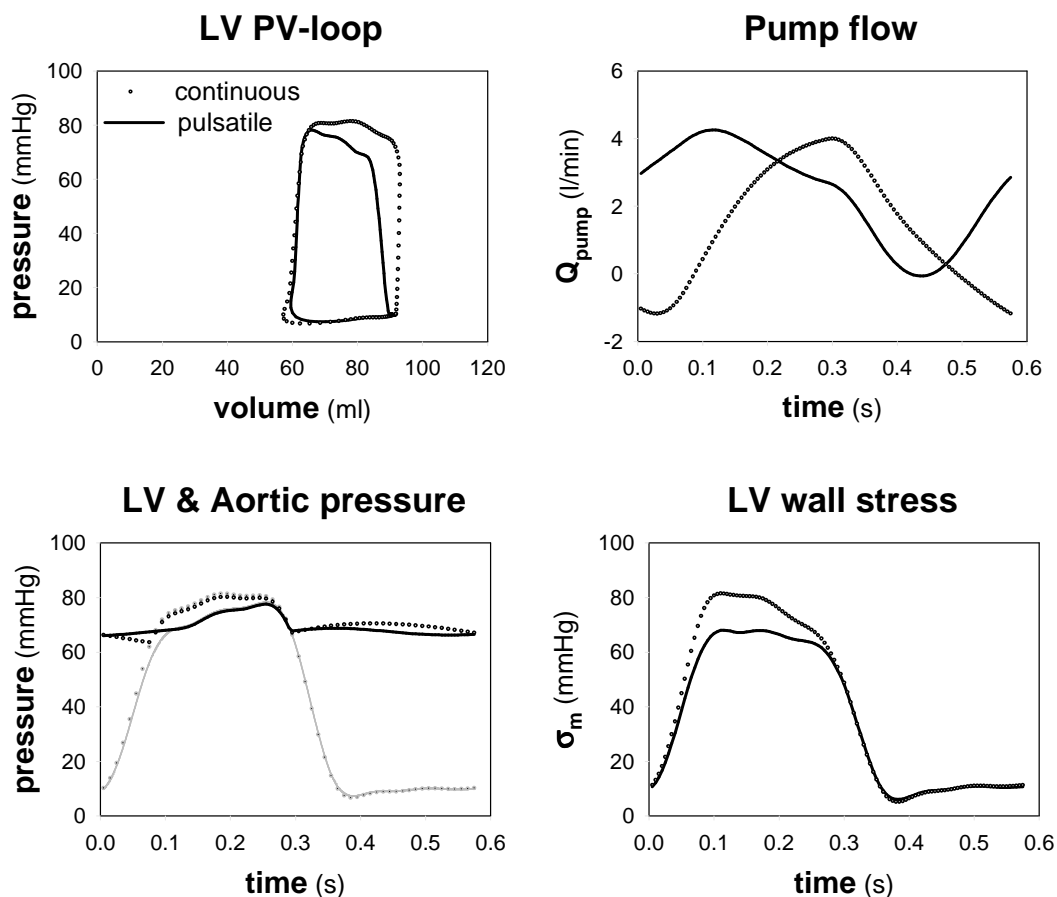


Fig. IV-17: Comparison of results obtained with a constant pump speed of 4000 rpm (dotted lines) vs. a pulsatile pump pattern with 20% phase shift and an average speed of 4000 rpm (solid lines). The gray lines represent left ventricular pressure, while the black lines in the same graph show aortic pressure.

5. Discussion

Although reduction of wall stress, LV pressure and end-diastolic volume is desirable for unloading of the heart, it is not yet clear whether complete unloading (where all flow is delivered by the pump and the aortic valve stays continuously closed) is more favorable than partial unloading. Our simulations in continuous mode show that complete unloading can only be achieved at high pump speeds. Complete unloading requires the pump to deliver enough energy to surpass the cardiac work thus elevating mean arterial pressure. Due to regulatory and compensatory effects in the real cardiovascular system, high pressures will be normalized by decreasing the vascular resistance (within a limited range), which is not the case in our simulations. Consequently, an overestimation of arterial pressure is present in our results.

Typical for unloading at high constant speeds is the triangular shape of the left ventricular PV-loop ^[155], as illustrated in Fig. IV-14. Even though isovolumic contraction and relaxation phases are very short in the normal heart, the pump evacuates blood rapidly from the LV resulting in volume variations during these phases. A phenomenon noticed at low pump speeds, when there is minimal unloading, is backflow through the pump due to the negative pressure head during diastole. According to our simulations, this is particularly true in highly contractile ventricles, although the main determinant is the generated arterial pressure.

It is clear that the pump (running at constant 4000 rpm) contributes appreciably to the total flow when it is cooperating with a weak heart. With increasing contractility (elastance), the ventricle assumes more work from the pump, which is reflected in increasing aortic flow and decreasing pump flow in Fig. IV-15. Such changes may be experienced clinically due to recovery of the heart or sympathetic response; however the variation in elastance will not commonly be as large as the range we simulated.

When heart rate increases during cardiac assist, it can be expected that the natural physiological responses dominate the parameter changes ^[196], which is seen in Fig. IV-15. This is somewhat expected, as the (time-varying) pressure drop over the pump does not drastically change as a consequence of heart rate changes. Pump flow is thus only altered by changes in inertia due to the more rapid

pressure variations. In contrast with the elastances, the simulated heart rate variations may occur in daily life.

Our data demonstrate that modulation of pump speed allows to unload the left ventricle without increasing the aortic pressure, by selecting the right phase shift. As compared to continuous speed operation, it would be impossible to decrease the load on the LV (by increasing the rpm) without an increase in arterial pressure. The use of modulated pump speed only causes limited changes in total flow and therefore these simulations suggest that a pulsatile pattern as used in this study can maintain perfusion while providing superior preload and afterload reduction to the LV.

Bearing in mind the analogy with the intra-aortic balloon pump, we anticipated that a counterpulsation pattern (highest pump speeds during diastole) would be ideal to enhance unloading and stress reduction. This operational mode only causes a mild increase in arterial pressure during systole, thus diminishing ventricular afterload compared to continuous speed operation. The higher pump flow during diastole reduces the end-diastolic LV volume, which results in a favorable shift on the Frank-Starling curve. In addition, counterpulsation augments flow and pressure in the aorta during diastole, thereby improving coronary perfusion as seen with intra-aortic balloon pumps. In order to assess the optimal phase shift yielding the most favorable unloading of the LV, we studied mechanical/energetic parameters such as derived oxygen consumption and wall stress. Our results indicate that a phase shift of approximately 20% yields most favorable results for these parameters, which supports the counterpulsation idea. In Fig. IV-17, the results of the simulations with a pulsatile pattern and a 20% phase shift are compared to the constant speed simulation at 4000 rpm. The influence of the pulsatile pattern is reflected in the pump flow, where it has to be taken into account that the pressure head over the pump varies. Further study is required to determine the optimal pulsatile pattern for this specific pump, but the pattern used in this study is easy to implement in control algorithms.

For this inverted sine wave pattern, we found that the pulsatile pump flow is higher than its constant speed counterpart up to a 40% phase shift. This is the result of concentrating pump energy in diastole, where it is most needed to overcome the adverse pressure head. During systole there is almost no pressure head over the pump and thus a sufficient flow can be obtained at a low rotational

speed. This lower speed also results in a lower aortic pressure during systole and consequently the LV has to perform less work to eject the blood.

All of our simulations were performed with the pump in synchronous pulsatile mode. In clinical practice, however, triggering for synchronous support can be difficult, especially in patients with recurrent arrhythmias. Asynchronous support is therefore favored. Several beats then have to be taken into account for evaluation and we expect that timing and time-shifts will also be important in that case.

In the simulations all parameters, except the one studied, were kept constant, thus neglecting the physiological response of the cardiovascular system. Since we considered sheep data, the simulations cannot simply be translated to clinical cases and as such, our results are to be seen as indicative, rather than absolute. This is particularly true for the calculated wall stress, which should be seen relative to the end-systolic value, where it is assumed that the wall thickness is 10 mm regardless of end-systolic volume. The most important consequence of keeping the parameters constant is the overestimation of arterial pressure. Nevertheless, the model gives a good view on the influence of unloading and the variations in effective wall stress.

For the pulsatile mode simulations, the physical limits of the rotary blood pump are not taken into account, meaning that the inertia of the rotor may restrict the possibilities for pulsatile support. This study is to be seen as a preliminary investigation of pulsatile support with a specific rotary blood pump, where the amplitude of the pulse pattern is arbitrarily chosen and the frequency defined by a previous animal study ^[179]. It remains to be studied whether the resulting acceleration and deceleration of the rotor can be achieved *in vitro* and *in vivo*. Furthermore, the characteristics of the pump we implemented were assessed at different constant speeds, while in the pulsatile pattern the working point actually shifts continuously from one characteristic to another. It is possible that a dynamic characteristic slightly differs from the combination of static characteristics. It can be expected that the pulsatile use of a rotary blood pump leads to higher shear inside the pump and consequently a higher hemolysis rate will appear. It has been demonstrated by Wang et al. and Tayama et al. ^[197,198], however, that it is possible to use a rotary blood pump in a pulsatile mode without increase in hemolysis, if the pump operation is restricted within certain limits. Finally, it should be studied whether pulsatile support with a rotary blood

pump is more or less susceptible to suction problems than continuous support. Our model currently does not allow simulation of suction, a problem that can best be evaluated *in vitro* and *in vivo*.

6. Conclusions

We used a validated mathematical model to investigate the unloading effect of a rotary blood pump (Medos-HIA microdiagonal pump). This effect was evaluated by hemodynamic data and mechano-energetic parameters derived from LV pressure-volume data. Our results indicate that for a rotary blood pump running at constant speed, complete unloading of the LV can only be achieved at high pump speeds.

A more efficient unloading is achieved by running the pump in a pulsatile mode in a counterpulsation pattern. This operation mode can decrease LV external work, wall stress, and oxygen consumption without impeding the flow. It is thus beneficial to have a low pump speed during ventricular systole and high pump speed during ventricular diastole.

7. Acknowledgements

The authors wish to thank Christoph Göbel for supplying the pump data and Takahiro Nishida for the valuable sheep data. They are also grateful to James Antaki for the thorough review.

This research was funded by a specialization grant of the Flemish Institute for the Promotion of Scientific-Technological Research in Industry (IWT-993171, S. Vandenberghe) and by a post-doctoral grant from the Fund for Scientific Research – Flanders (FWO Vlaanderen, P. Segers).

D. IN VITRO MODEL STUDY OF ROTARY BLOOD PUMP FAILURE AND VENTRICULAR ASSIST WITH A ROTARY BLOOD PUMP IN CONTINUOUS AND PULSATILE MODE

1. Introduction

The Medos Deltastream (Medos Medizintechnik GmbH, Stolberg, Germany) is a rotary blood pump with a diagonal flow path which is intended for use in miniaturized CPB circuits or ECMO systems. Nonetheless, the device is also applicable for short-term ventricular assist. In spite of three years of clinical experience and numerous animal trials, no detailed investigation of the heart-device interaction has been performed so far, according to our knowledge. Previous investigation was mainly focused on the safety and durability of the device, rather than its unloading capacities. Moreover, the device has the possibility to apply a pulsatile flow waveform but the interaction of that with a beating heart has not yet been assessed. The waveform is obtained via sinusoidal modulation of the rotational speed, and it has already been observed in mock loop testing ^[199] that the resulting pressure and flow waveforms do not fulfill the criteria for true pulsatile flow as stated in literature ^[200]. Nevertheless, the pulsatile pattern may have an important impact on the loading conditions of the heart.

This study investigates the interaction of the Deltastream device with an *in vitro* heart simulator in both continuous and pulsatile mode. Special attention is given to the load that is imposed on the heart by the device, but no autonomous nervous feedback mechanisms are simulated and thus only the pure hydraulic interaction is assessed.

2. Materials

An *in vitro* setup was constructed that consisted of a pneumatically driven heart simulator, an arterial afterload section and the Medos Deltastream device. The heart simulator consists of a left atrium and a left ventricle (LV), made out of

silicone rubber and contained in a Plexiglas housing filled with water. Details on the system were described earlier ^[145]. For this study, the ventricle was extended with a silicone tube at the apex to allow apical cannulation. The afterload section was also described earlier ^[187] and consists of a windkessel, a resistor with compressible foam, and a venous overflow reservoir. The Deltastream pump was connected between the heart simulator and the windkessel as to simulate apical to ascending aorta cannulation. The pump inflow cannula was 170 mm long with an inner diameter of 10 mm, while the outflow cannula consisted of 190 mm of the same tubing, and an additional 70 mm of ½" tubing to accommodate two separate flow probes for control and data acquisition. The test fluid was a 60/40 v/v% water-glycerin mixture with a kinematic viscosity of 3.65 mm²/s at an average temperature of 26°C.

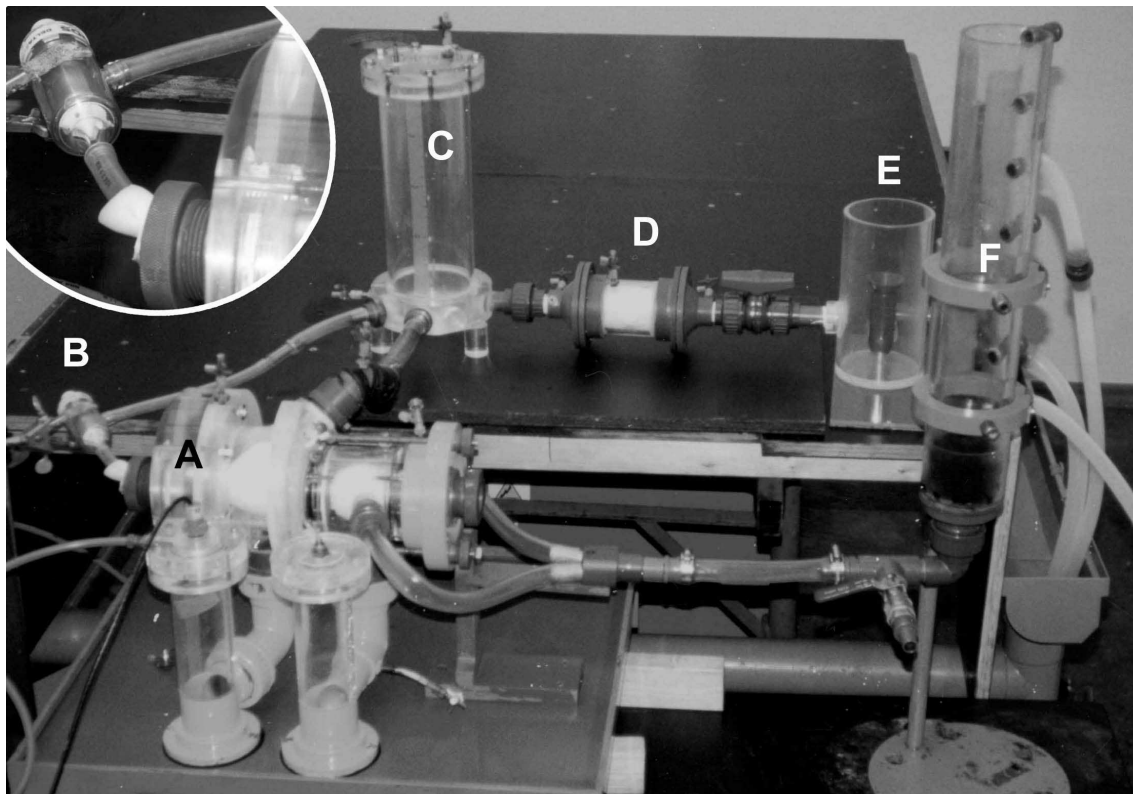


Fig. IV-18: Picture of the setup with the afterload section of the mock loop in the back, the heart simulator in the front, and the Deltastream pump on the most left. A: heart simulator. B: Deltastream. C: windkessel. D: resistor. E: venous overflow reservoir. F: preload (lung) reservoir.

The standard driver of the heart simulator is a computer-controlled pneumatic actuation system where a proportional valve follows a programmed pressure waveform based on feedback information of left ventricular pressure. However,

such a feedback control prevents unloading of the ventricle, where lower pressures than the predetermined curve are expected. The feedback pressure transducer was therefore set to a fixed (threshold) pressure value with a water column. As a consequence, the proportional valve acted as a simple on/off valve that was switched when the programmed pressure waveform crossed the threshold pressure. This resulted in an operation similar to the older drivers of pneumatic assist devices: systole was obtained by opening a valve between a pressurized buffer reservoir and the device. These drivers usually applied a slightly negative pressure in a separate buffer reservoir for diastole, while our system is restricted to atmospheric pressure.

The Deltastream pump was driven by a laboratory drive console, provided by the manufacturer, that allowed rotational speed control - where a fixed speed could be set - or pulsatile control. The console comes with two pressure sensors for feedback, which were connected to the LV (preload) and the windkessel (afterload). A flow probe - clipped on the pump outflow cannula - was also required. No triggering was available on the laboratory console so only asynchronous pulsatile support could be simulated. The pulsatile control mode imposed a sinusoidal rotational speed pattern upon the pump and its characteristics were derived from three parameters that could be set: pulse frequency, pulse pressure, and average flow rate. The software for the two control modes allowed data logging of the variables that were controlled or measured by the console. The logging interval, however, was not constant and the maximum sample frequency was approximately 10 Hz.

The data that were captured in the log file contained a time stamp, the preload and afterload pressure, the pump flow, the rotational speed, and the electrical power consumed by the pump. Further data were acquired with the controller of the heart simulator at a sample frequency of 200 Hz for at least 5 seconds under steady state conditions. These data included left ventricular pressure (P_{LV}) measured with a hi-fi cathetertip transducer (Millar Instruments Inc., Houston, TX) and aortic pressure (P_{ao}) measured in the windkessel with a DTX+ strain gauge pressure transducer (Ohmeda, Gent, Belgium). Aortic flow (Q_{ao}) was measured at the connection tube between the aortic valve and the windkessel with a H16C probe and HT207 flow meter (Transonic Systems Inc., Ithaca, NY) while the pump flow (Q_{pump}) was sampled at the pump outflow cannula with an H11X flow probe and HT109 flow meter. Additionally, the volume in the left

ventricle (V_{LV}) was acquired from an ultrasonic level meter (Superprox SM606, Hyde Park Electronics LLC, Dayton, OH) in the water column that communicates with the ventricle housing for pneumatic actuation.

For synchronization of the data captured with the heart simulator console and the Deltastream console, a signal generator was used to pass on a low frequency triangular signal (approx. 0.2 Hz) to a pressure channel on each console. Consequently, this signal was acquired and stored in the log files of both consoles.

3. Methods

3.1. Continuous mode

The Deltastream pump was ran according to a protocol that started with a baseline acquisition (BL) where the pump was shut off and the inflow cannula clamped. Next, the clamp was removed to simulate pump failure (0 rpm), which was followed by incrementally increasing the rotational speed from 1000 to 5000 rpm in steps of 1000 rpm. At each of the seven steps in this pump protocol, data acquisition was performed when a steady state was reached. This pump protocol was repeated for various contractile and rhythmic conditions of the heart. The heart's contractile state was varied by altering the pressure of the pneumatic buffer reservoir in the actuating system. The pressure level (PL) was set to obtain systolic aortic pressures of 80, 100, and 120 mmHg at baseline, and these conditions are further indicated as $PL80$, $PL100$, and $PL120$, respectively. $PL120$ simulated a healthy subject while $PL100$ and $PL80$ mimic assorted grades of left ventricular dysfunction. Within each pressure level, the heart rate (HR) was set consecutively at 50, 100, and 150 beats per minute (BPM), where 100 BPM comes closest to the clinically observed rates. The afterload was set to obtain a total vascular resistance of 1.2 mmHg·s/ml at $PL120$ and a heart rate of 100 BPM. The afterload was not varied during the measurements and thus there were 63 different conditions: 7 pump states, 3 heart rates, and 3 contractile states.

3.2. Pulsatile mode

All experiments in pulsatile mode were performed at $PL100$. Two combinations of heart rate and pump rate (PR) were tested at two different settings for pump flow and pulse pressure to assess the interaction between the pump and the heart. An overview of the four tested combinations is given in Table IV-4. Data were

acquired repeatedly over 10 second spans to create an observation of the changes in flow and pressure patterns over time.

Furthermore, a simulation of synchronous ventricular assist was performed where different trigger settings were analyzed. This was achieved by combining a heart rate of 100 BPM (at *PL100*) with a pump rate of 95 BPM while data were acquired over 150 consecutive heart beats (*HR 100 – PR 95*). This was repeated with a pump rate of 98 BPM where 165 heart beats were acquired (*HR 100 – PR 98*). As a result of the small difference in frequencies, each heart beat and pump beat had approximately the same period, but for each consecutive beat the onset of the heart beat was a little delayed with respect to the onset of the pump ‘beat’. In this way, co-pulsation, counter-pulsation, and all intermediate triggering forms were simulated. For each beat, the shift between the onsets of pump and heart beat was calculated and expressed as a percentage of the heart period. The onset of the heart beat was defined as end-diastole, while the onset of a pump beat was defined as the point where the rotational speed falls below the average of the sinusoidal speed variation pattern (see Fig. IV-19), which agrees with the minimal derivative.

Table IV-4: Overview of the tested combinations of heart rate and pump settings.

Combination (-)	Heart Rate (BPM)	Pump Rate (BPM)	Pump Flow (l/min)	Pulse Press. (mmHg)
1	100	50	2	40
2	100	50	3.5	20
3	80	60	2	40
4	80	60	3.5	20

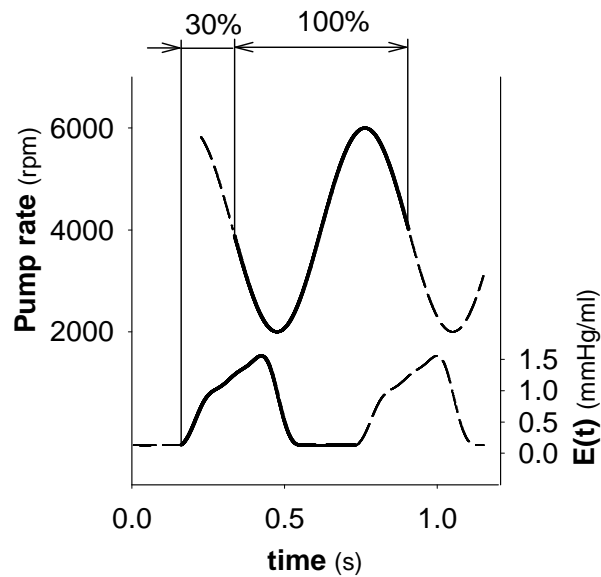


Fig. IV-19: Illustration of the phase shift definition, here indicating a shift of 30%.
E(t): left ventricular elastance.

3.3. Data processing

The data captured with the driving consoles of the heart simulator and the Deltastream pump were consecutively synchronized, interpolated, and merged to obtain one data file per measured setting. For the continuous mode data, an averaged beat was calculated from this file that was used for further calculation of average pressures and flows, hydraulic power generation (= flow x pressure head), stroke volume (SV), end-diastolic and end-systolic volume (EDV, ESV), and pressure volume area (PVA). This last parameter is the summation of the surface area within the left ventricular pressure-volume loop and the area between the end-systolic and end-diastolic pressure-volume relation in the same plane. For the calculation of these relations, a volume intercept (V_0) of 135 ml was assumed, based on the results of the pulsatile mode simulations (see Fig. IV-24). V_0 is the volume at which the ventricle cannot generate any pressure and it is therefore an intrinsic property of a ventricle and its contraction mechanism. In our *in vitro* model, however, V_0 is related to the dead volume in the rubber ventricle and thus PVA and other volume-related parameters should not be compared blindly to clinically observed values. Nonetheless, these parameters serve well as a means to compare the different interactions simulated in this experiment. It has been demonstrated that the PVA is a measure of oxygen consumption of the myocardium in a real heart ^[12].

The same pressure, flow, volume, and power parameters were derived for the pulsatile mode simulations, but based on individual beats instead of an averaged beat.

4. Results

4.1. Continuous mode

An example of baseline pressure and flow data is shown in panel A of Fig. IV-22 for a heart rate of 100 BPM and a pressure level of *PL100*. The results of the generated power and the resulting flows are displayed in Fig. IV-20 for the different pressure levels and rotational speeds for a heart rate of 100 BPM. The generated heart power increases with increasing pressure level, while the pump power is mainly sensitive to pump speed. As a result, the total power also increases with pump speed. The heart power that is generated at baseline is higher than any other. At a speed of 5000 rpm, the heart even ‘absorbs’ power, while aortic regurgitation occurs at that speed.

The total generated flow remains constant (mean \pm st. dev.: 4.8 ± 0.3 l/min), while the balance between pump flow and aortic flow shifts in favor of the pump flow for higher rotational speeds, where the pump also generates much more power. A pump speed of 0 rpm is a simulation of pump failure, and this can apparently result in regurgitation up to 2 l/min, depending on the remaining contractility (pressure level) of the heart. At a heart rate of 150 BPM, this regurgitant flow is higher (up to 3 l/min), and also the generated cardiac output is increased, thus leading to an equal total flow (4.7 ± 0.3 l/min). A heart rate of 50 BPM has an opposite effect, so lower regurgitation (1 l/min) and lower cardiac output yield a similar total flow (4.4 ± 0.3 l/min).

As a result of pump failure (0 rpm), the mean aortic pressure (MAP) drops from 80 mmHg at baseline (for *PL100*) to 43 mmHg (Fig. IV-21). Increasing pump speed augments the pressure gradually to a value of 147 mmHg at 5000 rpm. A heart rate of 150 BPM results in a MAP of 178 mmHg for the same condition. A similar trend is observed for the PVA, where the highest values are reached at a heart rate of 50 BPM: 10,445 mmHg·ml at baseline (*PL100*), compared to 8,177 mmHg·ml for the baseline value at 100 BPM.

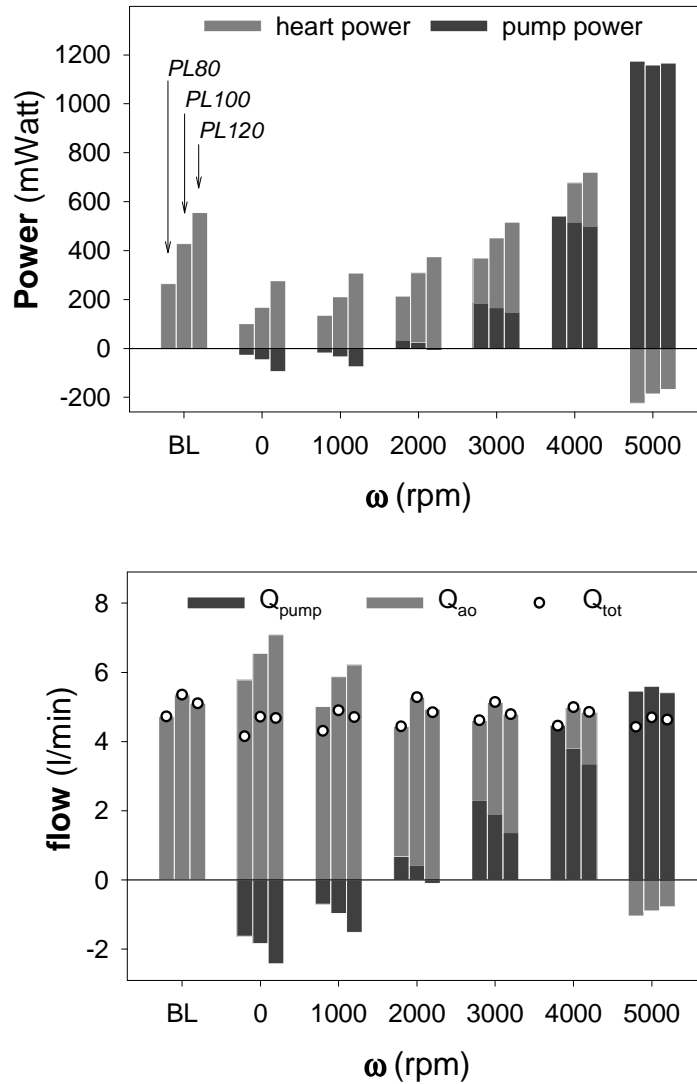


Fig. IV-20: Top panel: the power generated by the heart and the Deltastream pump as a function of the rotational speed. Bottom panel: Pump flow (Q_{pump}), aortic flow (Q_{ao}), and their sum (Q_{tot} , white dots) as a function of the rotational speed. The bars are grouped according to the pressure level (*PL80*, *PL100*, *PL120*), which simulates three different contractile states (see text). The heart rate was 100 BPM.

Pump failure results in an increase in stroke volume of 6 ml compared to BL (*PL100*, HR 100 BPM) and it takes a rotational pump speed of 3000 rpm to get the SV back to the baseline level. At a speed of 5000 rpm, the stroke volume has decreased 37% from baseline and measures 36 ml. For the same conditions, end-diastolic volume increases 10 ml from baseline if pump failure is simulated and it can be decreased 5 ml from baseline by setting a pump speed of 5000 rpm. Both SV and EDV are very dependent on the heart rate: while baseline SV and EDV at 100 BPM (*PL100*) are 57 and 235 ml, respectively, these values are 104 and 265 ml at 50 BPM, and 39 and 254 ml at 150 BPM. In fact, at 150 BPM the EDV is

not reduced with increasing pump speed, but it gradually rises to a value of 262 ml at 5000 rpm.

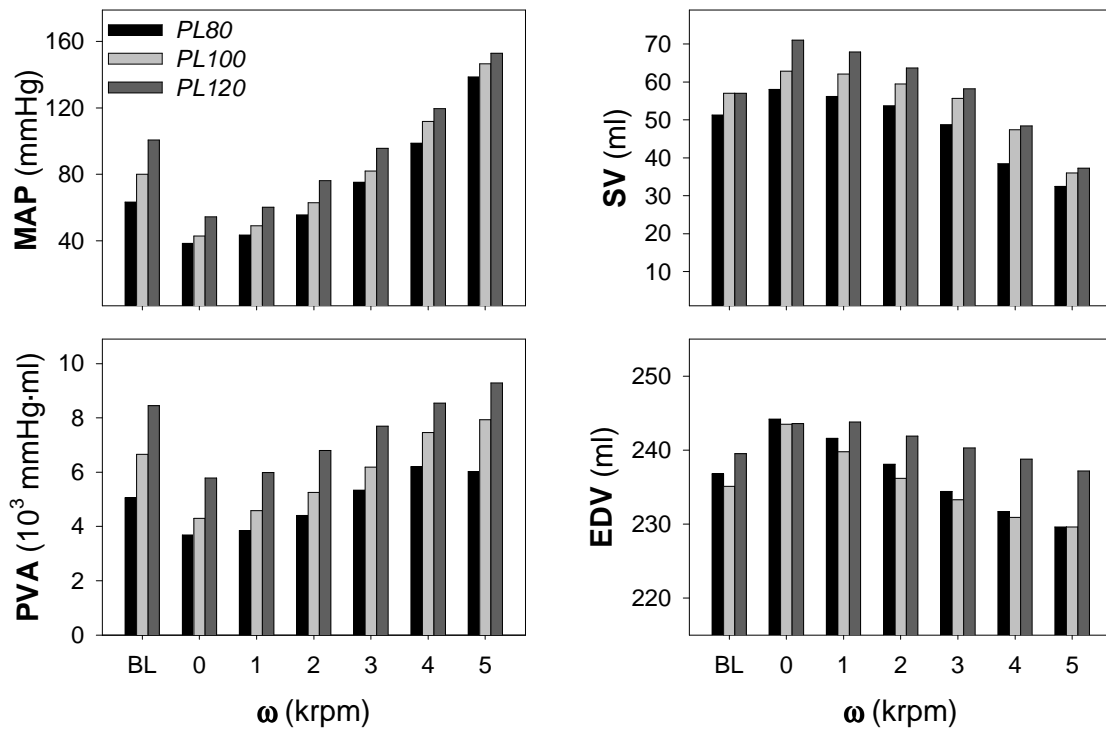


Fig. IV-21: The effect of rotational pump speed (ω) and pressure level (PL) on mean aortic pressure (P_{ao}), stroke volume (SV), pressure-volume area (PVA), and end-diastolic volume (EDV) at a heart rate of 100 BPM.

4.2. Pulsatile mode

A few examples of the heart-device interaction are shown in Fig. IV-22. Panel B and C show 2 samples of the combination of a heart rate of 100 BPM with a pump rate of 50 BPM. It can be observed that a pattern of 2 different alternating beats appears, which is most distinct in panel B. In panel C, which was acquired approximately 3 minutes later, the pattern is also present but the 2 beats are very alike and consequently the aortic pressure waveform looks almost normal. While the left ventricular pressure is generated by the heart at a rate of 100 BPM, the flow waveforms of panel C indicate that the ventricle is emptied alternately via the aortic valve and the pump. At times when the pump ‘beats’, outflow through the aortic valve is completely suppressed. The mean pump flow for this combination was set at 3.5 l/min on the drive console, while in both samples it turned out to be 4.3 l/min. Pulse pressure generated by the pump was set at 40 mmHg and it measured 39 mmHg in the data of panel B, while only 28 mmHg was reached in the data of panel C.

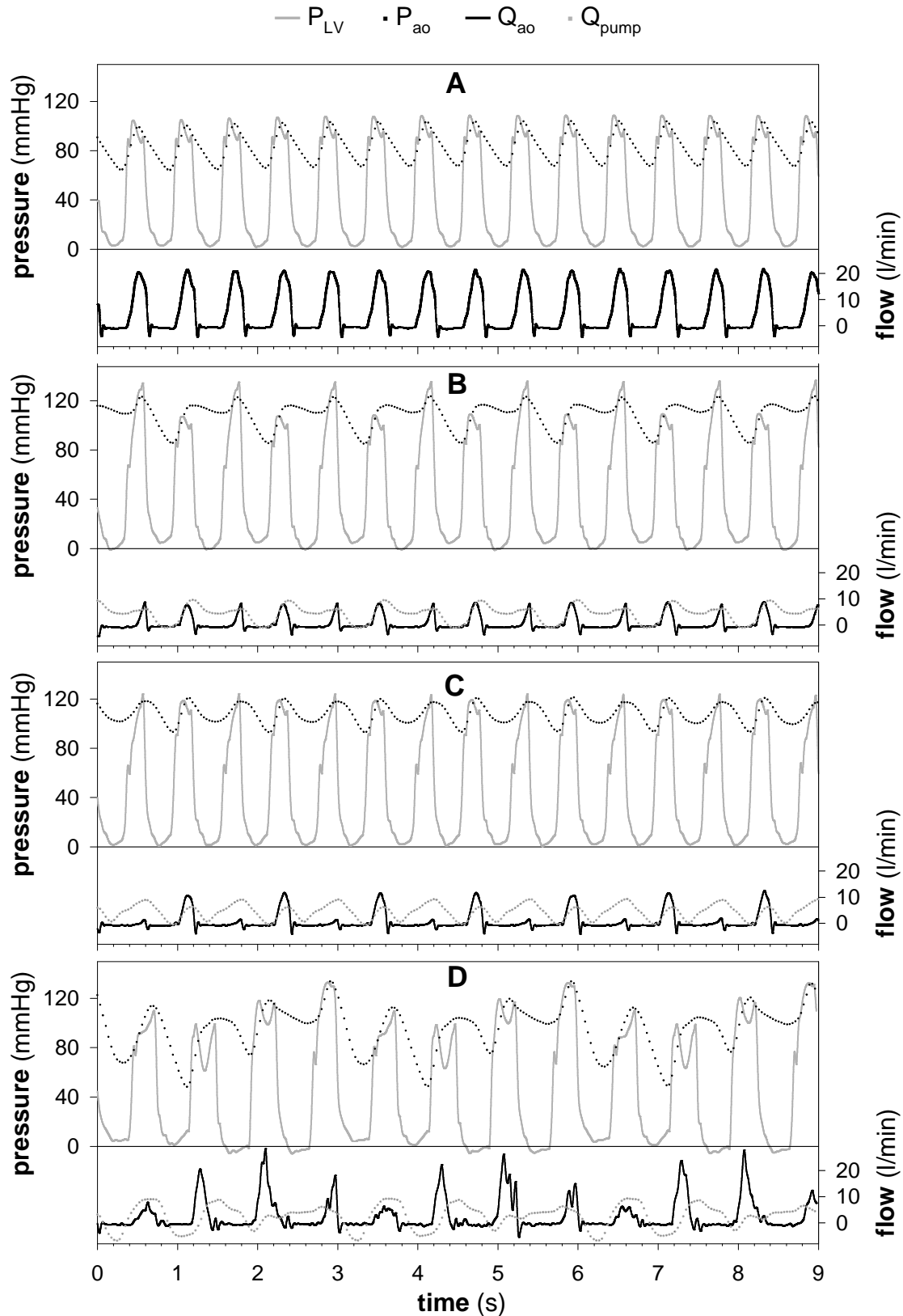


Fig. IV-22: Illustration of the interaction between the heart and a pulsating Deltastream diagonal pump. Panel A: baseline at a heart rate of 100 BPM. Panel B: Combination 2 of Table IV-4 with a heart rate of 100 BPM and a pump rate of 50 BPM. Panel C: Identical settings as panel B, but at a later time. Panel D: Combination 3 of Table IV-4: heart rate 80 BPM and pump rate 60 BPM. The flow scale is on the right hand side.

Panel D shows a sample of combination 3 of Table IV-2, where a heart rate of 80 BPM and a pump rate of 60 BPM are set. The mean pump flow was set at 2 l/min and it yielded 2.4 l/min, while the pulse pressure was set at 20 mmHg and the actual measured value was 86 mmHg (330% overestimation!) if pulse pressure is defined as the difference between maximum and minimum aortic pressure over the whole sample. Panel D further shows how a pattern of 4 consecutive heart beats is formed. This can best be observed in the left ventricular pressure, where each beat differs distinctively from the previous in waveform and amplitude. The aortic pressure also demonstrates a recurring pattern, which deviates very much from a normal aortic pressure pattern and exhibits various waveforms and pressure levels. The aortic flow is characterized in the same way, while the pump flow seems to have a pattern that consists of 3 beats in the same time span as the four beats of the pressure patterns.

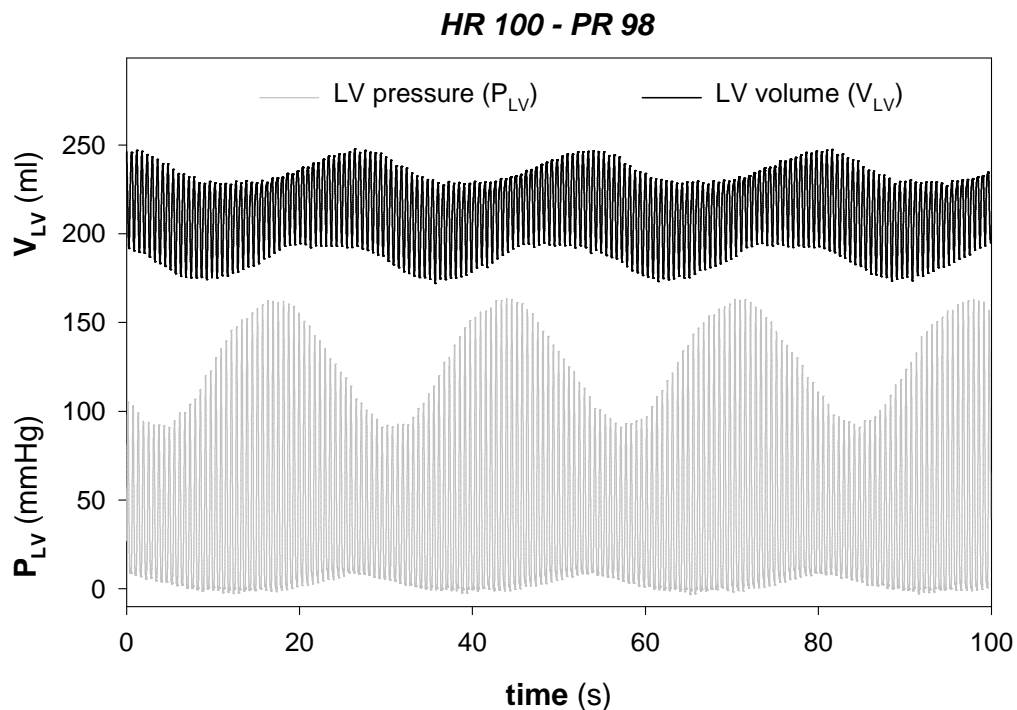


Fig. IV-23: Illustration of the effect of gradual phase shift change on left ventricular pressure and volume.

The simulation of synchronous ventricular assist at different trigger settings (phase shifts) by combining a heart rate of 100 BPM with a pump rate of 98 BPM results in a sinusoidal varying pattern in LV volume and pressure, as displayed in Fig. IV-23. This translates to a gradual shape change of the pressure-volume loops, as displayed in Fig. IV-24. The loop with the highest stroke

volume also yields the lowest systolic ventricular pressure and vice versa. The loop with the highest stroke volume was achieved when a phase shift of 38% was present. According to the definition given above, this means that the rotational speed decreases steeply approximately at end-systole, which corresponds to co-pulsation. The loop with the highest systolic ventricular pressure and lowest stroke volume occurred at a phase shift of 83%, which can be considered as counter-pulsation.

The varying phase shifts induce changes in loading conditions of the LV and consequently an end-systolic pressure-volume relationship (ESPVR) can be determined. The ESPVR is assumed linear and an iteration method ^[201] is used to estimate V_0 (135 ml), which is necessary for PVA calculation.

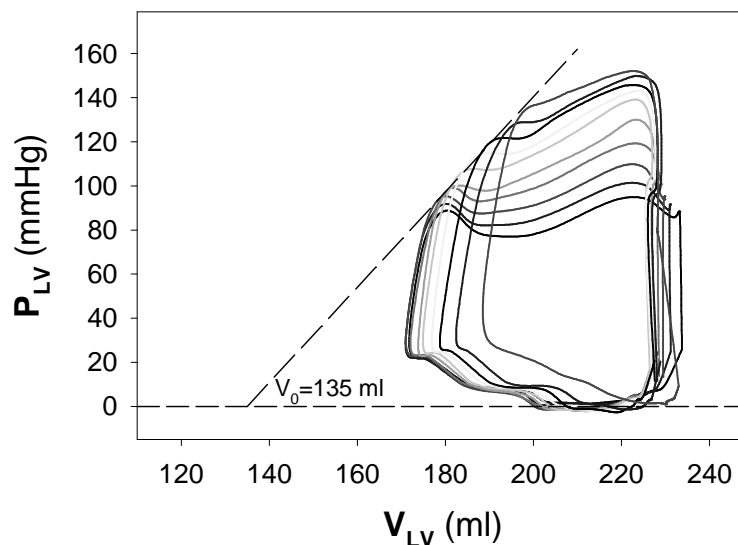


Fig. IV-24: Illustration of the change in left ventricular pressure-volume loops as a result of a shift in triggering, induced by a pump rate of 98 BPM and a heart rate of 100 BPM. The widest loop has a shift of 38% and it evolved to the smallest loop (shift: 83%) in 13 seconds. Every other beat is displayed.

An overview of averaged parameters is given in Fig. IV-25 for the whole range of phase shifts. It is found that the minimum MAP and PVA occur approximately at a 30% phase shift, while SV and EDV have their minimum at 83% and 64%, respectively for the *HR 100 – PR 98* combination. MAP then varies between 74 and 133 mmHg and the stroke volume between 44 and 64 ml. The mean pump flow stays constant over the whole phase shift range at 2.4 ± 0.1 l/min, while no trend could be found for the mean aortic flow, which yielded a total average of 2.7 ± 0.7 l/min.

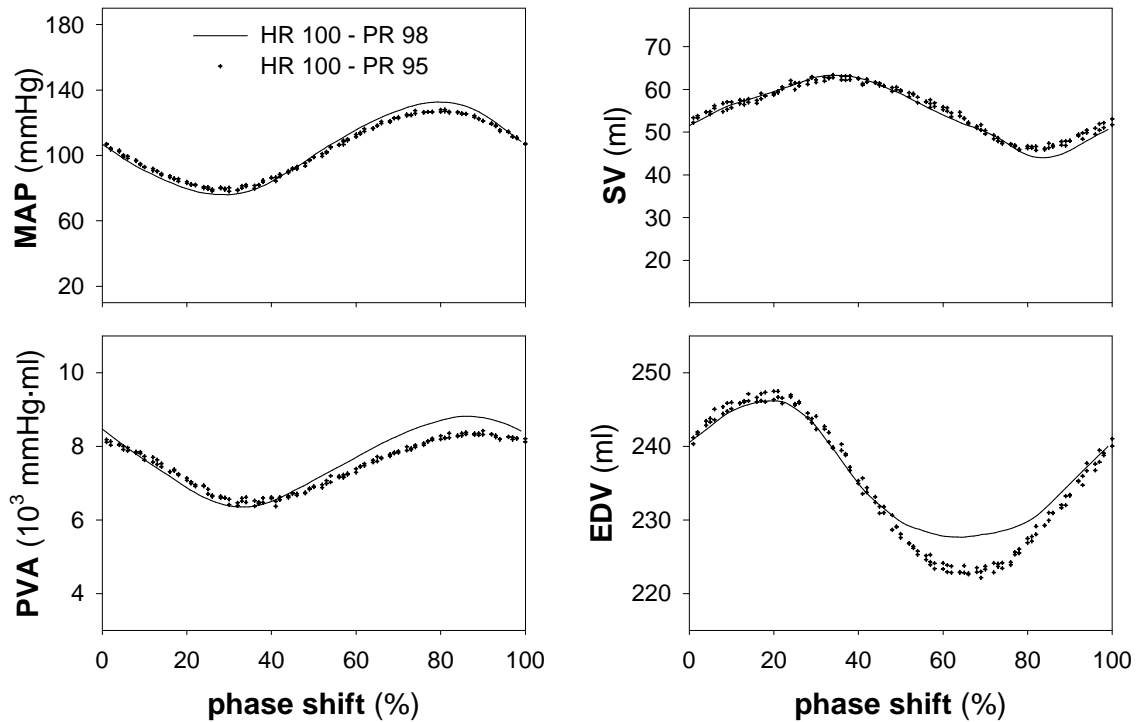


Fig. IV-25: Overview of the effect of the whole range of phase shifts. The cross marks indicate data points for which the shifts were obtained with a heart rate of 100 BPM and a pump rate (PR) of 95 BPM. The lines indicate that the shifts were obtained with a HR of 100 BPM in combination with a PR of 98 BPM.

5. Discussion

5.1. Continuous mode

The use of a rotary blood pump at a low continuous rotational speed can lead to regurgitation of fluid from the aorta to the LV through the pump. This, however, is compensated by a higher cardiac output in order to keep the total flow constant. A similar phenomenon was previously observed in healthy animals [202,203], but here it is clear that there are no biological compensation mechanisms involved. A possible explanation is that the ventricle gets better filled due to the regurgitation, and that the pneumatic actuation system can subsequently eject more fluid.

Fig. IV-20 indicates that the net flow through the pump at low rotational speed is negative, which means that the integral negative pump flow during heart diastole is larger than the integral positive pump flow that is generated during systole. This is due to three reasons: the longer duration of diastole, the higher (negative) pressure head during diastole, and the functioning of the aortic valve. The last two reasons are closely related: due to the valve the regurgitant flow can only

pass through the pump, while forward flow is split up in a part through the pump and a part through the valve. Opening of the valve also makes that ventricular and aortic pressure are approximately at the same pressure level, while the closed valve can bear a high pressure difference. However, the presence of the regurgitant flow path through the pump also alters the pressures, which can be determined from panel A in Fig. IV-21. The mean aortic pressure is low at a pump speed of 0 rpm because it communicates with the zero ventricular pressure during diastole. At high rotational speeds, the added pump energy is established as a pressure rise since the total flow stays constant. The MAP becomes extremely high because the pump keeps generating flow (and resulting afterload pressure) even during diastole, and because of the nonlinearity of the resistor in combination with the more continuous flow pattern.

In accordance with aortic valve insufficiency, regurgitation through the pump leads to a volume overload of the ventricle. This can be derived from the SV and EDV in Fig. IV-21. Although the relative change in EDV seems small, it should be stressed that the *in vitro* ventricle has a low ejection fraction and a large non-functional volume, which is comparable to a dilated failing heart. It is therefore more interesting to compare absolute volumes. The strong dependency of SV and EDV on the heart rate is also a limitation of our *in vitro* system where no Frank-Starling mechanism is implemented and filling occurs at atmospheric pressure. Consequently, a lower heart rate results in more time for filling and ejection, thus yielding a higher EDV and SV.

5.2. Pulsatile mode

The combination of a pulsatile rotary blood pump with a functioning LV clearly results in large, unphysiologic, variations in cardiovascular pressures and flows and the resulting load on the heart. A similar interaction can be expected for displacement type assist devices, although the waveforms produced by such a pump are more physiological. The pulsatile mode of the Deltastream pump theoretically generates a sinusoidal rotational speed pattern, and thus adds energy to the cardiovascular system in such a way. For characterization of the Deltastream pump and controller, it would be interesting to assess the response of the control algorithm to the observed variations. However, such an analysis could not be performed due to the undersampling of the pump speed on the drive console (10 Hz). Judging from the extreme variations, it can be stated that an

appropriate control algorithm is mandatory to compensate for this unphysiologic behavior.

If the combination of the two pulsating ‘pumps’ (heart and Deltastream) is compared to harmonic wave transmission theory, two phenomena can be observed. One is interference of waves at equal frequencies, where constructive and destructive interference can occur, dependent on the phase shift between the two waves. If the two waves are in phase (co-pulsation), the signals add up and the amplitude becomes the sum of the two wave amplitudes. If the waves are in counter-pulsation, the signals cancel out and the amplitude becomes small. This is similar to the data acquired at a heart rate of 100 BPM and a pump rate of 98 (if the difference in frequency is neglected), where the whole range of phase shifts was observed. This leads to times where there is co-pulsation and thus increase in amplitude, and times where there is a reduced amplitude. It should be taken into account that the pressure waves generated by the heart are a superposition of several harmonic waves and that the resulting interference is therefore more complex. Nonetheless, the (sinusoidal) rise and fall in pressures and volumes observed in Fig. IV-23 and in the data of Fig. IV-25 are clearly the result of interference that changes with phase shifts. The mean pump flow per beat does not really show this pattern because it is the primary controlled variable by the algorithm and is therefore approximately constant.

Another phenomenon that is known in wave transmission theory, is the combination of waves of different frequencies. With harmonics, this results in a recurring pattern that is called ‘beating’ in analogy with the sound formed when two such sound waves interfere. The beat frequency is the difference between the two original frequencies, and here it will be referred to as the ‘pattern frequency’ to avoid confusion. In the case of a heart rate of 100 BPM (1.667 Hz) and a pump rate of 50 BPM (0.833 Hz), the pattern frequency would be 0.833 Hz, or yield a pattern period of 1.2 seconds. This is the duration of 2 heart beats or 1 pump ‘beat’, which agrees with the data displayed in panels B and C of Fig. IV-22. For the combination of a heart rate of 80 BPM (1.333 Hz) and a pump rate of 60 BPM (1 Hz), a pattern period of 3 seconds occurs, which again relates to 3 pump beats at 60 BPM and 4 heart beats at 80 BPM. The 3-beat pattern can be observed in the pump flow of panel D (Fig. IV-22), while the 4-beat pattern is most apparent in the LV pressure.

If the pattern period is not an exact multiple of the individual beat periods, then a gradual shift will occur in the pattern. The length of the pattern will remain constant, but the shape of the waveforms will change cyclically due to altered (constructive/destructive) interference. This is in fact the phenomenon observed in the *HR 100 – PR 98* combination, where the pattern lasts only 1 beat and its variations relate to a gradual phase shift. A more apparent form of pattern changes is shown in panels B and C of Fig. IV-22, where the data were acquired for the same experiment, but just at a different time. Apparently the rates were not exactly 100 and 50 BPM, hence the shift. The closer the heart and pump frequencies are to a divider of the pattern frequency, the slower the shift in pattern shape will occur. Since the interaction can result in large variations in pressures and volumes, a fixed pump rate can lead to high load conditions and thus an automated trigger mechanism or feedback control is necessary to avoid extreme situations.

6. Study limitations

The *in vitro* model contains a drastic simplification of the afterload as seen by the heart and the pump. Nonetheless, such windkessel models have proven their value in the simulation of physiological arterial pressure and flow ^[126,133,134], even though they do not allow to study arterial perfusion on a detailed level.

The lack of baroreceptor feedback in our afterload model results in an overestimation of MAP in continuous mode (Fig. IV-21). It can be expected *in vivo* that resistance decreases to normalize the MAP, which would result in an increase in flow. On the other hand, a constant total flow in spite of cardiac assist was previously observed *in vivo* in healthy animals ^[202,204].

Due to the neglect of autonomous feedback mechanisms, the observed pressure and flow variations in pulsatile mode may appear more extreme than they will be observed *in vivo*. However, this means that in an *in vivo* setting a higher load is laid upon the nervous system and active control processes, such as the smooth muscle tone. In any case, it can be expected that stable, physiological pressure and flow waveforms are more appropriate for ventricular assist and that the here observed unphysiological hydrodynamic variations will also be experienced as unphysiological *in vivo*.

The heart simulator used in this study has no elastance-based control and consequently the sensitivity of the heart to preload (Frank-Starling mechanism) and afterload is ignored. Bypassing the original drive system with pressure feedback, however, results in a constant energy at end-diastole (buffer reservoir with fixed volume at given pressure), making the ejection afterload dependent: a lower afterload results in a higher flow (and thus stroke volume) and a lower pressure buildup. Therefore, the constant pneumatic energy that is delivered will result in a constant stroke work over a certain range of afterloads, which is similar to the *in vivo* findings of Glower et al. ^[13]. Afterload variations in the *in vitro* model will thus result in pressure volume loops as known in literature ^[4,12,178], similar to Fig. IV-24.

7. Conclusions

Experiments performed with the Deltastream diagonal pump in continuous mode demonstrated that a too low rotational speed leads to regurgitation. The flow effect is compensated by a higher cardiac output, while the pressure drops severely and may lead to underperfusion. Too high rotational speeds can result in a high mean arterial pressure while the total flow stays independent of the rotational speed.

A complex heart-device interaction appears when the same rotary pump is used in pulsatile mode. A repeating pattern with large pressure and flow variations emerges as a result of the interference between the pump's and the heart's pulsatile function. The resulting pattern is highly unphysiological and may change slowly as a result of phase shifts. This can lead to dangerous situations if no proper patient monitoring or pump control is implemented.

E. IN VIVO STUDY OF VENTRICULAR ASSIST WITH A ROTARY BLOOD PUMP IN CONTINUOUS MODE: IMPACT OF CANNULATION SITE[†]

1. Abstract

Ventricular assist devices are gaining ground in the therapeutic treatment of chronic heart failure. These devices are sometimes used as a bridge to recovery by unloading the left ventricle (LV) and restoring its function. It is therefore important to preserve the heart muscle and apply less invasive implantation methods. In this study ventricular unloading was achieved in 7 healthy sheep with a rotary blood pump at different pump flows. Ventricular cannulation via the left atrium (LA) and through the mitral valve was compared to atrial cannulation. The unloading of the heart was assessed with LV pressure-volume loops, derived energetic parameters and an estimate of LV wall stress.

No significant difference between the cannulations was found for any flow or pressure. LA cannulation, however, resulted in significantly lower stroke volumes and stroke work for all pump flows. Irrespective cannulation site, LV volumes and energetic parameters showed a significant decrease with increasing pump flow. From this study can be concluded that LV assist with a rotary blood pump can provide sufficient unloading with atrial cannulation.

2. Introduction

The clinical history of cardiac assist devices begins with the roller pump and centrifugal pumps that were used in cardiopulmonary bypass. They were followed by paracorporeal devices like the Abiomed BVS5000, the Thoratec VAD and the Berlin Heart, that are still popular for short-term and medium-term

[†] The contents of this section was accepted for publication in *Artif Organs* 2004: July issue

**The impact of pump speed and inlet cannulation site
on left ventricular unloading with a rotary blood pump**
Vandenberghe S, Nishida T, Segers P, Meyns B, Verdonck P

support ^[205-207]. For all these devices, cannulation of the left atrium was initially preferred for the inflow connection of the device to the circulation. Use of the (larger) intracorporeal devices like Novacor and HeartMate cleared the way for apical ventricular cannulation that is also foreseen in the design of newer generation devices. Rotary blood pumps take a prominent place within this new generation of assist devices, and keep gaining importance and popularity for the routine use of mechanical support for heart failure patients ^[58,82,208-210]. Some of the rotary blood pumps have already been used extensively in patients for long-term or even permanent cardiac assist ^[58,111,186,211], while others are still in a phase of *in vitro* or *in vivo* testing. The new designs are intended for intracorporeal use with an apical inlet cannulation, which is space saving and supposed to ensure a good inflow directly from the mitral valve. Atrial cannulation often results in severe complications: it is more prone to thrombus formation in the ventricle and on the cannula and it results in more bleeding, regardless of the lower pressure at that site. Furthermore, it has been reported that left ventricular cannulation with rotary blood pumps allows higher pump flows than left atrial cannulation ^[212]. This is due to the different pressure conditions combined with the different geometry and cannula approach angle. The flow generated by rotary pumps is inversely related to the pressure head, which implies that atrial cannulation will result in lower flow for comparable rotational pump speed. On the other hand, atrial cannulation preserves the myocardium and it provides an easier surgical insertion. This can be beneficial for the implantation of the newer and smaller devices, particularly miniaturized rotary blood pumps. These are intended to provide only partial unloading of the heart and thus atrial cannulation would be satisfactory. It would allow the implantation of these pumps through a left thoracotomy without the use of a heart-lung machine, thus sparing the patient a very traumatic surgical procedure.

The decision on the cannulation site should not only consider surgical complications and pump performance, but also the effect on the heart-device interaction. Especially with the growing application of assist devices as a bridge to recovery, the load on the heart (i.e., the left ventricle) should be taken into account.

In this study, the difference between left atrial and left ventricular cannulation for ventricular unloading with an implantable rotary blood pump is assessed *in vivo*.

The assist ratio was varied over a wide range. and special attention was given to the analysis of the load imposed on the left ventricle.

3. Methods

3.1. Surgical procedure and instrumentation

Seven healthy sheep with an average weight of 54 kg (range: 52-58 kg) were used for this study. All the animals received human care in compliance with the *Guide for the Care and Use of Laboratory Animals* published by the National Institutes of Health (NIH publication No. 86-23, Revised 1985). The sheep were all subjected to the same surgical procedure that was described previously^[179]. In short, a left thoracotomy was performed in the third intercostal space and the fourth rib was removed. A Medos-HIA microdiagonal pump (Medos Medizintechnik GmbH, Stolberg, Germany) was connected to the native circulation with a 50 Fr inflow cannula (29 cm long) inserted via the left atrial appendage and fixed with two purse string sutures. The tip of this cannula was initially positioned in the left atrium (LA) in 3 sheep and in the left ventricle (LV) through the mitral valve in the remaining 4 sheep. A 24 Fr outflow cannula (39.5 cm long) was sutured to the descending aorta. Each sheep was further instrumented with a high-fidelity catheter-tip pressure transducer (Millar Instruments Inc., Houston, TX), inserted in the LV via the apex and a 7 Fr conductance catheter (CardioDynamics BV, Leiden, The Netherlands) for LV volume measurement inserted via the left atrium. A disposable fluid filled pressure transducer was used for acquisition of the mean arterial pressure (MAP) in the left carotid artery. Mean flow through the ascending aorta (aortic flow, Q_{ao}) was monitored with an HT107 ultrasonic flow meter and H20A flow probe (Transonic Systems Inc., Ithaca, NY), while the flow through the pump (Q_{pump}) was monitored with a HT109 flow meter and H11X flow probe.

All parameters were continuously recorded on a heat-writing recorder (Nihon-Kohden Co, Tokyo, Japan), online digitized at 200 Hz and saved on a computer for further data processing.

3.2. Measurements

The measurement protocol started with the conductance catheter calibration^[213]. To assess the parallel conductance (V_c ; offset correction) of the surrounding tissue, 10 ml hypertonic saline (10% NaCl) was injected in the pulmonary artery.

The mean aortic flow during this steady state condition was retrospectively used for appropriate scaling of the acquired stroke volume (α scaling factor; gain correction). During these measurements, the pump was shut off and the inflow cannula clamped.

The inferior vena cava was then occluded to obtain pressure-volume (PV) loops at different preloads in order to assess the slope (E_{es}) and volume intercept (V_0) of the end-systolic pressure-volume relationship. We assumed that V_0 , being an intrinsic property of the heart, stayed constant throughout each cannulation protocol as described below.

With the inflow cannula still clamped, baseline data (BL) were acquired during steady state conditions. This was followed by unclamping of the cannula and subsequent acquisitions of the hemodynamic data during steady state conditions at increasing mean pump flows. Starting at $Q_{pump}=0$ l/min, the mean pump flow was increased with 0.5 l/min increments until complete unloading was achieved ($Q_{ao}=0$ l/min). Note that when $Q_{pump}=0$ l/min, the pump is running at a certain speed in order to keep the average flow through the pump at zero; this is not a simulation of pump failure, where the speed would be 0 rpm. After completion of this protocol, the inflow cannula of the pump was either advanced through the mitral valve into the LV (in 3 animals) or withdrawn through the mitral valve from the LV into the LA (in the remaining 4 animals), depending on the initial placement. The same protocol was then performed with the new cannulation, starting with a recalibration of the conductance catheter, followed by steady state measurements at BL and the same incrementally increasing pump flows.

3.3. Data processing

In one animal, the LV-cannulation part of the protocol was not performed while in another animal it was impossible to obtain calibration data (BL, vena cava occlusion and saline injection) of sufficient quality, also for the LV-cannulation. We excluded these data, leaving 7 data sets of LA-cannulation and 5 sets of LV-cannulation. An average beat was calculated from a minimum of seven sequential beats for each steady state acquisition. Hemodynamic parameters such as stroke volume (SV), end-systolic LV pressure (ESP), and mean arterial pressure (MAP) were derived from these beats.

Energetic parameters were calculated from the PV-loops to assess the unloading of the heart. The stroke work (SW) was calculated as the area within the PV-loop

and is a measure of the energy that the LV transfers to the blood. The potential energy (PE) was calculated as the area enclosed by the end-diastolic and end-systolic pressure volume relations and the descending limb of the PV-loop, and represents the energy consumed by the LV merely to contract. The sum of SW and PE gives the pressure-volume area (PVA), which is a measure of the oxygen consumption of the LV ^[12]. We further defined the mechanical efficiency (Meff (%)) of the LV as the percentage of the PVA that is taken by the SW (Meff = SW/PVA·100). Since the heart rate (HR) varies during the experiment and between each subject, the energetic parameters were multiplied by HR/60 to obtain values per second rather than per beat.

Additionally, the stress in the LV myocardium was estimated by assuming a thick-walled ellipsoidal geometry using the formula ^[21]:

$$\sigma = \frac{P \cdot D^2}{4 \cdot h \cdot (D + h)} \quad [\text{Eq. IV-14}]$$

With σ = meridional wall stress (mmHg); D = internal short-axis LV diameter (cm); P = LV pressure (mmHg); h = myocardial wall thickness (cm). These are all time-varying parameters.

Internal diameter D at any instant in time was derived from the volume measurements by ^[183]:

$$V_{LV} = \frac{7 \cdot D^3}{2.4 + D} \quad [\text{Eq. IV-15}]$$

with V_{LV} as instantaneous LV internal volume.

Wall thickness was not directly measured but its variation over the cardiac cycle was computed, based on the knowledge that myocardial volume stays constant throughout the whole experiment (LA and LV cannulation). An arbitrary value for this volume was calculated per sheep by assuming an end-systolic (index es) wall thickness (h_{es}) of 10 mm in the LA baseline measurements. With this assumption, myocardial wall volume V_w can be calculated as

$$V_w = \frac{7 \cdot (D_{es} + 2 \cdot h_{es})^3}{2.4 + D_{es} + 2 \cdot h_{es}} - V_{LVes} \quad [\text{Eq. IV-16}]$$

This fixed myocardial volume and the varying intra-ventricular volume allowed calculation (with the same formula) of the ventricular wall thickness throughout the averaged beat.

To obtain a single parameter as an indication of the overall LV wall stress for a certain pump setting, the stress was integrated over one beat, yielding the stress time integral (STI (mmHg·s/beat)). This was further multiplied by the heart rate (beats per second) to give a comparable value in mmHg. Since wall thickness was not directly measured but estimated on the basis of an arbitrary value, only the relative changes in wall stress and STI should be interpreted, rather than their absolute values.

All the data are presented by their mean values \pm standard deviation. Analysis was performed with paired t-tests to investigate the influence of the cannulation site and the pump flow level, and to determine the pump flow levels that yielded significant differences compared to baseline. The significance threshold was set at $p = 0.05$ for all tests.

4. Results

The effect of LA and LV cannulation on measured pressure volume loops is shown in Fig. IV-26 for subject #7 as a typical example, while Table IV-5 summarizes hemodynamic data measured in all subjects. The main effect of increasing the pump speed (and resulting pump flow) is the shift of the isovolumic ejection phase to lower volumes, thus a decrease in end-diastolic volume. The loops show a much smaller decrease in end-systolic volume and when averaged over all the subjects, it decreases from 65 ± 27 ml at BL to 58 ± 29 ml ($p = 0.12$) at a pump flow of 3.5 l/min for atrial cannulation. For ventricular cannulation, the numbers become 60 ± 14 ml at baseline and 53 ± 12 ml at $Q_{\text{pump}} = 3.5$ l/min ($p = 0.03$). The end-diastolic volume decreases more: from 95 ± 28 to 69 ± 27 ml ($p < 0.00$) for atrial cannulation and from 93 ± 11 to 68 ± 11 ml for ventricular cannulation ($p < 0.00$).

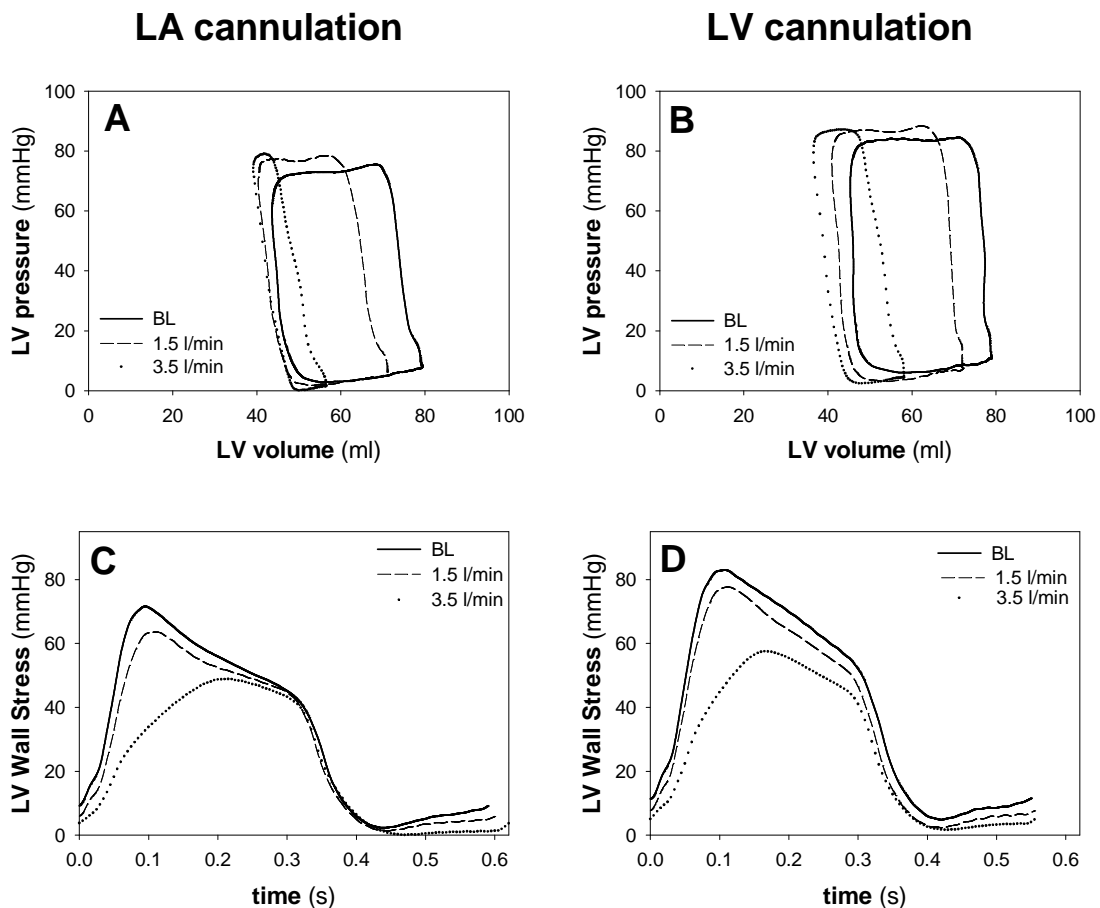


Fig. IV-26: Panel A and B show pressure volume loops of the left ventricle of subject #7 (see Table IV-5) with atrial and ventricular cannulation, respectively. The presented loops were acquired at baseline (BL) and with a pump flow of 1.5 and 3.5 l/min. Panel C and D show the according LV wall stress over one cardiac cycle.

As a result, the stroke volume decreases significantly under influence of the pump flow, which is demonstrated in panel A of Fig. IV-27. A pump flow of 1 l/min or more yields a stroke volume that differs significantly from BL, irrespective of cannulation site. Both the PV-loops and panel A of Fig. IV-27 show the impact of cannulation site on stroke volume: a significantly lower stroke volume is obtained with atrial cannulation. The difference increases with higher pump flows, but no interaction between cannulation site and pump flow was detected.

In the PV-loops shown in Fig. IV-26, there is an increase in ejection pressure due to the increased pump speed, but this is not an overall observation. There is no significant influence of pump flow or cannulation site on end-systolic pressure (Fig. IV-28). The end-diastolic pressure on the other hand, decreases with increasing pump flow and both cannulation site and pump flow have a

statistically significant impact for $Q_{\text{pump}} \geq 0.5$ l/min. Atrial cannulation results in lower end-diastolic pressures compared to ventricular cannulation (Fig. IV-28). While increased pump flow clearly diminishes the flow through the aortic valve (Fig. IV-27, panel C), there is hardly any gain in total blood flow (Fig. IV-27, panel D). On average, there is a slight (non-significant) increase in total flow when high pump flows are set, but there are also subjects that actually showed a small decrease in total flow by increasing the pump flow. For any given pump flow level, the type of cannulation has no effect on aortic flow, and hence on total flow.

LV wall stress is relieved by increasing the pump flow, as depicted in the STI plot of Fig. IV-29 (panel A). The impact of pump flow is significant, while no significant difference can be found for the different cannulations. A trend towards higher STIs for atrial cannulation can be seen in the graph. No significant influence of either cannulation or pump flow was detected for the PVA. The graph in Fig. IV-29 indicates a clear trend: the PVA – thus also the oxygen consumption – decreases with increasing pump speed. Atrial cannulation results in lower averages for PVA compared to ventricular cannulation and this for every pump flow. While stroke work of the left ventricle is significantly dependent on the cannulation site and the pump flow, the potential energy is independent of both. LA cannulation will result in a lower SW, just as increased pump flow will (Fig. IV-29, panel C). In combination with the trends in PVA, this results in a higher mechanical efficiency of the LV with LV cannulation. The mechanical efficiency also decreases significantly with increasing pump speed (Fig. IV-29, panel D).

Table IV-5: Overview of parameters derived from the left ventricular pressure-volume loops of all the subjects and for the two types of cannulation.

sheep	Q _{pump} (l/min)	LA cannulation				LV cannulation			
		ESV (ml)	SV (ml)	EDP (mmHg)	σ_{\max} (mmHg)	ESV (ml)	SV (ml)	EDP (mmHg)	σ_{\max} (mmHg)
1	BL	32.7	24.9	5.9	63.6	n/a	n/a	n/a	n/a
	1.5	32.8	18.6	5.1	61.3	n/a	n/a	n/a	n/a
	3.5	33.7	7.1	3.7	50.1	n/a	n/a	n/a	n/a
2	BL	108.7	33.4	8.9	90.7	77.7	39.7	9.5	61.0
	1.5	103.1	26.8	6.3	90.1	70.3	37.9	7.5	60.0
	3.5	101.0	10.9	5.4	86.5	64.8	29.7	6.0	50.3
3	BL	69.9	41.0	12.1	93.3	n/a	n/a	n/a	n/a
	1.5	52.0	31.6	7.5	69.6	n/a	n/a	n/a	n/a
	3.5	48.6	18.2	5.8	54.3	n/a	n/a	n/a	n/a
4	BL	44.2	37.6	6.6	68.7	45.5	40.9	8.1	72.4
	1.5	40.1	27.8	5.9	54.5	44.2	32.5	6.0	65.4
	3.5	39.3	9.4	4.8	39.7	42.5	15.9	4.4	50.7
5	BL	66.0	34.9	11.1	80.4	68.5	36.4	10.1	92.8
	1.5	58.1	28.7	9.0	71.7	60.4	26.3	7.6	77.7
	3.5	n/a	n/a	n/a	n/a	61.4	15.2	6.7	66.7
6	BL	86.5	33.2	9.4	96.4	60.9	33.3	12.2	79.4
	1.5	86.7	22.9	6.8	94.3	58.4	23.6	9.3	71.2
	3.5	87.4	9.8	5.8	90.1	59.0	11.0	7.7	62.2
7	BL	45.0	35.7	8.5	71.6	47.0	33.5	10.5	83.0
	1.5	41.0	30.9	6.1	63.5	41.9	31.2	7.7	77.7
	3.5	39.8	17.4	4.7	48.9	37.3	21.6	6.2	57.5

LA: left atrium; LV: left ventricle; Q_{pump}: pump flow; ESV: end-systolic volume; SV: stroke volume; EDP: end-diastolic pressure; σ_{\max} : maximum wall stress; BL: baseline (pump clamped)

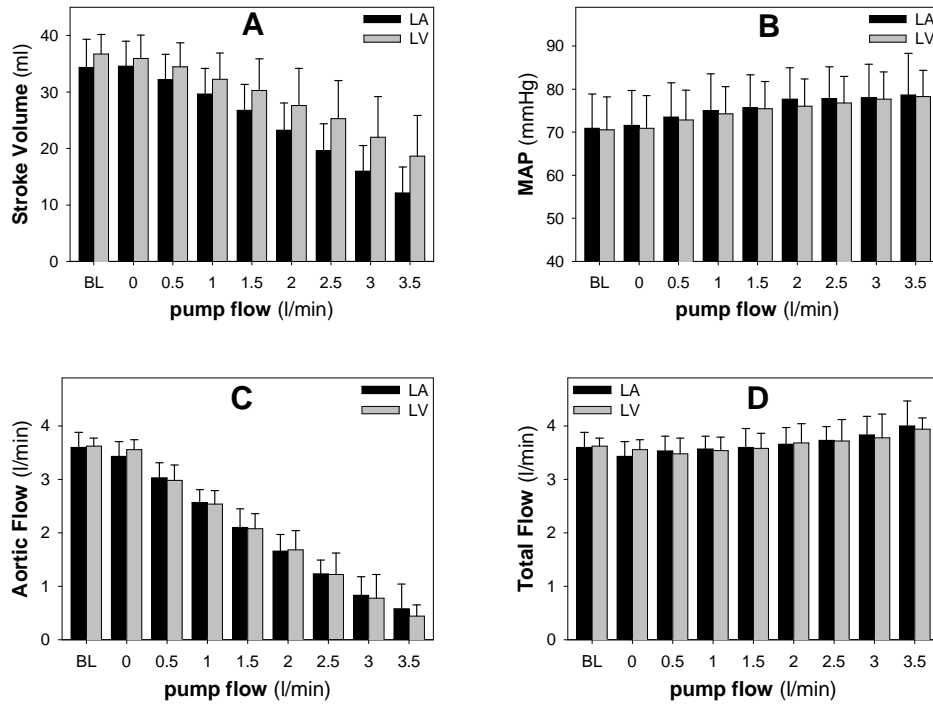


Fig. IV-27: The effect of pump flow and cannulation site on different hemodynamic parameters. The bars indicate the average over all subjects and the error bars indicate the standard deviation. A: stroke volume; B: mean arterial pressure; C: flow through the aortic valve; D: total blood flow. LA: left atrial cannulation; LV: left ventricular cannulation.

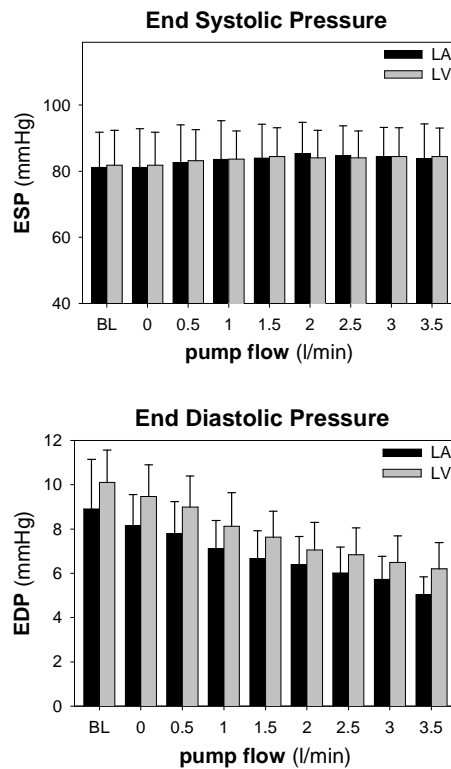


Fig. IV-28: The effect of pump flow and cannulation site on left ventricular end-systolic and end-diastolic pressure, expressed as mean + standard deviation.

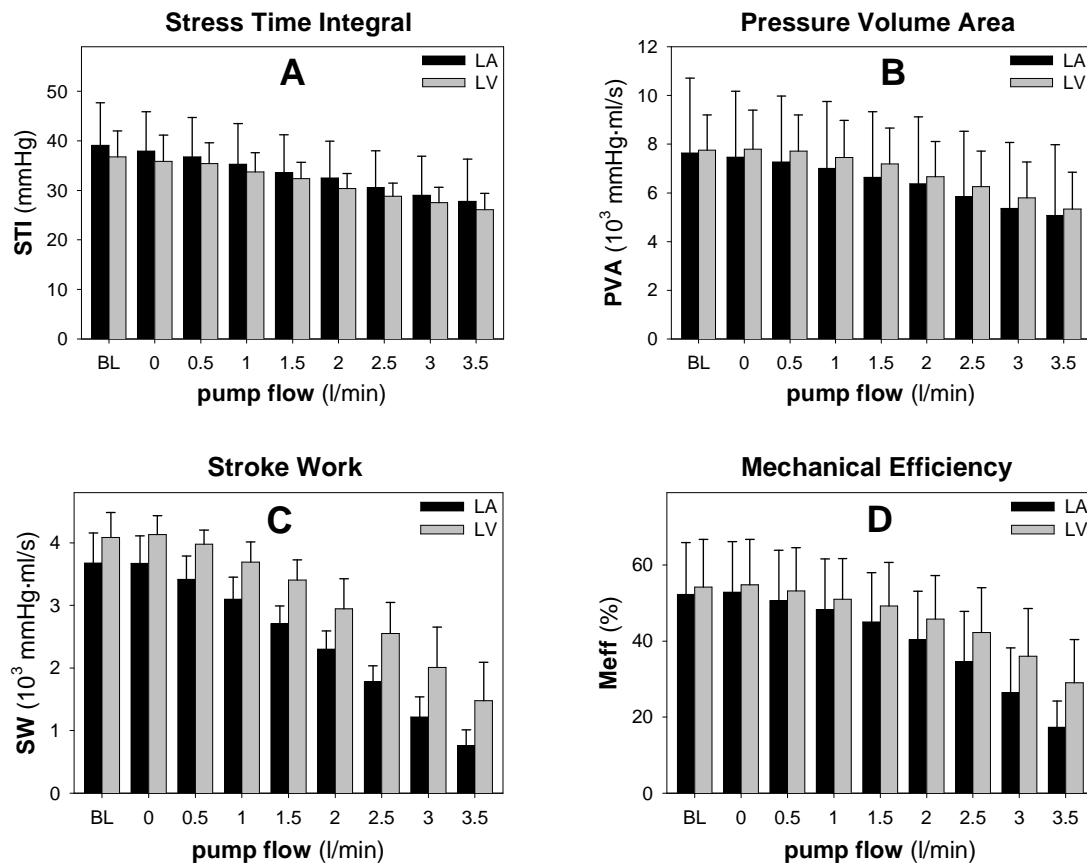


Fig. IV-29: The effect of pump flow and cannulation site on left ventricular wall stress (represented by stress time integral, panel A) and energetic parameters, all expressed as mean + standard deviation.

5. Discussion

With modern long-term cardiac assist, inflow cannulation is usually performed via the left ventricular apex, which damages the myocardium and further impedes left ventricular function. This study was intended to assess the hemodynamic influence of different cannulation options that preserve the myocardium. This approach may gain importance, given the potential use of assist devices as bridge to recovery. Obviously, for this application, myocardial damage due to the cannulation is to be avoided. An additional – methodological – advantage of our approach, where the atrial cannula is shifted through the mitral valve, is that all measurements are performed with the exact same cannula length and diameter. The only change from the pump's point of view is the completely different pressure condition: LV cannulation imposes a varying pressure head on the pump, while LA cannulation yields a constant pressure head. In fact, rotary blood pumps are often optimized for a working point of 5

l/min at a pressure head of 100mmHg, which approximates more the atrial cannulation situation than the ventricular.

An advantage of ventricular apical cannulation is the direct flow path from the mitral valve to the cannula inlet, and also the fact that LV filling through the mitral valve is not impeded. This is different in our experiment, where the flow actually has to turn 180 degrees to get from the mitral valve into the cannula, which may have consequences for thrombus formation and emboli. However, no hemodynamic evidence was found in this study to indicate that the cannula through the mitral valve hinders the valve function. Isovolumic ejection as well as isovolumic relaxation is present as vertical lines in the baseline PV-loops with LV cannulation, which indicates the absence of leakage or impeded filling. On the other hand, it can be observed that the LV end-diastolic pressure at baseline (Fig. IV-29) is higher with a cannula through the valve (LV cannulation) than without.

In spite of the different pressure conditions imposed on the pump, there is no effect of the cannulation site on either pump flow, aortic flow, or total flow. This is intrinsically due to the experimental protocol, where we choose to compare data at given pump flow levels, rather than at given pump rotation speeds. It has also been reported previously that cardiac assist does not augment the total blood flow in healthy animals ^[202,203], probably due to feedback mechanisms that normalize blood flow. Aortic pressure is most likely also normalized via baroreceptor feedback, but still a rise in mean aortic pressure is present for increasing pump flows. The rotary pump actually decouples the end-systolic LV pressure from the MAP, because the end-systolic pressure is not affected by the pump speed at all.

In an earlier animal experiment, Cohen et al. ^[214] measured aortic pressure, coronary flow, and myocardial oxygen consumption in swine with both atrial and ventricular apical cannulation in combination with a Biomedicus rotary blood pump. They found no significant difference between the two cannulations, but they reported local ventricular wall impairment as a result of the ventricular apical cannulation. This was also reported by Sethia et al. ^[215], who performed a similar study with atrial and ventricular apical cannulation in dogs and focused on regional ejection fraction around the cannulation site. These results are thus comparable to ours: the cannulation site has no significant impact on arterial or ventricular pressure or ejection fraction.

In contrast with these findings, Kono and colleagues^[216] recently stated that with a centrifugal pump, LV cannulation results in a sudden drop of LV pressure, volume, and oxygen consumption when the assist rate exceeds 75%. Since the authors only investigated the assist rate in steps of 25% (where 100% was their maximum attainable pump flow *in situ*), it is impossible to pinpoint the support level at which this sudden drop actually occurs. A similar conclusion, however, was drawn earlier by Pennock et al., Dennis et al., and Pierce et al.^[217]. They all found a sudden drop in myocardial oxygen consumption of the LV of about 50% by decompressing the LV completely, which they could only achieve with apical cannulation. In our present study, it is observed that a gradual – almost linear – trend can be seen for most parameters (Fig. IV-27-Fig. IV-29), which is also the case in Kono's study up to 75% support. No reduction in LV pressure was observed in our experiments, not even for a pump flow of 4.5 l/min (94% of total flow or 125% of BL flow) that was achieved in one animal. At this flow rate, the stroke volume was only 6 ml, while the end-systolic volume persisted at 38 ml. Seemingly, with the use of continuous flow support, the LV is first volume unloaded until 100% of the flow goes through the pump. Only higher flows result in decompression and pressure unloading with a marked reduction in oxygen consumption as a consequence. Nonetheless, this is an unwanted condition from clinical perspective because the aortic valve will remain closed and instigate additional risk for thrombus formation. This 'over unloading' with rotary blood pumps can also result in incidences of LV suction. This cannot have occurred in Pennock's study because he used gravitational draining, but we speculate that ventricular suction may have influenced Kono's experiments. Careful review of his Figure 4 reveals negative pressure levels in the LV. The only difference found by Kono et al. that is consistent for all their support levels is the external work (i.e., stroke work) that is always lower for LA cannulation and thus agrees with our findings.

Next to the stroke work, Fig. IV-29 indicates that also the LV pressure-volume area (indicative for oxygen consumption) benefits from LA cannulation. This could not be confirmed statistically due to the large variance. When expressing PVA relative to its baseline value per sheep, a significant influence of both cannulation site (atrial cannulation results in lower PVA) and pump flow are found (higher pump flow results in lower PVA), which indicates that all subjects show the same trend but at very different levels. The large variance is probably

attributable to the difficult determination of parallel conductance. Consequently, the position of the PV-loop on the volume axis varies considerably between subjects, also resulting in large variance on the potential energy. Combining our findings on SW, PVA and mechanical efficiency, it appears that the LV is most economical in energetic terms when atrial cannulation is applied. The transfer of energy to the blood, on the other hand, is more efficient when ventricular cannulation is used.

6. Study limitations

Although the conductance catheter offers great potential for *in vivo* hemodynamic analysis, its calibration (offset and gain factor) remains its Achilles heel. In this study, the conductance catheter was recalibrated after relocation of the cannula from LA to LV or vice versa. In all animals, there was a significant shift in baseline values (clamped cannula) for all volume and energetic related parameters. Obviously, baseline hemodynamic conditions may change in longer experimental settings in open chest animal preparations, but it is our feeling that at least part of the ‘baseline drift’ is due to catheter calibration. This study describes the results of an acute experiment in healthy animals and therefore does not allow to draw any conclusions for long-term outcomes. Chronic experiments would be especially interesting in a heart failure animal model to assess the evolution of the assisted heart and to identify the predisposition of a certain cannulation site to complications such as thrombo-embolic events. These studies, however, may also be performed retrospectively on available patient data from the many bridge to transplant cases performed over the past few years. Nevertheless, we believe that all the trends found in this study would be confirmed in the currently available chronic heart failure models.

7. Conclusion

Cardiac assist with a rotary blood pump can be performed with left ventricular or atrial inflow cannulation without damaging the myocardium. Ventricular cannulation through the mitral valve is more complex and does not prove to be beneficial from hemodynamic point of view. Moreover, for any given pump flow, atrial cannulation leads to significantly lower stroke work and hence a better energetic unloading of the left heart.

8. Acknowledgements

The authors are grateful to Miroslaw Zietkiewicz and Bartolomeij Perek for their assistance in the animal experiments.

This research was funded by a specialization grant of the Institute for the Promotion of Science and Technology in Flanders (IWT-993171, S. Vandenberghe).

CHAPTER V

Hydrodynamic Analysis of Heart - Pulsatile Catheter Pump Interaction

A. INTRODUCTION

1. Overview and rationale of the chapter

Positive-displacement (or volumetric) pumps were the first choice for ventricular assist devices in the early years of this treatment because they mimic the flow and pressure patterns generated by the native heart. Focus was also on full support where the device is able to take over the total blood flow, thus completely unloading the native heart. These volumetric pumps were therefore primarily judged by the flow they could generate at a certain pressure head, where 5 l/min was a requirement and higher flows were desirable to allow exercise. Examples of such high-flow devices are the pneumatic Medos VAD and Berlin Heart, and the electromechanical HeartMate VE and Novacor N100 (see chapter I).

High-flow volumetric pumps are already in routine clinical practice for about 20 years and records of extensive *in vitro* and *in vivo* tests are required for each device to obtain approval for clinical use. Consequently, all these devices (even the more recent) have been well characterized by the manufacturer. These devices all have some control algorithm implemented in electronic and/or software format and knowledge of these algorithms and the operation mechanism is necessary to properly characterize a device in all of its aspects (response to filling or critical situations, alarms, parameter estimation, etc.). Complete characterization of such devices is therefore complex and the necessary methods are device-dependent. Moreover, characterization and subsequent tuning of the control of high-flow volumetric devices is usually based on the output of the device and neglects the impact on the heart. Such characterization is therefore beyond the scope of this dissertation. Nonetheless, a simple (based on averaging of data) but universally applicable hydrodynamic characterization method for volumetric assist devices is presented in section B and applied in section C as an illustration and for reason of completeness. This section also describes in detail the construction and validation of the lumped *in vitro* model (mock circulatory system) with static preload, that is used for this characterization method and that was also used for the *in vitro* study described in chapter IV.

Partial support of a ventricle is accepted as a possible approach for heart failure patients that still have some native heart function. Volumetric pumps that generate a lower flow can be made smaller and allow rapid introduction and short-term use, which makes them ideal for stabilization of patients. The best known example, although strictly not a pump but a counterpulsation device, is the intra-aortic balloon pump (IABP). This device has become the standard mechanical support for stabilization of acute heart failure patients and is also applied in combination with pharmacological therapy for treatment of end-stage chronic heart failure. An alternative for the same field of application is the Impella pump, which is a rotary blood pump.

The main focus of this chapter is to investigate the application of a new minimally invasive device for stabilization and short-term support of heart failure patients: the PUCA II pump. First, section C compares the pumping capacities of the PUCA II for a specific condition to the capacities of high-flow VADs as an illustration of the different design criteria. Section D discusses the pumping capacities of the PUCA II in combination with a commercially available IABP driver in more detail. The pumping capacities were assessed in the *in vitro* model with a static and with a dynamic preload, where the combination of these data allowed quantification of the PUCA II contribution to total blood flow. Left ventricular unloading with the new device is discussed more in detail in section E, where the PUCA II is also used as a perfusion pump in the femoral artery and compared to the perfusion and unloading capacities of a commercially available IABP.

2. The PUCA II pump

The pulsatile catheter (PUCA) pump is a small ventricular assist device that consists of one catheter and a small pneumatic displacement pump. An overview of the development history of this device can be found in section D.2 and in the work of Mihaylov ^[218]. Over the course of time, many versions of the PUCA pump were manufactured and the working principle and the properties of the sample that was used in the studies described below are explained in the according sections.

The PUCA pump is currently distributed by Intra-Vasc.NL b.v. (Groningen, The Netherlands) under the name PulseCath. The ventricular assist device is available

in an open chest version for introduction with a sternotomy or thoracotomy, and in a closed chest version for introduction via the right subclavian artery. The closed chest version has a special tip (inflow cage) that allows the use of a dilator to facilitate the introduction. A prototype of this version was used in the studies below. Both devices use an introducer that measures pressures at the valve and at the catheter tip so that its correct position, as shown in Fig. V-1, can be determined from the pressure waveforms.

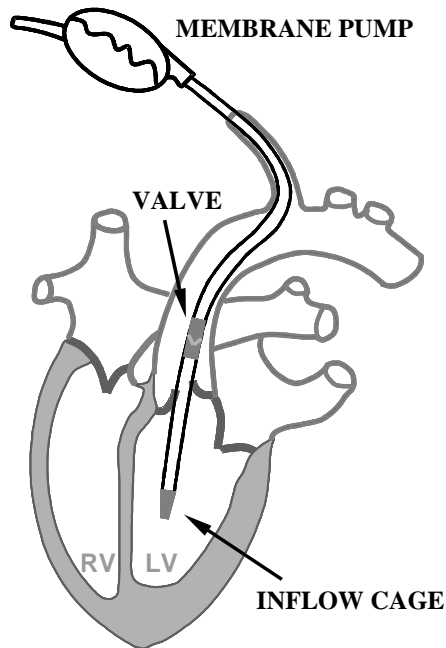


Fig. V-1: Schematic view of the position of the PUCA pump. RV: right ventricle. LV: left ventricle.

To date, the device has not been used in patients but was subject to extensive acute (2 hours) and chronic (4 days) animal testing. This revealed that the device can be used safely for this term, without causing blood damage or organ failure. As a result, approval for clinical application is granted and the first patient trial is expected soon.

B. HYDRODYNAMIC CHARACTERIZATION OF VENTRICULAR ASSIST DEVICES[†]

1. Abstract

A new mock circulatory system (MCS) was designed for evaluation and characterization of the hydraulic performance of ventricular assist devices (VADs). The MCS consists of a preload section and a multipurpose afterload section, with an adjustable compliance chamber (C) and peripheral resistor (R_p) as principal components.

The MCS was connected to a pulse duplicator system for validation, simulating a wide range of afterload conditions. Both pressure and flow were measured, and the values of the different components calculated. The data perfectly fits a 4-element electrical analogon (EA).

The MCS was further used to assess the hydrodynamic characteristics of the Medos VAD as an example of a displacement pump. Data were measured for various MCS settings and at different pump rates, yielding device specific pump function graphs for water and pig blood. Our data demonstrate (i) flow sensitivity to preload and afterload and (ii) the effect of test fluid on hemodynamic performance.

2. Introduction

Ventricular assist devices (VADs) are a means to support an end-stage heart failure patient and are generally used as a temporary bridge to cardiac transplantation. In order to actively bypass the diseased heart, blood is withdrawn via atrial or ventricular cannulation, and is pumped back into the systemic

[†] The contents of this section was published in Int J Artif Organs 2001;24:470-477:

Hydrodynamic characterisation of ventricular assist devices

Vandenbergh S, Segers P, Meys B, Verdonck P

circulation via a cannula in the aorta. Prior to experimental or clinical use, VADs are tested hydrodynamically to assess their hydrodynamic performance, their limiting factors, or their optimal working conditions with regard to supporting and unloading the heart. These tests are performed in a laboratory setup that mimics ventricular load. The compliance of the large vessels is usually modelled as a single elastic chamber (windkessel), while the resistance, which is mainly distributed over the arterioles, is compacted in one resistive element. Over the years, different models have been tested and it has been shown that hydraulic mock loops have, if well designed, the potential to accurately mimic the vascular system ^[131,132,134,219].

In this work, we present a new general-purpose mock circulatory system (MCS) to characterize and evaluate different types of ventricular assist devices. The characteristics of the MCS are assessed by direct measurement of its hydrodynamical properties, and by fitting an electrical analog (EA) model to the pressure and flow data measured in the hydraulic MCS. The setup allows insertion of VADs with displacement or rotary blood pumps and the characterization method was chosen in order to easily compare different devices. Data are presented for one particular displacement device (Medos VAD).

3. Materials and methods

3.1. Description of the mock circulatory system

The mock circulatory system (Fig. V-2) consists of a preload section (I) to fill the device under test (simulating atrial or ventricular cannulation) and an afterload section (III-V) that mimics the systemic circulatory tree. The ventricular assist device (II) is mounted between these two sections with interchangeable connectors, and an extra overflow (VI), buffer reservoir (VII) and circulation pump (VIII) are added to the system to guarantee a constant venous pressure (5 mmHg) and to uncouple preload and afterload.

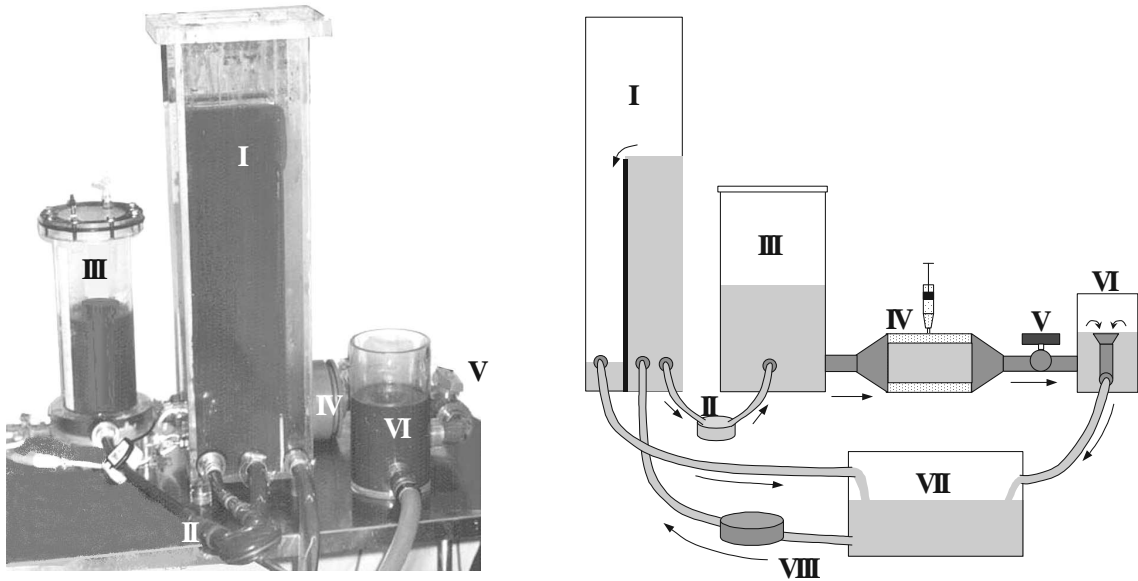


Fig. V-2: Photographic and schematic illustration of the mock circulatory system (MCS) during the Medos VAD test. I. Preload reservoir ;II. Medos VAD; III. Windkessel; IV. Resistance; V. Cutoff valve; VI. Afterload reservoir; VII. Buffer; VIII. Centrifugal pump.

The preload section is designed as a rectangular overflow reservoir with removable panels allowing to change the overflow height and thus the filling pressure of the device from 5 to 40 mmHg.

The major determinants of afterload pressure and flow are total arterial compliance (C) and total peripheral resistance (R_p)^[149]. The afterload section (also referred to as afterload model, AM) should therefore minimally consist of two major components: a windkessel (III) and a resistor (IV) to form a so-called RC-model^[124,220]. We designed the windkessel as a cylindrical container in which a variable volume of air is trapped. The compressibility of the air has the same effect as the elasticity of the vessel wall. The cylinder has an inner diameter of 100 mm and a height of 300 mm, resulting in a compliance range of 0 to 2 ml/mmHg. The resistor is constructed with a cylinder (\varnothing 100 mm, length 150 mm) in which an internal compartment is created with a cylindrical membrane. The test fluid is forced through a compressible foam (S-PPI3001.R, Uxem, Belgium) inside the membrane, which guarantees laminar flow. Adding water to the outer compartment (between cylinder and membrane) results in a compression of the foam and a controlled increase in resistance. The pressure-flow relation of the resistor is linear. The resistance can be accurately controlled between $0.6 \text{ mmHg}\cdot\text{s}\cdot\text{ml}^{-1}$ (no compression of the foam) and infinity (total compression).

To respect the high-frequency behavior of the arterial system, we placed a small entrance resistor (piece of foam) immediately proximal to the windkessel to simulate the characteristic impedance (R_c) of the aorta ^[126]. Furthermore, in the hydraulic model, the different components are connected with tubing of finite length and diameter and therefore the acceleration and deceleration of the fluid will introduce an inertance component (L). The electrical analog representation of the AM subsequently consists of 4 components: R_p , C , R_c and L (Fig. V-3) ^[125].

Luer-locks are present at strategic locations for easy pressure measuring (with DTX+ strain gauge transducers, Ohmeda, Gent, Belgium) and de-airing. All data is acquired with a home-made acquisition system, built around a National Instruments PCI 6024E DAQ-board in a Labview (National Instruments Corporation, Austin, TX) software environment.

3.2. Validation of the afterload model

Initial tests were performed with the afterload model connected to a pulse duplicator system ^[136]. The reproducibility and stability of the resistor and the windkessel were tested under pulsatile flow by setting the resistor to 4 different values and switching between 4 compliance settings (1750, 1250, 750 and 250 ml air) for each resistance. Pressure was measured at the inlet of the AM (P_{ao}), proximal ($P_{R,p}$) and distal ($P_{R,d}$) to the resistor, and in the windkessel (P_w). Flow (Q) was measured at the windkessel inlet with an ultrasonic flow probe (H16C or H11X, Transonic Systems Inc., Ithaca, NY).

3.2.1. Measuring R and C

Resistance is calculated directly from the measurements as $(P_{R,p}-P_{R,d})/Q$. Windkessel compliance was first tested statically, by incrementally injecting a certain volume of water and measuring the corresponding pressure rise. Since there is no undisputed method for compliance measurement during pumping, we applied several estimation methods (pulse pressure method ^[221], area method ^[222], decay time method ^[223]) using Q and P_w .

3.2.2. Electrical analogon fittings

In order to estimate total inertance and characteristic impedance of the AM, we fitted a 4-element electrical analog model (EA model; Fig. V-3) to the data. To fit the model (programmed in Matlab, The Mathworks Inc., Natick, MA), we

used Q as an input and minimized the difference between predicted and measured pressure (P_{ao}) by optimizing component values. The goodness of fit is expressed as RMSE (root mean squared error).

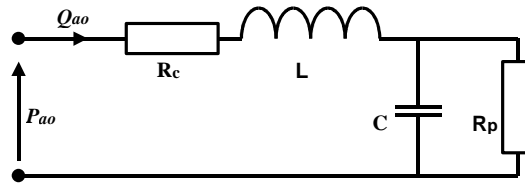


Fig. V-3: Electrical analogon (EA) of the MCS, presented as a modified 4-element windkessel model. Q_{ao} = aortic flow, P_{ao} = aortic pressure, R_c = characteristic resistance, L = inertance, C = total arterial compliance, R_p = peripheral resistance.

3.3. VAD tests

The mock circulatory system was used to test the Medos VAD (Medos Medizintechnik GmbH, Stolberg, Germany) over a wide range of filling pressures (5 - 40 mmHg), resistances (set as mean windkessel pressure; 60 – 160 mmHg) and compliances (0.3 - 1.6 ml/mmHg) and this for 5 different pump rates (40 – 120 BPM). The pump had a maximum stroke volume of 60 ml and the pneumatic pressure settings of this air driven membrane pump were kept constant at -10 mmHg and 160 mmHg for diastole and systole, respectively. Systolic time was set at 35% of the complete pump cycle. ½" PVC tubing was used as in- and outflow cannula (length 100 and 300 mm respectively) to connect the blood pump to the MCS. During VAD tests, pressure is measured in the preload reservoir and in the windkessel (which is comparable to human aortic pressure), while flow (Q) is measured at the same location as described above. All data is acquired at a 200 Hz sampling rate. Fluids used are water and pig blood at respective temperatures of 27 and 35°C .

4. Results

4.1. Validation of the afterload model

Data were obtained for 4 settings of resistance and compliance, yielding 16 different operating points. The measured values for R and the estimates for C (Pulse Pressure Method) are presented in Fig. V-4. It can be concluded that the range of R and C cover the patho-physiological range. Note that compliance varies not only by the amount of air that is trapped in the windkessel, but also with the mean pressure in the windkessel, and subsequently with the resistance.

Both Q and P_{ao} have a physiological morphology. P_{ao} is somewhat disturbed with reflections of the pressure waves that originate from opening and closing of the aortic valve. Due to the rigidity of the system, the resulting pressure peaks are higher than in the human body.

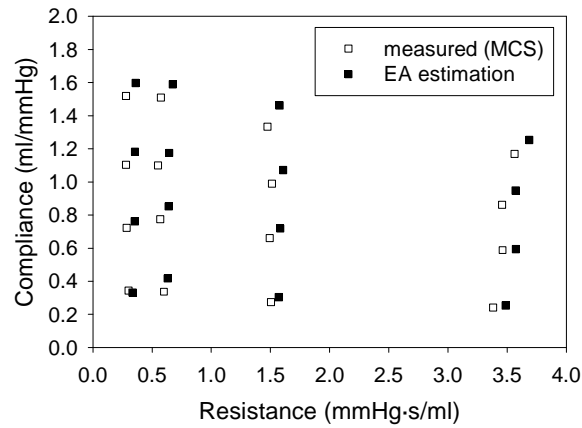


Fig. V-4: Comparison between measured parameter settings of C (estimated with pulse pressure method) and R_p and values estimated from the EA model fit.

The EA model fits the data very well, as reflected by the mean RMSE value of all measurements (mean \pm std. dev.: 2.8 ± 0.7 mmHg). Results for all 16 conditions are given in Table V-1. Fig. V-5 shows data measured with a high (3.38 mmHg·s/ml, see panel A) and an extremely low (0.29 mmHg·s/ml, see panel B) resistance. In both conditions, the model accurately predicts the measured pressure. In Fig. V-4, the values for C and R_p following from the 4-element EA model fit are compared to the actually measured resistance and the pulse pressure method estimate for compliance. The model slightly overestimates both R_p and C_{ppm} .

Table V-1: OVERVIEW OF MEASURED AND CALULATED PARAMETERS

setting id.	Compliance estimations [†]						4-element EA parameters [‡]				
	R_{meas} (mmHg·s/ml)	C_{static} (ml/mmHg)	C_{ppm} (ml/mmHg)	C_{area} (ml/mmHg)	C_{DTM} (ml/mmHg)	τ (s)	C (ml/mmHg)	R_p (mmHg·s/ml)	L (mmHg·s ² /ml)	R_c (mmHg·s/ml)	RMSE (mmHg)
R1C1	0.3	0.28	0.34	0.56	0.38	0.11	0.33	0.33	0.0051	0.054	4.69
R1C2	0.29	0.82	0.72	0.83	0.94	0.27	0.76	0.35	0.0055	0.024	2.96
R1C3	0.28	1.32	1.1	1.67	1.6	0.45	1.18	0.36	0.0055	0.02	2.94
R1C4	0.28	1.81	1.52	1.81	2.12	0.59	1.6	0.36	0.0056	0.018	2.54
R2C1	0.6	0.28	0.34	0.45	0.42	0.25	0.42	0.63	0.0042	0.071	3.57
R2C2	0.57	0.82	0.8	1.38	1.27	0.73	0.85	0.64	0.0051	0.031	3.2
R2C3	0.55	1.32	1.12	1.58	1.61	0.88	1.18	0.64	0.0059	0.017	2.81
R2C4	0.58	1.81	1.52	2.16	1.98	1.14	1.59	0.67	0.0058	0.017	2.76
R3C1	1.5	0.28	0.28	0.38	0.35	0.53	0.3	1.57	0.005	0.053	2.8
R3C2	1.49	0.82	0.67	0.65	0.74	1.09	0.72	1.58	0.0052	0.027	3.08
R3C3	1.51	1.32	1	0.94	1.13	1.7	1.07	1.61	0.0056	0.018	2.46
R3C4	1.48	1.81	1.33	1.67	1.52	2.24	1.46	1.58	0.0054	0.016	2.53
R4C1	3.38	0.28	0.24	0.27	0.26	0.89	0.25	3.49	0.0054	0.046	1.78
R4C2	3.46	0.82	0.57	0.65	0.63	2.15	0.59	3.58	0.0057	0.023	2.14
R4C3	3.46	1.32	0.86	1.21	0.96	3.3	0.95	3.57	0.0057	0.019	2.01
R4C4	3.56	1.81	1.17	1.34	1.29	4.58	1.25	3.69	0.0056	0.015	2.05

[†] Estimated from Q and P_w

[‡] Calculated from Q and P_{ao} fitting

R_{meas} : quotient of pressure difference over resistance and flow; C_{static} : statically measured compliance; C_{ppm} , C_{area} , C_{DTM} : compliance estimations with the pulse pressure method, the area method and the time decay method, respectively; τ : indication of decay time, product of C_{DTM} and R_{meas} ; C , R_p , L , R_c : values of the 4 elements of the EA model; RMSE : root mean squared error of the measured and fitted P_{ao}

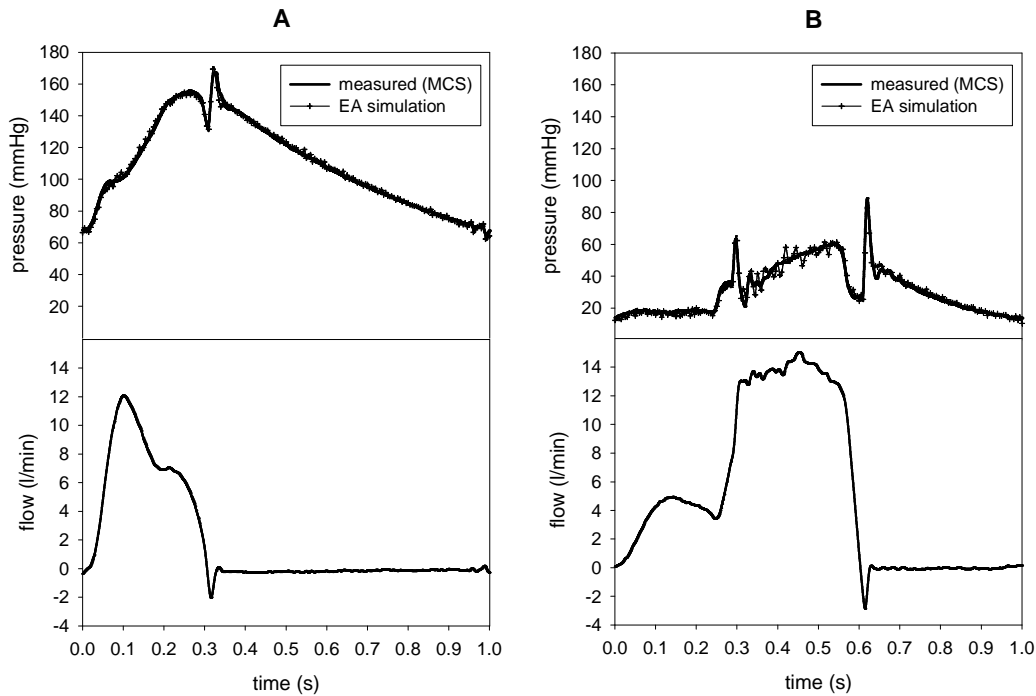


Fig. V-5: Measured aortic pressure and flow compared to the EA model fit for 2 different settings:
 A. R4C1 (see Table I) with an RMSE of 1.78 mmHg
 B. R1C2 (see Table I) with an RMSE of 2.96 mmHg

4.2. VAD tests

The data acquired during the Medos VAD tests was averaged over a sequence of at least 3 pulses. The 8 different preload and 8 resistance settings resulted in a series of 64 data points, plotted in a three-dimensional graph (Fig. V-6) for each pump rate and compliance setting.

The 3D graphs present average flow in relation to average preload and afterload (also referred to as mean arterial pressure (MAP)). A surface was interpolated between these points in order to allow a qualitative evaluation of the data: the slope of the surface in X and Y direction represent preload and afterload sensitivity of the device. To allow quantitative evaluation, a cut can be made in either direction through the surface, which yields two-dimensional preload-flow or afterload-flow graphs (representative data are shown in Fig. V-7). These 2D graphs are easier to interpret and allow a more detailed comparison between different devices.

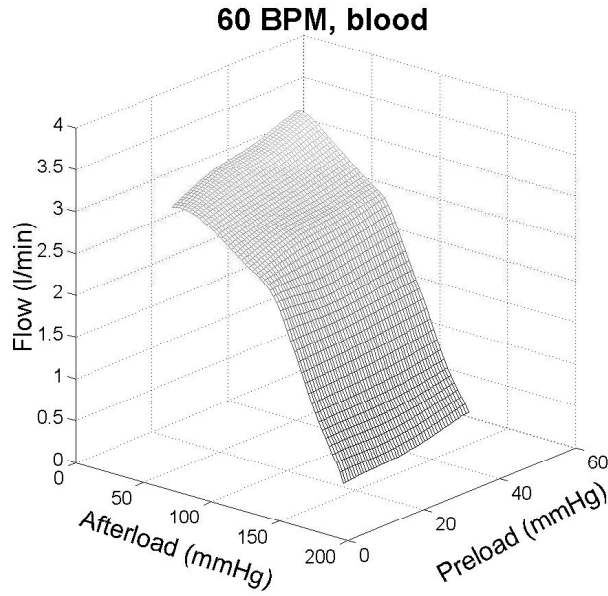


Fig. V-6: 3D graph of the Medos VAD characteristics as acquired in the MCS. Mean flow is presented in function of preload and afterload when pumping at a rate of 60 BPM with blood as a test fluid.

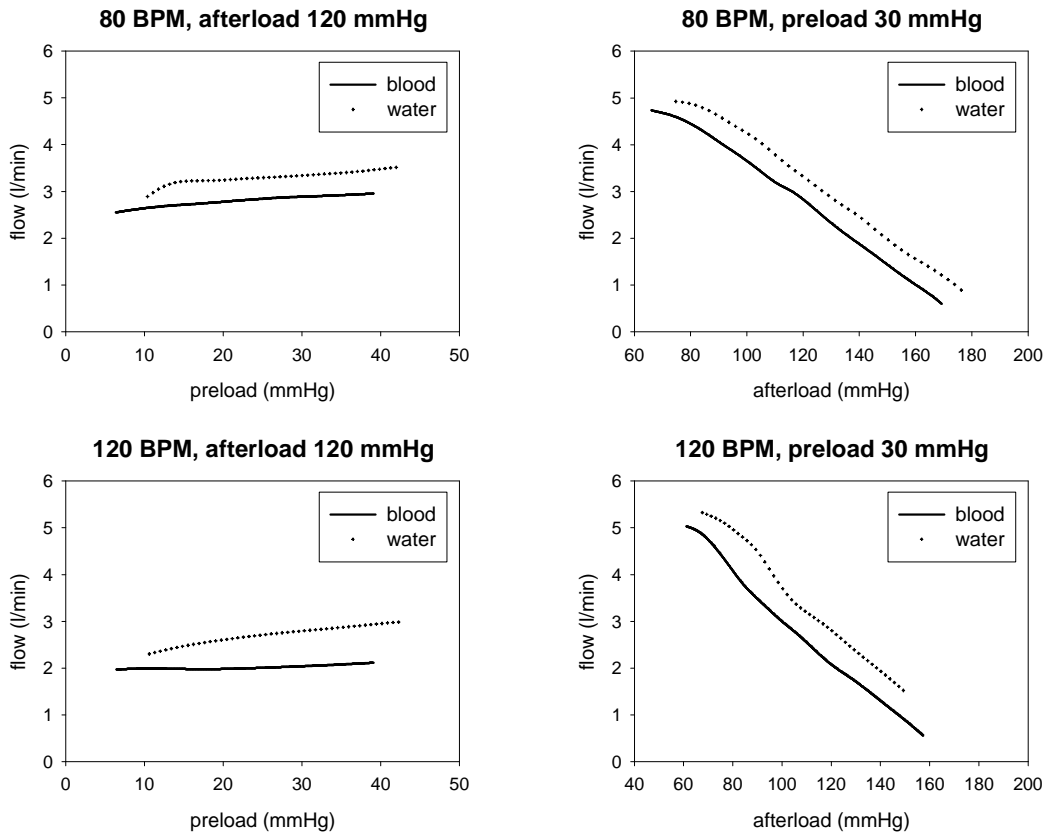


Fig. V-7: Illustrations of different hydrodynamic characteristics of the Medos VAD for different test fluids. Left: preload-flow graphs for 80 and 120 BPM at an afterload pressure of 120 mmHg. Right: afterload-flow graphs for 80 and 120 BPM at a preload pressure of 30 mmHg.

5. Discussion

The mock circulatory system appears an excellent simulation of the human systemic vascular system, covering the physiological and patho-physiological range of resistance and compliance. It is an afterload model that can not only be used for testing of ventricular assist devices, but it can also serve as a load for cardiac simulators in order to produce physiologically correct pressures and flows. The setup perfectly fits a modified 4-element EA model, consisting of peripheral resistance, compliance, characteristic impedance and inertance. Resistance and compliance estimated with the EA model correlate well to the measured values of R and the pulse pressure method estimate of C . The area method and decay time method produced unstable values and high overestimation of compliance for low resistances, due to an unclear distinction of the pressure decay. These findings are consistent with earlier observations [224,225]. Although we did not physically alter the entrance resistor in the afterload model during the experiments, the water level in the windkessel changes with different settings of R_p and C . This affects the fitted value of R_c : the larger R_p and C , the smaller R_c (Table I). In contrast, the inertance (determined by the fixed diameters and lengths of tubing and connector pieces) remains rather constant (mean \pm std. dev. = 0.0053 ± 0.0004 mmHg·s²/ml). Note that, though pressure wave travel and reflection do not appear in an electrical analog model, our model has no problem in fitting the measured pressure peaks. The reason is that we used the measured flow (which also results from incident and reflected waves) as an input to the model.

As there is a good correlation between actual AM parameters and 4-element EA model parameters, the EA model can be used to match the AM settings to human data. Fig. V-8 shows the aortic pressure of a patient with concentric hypertrophy as measured by Patel [226] and the model fit. The estimated parameters (see legend Fig. V-8) are within the range of the AM components, and consequently, it is possible to mimic this patient's afterload in the mock circulatory system.

Lumped mock systems can not be used to study wave propagation induced by blood pumps. Pressure waves originate upon ejection of the pump and from opening and closure of the valves in the mock system. Due to the stiff system, short wave travel distances, the absence of a bifurcating arterial tree and large reflections on the components and connectors, the pressure peaks in our AM are

larger than they are in the human aorta. Nevertheless, it is important to consider that relatively large pressure peaks may appear in the outlet cannula of an assist device since these cannulas are very rigid compared to the human aorta.

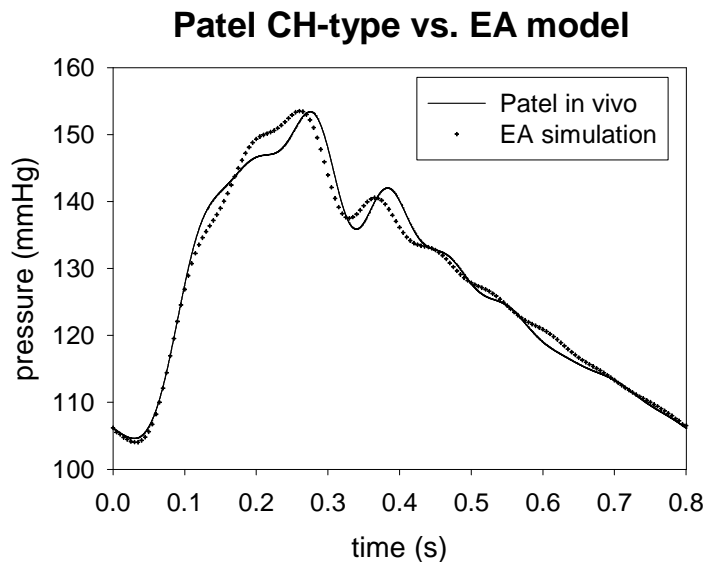


Fig. V-8: Aortic pressure measurement by Patel ^[226] in a patient suffering concentric hypertrophy, compared to the 4-element model fit. $R_p = 1.85 \text{ mmHg.s/ml}$, $C = 0.87 \text{ ml/mmHg}$, $L = 0.0016 \text{ mmHg.s}^2/\text{ml}$, $R_c = 0.071 \text{ mmHg.s/ml}$, resulting in an RMSE of 1.73 mmHg.

The 3D graphs that are produced as a result of VAD tests are a simple way to qualitatively evaluate pump performance. These characteristics clearly demonstrate the influence of preload, afterload and pump rate. High afterload leads to zero flow and higher flows can be reached when the filling pressure is higher. However, the latter relation is hardly distinguished at the lowest pump rate (40 BPM): the device has enough time to fill completely, even with low filling pressure. The influence of the preload increases with increasing pump rate; since the diastolic period shortens, the pump can only fill fast enough when the filling pressure is high. The effect of preload is only clearly present for low afterloads. When the afterload is high, the pump can only partially eject its contents and, therefore, filling is not the limiting factor and has little influence on the flow.

The afterload sensitivity increases with pump rate. It is easy to understand that for low afterloads, when the pump empties completely, a higher pump rate will result in a higher flow. At high afterload, the device has to build up pressure and squeeze the fluid through the resistor, which inevitably results in impeded stroke

volume and low flow. If the pump rate increases, the ejection time is reduced and as a result stroke volume is even more impeded and a lower flow will appear for the same afterload. Consequently, the relation between flow and afterload becomes steeper at higher pump rates and this slope is scarcely altered by the preload. Remarkable is the bend in the surface for a pump rate of 60 BPM. This sudden change in afterload sensitivity occurs between 100 and 120 mmHg and does not show at other pump rates.

Our experiments showed little or no effect of arterial compliance on pump characteristics. The test fluid, on the other hand, is an important parameter. Higher flows can be reached when water is used, but there is no difference in preload or afterload sensitivity: blood and water tests yield parallel pressure-flow relationships. All 3D graphs for water and blood show the same topology. The lower flow obtained with blood is due to its higher viscosity and density.

The extra energy loss created by this higher viscosity and density is distinct in all components of the MCS, the pump and the cannulas. Since the cannulas are relatively long and small, the density difference between water and blood, although small, has a marked influence on the inertance in these components. It is therefore important not only to work with a proper fluid, but also with the original cannulas or grafts. This may be difficult when a water-based mixture is used as a test fluid since most grafts are water-permeable. Consequently, VAD tests performed with (physiological) water as recommended for long-term reliability testing ^[123], may provide incorrect hydrodynamic data. Blood or a more convenient to use blood-analogous fluid should be used to correctly assess the hemodynamic pump performance.

From the point of view of patient support, mean flow is an important control parameter, and the preload-afterload presentation of the data may be a valuable tool in the device operating control. The data, however, do not allow determination of the limiting factor of a device. This would require an additional flow measurement at the inflow cannula to calculate the instantaneous pump volume and to study the filling and ejection separately. The pump may fill adequately, but may not have enough power to empty completely against a high pressure, or it may empty completely but only fill partially due to a low preload or insufficient suction of the pump. In this particular study, the Medos VAD was used with only one setting of systolic and diastolic pressure, while in clinical practice these settings are varied until an optimal flow is reached. In that way, the

limiting factor (low filling or low ejection) can be avoided, but this is not possible in most long-term electromechanical pulsatile ventricular assist devices. Therefore, it is recommended to study the pump characteristics with 2 separate flow meters for the inlet and outlet conduit.

6. Acknowledgements

This research is funded by a specialisation grant of the Institute for Innovation through Research and Technology in Flanders (IWT-991171). Patrick Segers is post-doctoral fellow funded by the Fund for Scientific Research - Flanders (FWO-Vlaanderen).

C. PUCA II PUMPING CAPACITIES VERSUS HIGH-FLOW VOLUMETRIC DEVICES

1. Introduction

The PUCA II catheter pump is intended for stabilization and short-term support of heart failure patients. Its main advantage is its small size and hence its option for fast and easy introduction in the left ventricle via a transvalvular pathway without causing permanent damage. Due to this application, the requirements and design criteria differ from traditional high-flow LVADs that are capable of taking over the complete workload of the heart. These devices are large and often make use of an inlet cannulation that damages the left ventricular apex. The small size of the PUCA II, on the other hand, compromises its pumping capacities. This section illustrates the difference in hydraulic performance of the PUCA II and two high-flow LVADs: the Medos VAD (Medos Medizintechnik GmbH, Stolberg, Germany) and the Novacor N100 (WorldHeart Corp., Ottawa, Canada). The comparison is based on the hydrodynamic characterization as described in section B.

2. Methods

The pump characteristics of the PUCA II in combination with an AutoCat IABP driver (Arrow Int., Reading, PA) were acquired from the *in vitro* mock circulatory system with static preload and lumped afterload. More details on this experiment can be found in section D. Similar measurements were performed for the Medos VAD in combination with its original pneumatic drive console and for the Novacor N100. All experiments were performed with a 60/40 v/v% water-glycerin mixture at room temperature.

For comparison of the pumping capacities of these devices, only the data acquired at a fixed rate of 80 BPM are discussed since this setting was available on all driving consoles. In a clinical environment, however, the PUCA II will function in ECG-triggered counterpulsation (synchronously) with the natural heart and thus the pump rate may vary. The Medos VAD can also be used with

ECG triggering, but (asynchronous) fixed rate operation is most common. The fixed rate mode of the Novacor is only used for implantation and weaning purposes, while the standard is Fill Rate Trigger mode (FRT). In this mode the pump automatically determines its filling and ejection timing with parameters derived from the internal volume variations, and thus pump rate also varies with the patient's condition. More information on the operation and working principles of the Medos VAD and the Novacor can be found in their respective manuals and in ^[56,57].

For these experiments, the PUCA II (with 40 ml stroke volume) was managed in “operator” mode and inflation and deflation timing were optimized before every data acquisition. The Medos VAD had a stroke volume of 60 ml and the driver was set to a pneumatic pressure of –10 mmHg for diastole and 160 mmHg for systole, and 35% systolic to diastolic time ratio. No additional settings were possible for the Novacor.

The protocol and the data processing for hydrodynamic characterization were explained in section B. In brief, for a given pump setting, the generated flow is measured for several combinations of preloads and afterloads. The data is averaged over a number of cycles and plot in a three-dimensional graph (the pump characteristic). For assessment of the preload- and afterload-sensitivity of the pump, two-dimensional cuts are made through the pump characteristic.

3. Results and discussion

The pump graphs obtained from the experiments with the three different ventricular assist devices are displayed in Fig. V-9. From these graphs it can be derived that the Medos VAD and the Novacor operate in similar flow ranges and show a high afterload sensitivity, while the PUCA II operates in a lower flow range and displays a much flatter surface, indicating that there is a smaller effect of afterload. The afterload sensitivities derived from the two-dimensional plots in Fig. V-10 are -0.12 , -0.78 , and $-0.66 \text{ ml}\cdot\text{s}^{-1}\cdot\text{mmHg}^{-1}$ for the PUCA II, Medos VAD, and Novacor, respectively. Note from Fig. V-10 that the afterload range for the PUCA II was lower than for the other pumps. The preload sensitivities in the same order are 0.11 , 0.46 , and $-0.07 \text{ ml}\cdot\text{s}^{-1}\cdot\text{mmHg}^{-1}$. These sensitivities determine the ‘physiological’ response to changes in the patient's condition. Since the fixed rate mode is mostly used in the hospital where the patient is

closely monitored, the settings of the pump drivers and the pump rate can be adjusted according to the patient's physical demands, thus eliminating the need for physiological response. Tweaking of the pump settings will then be required more often for highly sensitive pumps.

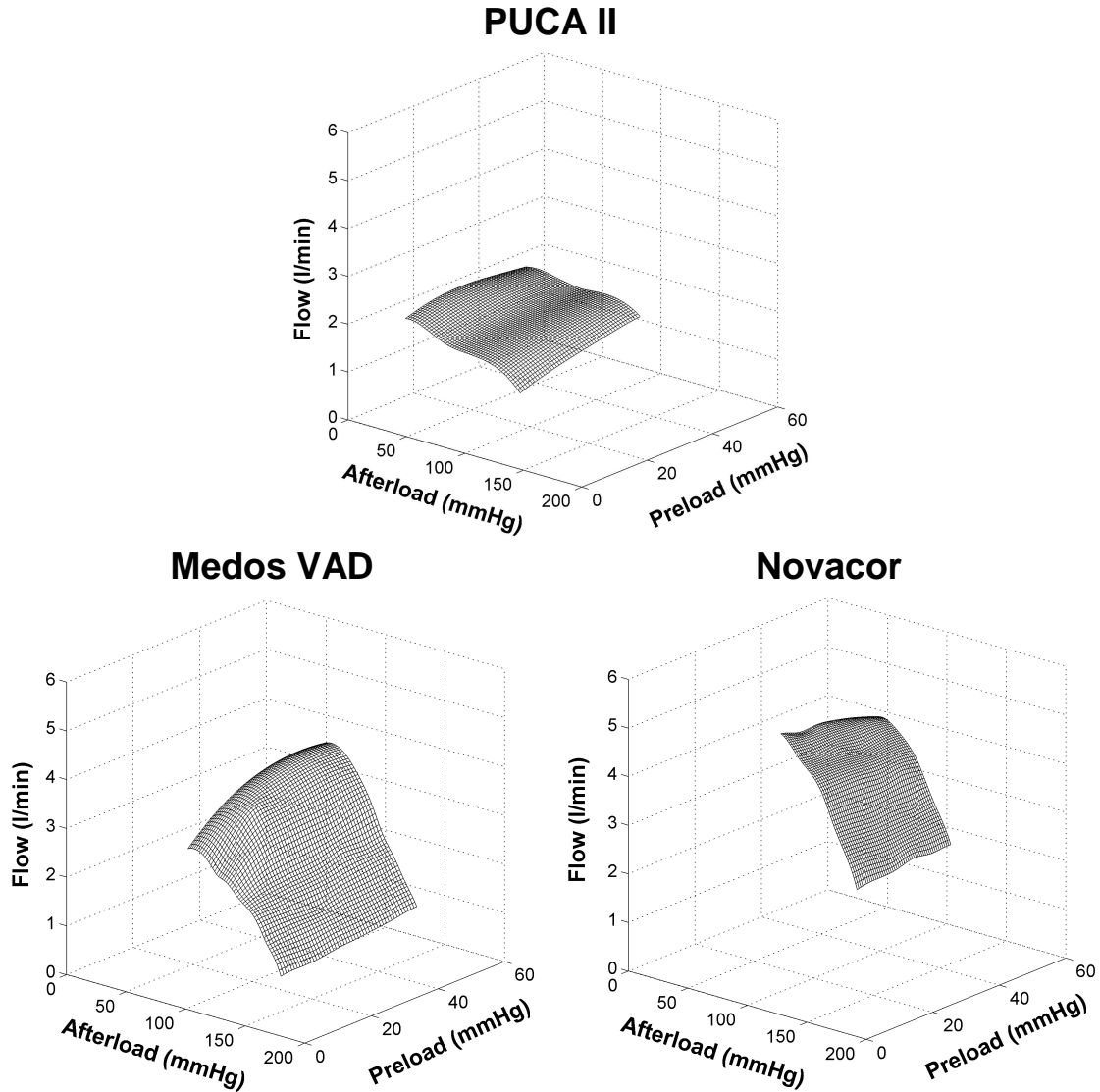


Fig. V-9: Pump characteristics of Novacor, Medos VAD, and PUCA II at 80 BPM.

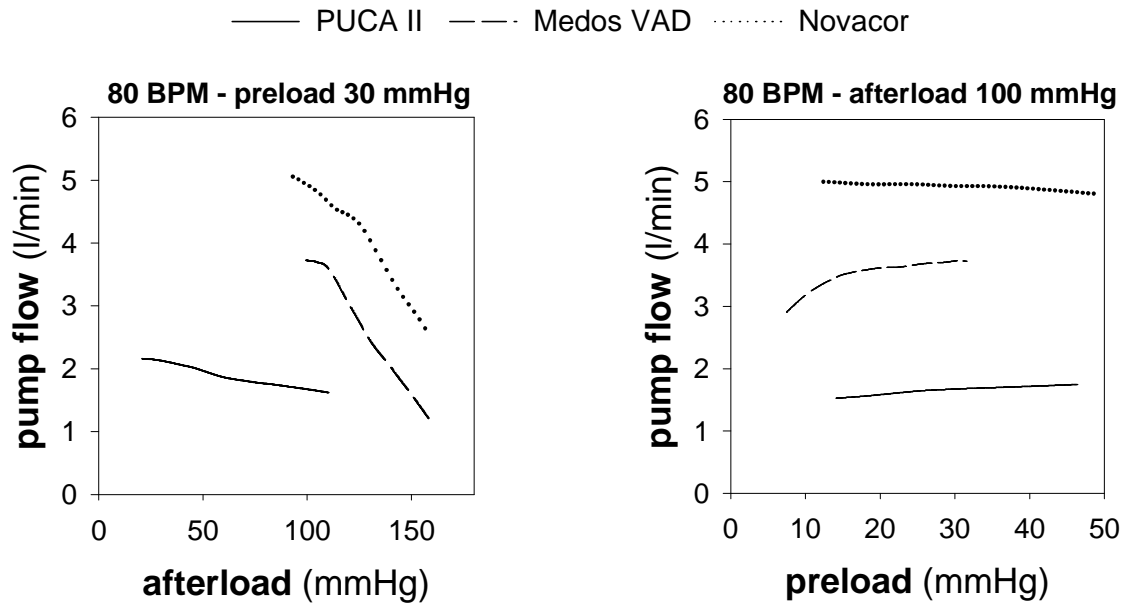


Fig. V-10: Two-dimensional cuts through the pump characteristics of Fig. V-9. Left: a cut parallel with the afterload-axis at a preload level of 30 mmHg. Right: a cut parallel with the preload-axis at an afterload level of 100 mmHg.

The different ranges of flow rates that are exposed in Fig. V-9 and Fig. V-10 are related to the different stroke volumes of the pump designs and do reflect the applications for which the pumps are developed. The Novacor, for instance, is intended for long-term use outside the hospital. It is therefore required that this pump can generate sufficient output when the patient performs physical activity. The Medos, on the other hand, is intended for short-term or medium-term use inside the hospital, where the patient will not be active and thus the pump output is calculated to obtain sufficient organ perfusion at rest. The PUCA II has the main benefit of being minimally invasive and its target application is support and stabilization. Even though high flows would be desirable, this device is not intended to take over the whole circulation.

Based on the pump rate of 80 BPM and the maximum stroke volume of each pump, the maximum obtainable flows in the experiments were 3.2, 4.8, and 5.8 l/min for the PUCA II, the Medos VAD, and the Novacor, respectively. Due to the combination of loading conditions and the constant (not optimized) driver settings, these maximum flows were not obtained for either device. Obviously, the flows generated by the Medos VAD can be increased by setting the systolic and diastolic pressures to higher absolute values. The designers of the PUCA II pump already demonstrated the importance of the pneumatic driver and the

driver settings in *in vitro* studies (see chapter VI, section B). A more powerful driver can overcome the inertance and resistance of the catheter and generate higher pump flows. The Novacor will also perform differently when operated in FRT and specifically for our setup - with continuous and unimpeded filling - the pump will adopt a higher pump rate and produce a higher flow.

A data set of each of the pump experiments was selected for comparable preload, compliance, and resistance settings and is shown in Fig. V-11 as an illustration. It is important to realize that in the pump characteristics, a similar afterload (i.e., the pressure at the pump's outlet) is obtained with different resistor settings for each pump. The necessary resistance to obtain a given afterload pressure is dependent on the pump's capacity to generate pressure and flow. For the data shown in Fig. V-11, however, it can be stated that the pumps were all inserted in the *in vitro* model with identical settings. Table V-2 gives an overview of parameters derived from these data sets, where it must be remarked that in the whole experiment a wide range of resistances was used to obtain the pump characteristics, and that the resistor was adjusted to obtain specific afterload pressures rather than specific resistance values. Hence the (relatively slight) discrepancy between the resistance values. Hydraulic power is the product of outlet flow and pressure, and the cycle work is the power integrated over one pump cycle.

Table V-2: Parameters derived from the data displayed in Fig. V-11.

	PUCA II	Medos VAD	Novacor
Preload (<i>mmHg</i>)	47.1	47.3	46.0
Resistance (<i>mmHg·s/ml</i>)	1.82	1.76	1.50
Compliance (<i>ml/mmhg</i>)	0.93	0.90	0.85
MAP (<i>mmHg</i>)	66.6	108.8	116.5
Pump flow (<i>l/min</i>)	1.90	3.70	4.38
Stroke volume (<i>ml</i>)	23.7	46.3	54.7
dp/dt_{\max} (<i>mmHg/s</i>)	90.5	232.1	428.9
Cycle work (<i>mWatt·s</i>)	219.9	746.7	1139.3
Max. hydr. power (<i>mWatt</i>)	920.7	4134.7	7561.2

From the data in Fig. V-11 and in Table V-2, it can be concluded that the Novacor is most powerful and that this results in a steep buildup of ‘arterial’ pressure (high dp/dt_{max}). This also means that when the pump is turned on, it will augment the output pressure to a high level in a few pumping cycles, even when there is no heart function to keep up the pressure. The PUCA II on the contrary, cannot build up pressure and therefore it can only maintain a low ‘aortic’ pressure level without residual heart function. It can also be noted that the Novacor ejects its large stroke volume in a short time period. The Medos VAD knows a longer ejection period, and the PUCA II needs even more time to gradually squeeze its smaller stroke volume through the resistor. The lower power of the PUCA II makes that, for the considered condition, it can only eject 59% of its volume, while this is 77% and 74% for the Medos VAD and Novacor respectively. It must be taken into account that the data were acquired at the windkessel of the lumped afterload model, where the inertia and resistance of the cannulas and catheter have already been overcome. The AutoCat driver of the PUCA II can generate pressures over 300 mmHg, while the Medos VAD was set at only 160 mmHg systolic pneumatic pressure and yet yields higher power at aortic level. This confirms once again that the resistance and inertia in the PUCA II catheter is an important limitation and simultaneous pressure measurements inside the pump chamber and in the aorta are necessary to experimentally determine the impact of these properties on PUCA II performance.

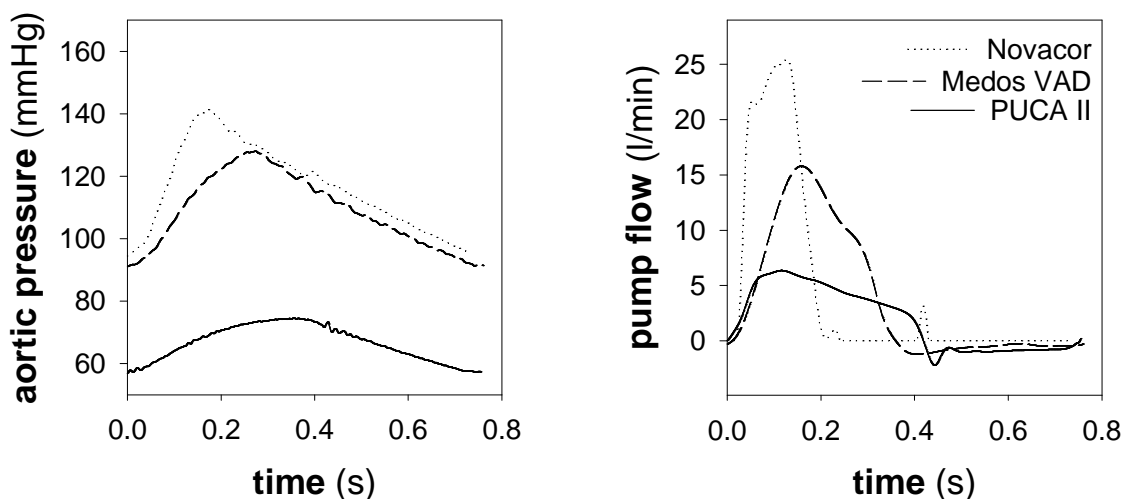


Fig. V-11: Illustration of the ‘aortic’ pressure and flow generated by the three compared pumps in similar conditions (see Table V-2).

4. Conclusions

Comparison of the PUCA II pump to the Medos VAD and Novacor system revealed a high disparity in pump capacities, which is in accordance with their target application and design criteria. The high-flow Medos VAD and Novacor can generate more power, resulting in higher pump output and a higher pressure level than the PUCA II. They are, however, very sensitive to afterload variations whereas the PUCA II flow is hardly influenced by loading conditions.

D. IN VITRO EVALUATION OF THE PUCA II INTRA-ARTERIAL LVAD[†]

1. Abstract

The ‘pulsatile catheter’ (PUCA) pump is a minimally invasive intra-arterial left ventricular assist device intended for acute support of critically ill heart failure patients. To assess the hydrodynamic performance of the PUCA II, driven by an Arrow AutoCat IABP driver, we used a (static) mock circulatory system in which the PUCA II was tested at different loading conditions. The PUCA II was subsequently introduced in a (dynamic) cardiovascular simulator (CVS) to mimic actual *in vivo* operating conditions, with different heart rates and 2 levels of left ventricular (LV) contractility.

Mock circulation data shows that PUCA II pump performance is sensitive to afterload, pump rate and preload. CVS data demonstrate that PUCA II provides effective LV unloading and augments diastolic aortic pressure. The contribution of PUCA II to total flow is inversely related to LV contractility and is higher at high heart rates. We conclude that, with the current IABP driver, the PUCA II is most effective in 1:1 mode in left ventricles with low contractility.

2. Introduction

Cardiac assist devices are generally durable devices that are capable of maintaining the circulation of a patient suffering from severe heart failure for prolonged periods. Apart from these devices, there is also need for circulatory support devices that can be introduced rapidly in case of sudden cardiac failure or as a treatment of the low output syndrome (LOS). These minimally invasive resuscitation methods are required for short-term to medium-term periods to stabilize the patient and to give the clinicians the time to outline a treatment

[†] The contents of this section was published in Int J Artif Organs 2003;26(8):743-752:

***In vitro* evaluation of the PUCA II intra-arterial LVAD**
Vandenberghe S, Van Loon JP, Segers P, Rakhorst G, Verdonck P

strategy. Examples of such devices are the intra-aortic balloon pump (IABP), first used by Kantrowitz in 1967 [227], the Hemopump [228], and more recently the Impella pumps [61]. All these devices allow fast introduction without need for thoracotomy, they provide unloading of the heart, improve perfusion of major organs and result in increased coronary blood flow [121,229].

An apparatus that aims to combine the advantages of the aforementioned devices is the pulsatile catheter (PUCA) pump, which delivers both pulse *and* blood flow to the arterial system [218,230]. It comprises a valved catheter that can be introduced transarterially (e.g., in the subclavian artery) and shifted retrograde into the left ventricle. Blood is drawn from the left ventricle and ejected in the aorta through the incorporated valve (Fig. V-12).

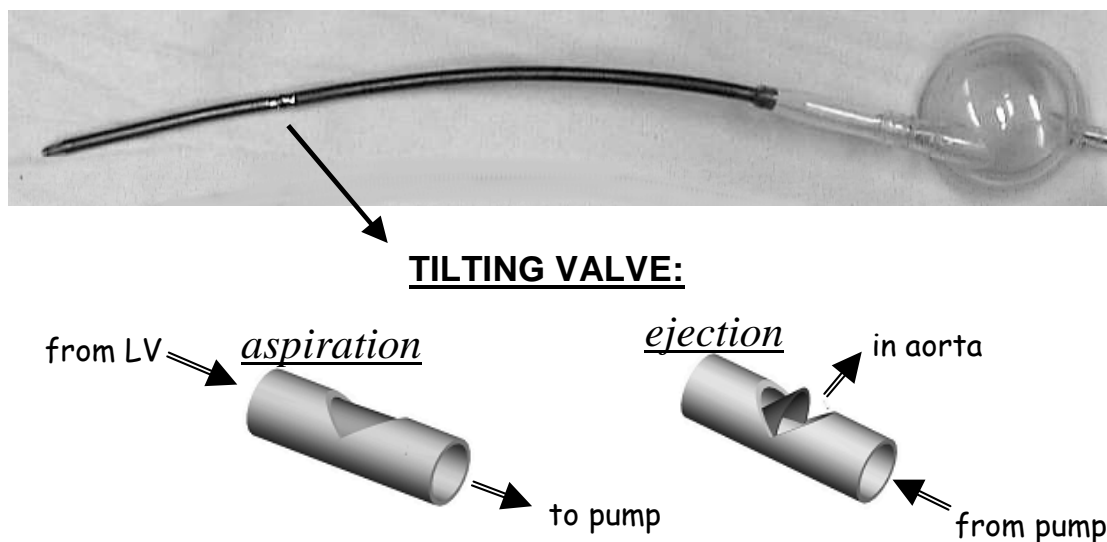


Fig. V-12: Picture of the PUCA II catheter and membrane pump, with a detailed drawing of the tilting valve.

The principle of the PUCA pump was invented by Dr. Rakhorst based on an idea of Hans Zwart who tested a closed chest cardiac assist system in dogs [231]. The first thick-walled prototypes of pulsatile catheters (1 mm wall thickness) were produced by Dr. Kolff and Dr. Hennig between 1990 and 1992. Thin-walled, dual valved, PUCA pumps have been manufactured since 1995 and extensively tested *in vitro* and *in vivo* at the Department of Biomedical Engineering of Groningen University, The Netherlands [218].

Currently, a more recent, single-valved, version of the PUCA pump (PUCA II) is in a test phase and its first clinical use is expected soon. This PUCA II is also a thin-walled catheter (wall thickness: 0.3 mm) but has only one tilting valve

incorporated into the catheter wall, which allows ejection of blood in the ascending aorta. The catheter is connected to a custom-made membrane pump which can be actuated by most commercially available IABP drivers and drivers for pneumatic cardiac assist devices.

In this study we assessed the pump characteristics and the efficiency of the PUCA II pump driven by an Arrow AutoCat IABP driver in a mock loop. Additionally, we evaluated the functioning of this device in combination with a hydraulic bench model of the cardiovascular system.

3. Materials and Methods

To obtain the pump characteristics of the system we first inserted it in a ‘static’ *in vitro* mock circulatory system, representing a physiological afterload. The only pumping action in this setup was delivered by the PUCA II.

Secondly, we used a ‘dynamic’ *in vitro* model or cardiovascular simulator (CVS). This consists of a pulse duplicator as simulation of the left heart and a distributed afterload system which allows realistic introduction and positioning of the device.

3.1. PUCA II setup

The PUCA II catheter (Intra-vasc BV, Groningen, The Netherlands) consists of a 28 cm long 21 Fr reinforced polyurethane shaft that incorporates a stainless steel inflow cage at the tip and an outflow valve located 10 cm distally ^[56,230]. The catheter is connected to a paracorporeally placed, pneumatically driven, single-port valveless membrane pump with a stroke volume of 40 ml. The catheter valve is designed as to direct blood flow from the left ventricle (LV) to the membrane pump during the aspiration phase, and to direct the blood into the ascending aorta during pump ejection.

For this study, the pump was driven by an AutoCat intra-aortic balloon pump driver (Arrow Int., Reading, PA), which allowed us to run the pump in either ‘autopilot’ or ‘operator’ (manual) mode. The latter allows to adjust inflation and deflation timing. The pump to heart frequency ratio can be set to 1:1 or 1:2 in both operating modes.

3.2. Static model

The static model is a lumped representation of the human cardiovascular system [187]. It consists of a preload reservoir, simulating the LV and providing a constant filling to the pump, and an afterload section. This latter section mimics systemic arterial compliance and total peripheral resistance with a windkessel and a resistive element with a compressible foam. The PUCA II was inserted in the model via the ‘aortic’ tubing that connects the preload reservoir to the windkessel. The catheter was positioned with the valve in the ‘aorta’ and its tip sealed in the preload reservoir as to simulate a perfectly closed aortic valve. Consequently, the only flow path from the preload reservoir (LV) to the windkessel was through the PUCA II catheter.

Pressure data were acquired with DTX+ pressure transducers (BD, Franklin Lakes, NJ) in the preload reservoir, the windkessel (aortic pressure) and just after the resistor (venous pressure). Flow was measured at the membrane pump exit port and at the ‘aorta’ between preload and windkessel with 10C and H16C flow probes on a T206 and HT207 flow meter (Transonic Systems Inc., Ithaca, NY), respectively. Since there is no valve in the exit port, there is both forward and backward flow with a mean of 0 l/min. The positive (forward) part of this flow is normally used to monitor the PUCA II system and we will refer to it as the ‘indicated pump flow’ (Q_{puca}).

3.3. Dynamic model

This model is composed of a pulse duplicator system and a silicone arterial tree, simulating the systemic circulation (see Fig. V-13). The pulse duplicator consists of 2 silicone sacs representing the left atrium and ventricle with a bileaflet and a bovine pericard valve as mitral and aortic valve respectively. The sacs are suspended in a water-filled housing and are actuated by a computer controlled pneumatic driver [136].

The elastic arterial tree consists of an aorta with 8 branches representing the main arteries to the head, the arms, the kidneys and splanchnic organs and the legs. These arteries are present on both the left and right side, and are connected conform anatomical reality (cf. brachiocephalic trunc). Arterial dimensions are derived from literature as to mimic a 1.8 m tall male of 85 kg [138], with some adaptations since several arteries are bundled for ease of construction. The arteries end in a resistor with a compressible foam and a venous overflow system

that allows volumetric measurement of the mean flow through every branch. The PUCA II catheter was introduced in the right subclavian artery and was positioned through the aortic valve using the standard technique with a guiding pressure catheter.

Pressure measurements were performed in the LV with a pigtail catheter and DTX+ transducer and in the ascending aorta with a Millar hi-fi transducer (Millar Instruments Inc., Houston, TX). Flow distribution over the model was measured with the overflow system.

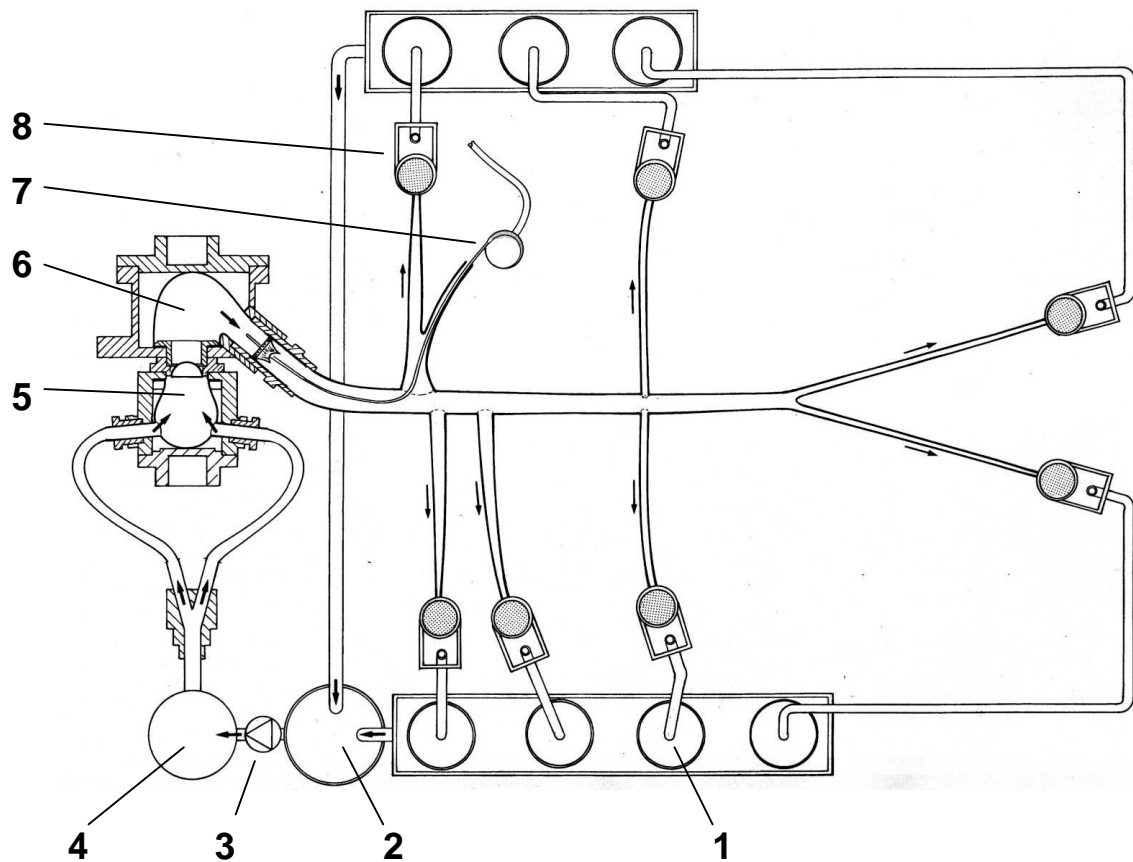


Fig. V-13: Overview of the model setup: 1. collection container; 2. buffer reservoir; 3. centrifugal pump; 4. lung reservoir with weir; 5. left atrium; 6. left ventricle; 7. PUCA pump; 8. variable resistor combined with an overflow reservoir.

4. Protocol

All experiments were performed with a 60/40 v/v% water-glycerin mixture at room temperature (kinematic viscosity: $3.7 \text{ mm}^2/\text{s}$, density 1093 kg/m^3) and with the AutoCat driver set to ‘operator’ mode. All data were sampled at 200 Hz for at least 5 seconds in an equilibrium state, which allowed us to calculate an average, representative beat.

4.1. Static model

Measurements in the static model were performed at 60, 90 and 120 beats per minute (BPM) in 1:1 mode. An electronic patient simulator supplied ECG triggering and arterial pressure feedback for the AutoCat driver. Each pump rate was combined with different settings of preload (filling pressure of 10, 20, 30 and 40 mmHg) and afterload. The latter was set by varying the resistor to obtain mean windkessel pressure values of 20, 40, 60, 80, and 100 mmHg at 60 BPM with a filling pressure of 10 mmHg. The static model experiments allowed us to compose a pump graph and to calculate the efficiency of the pump as the ratio of the total ‘aortic’ flow to the indicated pump flow. This efficiency was plotted as a function of mean arterial pressure (MAP) for each pump rate (Fig. V-15).

$$\eta = \frac{Q_{ao}}{Q_{puca}} = \frac{\text{actual total aortic flow}}{\text{indicated PUCA pump flow}} \quad [\text{Eq. V-1}]$$

4.2. Dynamic model

In the dynamic model, the heart and PUCA II were also set to 60, 90 and 120 BPM, but a different protocol was followed to assess the gain of the PUCA II over the native heart function. For each heart rate, data were acquired with the pump switched off (control 1), then with the pump in 1:1 mode, afterwards in 1:2 mode, and finally a last acquisition was performed with a switched off pump (control 2) to control the stability of the model. These measurements were done for 2 levels of LV contractility (by adjusting the pneumatic pressure level) as to obtain a maximum aortic pressure of 70 (low contractility) and 120 mmHg (high contractility) at 60 beats/min, respectively. This resulted in 6 test series (3 heart rates and 2 contractilities). Inflation and deflation timing of the PUCA II was adjusted by an experienced IABP operator to obtain optimal counterpulsation. ECG triggering was delivered by the pulse duplicator controller and true arterial pressure was fed back to the AutoCat driver.

It was not possible to determine the pump efficiency in the dynamic model since total aortic flow (Q_{ao}) is not only generated by the pump but it is composed of effective PUCA II pump flow and cardiac output. Therefore $Q_{ao} = Q_{puca} \cdot \eta + Q_{heart}$, with η = efficiency and Q_{heart} = flow delivered by the heart, both unknown. We estimated the efficiency by interpolating it for the MAP from the static model results. Thus we were able to split up Q_{ao} and to calculate the actual contribution of the PUCA II to total flow when working in combination with a pumping

ventricle. To study the main effects of heart rate, pump mode and contractility on mean arterial pressure (MAP), flow, and pulse pressure, a 3-way ANOVA was performed with Tukey post-hoc tests at a significance level of $p = 0.05$.

5. Results

5.1. Static model

Representative examples of data measured in the static model are given in Fig. V-14. Typical is the uni-directional aortic flow, which follows the positive part of the bidirectional flow at the membrane pump outlet. During peak ejection the aortic flow is smaller than the pump outlet flow, indicating that there are some minor losses. During the aspiration phase of the pump, the aortic flow is slightly negative. The pump rate of 60 BPM shows a larger peak ejection loss and a larger negative flow compared to 90 and 120 BPM.

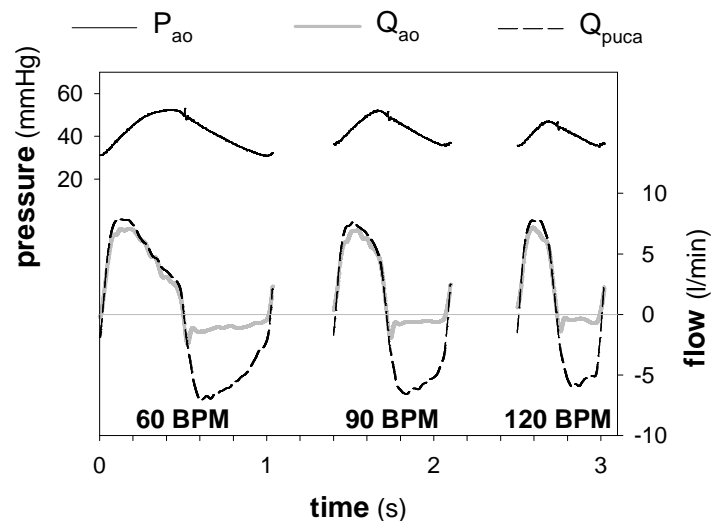


Fig. V-14: Data measured in the static model at 60, 90 and 120 BPM. All these data were measured with a preload pressure of 30 mmHg, a resistance of 1.0 mmHg-s/ml, and a compliance of 1.1 ml/mmHg.

The top panel of Fig. V-15 shows the pump graphs measured at a pump rate of 90 BPM for the 4 levels of preload. The presented flow is the aortic flow, i.e., the effective flow running through the setup. The highest preload yields the highest, most powerful, pump characteristic. It can also be derived from this graph how preload changes have an influence on afterload, since the data points acquired with higher preloads are also shifted rightward, while there were no changes in the resistance.

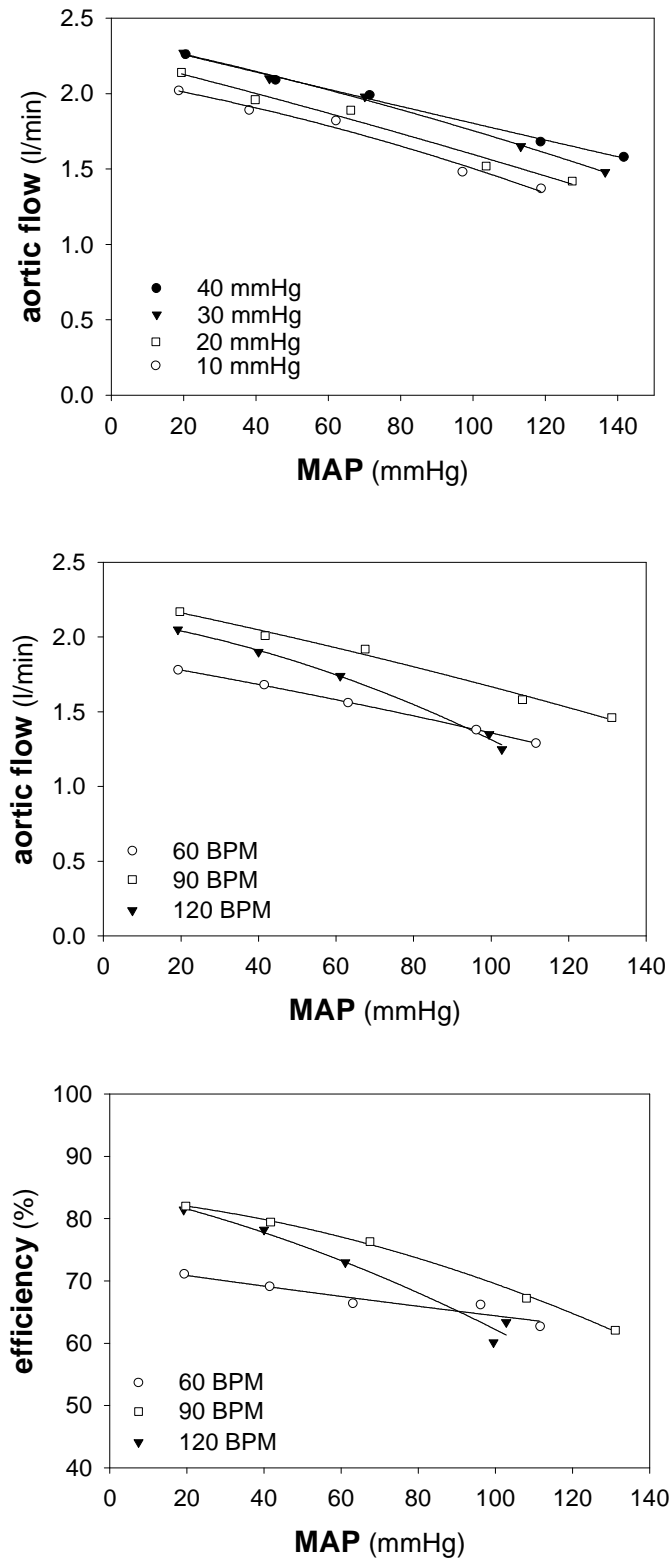


Fig. V-15: Results from the static model experiment. Top panel: pump graph at 90 BPM, demonstrating the influence of preload pressure (10 – 40 mmHg). Middle panel: averaged pump graphs of 60, 90 and 120 BPM. Bottom panel: efficiency plot for the three different pump rates. The 'aortic flow' in the pump graphs is the effective total flow running through the whole setup.

To better visualize the effect of heart rate on the pump graph, we calculated an average pump graph (averaging the effect of preload) for each heart rate. The result is given in the middle panel of Fig. V-15. In addition, we calculated the efficiency of the pump at the different heart rates (bottom panel of Fig. V-15). At low afterload pressures (< 50 mmHg), the PUCA II efficiency is about the same for 90 and 120 BPM (approximately 80%), while the same system running at 60 BPM has a 10 % lower efficiency. The efficiency at 60 BPM is hardly influenced by variations in afterload. For the other pump rates, efficiency decreases with increasing afterload, where it is best preserved with the PUCA II running at 90 BPM.

5.2. Dynamic model

The cardiovascular simulator proved to be stable with small variability in flow distribution and LV and aortic pressure when compared before and after each test series: maximum differences of 3% and 5% were found between control 1 and control 2 for LV and aortic pressure, respectively. Consequently, we used the average of the 2 control states for further data analysis and labeled it as 'CTRL'.

Panel A of Fig. V-16 shows aortic pressure, LV pressure, and pump outlet flow generated by the CVS (60 BPM) in a control state, i.e., with the PUCA II in position but switched off. In panel B, the pump has been switched on in 1:1 mode at the same heart rate. Due to the counterpulsation, the systolic LV pressure is decreased and the aortic pressure is increased during diastole. When deflation timing is set correctly, the aortic pressure decreases again at the end of diastole, but it always remains at a higher level compared to the control state. This means that, as a consequence of the PUCA II pump, the LV reaches a higher pressure during the isovolumic contraction phase, but that pressure doesn't rise much more during the ejection phase because of pump aspiration. So, during the initial contraction phase the LV works against a higher afterload than normal, followed by a lower afterload that effectively unloads the ventricle. Also in Fig. V-16, panel C illustrates the acuteness of the unloading effect in 1:2 mode, where assisted beats alternate with unassisted beats. This results in a higher aortic pressure during the diastole of the assisted beats, in comparison with the diastolic aortic pressure in 1:1 mode. In the 1:2 mode there is also a significantly higher pulse pressure (135% of CTRL) generated at half the heart rate. This is in contrast with the 1:1 mode, where aortic pulse pressure is significantly lower compared to the control state (74% of CTRL). In both modes the pulse pressure

is inversely correlated to the heart rate. The unloading effect of the PUCA II is less pronounced in ventricles with a higher contractility. LV pressure is hardly reduced and the ‘bump’ in the diastolic aortic pressure is smaller, as shown in panel D.

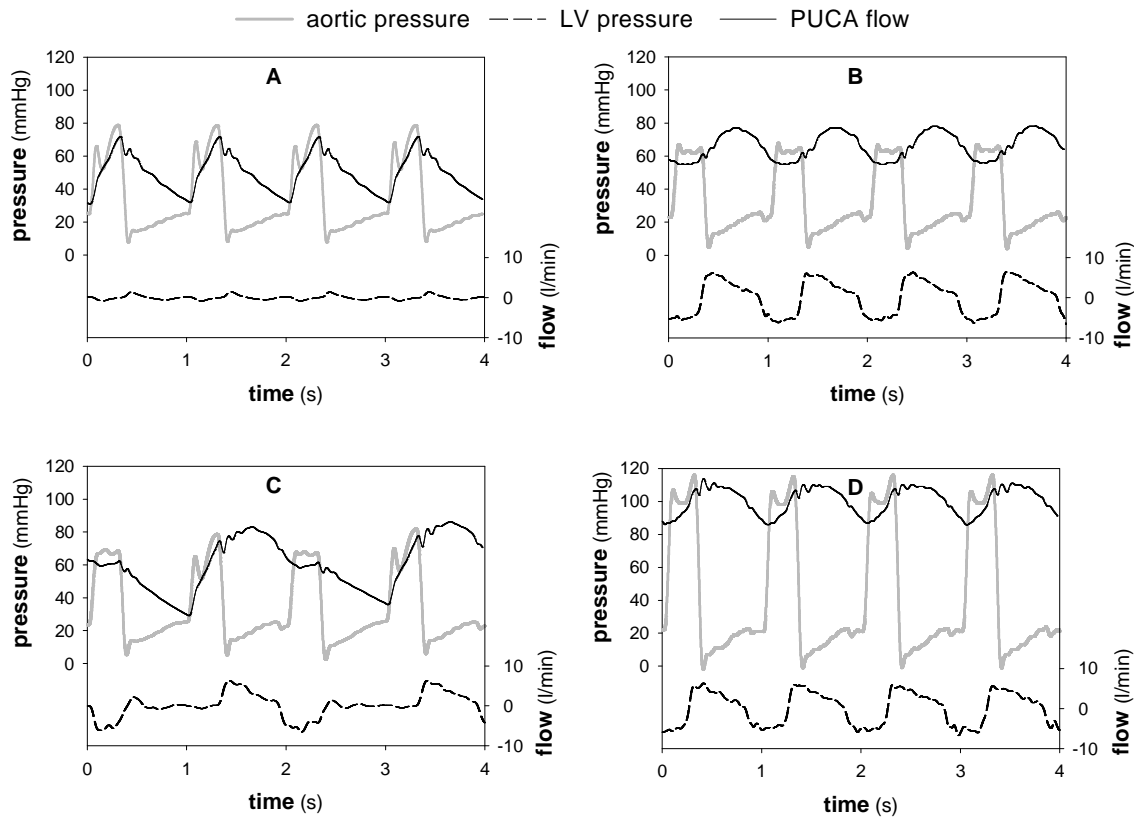


Fig. V-16: Data measured in the dynamic model. Panel A: low LV contractility and PUCA II switched off. Panel B: low contractility and PUCA II working in 1:1 mode. Panel C: low contractility and PUCA II working in 1:2 mode. Panel D: high contractility and PUCA II working in 1:1 mode.

It is obvious that mean aortic pressure and total flow are increased by the use of the PUCA II pump, and that this increase is most expressed in 1:1 mode. This can be derived from Fig. V-17 (middle panel), where the highest flow rise occurs at 120 BPM for 1:1 mode at low contractility (167% of CTRL). Fig. V-17 also clearly demonstrates that the level of contractility - rather than the pump settings - causes the main effect on flow and arterial pressure. There is a significant difference in MAP and mean flow obtained in the two pump modes compared to CTRL. There is, however, no significant difference between the 2 pump modes themselves. The heart rate also exerts little influence on both variables: a significant difference could only be detected between 60 and 120 BPM.

The bottom panel of Fig. V-17 shows the pump flow as indicated by PUCA II (Q_{puca}), i.e., the positive part of the membrane pump outlet flow. When considering the low contractility in 1:1 mode, Q_{puca} is higher than the total flow generated in the whole system (middle panel of Fig. V-17), which can only be explained by the presence of losses. This confirms that, as in the static model experiments, one needs to account for an efficiency factor lower than 100%. As described in the methods section, we used the efficiency as assessed in the static model to calculate the separate contributions of the heart and the PUCA II to total flow. The results are given in Fig. V-18 for 1:1 mode. For the low contractile ventricle, PUCA II contributes for approximately 80% to total flow, while for the high contractile ventricle its contribution becomes less than 50%. The contribution is also dependent on the pump rate.

6. Discussion

6.1. Static model

Due to the losses that appear at peak ejection and during pump aspiration, the indicated pump flow is an overestimation of the effective flow. Therefore, the introduction of an efficiency factor is justified to account for the losses over the valve. In analogy with cardiac valves, it can be assumed that the flow losses consist of 2 parts: the volume that is needed to tilt the valve and the leakage through the valve when it is in a certain position. The difference with cardiac valves is that the tilting valve of the PUCA II also shows losses during ejection: a certain volume slips by the opened valve and runs towards the tip of the catheter. The 'lost' volume needed to tilt the valve is in fact re-aspired from the aorta (in the beginning of the aspiration phase, during valve closure) or re-ejected in the LV (during valve opening).

The losses are clearly influenced by the pump rate, which determines the timing of the tilting behavior and the period of leakage. It can be expected that another determinant is the pressure level of preload and afterload, and the pressure generated in the pump, which is dependent of the feedback signal. These pressures determine the time varying pressure head over the valve, which, in turn, determines the leakage and the torque needed to tilt the valve. The combination of these determinants leads to higher losses and lower efficiency with PUCA II working at 60 BPM compared to the other pump rates. This discrepancy is not due to alterations in the setup because data was acquired for

all pump rates consecutively for a certain resistance setting, before switching to the next resistance setting.

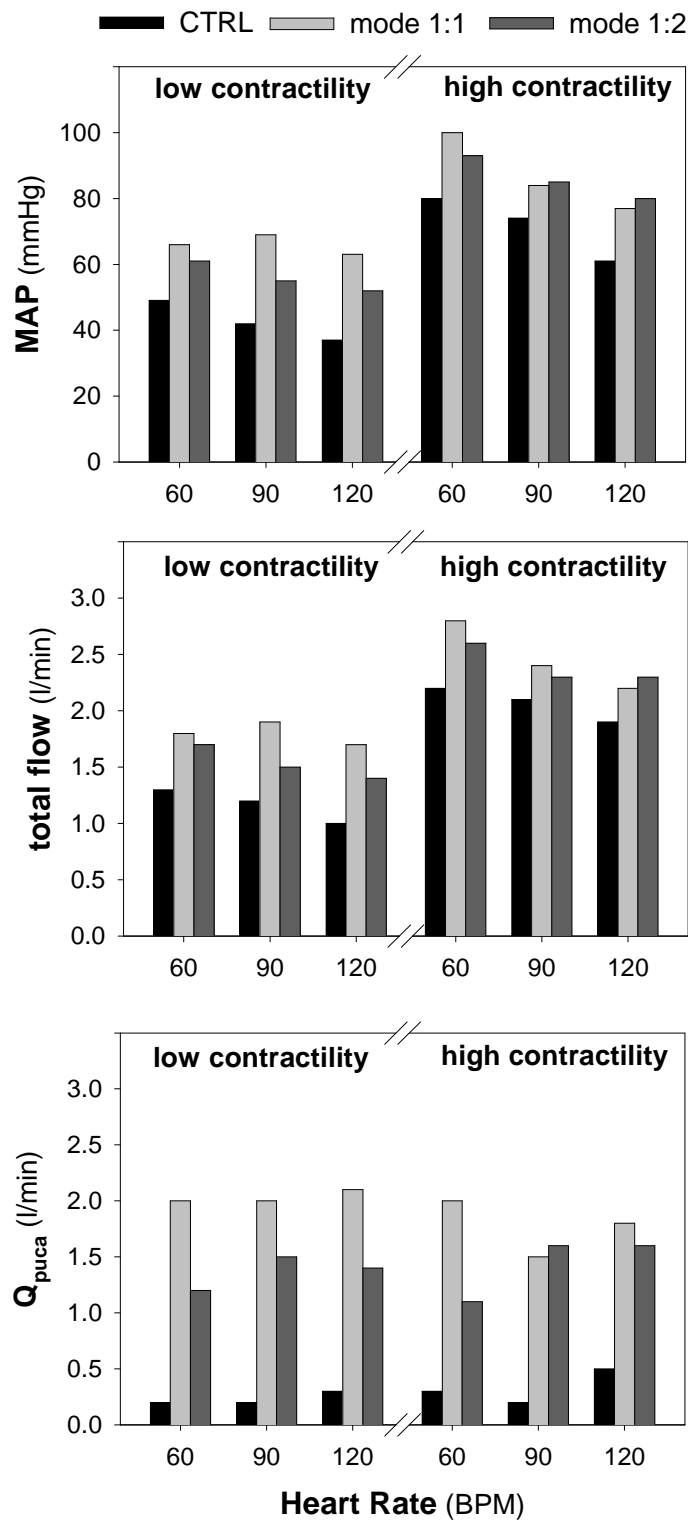


Fig. V-17: Summary of dynamic model results for mean arterial pressure (MAP), total flow and indicated pump flow (Q_{puca}). The data is bundled with respect to the different modes, heart rates and contractilities.

It is important to realize that the pressure and flow in the static model are solely generated by the PUCA II system itself, and therefore only a limited range of pressures and flows could be obtained. Consequently the pump graph is a characteristic of the system as such, without interactions or external influences. To obtain the pump graph, a wide range of resistances had to be set, part of them with unrealistically high values (max. total vascular resistance: 5.2 mmHg·s/ml). However, this is just a means to obtain different working points on the characteristic and this does not influence the characteristic in any way.

An important issue in the experimental setting is the viscosity of the test fluid. While we only reported the data measured with the water-glycerin mixture, we also performed tests with water as a test fluid. In these tests, generated flows were on average 30% higher than the ones reported here, the values being comparable to the values found in former tests performed at Groningen University ^[230]. In our experience, the 60/40 v/v% water-glycerin mixture is a good substitute for blood as a test fluid ^[187].

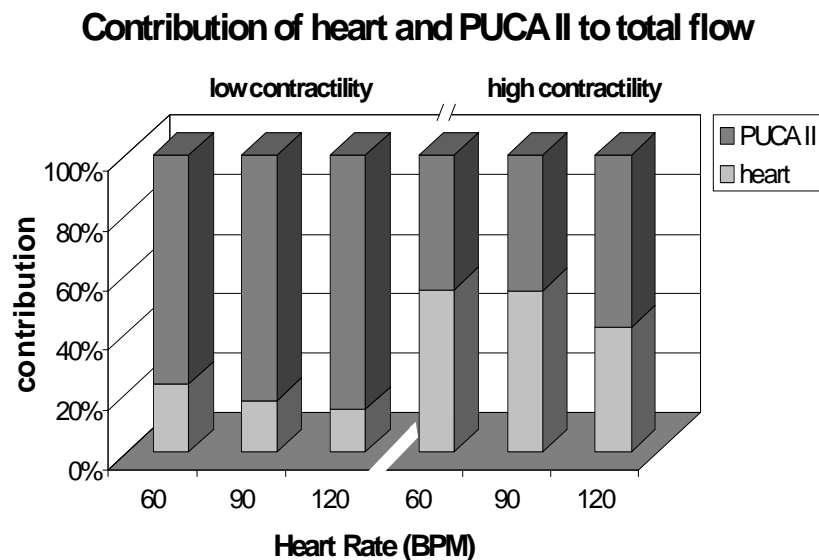


Fig. V-18: Relative contribution of the cardiac simulator (heart) and the PUCA II assist system (in 1:1 mode) to total flow.

6.2. Dynamic model

Our data clearly demonstrate the unloading effect of the PUCA II (Fig. V-16). The maximum LV pressure is reduced and the aortic pressure is increased during diastole, which should result in reduced LV wall stress and improved coronary

perfusion, respectively. The fact that the aortic pressure during isovolumic contraction is increased as a consequence of the assist system will result in a delayed opening of the aortic valve. A more aggressive pump aspiration should result in a faster pressure drop just before the contraction, normalizing the aortic valve behavior and further improving LV unloading. Fig. V-16 also reveals that the unloading is much more effective when an LV with low contractility is simulated. Apparently it is more difficult for the PUCA II to drag down higher LV pressures.

When the indicated pump flow (Q_{puca}) and the total flow (Q_{ao}) are compared (Fig. V-17), total flow is only slightly higher or sometimes even lower than indicated pump flow, indicating that an efficiency factor ($< 100\%$) has to be taken into account and that the indicated pump flow is an overestimation of the effective flow.

It can be questioned whether the efficiency obtained in the static model is valid for the dynamic model. Therefore, we performed extra measurements (at a fixed rate of 80 BPM which does not require an ECG feedback) in the static model and in the cardiovascular simulator, without actuating the LV (simulating heart block). In these conditions, total flow is generated solely by PUCA II and the efficiency can then be calculated as the ratio of total flow to indicated pump flow. When interpolated for MAP on the efficiency plot produced by the real static model, the difference between measured and interpolated efficiency was less than 1%. We acknowledge that this concerns only one data point, measured again under static preload conditions, but it suggests that the efficiency transfer from static to dynamic model is valid and that Fig. V-18 is a reasonable presentation of the contributions of heart and PUCA II to total flow.

Our data show only a moderate gain in total flow when the pump is switched on, and since there is only little difference between Q_{puca} and Q_{ao} , it suggests that the contribution of the heart decreases by assisting it. Further exploration of the data effectively revealed that the flow generated by the LV decreases when it is unloaded. This decrease seems sensitive to heart rate: at 60 BPM (high contractility), the assisted LV pumps approximately 67% of the CTRL flow, while at 120 BPM this contribution drops to 53%. This observation is analogous to findings in experiments with healthy animals where there was no augmentation of cardiac output due to LV assist^[202,203]. The pumping principle is probably the cause of this: blood is temporarily stored into an extracorporeal

chamber (the membrane pump) and inserted back into the cardiovascular system at another time in the heart cycle. The blood that goes to the membrane pump is in fact ‘stolen’ from the cardiac output. Meanwhile, a part of the pumping energy is wasted on transport of the blood from and to the pump, where inertia plays an important role because the flow direction in the thin catheter has to be reversed.

Data measured at control conditions (Fig. V-17, lower panel) show that there is flow when the pump is switched off. This is actually the result of the influence of the pumping LV on the pump membrane through the PUCA II catheter, which was also confirmed visually: the membrane moved synchronous with the pumping LV. It can also be seen in Fig. V-16 (panel A) that there is a small forward and backward PUCA flow in the control state. Since the positive part of this flow is presented in the plot of Fig. V-17, it appears as if the PUCA II was pumping, but the valve stayed closed and the actual net flow was 0 l/min.

We found that the impact of the assist system is most obvious in a ventricle with low contractility, although the contribution to a ventricle with high contractility is still substantial. A plausible explanation for the influence of the contractile state is the increased aortic pressure in the presence of a high contractile ventricle, which imposes a higher afterload on the PUCA II pump, compared to the low contractility situation. In the filling phase, the blood is possibly more ejected into the pump by the ventricle, while in a low contractile state it is sucked out of the ventricle by the pump. This contractile influence can probably be eliminated by the use of an IABP driver that can generate higher pressures, in order to obtain the maximal stroke volume under all physiological conditions.

6.3. Study limitations

This study makes use of *in vitro* models that mimic anatomical reality and simulate physiological processes. Due to the complexity of the human body, simplifications had to be implemented and we also faced inherent limitations of the setup’s construction. The construction of our static model setup, for instance, only allowed for a limited preload range between 10 and 40 mmHg, which is relatively low. In reality, the preload of the pump is left ventricular pressure, which averages (over the complete cardiac cycle) to approximately 40 mmHg. During ventricular ejection however, a preload pressure of 100 mmHg can easily be obtained, while during diastole the preload will tend more to 0 mmHg. It would be more realistic to have a varying preload, but then timing is a crucial

factor again, which complicates the assessment of pump characteristics. Therefore, we chose to use a constant preload pressure for the pump graph determination, since an additional evaluation of the PUCA II performance was accomplished in the dynamic model anyway. The effect that a higher constant preload pressure would have on the hydraulic performance is unclear. On one hand, it improves filling of the membrane pump, but on the other hand, it alters the tilting behavior and the leakage of the valve.

The pulse duplicator's unphysiological response to heart rate changes is a known limitation of the dynamic model which is due to the inertia of the actuating system. The middle panel of Fig. V-17 shows how the control cardiac output decreases when the heart rate is increased. This gives the false impression that the effect of the PUCA II pump is hardly influenced by the pump rate when working in combination with a pumping ventricle, which is in contrast to the static model data. The middle panel of Fig. V-17 also reveals that the total flow during control conditions was rather low (below 2.5 l/min), indicating that the peripheral resistance in the model (calculated retrospectively to be 2.1 mmHg·s/ml) may have been too high, potentially limiting the clinical relevancy of our observations. We believe that this is not the case, and this for two reasons. Firstly, LVAD's are used in patients with poor cardiac performance. Cardiac output, measured in the clinical setting, may indeed be this low^[232,233], especially in patients with severe heart failure, where Linde et al. reported average CO values of 1.9 l/min^[233]. As such, the simulations labeled as 'high contractility' do reflect (severe) patho-physiological flow conditions. Secondly, although the absolute flow level is of importance, we have demonstrated in the static model experiments that the efficiency of the PUCA pump is determined by the variation in time of the pressure head over the tilting valve (determined by the heart rate and pressure level). From this perspective, the 'low' contractility state with sub-normal blood pressures are representative for the PUCA-pump operating under patho-physiological pressure conditions, while the 'high' contractility state is representative for the PUCA-pump performance under normal pressure conditions. The lower the afterload (arterial pressure levels as one can expect in patients with cardiogenic shock), the higher the efficacy of the PUCA II, and the higher the effectively ejected blood volume will be. Nevertheless, the high relative contribution of PUCA II to total flow in the low contractility setting as

depicted in Fig. V-18, should be interpreted with care, taking into account the low basal flow level during these conditions.

7. Conclusion

We evaluated the pump performance of the PUCA II intra-arterial LVAD in combination with an Arrow AutoCat driver. Pump characteristics and efficiency were first measured in a static mock circulation, after which the PUCA II was tested in a pulsatile cardiovascular simulator. We conclude that the used driver-pump-catheter combination is most effective for the combination of relatively high heart rates and low residual contractility. The low contractility yielded the best ventricular unloading and diastolic aortic pressure augmentation. We expect that the performance of the system can be further improved by the use of a more powerful driver and by reduction of the valve leakage.

8. Acknowledgements

The authors wish to express their gratitude to Alain Storms and Hans Josemans for their advice on the AutoCat driver and to Ilse Van Tricht for patiently managing the overflow system. They also thank professor Brouwer and dr. Verkroost of the Department of Thoracic Surgery, University Hospital Nijmegen for reviewing the manuscript.

This research was funded by a specialization grant of the Institute for the Promotion of Science and Technology in Flanders (IWT-993171, S. Vandenberghe) and by a post-doctoral fellowship from the Fund for Scientific Research – Flanders (FWO Vlaanderen, P. Segers).

E. IN VITRO ASSESSMENT OF THE UNLOADING AND PERFUSION CAPACITIES OF THE PUCA II AND THE IABP[†]

1. Abstract

The PUCA II pump is a minimally invasive intra-arterial left ventricular assist device that can be used as an alternative for the intra-aortic balloon pump (IABP). In this study, we assessed the cardiac unloading and organ perfusion capacities of both PUCA II and IABP in an *in vitro* setup, consisting of a heart simulator and a silicone arterial tree, mimicking anatomical geometry and flow distribution. The IABP was positioned in the descending aorta, while the PUCA II was tested both in ‘trans-aortic’ and ‘abdominal’ position. All devices were driven by the same Arrow AutoCat IABP driver at different pump rates. Apart from flow, arterial pressure, and pulse pressure, we also calculated hemodynamic indices for myocardial oxygen supply and demand.

The ‘abdominal’ PUCA II assist and the IABP both provide mild unloading of the heart, and a limited improvement of arterial pressure and flow. The ‘trans-aortic’ PUCA II assist greatly enhances flow and pressure, but does not unload the heart properly in the tested configuration.

2. Introduction

Patients suffering from progressive cardiac failure are often supported with an intra-aortic balloon pump (IABP) when the disease comes to an end-stage. The IABP is a counterpulsation device that was first used by Kantrowitz^[227] and is already in use for three decades to stabilize heart failure patients, or for the treatment of acute cardiac failure. The pump is used for short-term or medium-term application and its main advantage is the fast, minimal invasive insertion

[†] The contents of this section was published in *Perfusion* 2004;19:25-32

***In vitro* assessment of the unloading and perfusion capacities
of the PUCA II and the IABP**

Vandenberghhe S, Segers P, Josemans H, Van Loon JP, Rakhorst G, Verdonck P

that can be done in a cathlab, or even by trained ER staff. The pulsatile catheter (PUCA) pump is a device that combines the counterpulsation principles of the IABP with an actual blood pump. The newest version of this device (PUCA II) consists of a thin-walled catheter with one single tilting valve incorporated into the catheter wall. The catheter can be introduced transarterially and shifted retrograde into the aorta or the left ventricle. The catheter is connected to a custom-made membrane pump which can be actuated by most commercially available IABP drivers and drivers for pneumatic cardiac assist devices.

Both the IABP and the PUCA II are expected to support the patient's heart by increasing the blood flow, unloading the myocardium and improving end-organ and coronary perfusion. We used an *in vitro* setup to assess these characteristics from a commercially available IABP and from the PUCA II. The latter was placed both in the normal trans-aortic position (designated 'aortic') where it runs through the aortic valve in the left ventricle, and in an 'abdominal' position where it's main benefit is expected to be an increase in abdominal organ perfusion.

3. Materials

3.1. *In vitro* setup

The *in vitro* model is composed of a pulse duplicator system and a silicone rubber arterial tree, simulating the systemic circulation ^[136] (see Fig. V-19). The pulse duplicator consists of two silicone sacs, representing the left atrium and ventricle, actuated by a computer controlled pneumatic driver to obtain physiological intraventricular pressures. A bileaflet and a bovine pericard valve are used as mitral and aortic valve, respectively. The elastic arterial tree consists of a tapered aorta with eight branches representing the main arteries to the head, the arms, the abdominal organs and the legs, on both left and right side. Arterial dimensions are derived from literature as to mimic a 1.8 m tall male weighing 85 kg ^[138]. The arteries in the abdominal region were bundled and simply represented by equivalent renal arteries, whose cross sectional areas were adapted accordingly. Each branch ends in a resistor with a compressible foam and a venous overflow system that allows volumetric measurement of the mean flow through every branch. The test fluid, a 60/40 v/v% water-glycerin mixture (kinematic viscosity: 3.7 mm²/s, density 1093 kg/m³), was channeled from the overflow system to a collector, where it was pumped up again into a preload

reservoir that mimics the lungs. The flow distribution over the entire model was set according to literature values ^[234], where the major portion of the flow (>50%) goes to the abdominal region in patients at rest.

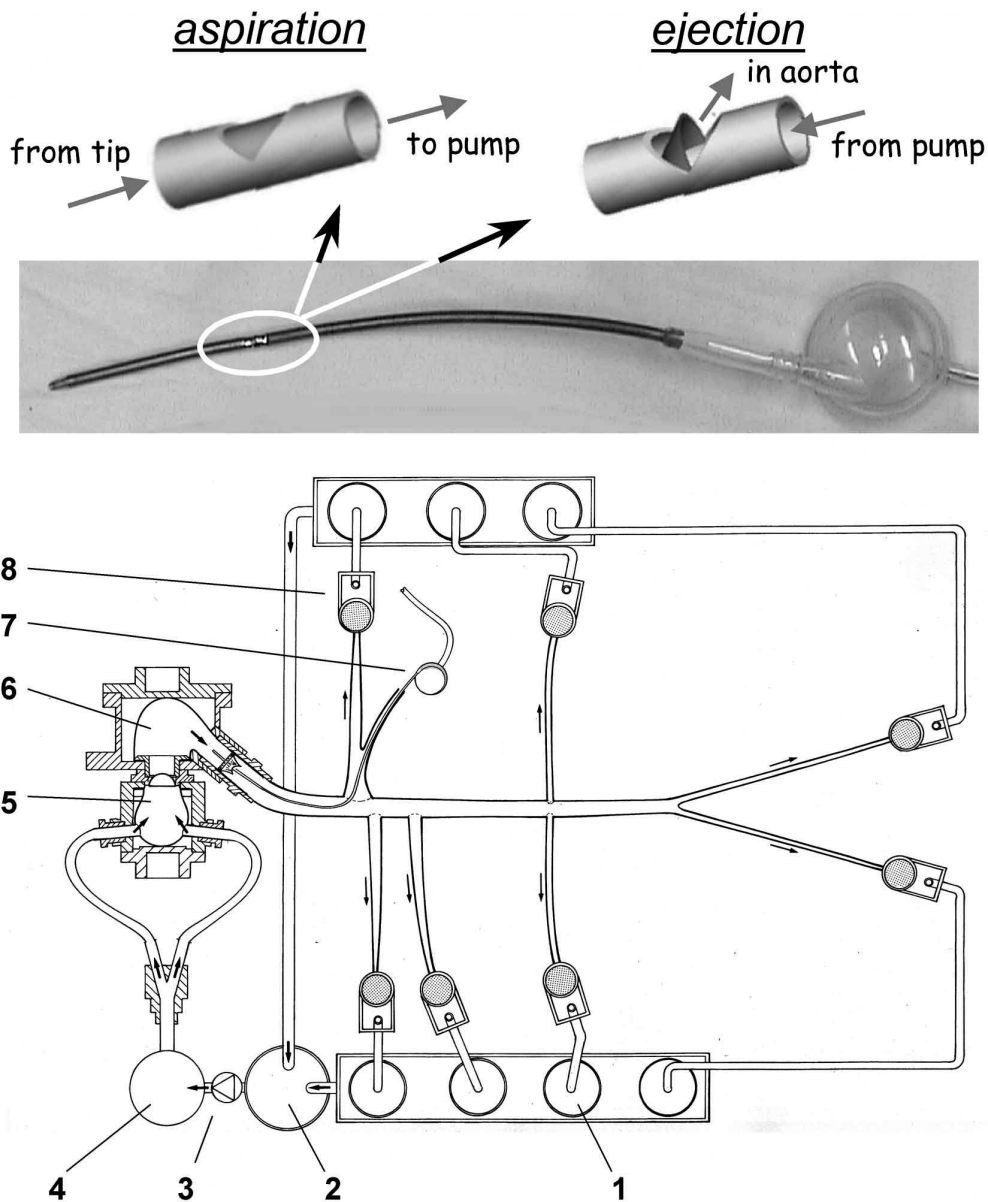


Fig. V-19: Top: picture of the PUCA II catheter and membrane pump and a detailed drawing of the tilting valve. Bottom: overview of the model setup. 1. collection container, 2. buffer reservoir, 3. centrifugal pump, 4. lung reservoir with weir, 5. left atrium, 6. left ventricle, 7. PUCA II catheter and membrane pump in trans-aortic position, 8. variable resistor combined with an overflow reservoir.

3.2. PUCA II and Intra-Aortic Balloon Pump

The PUCA-II catheter (Intra-Vasc.NL b.v., Groningen, The Netherlands) consists of a 28 cm long 21 Fr reinforced polyurethane shaft that incorporates a stainless steel inflow cage at the tip and an outflow valve located 10 cm distally ^[218,230].

The catheter is connected to a pneumatically driven, single-port, valveless membrane pump with a stroke volume of 40 ml that is placed paracorporeally. The catheter's tilting valve is designed specifically for the trans-aortic position, as to direct blood flow from the left ventricle (LV) to the membrane pump during the aspiration phase, and to direct the blood into the aorta during pump ejection.

3.2.1. Trans-aortic position (PUCAao)

The PUCA II catheter was introduced in the right subclavian artery and positioned through the aortic valve using the standard technique with a guiding pressure catheter^[235]. To seal the setup, the subclavian artery was tied up around the PUCA II and thus occluded one of the eight branches.

3.2.2. Abdominal position (PUCAabd)

To simulate the use of the PUCA II as an organ perfusion pump, the same catheter was introduced through the left femoral artery and shifted retrograde until the valve was positioned at the bifurcation site of the renal arteries. In this position, the femoral artery was occluded.

3.2.3. Intra-aortic balloon setup (IABP)

An 8 French Narrowflex Intra-aortic balloon catheter (Arrow Int., Reading, PA) was inserted via the left femoral artery for the IABP experiment. The balloon (40 ml stroke volume, 26 cm length and 15 mm inflated diameter) was positioned in the descending aorta and the femoral artery was occluded for sealing purposes.

3.3. Measurements

Both the intra-aortic balloon and the PUCA II were driven by an AutoCat IABP driver (Arrow Int., Reading, PA). The required ECG feedback for the driver was provided by the computer control of the pulse duplicator. All experiments were performed with the AutoCat driver set to 'operator' mode, while an experienced IABP operator adjusted the inflation and deflation timing to obtain optimal counterpulsation with the devices in a 1:1 mode. All three devices (PUCAao, PUCAabd, IABP) were tested with the cardiac simulator running at two levels of ventricular contractility (low and high) at three heart rates (60, 90, and 120 BPM). The pressure level of the pneumatic controller of the pulse duplicator was adjusted to obtain the different contractility levels, i.e., systolic aortic pressure of 70 mmHg (low contractility) and 120 mmHg (high contractility) during control conditions (no support). As such, six different hemodynamic conditions were

obtained for each device, resulting in a total of 18 runs (3 devices, 2 contractilities, 3 heart rates). Because our simulator is not subject to biovariability, no measurements were repeated. Instead we performed control measurements (CTRL) with the device shut off at the beginning and end of each run and compared these to assess the stability of our *in vitro* setup. Consequently each run consisted of the following three steps: CTRL, pumping in 1:1 mode, CTRL. For each step, pressure data were sampled at 200 Hz and captured for at least 5 seconds when a steady state condition was present. Pressure was measured in the LV (P_{LV}) with a pigtail catheter and a DTX+ pressure transducer (BD, Franklin Lakes, NJ) and in the ascending aorta (P_{ao}) with a Millar high-fidelity transducer (Millar Instruments Inc., Houston, TX). Flow distribution over the model (Fig. V-20) was measured with the overflow system. Total mean flow was calculated by summation of mean regional flows.

To assess cardiac unloading and perfusion capacities of the assist devices, cardiac oxygen demand and supply were estimated from the LV and aortic pressure curves ^[236,237]. The tension time index (TTI) is a marker for oxygen demand, and is calculated as the area under the LV pressure curve during systolic ejection, multiplied by the heart rate (HR) to express it per minute. The diastolic time index (DTI) is a measure of perfusion or oxygen supply and is defined as the area under the aortic pressure curve during diastole, also multiplied by HR.

$$TTI = \int_{\text{systole}} P_{LV} dt \cdot HR \quad (\text{mmHg}\cdot\text{s}/\text{min}) \quad [\text{Eq. V-2}]$$

$$DTI = \int_{\text{diastole}} P_{ao} dt \cdot HR \quad (\text{mmHg}\cdot\text{s}/\text{min}) \quad [\text{Eq. V-3}]$$

4. Results

The variability in the flow distribution appeared to be small. The control values at the beginning and end of each run were compared for LV and aortic pressure. The maximum differences found were 3% and 5% of the average, respectively. This demonstrates the stability of the setup and allowed to use the average of the control measurements for each run for further processing.

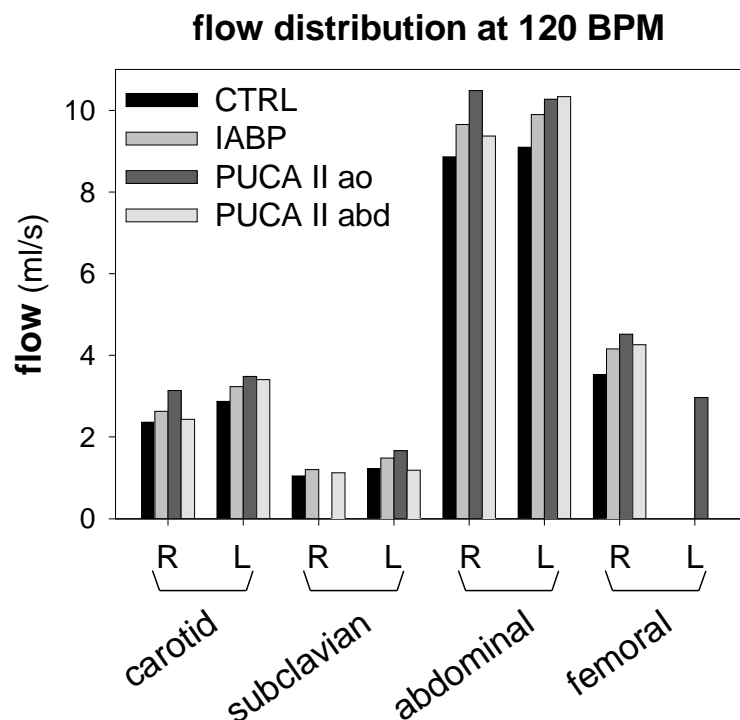


Fig. V-20: Flow distribution over the 8 arterial branches when applying the different devices. The CTRL set is taken from the IABP experiment. All these data were captured at a heart rate of 120 BPM and the high contractility setting. ao = aortic, abd = abdominal, R = right, L = left.

The flow distribution over the whole arterial tree and the influence of the different devices is given in Fig. V-20 for the high contractility condition and a HR of 120 BPM, with the CTRL data taken from the IABP experiment. IABP increases total flow, but the largest effect is obtained with the PUCA II in trans-aortic position (PUCAao).

The effect of IABP or PUCA II support on ventricular and aortic pressure is demonstrated in Fig. V-21, where cardiac cycle samples are shown for the three different heart rates during the low contractility condition. Data indicated as CTRL (panel A) are again taken from the IABP experiment (with the pump off).

Aortic pressure in the IABP experiment shows a high diastolic peak, being the result of a steep pressure rise and fall at the beginning and the end of diastole, respectively. This sudden pressure decrease at end-diastole leads to a very low aortic (afterload) pressure at the onset of ejection. Aortic pressure behaves similar in the PUCAabd experiment, except that the obtained pressure peak is lower and the rise and fall of diastolic pressure is less steep. In contrast, PUCAao data display only a slight bump in diastolic aortic pressure (Fig. V-21, panel C). This is the result of a much slower pressure rise and fall, leading to an elevated end-diastolic pressure. The shape of the LV pressure waveform is not altered by the IABP, but it is shifted to a lower level compared to CTRL, similar to what happens with the PUCA II in abdominal position. In the PUCAao experiment, however, LV pressure has a flattened waveform, keeping the pressure constant throughout systole.

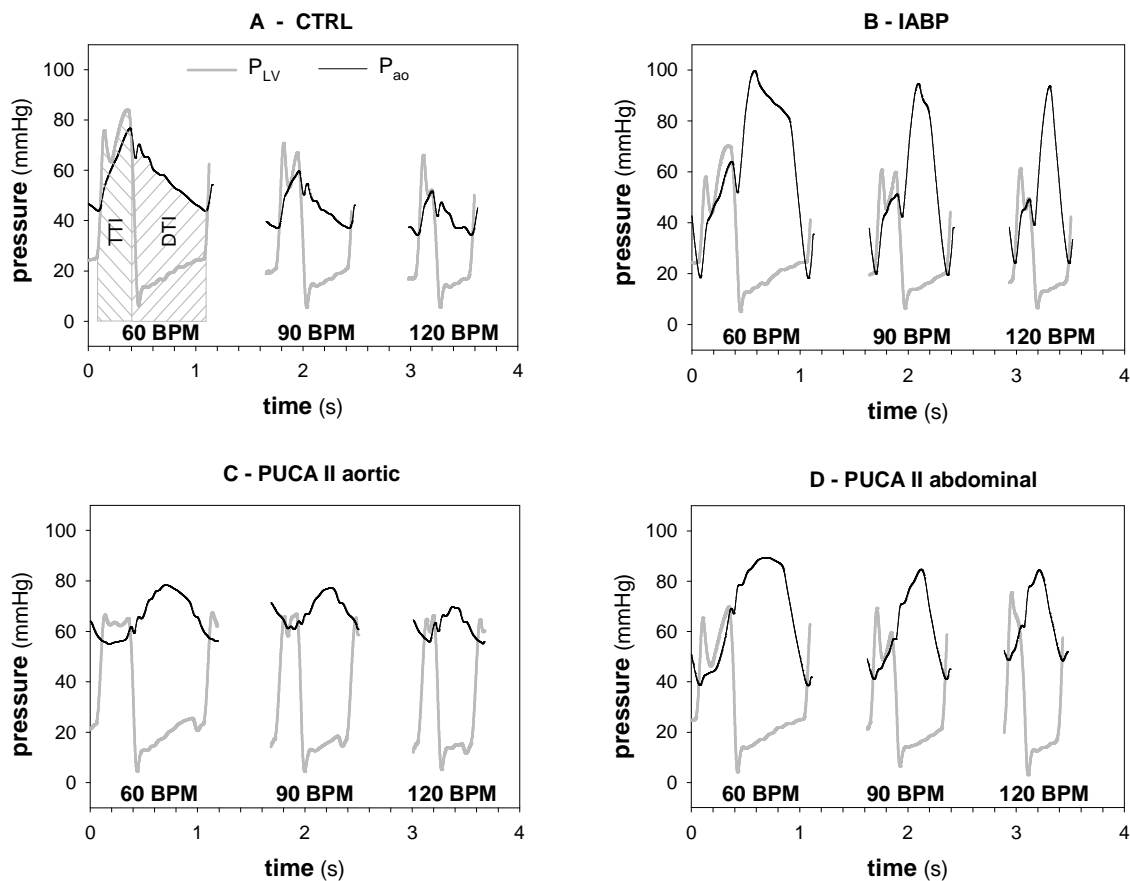


Fig. V-21: Raw aortic (black) and left ventricular (gray) pressure data from the different experiments. The data shown was captured at the low contractility setting, at different heart rates (60, 90, and 120 BPM). The CTRL data are taken from the IABP experiment. In the CTRL panel is illustrated how TTI ($\sim O_2$ demand) and DTI ($\sim O_2$ supply) are calculated.

The pressure increase in diastole results in an elevated MAP. In Fig. V-22 (panel B), this is presented as the change in MAP compared to the CTRL value (which was obtained in the same test series), thus allowing to judge the effect of switching the pump on. There is a very high increase in MAP by use of the PUCA II in the trans-aortic position (range 20 mmHg) and a moderate increase by using it abdominally or by the IABP (about 10 mmHg). The pressure rise seems to depend on the level of contractility, where all devices have more difficulties to further increase the pressure in the presence of a high contractile LV (averaging all control measurements, MAP is 49 ± 7 mmHg for the low contractility versus 74 ± 8 mmHg for the high contractility experiments, $P < 0.05$). Panel A of Fig. V-22 leads to similar conclusions for the total flow: PUCAao provides the highest increase in total flow, which is again most outspoken in the low contractility experiments where flow levels are lower than in the higher contractility setting (averaged CTRL flow is 1.3 ± 0.15 and 2.0 ± 0.17 l/min in the low and high contractility conditions, respectively; $P < 0.05$). Note that the IABP and PUCAabd also seem to demonstrate a contractility dependency for the flow.

PUCA II in the trans-aortic position yields higher DTI (~ oxygen supply) values than PUCAabd or the IABP, as shown in Fig. V-22 (panel C). The data are presented relative to their respective CTRL values and show that using the PUCA II in a low contractile ventricle at high heart rates can almost double the oxygen supply (98% increase). The tension time index (TTI) is an indication of how well the ventricle is unloaded; a decreased TTI results from reduced LV pressure and/or shorter exposure of the myocardium to high pressure, resulting in decreased wall stress and oxygen consumption. Our results (Fig. V-22, panel D) indicate that IABP and the abdominally placed PUCA II reduce the oxygen demand of the LV, while on the contrary, PUCA II in trans-aortic position slightly increases the demand, thus loading the ventricle. Especially at 120 BPM there is a noteworthy increase in TTI of 25.5% under low contractility conditions. The influence of contractility (more modest changes in high contractility conditions) on DTI and TTI can be appreciated from Fig. V-22.

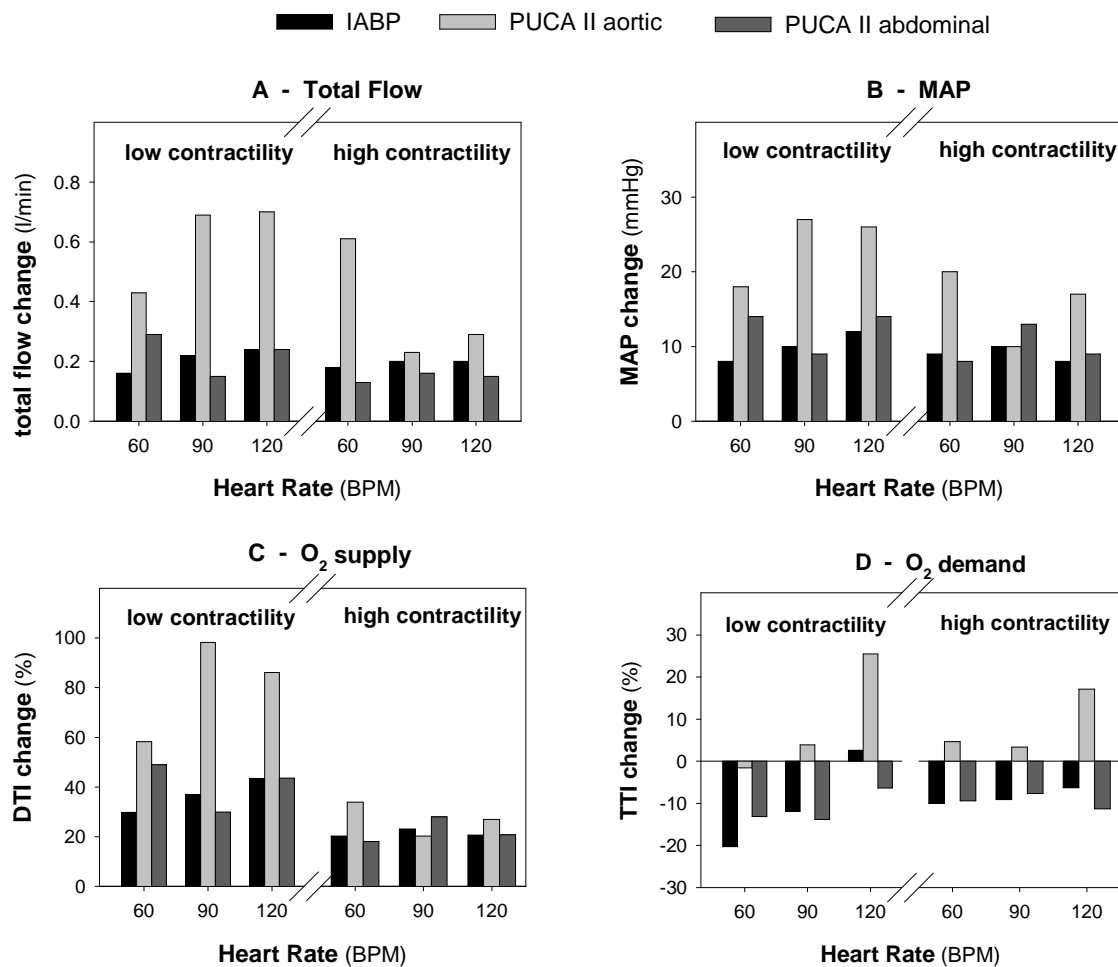


Fig. V-22: Effect of the devices on total flow, mean arterial pressure (MAP), diastolic time index (DTI), and tension time index (TTI). The results are expressed for all the tested heart rates and contractilities. The top panels display for each experiment the difference between the respective CTRL value and the value obtained during assist, thereby illustrating the changes that occur by switching on a device. For the bottom panels, these differences are expressed relative to the CTRL value.

To characterize the effect of the devices on aortic pressure, we also calculated the changes induced by the different devices in end-diastolic pressure (Fig. V-23, top panel) and pulse pressure (bottom panel). The use of the PUCA II in the trans-aortic position results in a large increase in end-diastolic aortic pressure, while the IABP is capable of dragging this pressure down. The opposite is seen in the pulse pressure, that is reduced by the PUCAao and increased by the IABP and (to a lesser extent) PUCAabd. The pulse pressure is in some cases even doubled by IABP application (highest increase = 217%), which is in accordance with the raw data from Fig. V-21. Again, the induced changes are less pronounced in the high than in the low contractility conditions (Fig. V-23).

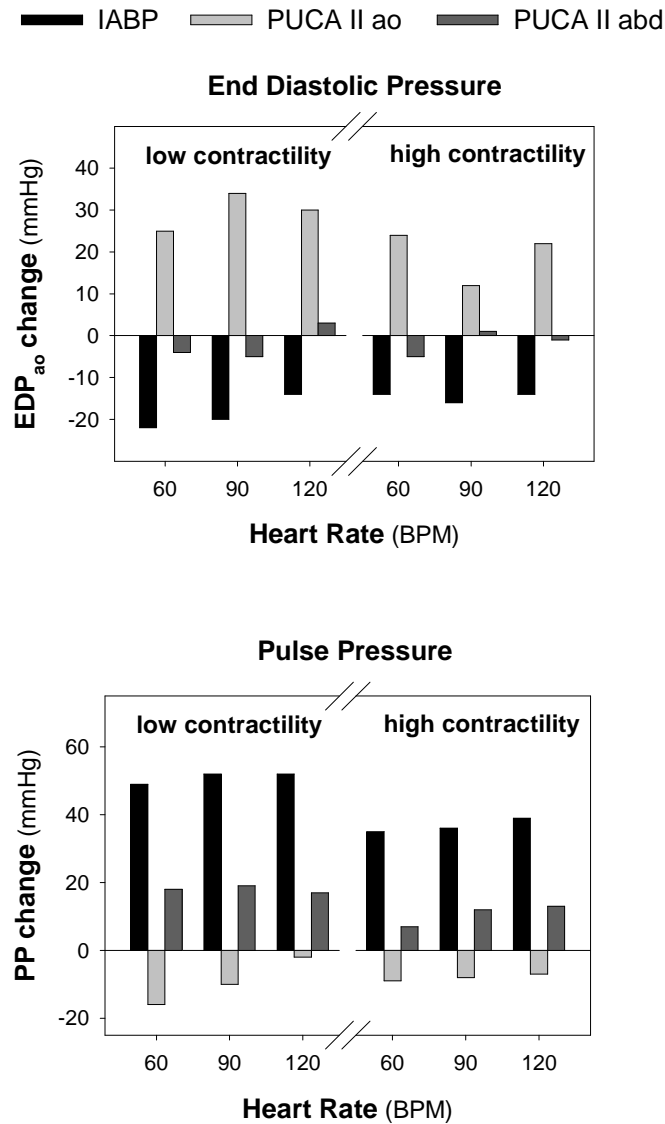


Fig. V-23: End-diastolic pressure changes and pulse pressure changes obtained in the different experiments, for all the tested heart rates and contractilities.

5. Discussion

Overall, our results show that the PUCA II pump, when used in the abdominal position, yields similar hemodynamic effects as obtained with a standard intra-aortic balloon pump. Both assist methods increase mean systemic arterial pressure and flow to the same extent, and their impact on oxygen supply (approximated by DTI) and oxygen demand (TTI) is also comparable. This is not surprising, since in se, they use the same principle of aortic counterpulsation to augment coronary perfusion and flow: a certain volume is injected in the aorta during diastole and retrieved again during systole. The major difference is that the IABP displaces gas (helium) while the PUCA II pumps blood, which results

in larger inertial forces. This can be noticed in the raw data of Fig. V-21, where the pressure rise and fall are less steep in the PUCAabd experiment, compared to the IABP. Consequently, the IABP is capable of increasing the pressure more rapidly during diastole, and decreasing it quickly again at the end of diastole, before the contraction starts. The PUCAabd shows little effect on end-diastolic pressure.

When PUCA II is used in the trans-aortic position, it performs better as an assist device in terms of displaced blood volume, but it augments the end-diastolic pressure, thereby increasing the load on the heart as quantified by TTI. It has been shown that increased end-diastolic pressure causes a later opening of the aortic valve, at a higher intraventricular pressure, resulting in increased stroke work of the ventricle ^[238]. This incapability of dragging down the end-diastolic pressure has the advantage that the increase in DTI is much higher, which should have favorable effects on coronary perfusion. Although the diastolic pressure peak is not very high in the PUCAao experiment, the pressure stays high throughout the whole diastole as well as during systole. For PUCAabd and IABP, the diastolic peak pressure is high, but pressure varies much more over the diastolic period, and is gradually built up in systole, starting from a low end-diastolic pressure. Consequently, the MAP is highest in the PUCAao experiment, and since total vascular resistance stays constant in the *in vitro* setup, the gain in total flow is highest for the PUCA II in trans-aortic position.

In terms of hemodynamic performance, there is clearly a difference between IABP and PUCAabd on one hand, and PUCAao on the other. These differences originate from the fact that with PUCA II in trans-aortic position, blood is aspirated from the left ventricle, while IABP and PUCAabd work directly in the aorta, allowing a fast pressure drop there. The advantage of PUCAao is that it actually moves blood from the left ventricle to the aorta instead of just displacing it in and out of the aorta. Therefore the PUCAao actually pumps along with the natural circulation, thus more drastically increasing the flow and the mean arterial pressure. It can also be observed from the pressure waveforms in Fig. V-21 that LV pressure is nearly constant throughout systole in the PUCAao experiment. In this setting, PUCA II does not decrease the LV pressure more than IABP or PUCAabd, but it smears out the waveform more equally over the systole. Consequently, applying PUCA II directly in the LV does not unload the ventricle as one might anticipate, which was already indicated by the increase in

TTI. We hypothesize that the suction pressure in the membrane pump is not high enough for optimal assist, since the blood instigates substantial inertia that has to be overcome.

An important issue with the trans-aortic application of the PUCA II is the transvalvular position of the catheter, which may augment valvular regurgitation of valves that are often stenotic in the clinical setting. Although the placement itself is relatively simple ^[235], it also results in an obstruction of the ejection of the LV, which may also explain the lack of unloading. In addition, in previous experiments ^[239], we have calculated that the tilting valve of the PUCA II catheter directs approximately 80% of the membrane pump output into the aorta (80% efficiency), meaning that a small amount of blood is returned to the left ventricle during cardiac diastole. This observation, together with valvular regurgitation, contributes to the fact that the diastolic aortic pressure does not peak as high in the PUCAo experiment as in the other experiments.

While the correct functioning of PUCA II in transaortic position requires the tilting valve, this is not a necessity when it is used abdominally. The only argument in favor, besides manufacturing standardization, is that the flow could be directed more organ-specific by placing the tilting valve at a targeted arterial bifurcation. This effect, however, was not observed in the measured flow distributions (Fig. V-20), where we were not able to detect any specific abdominal gain.

6. Study limitations

This study reports the hemodynamic impact of three different cardiac assist methods, all counterpulsation based. Since it is an *in vitro* study, important biological and physiological feedback mechanisms are neglected, thus only the pure mechanical effects are visible. This means that the changes in MAP are probably overestimations of the real clinical situation, where an increase in MAP, if unphysiological, will be countered by a decrease in vascular resistance and consequently a higher increase in flow.

We quantified the unloading capacities using TTI and DTI. Although these indices do not give an absolute indication of the oxygen consumption or supply, we believe that they at least allow to indicate which of the tested devices and in which mode will have the highest impact on oxygen demand and supply.

Our pulse duplicator shows an unphysiological heart rate dependency, where increases in heart rate result in decreased ventricular pressure and stroke volume. Also, the flow levels in our study are rather low, mainly because of a rather high systemic vascular resistance. However, comparable low flows (<2 l/min) have also been reported clinically ^[233]. Moreover, we have found previously that it is mainly the pressure level and pressure gradient over the catheter that determines the performance of the PUCA II, rather than the absolute flow levels in the model ^[239]. The observed differences in IABP and PUCA II performance between the low and high contractility conditions, reported in this study, are therefore the consequence of the different pressure levels at which the model operates and that the devices undergo.

7. Conclusion

We compared the hemodynamic effect of an intra-aortic balloon pump with a PUCA II pulsatile catheter that was used both in a trans-aortic and abdominal position. We found that the latter application has no directly measurable hemodynamic advantage over the traditional IABP, when both devices use the same driver. When the PUCA II is used in trans-aortic position, however, it yields an important augmentation of flow and arterial pressure, and thus possibly coronary perfusion. The disadvantage of this application is that it does not unload the heart in terms of tension time index. Further studies, using a specifically designed and more powerful pneumatic driver, are needed to resolve this shortcoming.

8. Acknowledgements

The authors wish to express their gratitude to Alain Storms for his assistance with the AutoCat driver and to Ilse Van Tricht for patiently managing the overflow system. They are also grateful to Marcel Antheunis and Martin Van Daele for their technical assistance. This research was funded by a specialization grant of the Institute for the Promotion of Science and Technology in Flanders (IWT-993171, S. Vandenberghe) and by a post-doctoral fellowship from the Fund for Scientific Research – Flanders (FWO Vlaanderen, P. Segers).

CHAPTER VI

Conclusions

A. SUMMARY OF THE ROTARY BLOOD PUMP STUDIES

1. Introduction

This section summarizes the results found in chapter IV and compares the different models that were applied. The discrepancies and agreements between the models are discussed to give an idea of the validity of the different models and the conclusions drawn from the performed studies. The three models used are the mathematical model, the *in vitro* model with the heart simulator as dynamic preload, and sheep as an *in vivo* model.

The studies performed with the models focus on three fields: failure of a rotary blood pump, unloading with a rotary blood pump at constant rotational speed, and unloading with a modulated (sinusoidal) rotational speed. The latter study was not performed *in vivo*, and the discussion of pump failure *in vivo* is based on work by Nishida et al. ^[179].

An *in vivo* model is obviously the most realistic since it incorporates the whole circulatory system and all the control mechanisms, whereas the other models neglect the pulmonary circulation and neurohumoral control. Discrepancies between the models can also be due to the use of two different pumps: the Deltastream pump used in the *in vitro* model is more powerful than the microdiagonal pump that was applied in the other models. Further, the *in vitro* model simulated human flow levels, while the other models simulated sheep.

It can be questioned how well the sheep data relate to patient data, but the overall goal of these studies was to gain insight in the heart-device interaction and not to predict specific situations and outcomes. After all, the large variety in patient conditions and ventricular assist devices used in clinical practice only allows to draw general conclusions, which are valid for all rotary blood pumps.

2. Pump failure

The fear of sudden failure of a rotary blood pump is based on the valveless design that may lead to regurgitation (backflow) through the pump and subsequent overloading of the left ventricle (LV) and decreased cardiac output.

Nishida et al. analyzed hemodynamic data of healthy sheep and sheep with chronic heart failure (microsphere injection) at baseline (BL; without an assist device) and after 15 minutes of pump failure (PF). The simulation of this study with a mathematical model yielded good agreement, especially at BL. It was found from both models that subjects with heart failure are more sensitive to pump failure, and these subjects distinguish themselves from healthy subjects with a significantly higher end-diastolic volume (EDV) and a significantly lower mean arterial pressure (MAP). Heart failure subjects further demonstrate a lower total systemic flow (Q_{tot}) and pressure volume area (PVA) and higher LV wall stress compared to healthy subjects. The simulated heart failure, however, is relatively mild compared to the heart failure observed in critically ill patients. Animal models simply can not survive the drastic hemodynamic conditions that can be found in the clinical setting.

Both studies demonstrate how sudden pump failure leads to a significant increase in LV stroke volume (SV) and aortic flow (Q_{ao}), as shown in Table VI-1. Also the PVA and EDV increased, but this was only significant in the *in vivo* model. The mathematical model further indicated an increase in LV wall stress (stress time integral, STI). However, Q_{tot} and MAP remained constant in spite of the pump failure, and it was concluded from both models that an acute life-threatening situation did not occur in the healthy nor in the heart failure group.

If the *in vitro* simulations with a baseline systolic pressure level of 120 mmHg are considered healthy and the pressure level of 80 mmHg considered as heart failure, then the latter category distinguishes itself by a slightly lower EDV and SV and thus a lower total flow. A much lower MAP and PVA are also present and therefore all these parameters agree with the *in vivo* and mathematical difference between healthy and heart failure subjects, apart from the EDV. In a biological heart, dilatation due to heart failure is the consequence of a remodeling process on cellular level that changes the composition of the myocardium. This can not be simulated *in vitro* and the observed LV volume changes are merely

the result of the passive elastic properties of the rubber ventricle and the governing pressures, and are therefore very limited.

Table VI-1: Comparison of baseline (BL) and pump failure (PF) in the three available models.

	MATH MODEL	<i>IN VITRO</i>	<i>IN VIVO</i>
	PF vs. BL	PF vs. BL	PF vs. BL
Q_{ao}	>*	>	>*
Q_{tot}	=	=	=
MAP	=	<	=
EDV	>	>	>*
SV	>*	>	>*
PVA	>	<	>*
STI	>*	n.a.	n.a.

* statistically significant with $p < 0.05$

n.a.: not available

No repeated measures were performed in the *in vitro* model.

In vivo relations derived from Nishida et al. ^[179].

Parameter abbreviations are defined in the text.

The effect of pump failure was established *in vitro* by an increase in SV, EDV, and aortic flow while total flow is preserved, all in accordance with the other model data. In contrast with the other models, the *in vitro* model predicts a strong decrease in MAP and PVA as a result of pump failure. This disparity is due to a combination of three things. First there is the sensitivity of the afterload to pulse, yielding a higher resistance with continuous flow. Secondly, the MAP decrease can be explained by the unphysiologic control of the heart simulator, that does not respond to (preload) volume changes and leads to lower LV pressure and the false impression that pump failure diminishes myocardial oxygen consumption (lower PVA). Thirdly, Fig. IV-6 and [Eq. IV-4] in section A demonstrate that the resistance of the Deltastream pump used in the *in vitro* study is approximately three times smaller compared to the microdiagonal pump used in the other studies. This explains the higher backflow (up to 3 l/min) and decreased MAP (approx. 40 mmHg), which lead to a life-threatening situation according to the *in*

vitro model. The importance of pump and cannula resistance for pump failure was pointed out before by Antaki et al. [240], and it was briefly mentioned in section B that mathematical model simulations with shorter cannulas led to higher forward and backward flow through the pump.

Apart from the pump and cannula properties, also the condition of the heart is an important determinant for the effect of pump failure. In all models it appears that the total flow remains constant during pump failure as a result of an increase in flow through the aortic valve. As mentioned before, the simulated heart failure in the sheep and mathematical model is relatively mild compared to clinically observed heart failure. It is very likely that patients with severe heart failure lack the necessary preload reserve to generate the extra aortic flow and consequently a life-threatening situation may occur. The importance of residual cardiac function is also illustrated by clinical experience: in patients that are treated before preterminal heart failure presents, a rotary blood pump can be turned off routinely for a five minute echocardiographic evaluation without adverse effects [241]. In more severe heart failure patients on the other hand, switching off a rotary blood pump may lead to unconsciousness within seconds (H. Schima, personal communication).

3. Unloading with constant rotational speed

When comparing the mathematical model findings for LV unloading with the results of the *in vitro* and *in vivo* studies, it should be taken into account that a whole different range of pump flows (Q_{pump}) was investigated. The *in vitro* and *in vivo* models are both limited to pump flows that approximate the baseline aortic flow (5.3 and 3.6 l/min, respectively) while the pump flows simulated in the mathematical model exceed the baseline flow (3.5 l/min) by far. Exceeding this flow results in a permanent closure of the aortic valve as was observed in the mathematical model simulations at 6000, 8000, and 10000 rpm. This effect was reached with the Deltastream in the *in vitro* model only at the highest speed used (5000 rpm, $Q_{\text{pump}} = 5.6$ l/min), and not at all in the *in vivo* unloading study (max. $Q_{\text{pump}} = 3.5$ l/min).

The mathematical model shows that there is little LV unloading as long as the aortic valve still opens, but once the pump flow gets higher (as of 6000 rpm), MAP and Q_{tot} increase markedly while LV pressure decreases, indicating

effective unloading. This is in fact in accordance with a prediction of the *in vivo* study (also based on literature data): increase in rotational speed first leads to complete volume unloading ($SV = 0$ ml), followed by LV pressure unloading at higher speeds. The *in vitro* model confirms that an increase in rotational speed results in a decrease in SV , and this is also found for the mathematical model in a comparable speed range, i.e., up to the point where the aortic valve stays closed (6000 rpm). For the higher speed range, however, the isovolumic phases disappear and a triangular PV-loop is observed, yielding a higher SV than at low speed. In numbers, the SV in the mathematical model study goes from 38 ml at 2000 rpm to 30 ml at 6000 rpm and to 48 ml at 10000 rpm. A similar observation was made by Kono et al. ^[216] who performed an *in vivo* unloading study with a rotary blood pump at higher flows. Once over the ‘threshold pump flow’ where the aortic valve stays closed, the PV-loops become triangular with a lower maximal pressure and shifted to lower volumes, completely in accordance with our mathematical model data.

In summary, it can be concluded from the combination of all the models that LV unloading with a rotary blood pump at low constant rotational speed leads to a decrease in SV and EDV , while ESV , MAP , LV pressure and Q_{tot} stay constant. Increase in rotational speed only amplifies the effect on SV and EDV , while augmented pump flow is compensated by diminished aortic flow. This is translated in the PV-plane as narrowing rectangular loops that maintain the same height. Once the ‘threshold flow’ (permanently closed aortic valve) is reached, Q_{ao} can not decrease further due to the valve function. Increase in rotational speed is then established as an increase in total flow, an increase in aortic pressure, and a decrease in LV pressure (pressure unloading). PV-loops get a triangular shape (higher SV), shrink in height, and shift further to the left, indicating a decreased oxygen demand.

The *in vitro* model findings deviate from this explanation as far as MAP is concerned: it is not preserved up to the ‘threshold flow’ but it is decreased from baseline at low rotational speeds and it then gradually increases with increasing pump speed (\sim flow). Again, this is due to the unphysiologic behavior of the heart simulator and afterload and the low pump resistance of the Deltastream pump.

It seems obvious from the model findings that a rotary blood pump can only provide strong unloading and increased perfusion if it ‘overpowers the heart’s

capacity' by generating flows above the baseline aortic flow. However, the consequent permanent closure of the aortic valve imposes additional risks such as thromboembolism and therefore it may be desirable to use a pump below the 'threshold flow'. The LV will then only be volume unloaded and there will be no total flow augmentation, but the pump will take over a part of the flow from the LV and thus (slightly) limit the work and the oxygen demand of the LV. This application is restricted to hearts with sufficient residual function and cardiac output where resting the heart has priority over increasing the perfusion. The availability of miniaturized rotary blood pumps is therefore important, so they can be implanted in a less invasive way in an earlier stage of heart failure and thereby promote the recovery of the diseased LV.

4. Unloading with modulated rotational speed

From the modulated rotational speed (sine wave pattern) studies performed *in vitro* and in the mathematical model, it can be concluded that counterpulsation is the most desirable triggering for LV unloading with synchronous ventricular assist. According to the definitions used in the studies, counterpulsation relates to low phase shifts between the onset of LV systole and the onset of pump 'diastole'. Consequently, a high rotational speed (pump 'systole') will be reached during LV diastole and thus the preload of the LV will be reduced. Moreover, the low speed during systole will still allow the aortic valve to open. Counterpulsation with a rotary blood pump further leads to increased average pump flow, decreased mean arterial pressure and decreased PVA and myocardial wall stress. Also the external work delivered by the LV is diminished according to the mathematical model. The *in vitro* model confirms the decrease in MAP and PVA for low phase shifts and it further shows an increase in SV. However, a major drawback of counterpulsation as it was investigated here, is the decrease in pulse pressure. A high speed during diastole and a low speed during systole can flatten the arterial pressure waveform, which may result in altered organ perfusion.

When a rotary blood pump is used in a pulsatile way but untriggered (asynchronously), it leads to complex interference patterns that can result in slow but large variations in pressures, volumes, and flows and are therefore undesirable. This was only assessed in the *in vitro* model and could therefore not be confirmed.

B. SUMMARY OF THE PUCA II STUDIES

1. Introduction

The thin-walled, single-valved pulsatile catheter (PUCA II) is unique as a ventricular assist device. It is small and can therefore be deployed rapidly by minimally invasive introduction via the subclavian artery, thus lending itself for an unexplored field of LVAD application: bridge to bridge. The PUCA II works according to the counterpulsation principle of the intra-aortic balloon pump (IABP), yet, it also pumps blood. Due to its small size, however, its pumping capacities are lower compared to traditional high-flow LVADs. This was illustrated in chapter V (section C), where the PUCA II was compared to the Medos VAD and the Novacor assist device. The comparison was based on hydraulic performance of the pumps as such (no heart interaction) in a specific setting: a fixed rate of 80 BPM. Three-dimensional graphs were constructed to show the generated pump flow in function of preload and afterload. The generated hydraulic energy at arterial level was further calculated for identical settings of preload, resistance, and compliance. From this comparison it is obvious that the Medos VAD and the Novacor generate similar flows (4-5 l/min) while the PUCA II demonstrated lower flow capacities (≈ 2 l/min). Also the cycle work generated by the Novacor was approximately 5 times higher than the PUCA II work for the tested conditions. The Medos VAD delivered 3.4 times more work and this resulted in a rapid ejection with high peak flow and pressure rise for the Novacor, a more gradual ejection for the Medos VAD, and a slow ejection and pressure rise for the PUCA II. The flow and power findings reflect the target applications of the different devices, where the Medos VAD and the Novacor aim at taking over the complete LV workload respectively for medium-term (in hospital) and long-term (out of hospital) episodes. In contrast, the PUCA II is intended for short-term stabilization and support.

Up to date, independent research of the performance of the PUCA II and its interaction with the left ventricle is inexistent. The only available information comes from basic *in vitro* testing ^[230,242], mathematical model simulations ^[243], and extensive *in vivo* testing ^[202,218,235] by the designers themselves. The

following section summarizes these studies, that resulted in an evolution in the design from a thick-walled dual-valved catheter to its current design. The studies performed in the Hydraulics Laboratory with the current design of the PUCA II are summarized in the last section.

2. Available information on PUCA

The current PUCA II pump is a second-generation device, developed from the dual-valved PUCA I. A mathematical model study with the latter concluded that the flow resistance of the valves seemed a more important determinant of the pump capacity than the governing pressures and patient hemodynamics ^[218]. It was further found that optimal total systemic flow, increase in myocardial O₂ supply and decrease in O₂ consumption could be obtained if the pump was used in 1:2 mode, generated 3 l/min, and was triggered for counterpulsation ^[243]. The same study stated that a lower flow is detrimental for perfusion but more favorable for LV unloading because it limits the aortic pressure (with constant resistance) and therefore decreases the O₂ consumption, which dominates the O₂ supply/consumption ratio.

In vitro testing was performed by the developers in a rudimentary mock loop with a water column as an afterload ^[230]. One study focused on the effect of the driver used on PUCA II performance and compared a driver for pneumatic VADs to a driver for an IABP. The 21 Fr PUCA II catheter had a length of 25 cm and membrane pumps with a stroke volume of 65 and 55 ml were used. It was concluded that PUCA II performs best if the IABP driver was used in combination with the 55 ml pump, leading to a pump flow of 2.8 l/min at 80 BPM. The beneficial effect of the IABP driver is due to the higher and faster pressure development, specifically intended for counterpulsation purposes. Previous *in vitro* studies with the dual-valved PUCA I had also revealed an important influence of the driver and its timing and control strategy ^[242].

Another *in vitro* study with the PUCA II assessed the leakage over the tilting valve during aspiration and ejection generated by a pneumatic artificial heart driver ^[244]. A flow of 1.7 l/min could be produced and caused aspiration and ejection leakage of 17 % and 5 %, respectively. Ejection leakage was defined as the portion of catheter flow that goes to the tip, while aspiration leakage was the portion of catheter flow that did not come from the tip.

Acute animal experiments were performed to assess the optimal driving mode for a 25 Fr PUCA I ^[202]. It was found that asynchronous assist in calves provided sufficient flow (mean: 2.8 l/min) and a significant reduction in myocardial O₂ consumption, and is suitable for patients suffering from cardiac arrhythmias. Synchronous assist, however, delivered superior flow (mean: 2.9 l/min) and O₂ consumption reduction, together with maximum coronary flow. Animal experiments with a 40 cm long 21 Fr PUCA II demonstrated flows of 1.2 – 1.4 l/min ^[244].

3. PUCA II studies performed at the Hydraulics Laboratory

The *in vitro* studies with the PUCA II pump described in this dissertation focus on assessment of the pump capacities and the unloading and perfusion capacities. The same version of pump and driver were used throughout: a 28 cm long, 21 Fr catheter with a valve located 10 cm from the tip, a single-port valveless membrane pump with a stroke volume of 40 ml, and an Arrow Autocat IABP driver. All our experiments were performed with a water-glycerin mixture (60/40 v/v%) to mimic the viscosity of blood. The importance of a blood-analogue fluid for pulsatile pump studies was demonstrated in section B of chapter V.

Rather than estimating the PUCA II valve leakage during aspiration and ejection, the efficiency of the pump over a whole beat was derived from the *in vitro* experiment with a static preload and lumped afterload. This efficiency proved to be related to the afterload, expressed as mean arterial pressure (MAP). The knowledge of this efficiency (varying between 60% and 80%) allows better estimation of the actual pump flow, which is always overestimated by measurements at the membrane pump outlet (indicated pump flow). The actual flow is then relation of the preload, afterload and the pump frequency. At a MAP of 100 mmHg and a preload of 40 mmHg, for instance, a pump frequency of 90 BPM was superior to 60 BPM or 120 BPM in terms of actual pump flow, which was maximally 1.9 l/min. From the experiment with a heart simulator as dynamic preload, it was concluded that the PUCA II provides a significant contribution to total flow (over 80%), especially in a failing heart and at high heart rates. However, it has to be taken into account that extreme low total flows were present in these simulations. It was also found that 1:1 mode provides superior flow and MAP to 1:2 mode at all heart rates, and that this performance is likely related to the used driver. Attention should be paid to the fact that 1:2 mode in

the Arrow Autocat driver means that every other pump beat is skipped, while in the previously performed studies 1:2 mode was defined as one long pump beat stretched out over 2 heart beats.

When the PUCA II is used in its standard position through the aortic valve, it provides much higher flow compared to an intra-aortic balloon pump (IABP). Also the myocardial O₂ supply estimated from the pressure data is superior with the PUCA II, while the IABP provides lower flow but better unloading as indicated by O₂ consumption. When the PUCA II is placed in an abdominal position, the hemodynamic effect correlates well with the IABP findings. This is in agreement with a mathematical model study of Verkerke et al., where it is stated that a choice has to be made between flow augmentation and LV unloading, depending on the patient needs ^[243]. It appears that the PUCA II in trans-aortic position in combination with an Arrow Autocat driver is suitable for maintaining pressure and flow in heart failure patients, but not for LV unloading. However, a more powerful driver may lead to both pressure and flow augmentation, and LV unloading.

4. Conclusion

Making a roundup of all existing PUCA studies is complicated by the fact that two different devices (PUCA I and PUCA II) were manufactured in many different versions and actuated by various drivers. The tested PUCA II catheters differ in length (from 25 to 40 cm), distance from tip to valve (8, 10, or 12 cm), and wall thickness (0.3 or 0.5 mm). Membrane pumps for the PUCA II tests were also manufactured in sizes from 40 ml to 65 ml stroke volume.

Nevertheless, taking into account these device variations, the different test fluid and the different definition of pump flow (actual produced forward flow vs. indicated flow at the pump outlet), all studies performed with the PUCA II yield similar results. The generated flow is insufficient to take over the circulation of a patient completely, but it can provide flow and pressure augmentation in a range that is acceptable to stabilize and support heart failure patients for a short-term. Consequently, this device has potential to become a useful tool in heart failure management.

C. LESSONS LEARNED FOR FUTURE MODELING OF CARDIAC ASSIST

1. Introduction

New cardiac assist devices slowly infiltrate in the hospitals for treatment of end-stage heart failure patients. Investigation of their hemodynamic impact on the native cardiovascular system is often performed by creating a model of the device and the human circulation, rather than investigating real patient data. The advantage of such modeling is that it is systematically reproducible and it can be used to simulate a broad range of patient conditions and hemodynamic disturbances. The most popular ways for simulating the heart-device interaction are mathematical ‘lumped parameter’ models and *in vitro* fluidic models. The latter are often also constructed of a series of ‘lumped’ mechanical components that represent otherwise distributed properties. Regardless of the model type and its extensiveness, by definition, any cardiovascular model is an approximation of the prototype human circulatory system, and typically fails to reproduce the complexity of its humoral, neural, thermal, and mechanical regulation mechanisms.

Simplifications and approximations with respect to reality are the basis of modeling, but the extent of simplification should depend on the goal of the simulation studies. The use of the mathematical and *in vitro* models described in this dissertation revealed two major shortcomings of which it can be expected that they are also apparent in other models used in this research field. A first shortcoming concerns modeling of total vascular resistance, while a second shortcoming is the simulation of cardiac dynamics. Even though several models worldwide have proven their value in basic cardiovascular research, their application for ventricular assist studies has to be approached with caution because of these issues.

2. Resistance issues

2.1. Control mechanisms

One important component in modeling the vascular system - the afterload of the pump and the heart - is the total vascular resistance (TVR). The mechanisms that control this parameter have been modeled extensively in several ways^[245-249], but few attempts have been undertaken to implement these mechanisms in models of cardiac assistance^[135,250,251]. The main effect of neglecting the negative feedback mechanisms that normally regulate TVR is that mean arterial pressure (MAP) is much more dependent upon flow than observed physiologically. In other words, by excluding the intrinsic reflex that normalizes pressure (by vasodilatation), a model will falsely predict acute hypertension at high aortic flows.

In the healthy cardiovascular system, an augmentation of total flow by the use of an assist device or as a result of exercise would lead to a decrease in TVR to facilitate the higher flow and to limit the rise in blood pressure^[252]. The *in vivo* experience with ventricular support in sheep (chapter IV, section E), however, indicates that no normalization of the arterial pressure is necessary as long as the pump flow does not exceed the baseline unsupported cardiac output. This restriction beholds that the total flow stays constant because the pump flow is countered by a decrease in flow through the aortic valve. In other words, as long as the pump flow is limited to baseline cardiac output, there is no condition that compares to exercise.

The same conclusion can be drawn from the *in vitro* interaction study of chapter IV (section D), where regurgitation of the aortic valve even helped to normalize total flow. A similar phenomenon was observed in the studies with the PUCA II pump: cardiac output was reduced in compensation for the supplemental pump flow. Nonetheless there was an increase in total flow and concomitant rise in MAP of 27 mmHg: a condition that is typically normalized *in vivo* by downregulation of TVR.

Much higher flows were obtained in the mathematical model study in chapter IV (section C), where ventricular assist was simulated at various rotational speeds. A speed of 6000 rpm resulted in a situation where the total blood flow in sheep was generated by the microdiagonal pump, yielding a permanently closed aortic valve. In patients, total unloading and a permanently closed aortic valve can be expected at a speed of 7000 rpm, which relates to the design point of the

microdiagonal pump. Further increase of the pump speed resulted in a decoupling of aortic and left ventricular pressure in the simulation, where the latter indicated a decompression of the left ventricle. The aortic pressure, however, augmented to extreme values: 156 mmHg at a total flow of 8 l/min at 10000 rpm. Such a high total flow mimics the perfusion needs of a sheep during exercise, and consequently a regulation of TVR can be expected *in vivo* to maintain the MAP within normal physiological limits.

One way to prevent the overestimation of aortic pressure in the mathematical model would be a basic implementation of autonomous baroreceptor feedback. It is, however, important to take into account that there are slow and fast pathways, because this influences the instantaneous interaction between the pump and the cardiovascular system when pulsatile support is used. This becomes essential when the influence of synchronous and asynchronous support and their timing is modeled.

2.2. Linearization

It is practically impossible to mimic the vascular tree with its multitude of branching arterioles and capillaries, which generate resistance in a unique way. Nonetheless, TVR (mainly generated in the arterioles) can be assumed linear, as seen in Poiseuille flow patterns ^[253]. This means that the pressure drop over the vascular system is linearly related to the flow through it, or that the resistance value, TVR, is constant and independent of the flow level. This presumes that the above-mentioned feedback mechanisms are neglected.

Simulating the linearity of TVR in a mathematical model is not problematic since an ideal resistor is modeled as a simple constant. Of more concern with respect to stability and linearity is the physical construction and regulation of *in vitro* resistors, which are preferably assembled in a lumped, spatially condensed way. Various designs have been used by others: slide valves, needle valves or ball valves ^[132]; compressed tubes or foam ^[131,187]; porous or perforated aluminum oxide or plastic ^[126,134,251,254]; tubing clamps ^[141]; bundles of capillary tubing ^[255]. From the experience gained during the research described in this dissertation, it was found that the best resistor is still the one designed by Westerhof et al. that was extensively described in a 1971 publication ^[126]. It shows not only a strong linear behavior between flow and pressure drop, but also a good linearity in regulation in the physiological range: each increment in slide position results in a

similar change in resistance, regardless of the resistance value. Consequently, this type of resistor was mimicked by other research groups ^[134,251,254].

Regardless of the design of the resistor, there is still a large nonlinearity introduced in each *in vitro* system by the other components and the connections between them. Since Poiseuille flow is rarely present at these sites, energy losses will occur that result in pressure drops related to the square of the flow. This nonlinear resistance behavior of an *in vitro* system has important consequences, since over a heart period the flow ranges from slightly negative values at aortic valve closure to peak flows of more than 400 ml/s at rest. Consequently, in a nonlinear system, the instantaneous resistance value will vary over a wide range, which is certainly not physiological and may result in incorrect conclusions. A way to overcome this weakness of *in vitro* models is to incorporate an active (computer controlled) resistor that keeps the resistance value constant by means of instantaneous pressure and flow feedback. An example of this was reported by O’Leary et al. ^[251], except that their control was not instantaneous and the necessary regulation time was unconstrained.

3. Cardiac modeling issues

In the modeling of cardiac assist devices, the interaction between the left ventricle (LV) and an LVAD is usually of concern. This interaction is governed by the sensitivity of both the LV and the LVAD to changes in load. As discussed in chapter III, the original time-varying elastance theory of Suga and Sagawa ^[8] is the most common way to account for this behavior by the LV. This model is relatively straightforward to implement in mathematical models, and most recently has been implemented with *in vitro* models ^[143]. This theory, first described in the early 1970s, states that the ratio of pressure and volume in the LV obeys a prescribed function of time, termed “elastance”:

$$p(t) = E(t) \cdot [V(t) - V_0] \quad [\text{Eq. VI-1}]$$

with:

- p(t): time varying pressure (mmHg)
- V(t): time varying volume (ml)
- E(t): time varying elastance (mmHg/ml)
- V₀: an offset constant (ml)

Under the conditions studied, the elastance curve has been observed to be independent of loading. Consequently, the maximum value of this function (E_{es},

end-systolic elastance) has been used widely as a marker of the contractility of the LV. Because it is independent of preload and afterload, each individual has its own elastance curve that only changes when the basic contractile function of the heart changes, e.g., under influence of sympathetic/parasympathetic stimuli, inotropic drugs, disease, or healing processes ^[7]. In fact, normalization of this curve with respect to time and amplitude results in a general curve that is typical for the species, which is an appealing feature for modeling ^[10,150,155].

The studies of Suga, Sagawa, and many of their successors were performed in intact (whether or not isolated) animal hearts and under physiological conditions. During cardiac assist with displacement-type blood pumps, however, the heart is subjected to quickly varying loading conditions. When such a device is used in a counterpulsation manner, for instance, extreme unloading occurs during LV systole. Consequently, it should be questioned whether the original elastance theory is still valid for mechanically supported hearts.

3.1. Elastance and a rotary blood pump

The data in Fig. VI-1 were acquired from an acute study in seven healthy sheep that underwent implantation of the Medos-HIA microdiagonal pump (described in chapter IV, section E). The pump was operated at several mean pump flows, as seen in the figure. Data were also acquired at baseline (BL) where the device was shut off and the cannulas clamped. Each animal was instrumented with a conductance catheter (CardioDynamics BV, Leiden, The Netherlands) and a Millar hi-fi cathetertip pressure transducer (Millar Instruments Inc., Houston, TX) in the left ventricle.

The elastance curves in the right panel of Fig. VI-1 all originate from one animal with atrial inflow cannulation. For each pump flow level, several sequential beats were averaged to obtain the displayed curve, which was then normalized in time to filter the variations in heart rate for better comparison. The curves demonstrate how increasing pump flow results in a gradual change in E_{es} , stretching the elastance curves vertically. It can not be excluded that there is no increased functionality due to improved coronary perfusion, but the time between each subsequent measurement was no more than two minutes and it is unlikely that the myocardial condition improves in this time. The displayed E_{es} changes are clearly a result of the heart-pump interaction and it can be concluded that E_{es} alone

cannot be used to quantify the condition of the LV (contractility) during cardiac assist with a rotary blood pump.

in vivo LV data with microdiagonal pump support

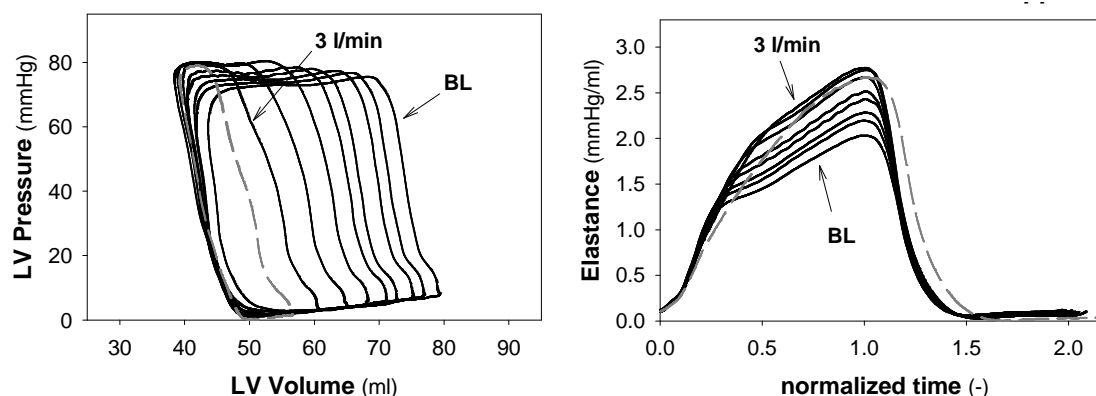


Fig. VI-1: Left ventricular pressure-volume loops (left) and the according elastance curves (right) of a sheep with a Medos-HIA microdiagonal pump with left atrial inflow cannulation. The black curves show data acquired at baseline (BL) and pump flows of 0, 0.5, 1, 1.5, 2, 2.5, and 3 l/min. The curves are arranged between 'BL' and '3 l/min' in that respective order. The gray dashed line shows similar data at a pump flow of 3.5 l/min in the same sheep.

Consequently, it is incorrect for mathematical and *in vitro* models to scale a predefined $E(t)$ waveform with a fixed E_{es} . Moreover, if the elastance curves of Fig. VI-1 are also normalized with respect to amplitude, they all coincide for the diastolic part but the systolic part is different for each flow level: less steep for increasing pump flows. This indicates that higher pump flows slow down intraventricular pressure rise. The differences are relatively small, but this indicates that it is even incorrect to use one predefined waveform for normalized elastance if cardiac support with a rotary blood pump is simulated.

For the particular sheep data shown in Fig. VI-1, it was also found that increasing the pump flow above 3 l/min resulted in a gradual decrease of E_{es} (see Fig. VI-2) and a deformation of the waveform (see dashed line in Fig. VI-1). The maximum elastance point shifted to an earlier time in the cycle thus resulting in a longer time-normalized curve. This means that the cardiac assist also influences the systolic/diastolic time ratio. A similar phenomenon was observed in all seven sheep, for both left atrial and left ventricular cannulation, but the pump flow level as of which the waveform deformation sets on varied between subjects. This level relates to the 'threshold speed' (or threshold flow) as described in section A

of this chapter. This is the point where the aortic valve stays permanently closed and decompensation of the LV begins, resulting in a pressure decrease.

The analysis of these data presumed that V_0 of the $E(t)$ function for each sheep at baseline remained constant over the range of support levels studied. This was done because controlled preload variations (necessary for V_0 calculation) could not be performed repeatedly in between the acquisitions. It can be argued that V_0 shifts as a result of the level of unloading and therefore the resulting elastance curves with the corrected V_0 actually coincide – thereby implying a constant level of contractility. We therefore scaled the E_{es} of the different curves of Fig. VI-1 to the baseline E_{es} by adjusting V_0 (see Fig. VI-2). This revealed a linear relationship between the pump flow and the corrected V_0 's up to the threshold flow. Once higher pump flows are reached, the necessary V_0 correction, deviates strongly from this relationship. If the argument that V_0 shifts during cardiac support is correct and if the pump flow is kept below the threshold flow, time-varying elastance theory could be corrected for rotary blood pump use as:

$$p(t) = E(t) \cdot [V(t) - V_0(Q_p)] \quad [\text{Eq. VI-2}]$$

Where $V_0(Q_p)$ describes the linear relationship between pump flow and V_0 . The use of [Eq. VI-2] in a cardiac model would allow to use one constant E_{es} value to scale a predefined $E(t)$ waveform. The term $V_0(Q_p)$, however, is related to a non-cardiac parameter (pump flow) and therefore does not model the heart as such. A proper cardiac model describes heart function with parameters known to the heart and independent of extra-cardiac influences such as load or pump flow. Consequently, a cardiac model on hemodynamic level is limited to pressure and volume and their time derivatives. Even if $V_0(Q_p)$ is known and [Eq. VI-2] is used in a cardiac model, there is still the issue of waveform morphology. Possibly, the discrepancies between the systolic parts of normalized elastance curves can be overcome with time-varying V_0 , but this means that a different function has to be defined for each flow level. This has the following drawbacks:

- i) Since the relations of V_0 in function of pump flow and time are unknown in clinical practice, such a V_0 -corrected elastance theory cannot be used for evaluation of heart function.
- ii) A cardiac model based on such a theory is complex, and it contains more extra-cardiac parameters that limit the applicability of the model to specified situations.

iii) This theory would still only be valid within a limited flow range, up to the threshold flow.

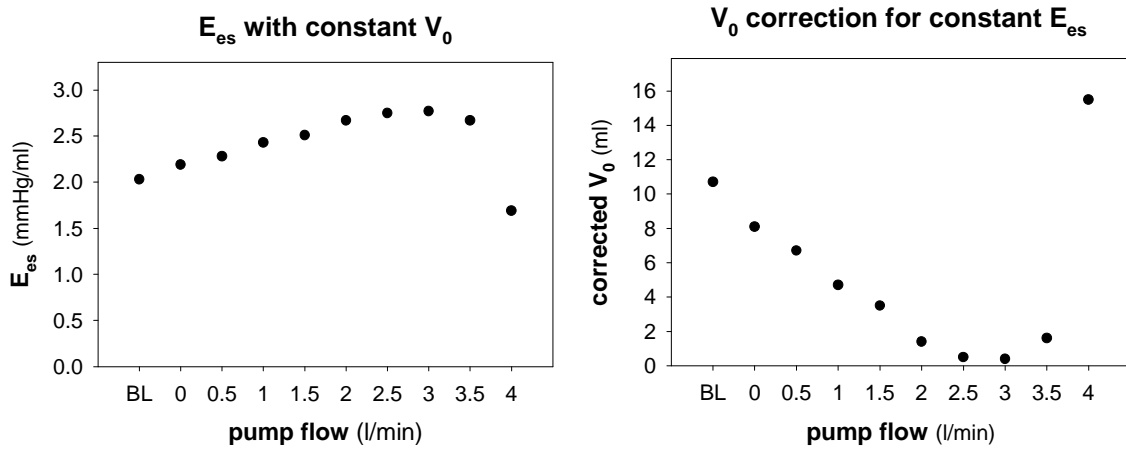


Fig. VI-2: Left: end-systolic elastance at different pump flows, derived from Fig. VI-1, where $V_0 = 10.7$ ml for all data. Right: V_0 that is necessary to obtain the baseline (BL) E_{es} of 2.03 mmHg/ml at every pump flow.

3.2. Elastance and a positive-displacement pump

The data in Fig. VI-3 were acquired from a healthy calf that underwent an implantation of a Novacor N100 left ventricular assist device as part of a surgical training program (unpublished data P. Steendijk, personal communication). The Novacor was implanted with apical and ascending aorta cannulation and the animal was instrumented with a 5-segment conductance catheter with hi-fi pressure transducer tip (CardioDynamics BV, Leiden, The Netherlands) in the left ventricle. Fig. VI-3 shows a data sequence where the Novacor was pumping in a fixed rate mode and subsequently switched off. The ‘Novacor on’ part demonstrates the interaction between the native heart and the device: the asynchronous support is obvious from the repeated sequence of four beats in the pressure plot (top panel), which is similar to the findings with the use of the Deltastream pump in pulsatile mode (see Fig. IV-22). These varying LV pressures indicate that the native heart is subject to quickly varying load conditions.

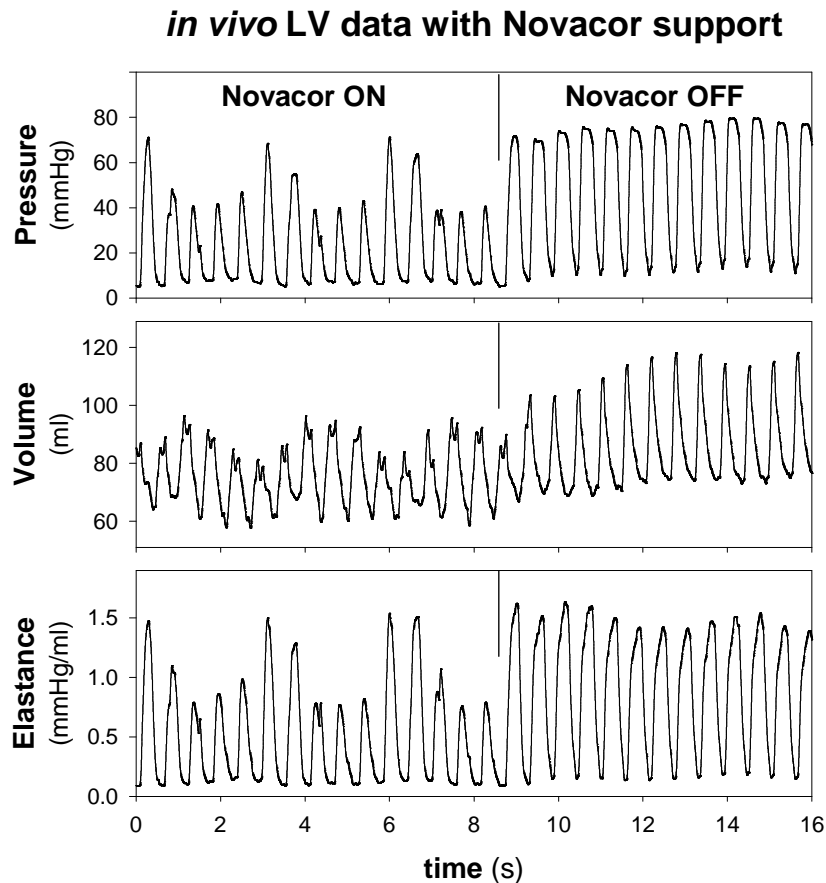


Fig. VI-3: Left ventricular pressure, volume, and elastance measured in a calve with a Novacor assist device. The device was pumping in fixed rate mode and then switched off. The graphs show one continuous data sampling interval of 16 seconds.

The bottom panel of Fig. VI-3 displays the elastance calculated from the acquired pressures and volumes according to [Eq. VI-1], where V_0 equals 25 ml. The right hand side ('Novacor off') shows very stable elastance curves, while the 'Novacor on' side shows sequential beats with very different maxima (E_{es}). A similar phenomenon was observed by Yoshizawa et al. who estimated the maximal elastance with an algorithm based on aortic pressure and flow ^[256]. Correction techniques based on V_0 as described in section 3.1 were applied in vain: large beat-to-beat variations in elastance were persistent. According to the (load independent) time-varying elastance theory, this would mean that the contractility of the heart changes from beat to beat. Since contractility is considered an intrinsic property of the heart muscle (its 'strength'), it should only change gradually and thus the observed rapid variations in elastance result from the heart-device interaction. This finding makes E_{es} an unreliable indicator for LV contractility under ventricular assist with a positive-displacement pump.

In fact, normalization of all the separate beats with respect to time and amplitude results in a series of coinciding graphs for the ‘Novacor off’ section while the ‘Novacor on’ normalized graphs differ considerably from this and from each other (Fig. VI-4).

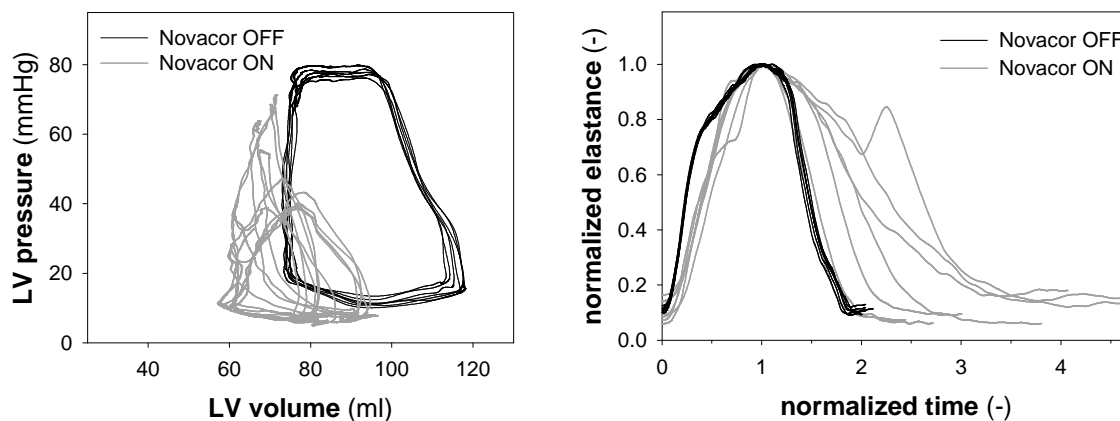


Fig. VI-4: Pressure-volume loops (left) and normalized elastance curves (right) composed with the data of Fig. VI-3.

3.3. Prospects

The previous paragraphs indicate that the original time-varying elastance theory falls short for an assisted heart. It cannot be used reliably to assess the contractility of the native heart, and it fails to accurately describe heart function in models of assisted hearts. Consequently, there is need for a correction or an alternative for this theory, which has proven its value in unassisted hearts.

Suga and Sagawa extended their own time-varying elastance model already in 1980 to account for inaccuracies in pressure estimation of differently loaded heart beats ^[257]. They therefore included terms that are related to instantaneous volume variation, peak ejection velocity, and the total ejected volume. Nowadays, several models have been developed that mimic left ventricular function not only by elastance, but also with additional resistive and inertial components ^[160,258,259], or by its isovolumic characteristics ^[163] (see Chapter III). Such models yield a more accurate representation of natural cardiac pressure and volume variations, but so far they have not been evaluated for assisted hearts and they are very rarely used in cardiac assist models.

To determine the elastance curve of a specific heart according to the original theory, one needs pressure and volume curves under several loading conditions to determine V_0 and the elastance curve. This, however, is not sufficient for a

more complicated model. The elastance-resistance model for instance, additionally requires data sampled during an isovolumic beat to determine the ventricular resistance, and the isovolumic description requires multiple isovolumic beats at different volumes. Consequently it is not obvious to acquire the necessary data for accurate cardiac modeling from experiments that focus on cardiac assist. Moreover, the presence of the device and the associated mutilation of the heart (e.g., by apical cannulation) have an impact on the remaining heart function, and should be incorporated in the cardiac model. It is therefore recommended to assess data for cardiac modeling with the device in place but with its cannula clamped.

4. Conclusion

A resistor that models (part of) the hydraulic load of the vascular system is prone to two major shortcomings: nonlinearity (only in *in vitro* systems) and the lack of control as in the mammalian body. The first shortcoming can be minimized by a resistor design according to Westerhof's criteria, or by feedback control of the resistance value. The second shortcoming requires feedback control algorithms that can be used in both mathematical and *in vitro* models, but their realization with the proper response time will be more difficult *in vitro*. Both shortcomings result in an overestimation of arterial pressure if total systemic flow augmentation by the assist device is modeled.

A cardiac model that is based on the original time-varying elastance theory of Suga and Sagawa would have one elastance curve implemented from which the LV pressure and volume that have to be generated are calculated. This is most common in mathematical models, but it has also been implemented in *in vitro* models. The data presented in this chapter, however, indicate that the elastance curve varies as a result of the interaction between the heart and an assist device and that the original time-varying elastance theory is not appropriate for this kind of modeling.

Further investigation is necessary to better quantify, understand, and model the behavior of the heart (specifically the LV) under cardiac assist. Further development and validation of models should preferably be performed with different types of assist devices and experimental methods to corroborate the results observed in these studies.

D. FINAL THOUGHTS AND COMMENTS

The use of ventricular assist devices was popularized in the mid 1980s, when specialized centers offered the possibility to implant Novacor or HeartMate devices. Meanwhile, more devices are available and they can be implanted in more hospitals worldwide. Monitoring techniques have also improved over the years and consequently there are tons of patient data that contain some information on the effect of a ventricular assist device on the failing heart.

Only a small part of these data, however, has been purposely acquired for research goals. These data reflect the use of assist devices with many variables: different devices, different pump settings, different patient conditions, different pharmacological treatment. Even large randomized trials are not suitable for gaining insight in the heart-device interaction because their main goal is to evaluate clinical outcome. After all, patient management aims at the longest and most comfortable survival, rather than at studying the effects of a particular application.

Still, thorough understanding of the heart-device interaction on multiple levels is necessary to improve the treatment and survival of heart failure patients, preferably by healing their own heart (bridge to recovery). Animal models are a useful alternative to patient data, even though it is difficult to create an animal model with similar heart failure conditions as observed in clinical practice. It is also not necessary to sacrifice animal lives for every study that pursues more insight in the heart-device interaction. *In vitro* models and mathematical models are cheaper and more fit for investigation of, for instance, specific parameters that are difficult to acquire *in vivo* or the impact of certain pump settings. Even though they are simplifications of reality and their results need to be analyzed critically, such models are stable, relatively easy to manage and not subject to biodiversity.

In vitro modeling, *in vivo* (animal) modeling, and mathematical modeling are viable alternatives for patient studies. The research described in this thesis with these models intends to be another paving stone on the path that leads to insight in the heart-device interaction on hemodynamic level.

References

1. West JB. *Best and Taylor's physiological basis of medical practice*. 12th ed. Baltimore: Williams & Wilkins; 1990.
2. Levick J. *An introduction to cardiovascular physiology*. 2nd ed. Oxford: Butterworth-Heinemann Ltd.; 1995.
3. Darovic GO. *Hemodynamic monitoring: Invasive and noninvasive clinical application*. 2nd ed. Philadelphia: W.B. Saunders Company; 1995.
4. Strackee J, Westerhof N. *The physics of heart and circulation*. 1st ed. Bristol: IOP Publishing Ltd.; 1993.
5. Yellin E. The momentum of mass, the momentum of ideas, and diastolic function. In: Ingels N, Daughters G, Baan J, Covell R, Reneman R, Yin F, eds. *Systolic and diastolic function of the heart*. Amsterdam: IOS Press, 1995.
6. Katz AM. Ernest Henry Starling, his predecessors, and the 'law of the heart'. *Circulation* 2002;106(23):2986-92.
7. Suga H, Sagawa K, Shoukas AA. Load independence of the instantaneous pressure-volume ratio of the canine left ventricle and effects of epinephrine and heart rate on the ratio. *Circ Res* 1973;32(3):314-22.
8. Suga H, Sagawa K. Instantaneous pressure-volume relationships and their ratio in the excised, supported canine left ventricle. *Circ Res* 1974;35(1):117-26.
9. Fung Y. *Biodynamics: Circulation*. 1st ed. New York: Springer-Verlag; 1984.
10. Senzaki H, Chen CH, Kass DA. Single-beat estimation of end-systolic pressure-volume relation in humans. A new method with the potential for noninvasive application. *Circulation* 1996;94(10):2497-506.
11. Suga H. Total mechanical energy of a ventricle model and cardiac oxygen consumption. *Am J Physiol* 1979;236(3):H498-505.
12. Suga H. Cardiac mechanics and energetics--from e_{max} to pva. *Front Med Biol Eng* 1990;2(1):3-22.
13. Glower DD, Spratt JA, Snow ND, Kabas JS, Davis JW, Olsen CO, et al. Linearity of the Frank-Starling relationship in the intact heart: The concept of preload recruitable stroke work. *Circulation* 1985;71(5):994-1009.
14. Sharir T, Feldman MD, Haber H, Feldman AM, Marmor A, Becker LC, et al. Ventricular systolic assessment in patients with dilated cardiomyopathy by preload-adjusted maximal power. Validation and noninvasive application. *Circulation* 1994;89(5):2045-53.
15. Takagaki M, McCarthy PM, Chung M, Connor J, Dessoffy R, Ochiai Y, et al. Preload-adjusted maximal power: A novel index of left ventricular contractility in atrial fibrillation. *Heart* 2002;88(2):170-6.
16. Gorcsan J, 3rd. Load-independent indices of left ventricular function using automated border detection. *Echocardiography* 1999;16(1):63-76.
17. Sarnoff SJ, Braunwald E, Welch GH, Jr., Case RB, Stainsby WN, Macruz R. Hemodynamic determinants of oxygen consumption of the heart with special reference to the tension-time index. *Am J Physiol* 1958;192(1):148-56.
18. Alpert N. *Cardiac hypertrophy*. New York: Academic press; 1971.

19. Segers P, Stergiopoulos N, Schreuder JJ, Westerhof BE, Westerhof N. Left ventricular wall stress normalization in chronic pressure- overloaded heart: A mathematical model study. *Am J Physiol Heart Circ Physiol* 2000;279(3):H1120-7.
20. Arts T, Bovendeerd PH, Prinzen FW, Reneman RS. Relation between left ventricular cavity pressure and volume and systolic fiber stress and strain in the wall. *Biophys J* 1991;59(1):93-102.
21. Falsetti HL, Mates RE, Grant C, Greene DG, Bunnell IL. Left ventricular wall stress calculated from one-plane cineangiography. *Circ Res* 1970;26(1):71-83.
22. American Heart Association. Heart disease and stroke statistics - 2003 update. Dallas: American Heart Association; 2002.
23. World Health Organisation. World health report 2003: Shaping the future: WHO; 2003.
24. Nationaal Instituut voor de Statistiek. Gezondheidstoestand. Available at: http://www.statbel.fgov.be/figures/d364_nl.asp#1. Accessed February 12, 2004
25. Baker DW, Hayes RP, Massie BM, Craig CA. Variations in family physicians' and cardiologists' care for patients with heart failure. *Am Heart J* 1999;138(5 Pt 1):826-34.
26. Remme WJ, Swedberg K. Guidelines for the diagnosis and treatment of chronic heart failure. *Eur Heart J* 2001;22(17):1527-60.
27. Ganiats TG, Browner DK, Dittrich HC. Comparison of quality of well-being scale and nyha functional status classification in patients with atrial fibrillation. *Am Heart J* 1998;135(5):819-24.
28. Cohn JN, Archibald DG, Ziesche S, Franciosa JA, Harston WE, Tristani FE, et al. Effect of vasodilator therapy on mortality in chronic congestive heart failure. Results of a veterans administration cooperative study. *N Engl J Med* 1986;314(24):1547-52.
29. McDonald CD, Burch GE, Walsh JJ. Alcoholic cardiomyopathy managed with prolonged bed rest. *Ann Intern Med* 1971;74(5):681-91.
30. Stevenson LW, Kormos RL, Bourge RC, Gelijns A, Griffith BP, Hershberger RE, et al. Mechanical cardiac support 2000: Current applications and future trial design. June 15-16, 2000 bethesda, maryland. *J Am Coll Cardiol* 2001;37(1):340-70.
31. Lee TH, Hamilton MA, Stevenson LW, Moriguchi JD, Fonarow GC, Child JS, et al. Impact of left ventricular cavity size on survival in advanced heart failure. *Am J Cardiol* 1993;72(9):672-6.
32. Starling RC, Young JB. Surgical therapy for dilated cardiomyopathy. *Cardiol Clin* 1998;16(4):727-37.
33. Kashem A, Kashem S, Santamore WP, Crabbe DL, Margulies KB, Melvin DB, et al. Early and late results of left ventricular reshaping by passive cardiac-support device in canine heart failure. *J Heart Lung Transplant* 2003;22(9):1046-53.
34. He KL, Shimizu J, Yi GH, Gu A, Kashem MA, Crabbe DL, et al. Left ventricular systolic performance in failing heart improved acutely by left ventricular reshaping. *J Thorac Cardiovasc Surg* 2003;126(1):56-65.
35. McCarthy PM, Takagaki M, Ochiai Y, Young JB, Tabata T, Shiota T, et al. Device-based change in left ventricular shape: A new concept for the treatment of dilated cardiomyopathy. *J Thorac Cardiovasc Surg* 2001;122(3):482-90.
36. Fukamachi K, Inoue M, Doi K, Schenk S, Nemeh H, Dessoffy R, et al. Device-based left ventricular geometry change for heart failure treatment: Developmental work and current status. *J Card Surg* 2003;18 Suppl 2:S43-7.
37. Schenk S, Reichenspurner H, Boehm DH, Groetzner J, Schirmer J, Detter C, et al. Myosplint implant and shape-change procedure: Intra- and peri-operative safety and feasibility. *J Heart Lung Transplant* 2002;21(6):680-6.

38. Kass DA, Baughman KL, Pak PH, Cho PW, Levin HR, Gardner TJ, et al. Reverse remodeling from cardiomyoplasty in human heart failure. External constraint versus active assist. *Circulation* 1995;91(9):2314-8.
39. Acorn Cardiovascular Inc. Corcap™ cardiac support device - product fact sheet. Available at: <http://www.acornev.com/htmlsite/indexb.htm>. Accessed November 18, 2003
40. Sabbah HN. The cardiac support device and the myosplint: Treating heart failure by targeting left ventricular size and shape. *Ann Thorac Surg* 2003;75(6 Suppl):S13-9.
41. Raman JS, Byrne MJ, Power JM, Alferness CA. Ventricular constraint in severe heart failure halts decline in cardiovascular function associated with experimental dilated cardiomyopathy. *Ann Thorac Surg* 2003;76(1):141-7.
42. Oz MC, Konertz WF, Kleber FX, Mohr FW, Gummert JF, Ostermeyer J, et al. Global surgical experience with the acorn cardiac support device. *J Thorac Cardiovasc Surg* 2003;126(4):983-91.
43. Taylor DO, Edwards LB, Mohacsi PJ, Boucek MM, Trulock EP, Keck BM, et al. The registry of the international society for heart and lung transplantation: Twentieth official adult heart transplant report--2003. *J Heart Lung Transplant* 2003;22(6):616-24.
44. The Organ Procurement and Transplantation Network. Annual data reports by organ. Available at: http://www.optn.org/data/annualReport.asp?url=/data/AR2002/ar02_main_organ.htm. Accessed November 18, 2003
45. Pantalos GM. A selective history of mechanical circulatory support. In: Lewis T, Graham TR, eds. *Mechanical circulatory support*. London: Edward Arnold, 1995;3-12.
46. Kuo J, Graham TR. The choice of blood pump for cardiopulmonary bypass. In: Lewis T, Graham TR, eds. *Mechanical circulatory support*. London: Edward Arnold, 1995;153-8.
47. Arabia FA, Smith RG, Rose DS, Arzouman DA, Sethi GK, Copeland JG. Success rates of long-term circulatory assist devices used currently for bridge to heart transplantation. *Asaio J* 1996;42(5):M542-6.
48. Barker LE. The total artificial heart. *AACN Clin Issues Crit Care Nurs* 1991;2(3):587-97.
49. Olsen DB. The fda and the artificial heart. *Artif Organs* 1990;14(3):173.
50. Goldstein DJ, Oz MC. *Cardiac assist devices*. Armonk: Futura Publishing Company Inc.; 2000.
51. Golding LAR. The development and clinical use of centrifugal blood pumps. In: Lewis T, Graham TR, eds. *Mechanical circulatory support*. London: Edward Arnold, 1995;153-8.
52. Liotta D, Hall CW, Cooley DA, De Bakey ME. Prolonged ventricular bypass with intrathoracic pumps. *Trans Am Soc Artif Intern Organs* 1964;10:154-6.
53. Frazier OH, Fuqua JM, Helman DN. Clinical left heart devices: A historical perspective. In: Goldstein D, Oz M, eds. *Cardiac assist devices*. Armonk, NY: Futura Publishing Co., 2000;3-13.
54. Aaronson KD, Eppinger MJ, Dyke DB, Wright S, Pagani FD. Left ventricular assist device therapy improves utilization of donor hearts. *J Am Coll Cardiol* 2002;39(8):1247-54.
55. Petrucci R, Kushon D, Inkles R, Fitzpatrick J, Twomey C, Samuels L. Cardiac ventricular support. Considerations for psychiatry. *Psychosomatics* 1999;40(4):298-303.
56. Mihaylov D, Verkerke GJ, Rakhorst G. Mechanical circulatory support systems: A review. *Technol Health Care* 2000;8(5):251-66.
57. Delgado DH, Rao V, Ross HJ, Verma S, Smedira NG. Mechanical circulatory assistance: State of art. *Circulation* 2002;106(16):2046-50.

58. Song XW, Throckmorton AL, Untaroiu A, Patel S, Allaire PE, Wood HG, et al. Axial flow blood pumps. *Asaio Journal* 2003;49(4):355-64.
59. Reul H, Kaufmann R, Siess T. Cardiac assist devices. In: Verdonck P, ed. *Intra and extracorporeal cardiovascular fluid dynamics*. Southampton: Computational Mechanics Publications, 1998;233-57.
60. World Heart Corporation. Mr. L: A record of long-term support. Available at: http://www.worldheart.com/section5/novacor_patient_4.htm. Accessed November 18, 2003
61. Siess T, Nix C, Menzler F. From a lab type to a product: A retrospective view on impella's assist technology. *Artif Organs* 2001;25(5):414-21.
62. Trumble DR, Magovern JA. Muscle powered blood pump: Design and initial test results. *Asaio J* 1999;45(3):178-82.
63. Patel NC, Jothi M, Trivedi DB, Sabino G, Daly P, Booker PD, et al. Post-cardiotomy mechanical circulatory support using a conventional bypass circuit in children. *Eur J Cardiothorac Surg* 2001;20(4):811-5.
64. Frazier OH. First use of an untethered, vented electric left ventricular assist device for long-term support. *Circulation* 1994;89(6):2908-14.
65. Hetzer R, Muller JH, Weng YG, Loebe M, Wallukat G. Midterm follow-up of patients who underwent removal of a left ventricular assist device after cardiac recovery from end-stage dilated cardiomyopathy. *J Thorac Cardiovasc Surg* 2000;120(5):843-53.
66. Hetzer R, Muller JH, Weng Y, Meyer R, Dandel M. Bridging to recovery. *Ann Thorac Surg* 2001;71(3 Suppl):S109-13; discussion S14-5.
67. Loebe M, Hennig E, Muller J, Spiegelsberger S, Weng Y, Hetzer R. Long-term mechanical circulatory support as a bridge to transplantation, for recovery from cardiomyopathy, and for permanent replacement. *Eur J Cardiothorac Surg* 1997;11 Suppl:S18-24.
68. Sodian R, Loebe M, Schmitt C, Potapov EV, Siniawski H, Muller J, et al. Decreased plasma concentration of brain natriuretic peptide as a potential indicator of cardiac recovery in patients supported by mechanical circulatory assist systems. *J Am Coll Cardiol* 2001;38(7):1942-9.
69. Barbone A, Holmes JW, Heerdt PM, The AH, Naka Y, Joshi N, et al. Comparison of right and left ventricular responses to left ventricular assist device support in patients with severe heart failure: A primary role of mechanical unloading underlying reverse remodeling. *Circulation* 2001;104(6):670-5.
70. Frazier OH. Left ventricular assist device as a bridge to partial left ventriculectomy. *Eur J Cardiothorac Surg* 1999;15 Suppl 1:S20-5; discussion S39-43.
71. Thalmann M, Schima H, Wieselthaler G, Wolner E. A review on physiology of continuous blood flow in recipients of rotary cardiac assist devices. *J Heart Lung Transplant* 2004;In press.
72. Allen G, Murray K, Oslon D. The importance of pulsatile and nonpulsatile flow in the design of blood pumps. *Artif Organs* 1997;21(8):922-8.
73. Nosé Y, Kawahito K. Development of a non-pulsatile permanent rotary blood pump. *Eur. J. Cardio-Thorac. Surg.* 1997;11:S32-S8.
74. Nosé Y, Kawahito K, Nakazawa T. Can we develop a non-pulsatile permanent rotary blood pump? Yes, we can. *Artif Organs* 1996;20(6):467-74.
75. Yozu R, Golding L, Yada I, Harasaki H, Takatani S, Kawada S, et al. Do we really need pulse - chronic nonpulsatile and pulsatile blood-flow - from the exercise response viewpoints. *Artif. Organs* 1994;18(9):638-42.

76. Jett G. Physiology of nonpulsatile circulation: Acute versus chronic support. *ASAIO J* 1999;45:119-22.
77. Litwak KN, Kihara S, Kameneva MV, Litwak P, Uryash A, Wu Z, et al. Effects of continuous flow left ventricular assist device support on skin tissue microcirculation and aortic hemodynamics. *Asaio J* 2003;49(1):103-7.
78. Litwak K. Author's reply to a letter to the editor. *ASAIO J* 2003;49(5):614.
79. Undar A. Universal and precise quantification of pulsatile and nonpulsatile pressure flow waveforms is necessary for direct and adequate comparisons among the results of different investigators. *Perfusion-UK* 2003;18(2):135-6.
80. Shepard R, Simpson D, Sharp J. Energy equivalent pressure. *Arch Surg* 1966;93(5):730-40.
81. Schima H, Trubel W, Moritz A, Wieselthaler G, Stohr H, Thoma H, et al. Noninvasive monitoring of rotary blood pumps: Necessity, possibilities, and limitations. *Artif Organs* 1992;16(2):195-202.
82. Wieselthaler GM, Schima H, Hiesmayr M, Pacher R, Laufer G, Noon GP, et al. First clinical experience with the debakey vad continuous-axial-flow pump for bridge to transplantation. *Circulation* 2000;101(4):356-9.
83. Nakata K, Shiono M, Orime Y, Hata M, Sezai A, Saitoh T, et al. Effect of pulsatile and non-pulsatile assist on heart and kidney microcirculation with cardiogenic shock. *Artif Organs* 1996;20(6):681-4.
84. Nishinaka T, Tatsumi E, Nishimura T, Shioya K, Ohnishi H, Taenaka Y, et al. Change in vasoconstrictive function during prolonged nonpulsatile left heart bypass. *Artif Organs* 2001;25(5):371-5.
85. Shomura Y, Tanaka K, Takabayashi S, Hioki I, Tenpaku H, Maze Y, et al. Afferent and efferent nerve activity of arterial baroreceptor reflex under nonpulsatile systemic circulation. *Artif Organs* 1999;23(6):513-7.
86. Ninomiya I, Irisawa H. Aortic nervous activities in response to pulsatile and nonpulsatile pressure. *Am J Physiol* 1967;213(6):1504-11.
87. Nishimura T, Tatsumi E, Taenaka Y, Nishinaka T, Nakatani T, Masuzawa T, et al. Effects of long-term nonpulsatile left heart bypass on the mechanical properties of the aortic wall. *Asaio J* 1999;45(5):455-9.
88. Nishimura T, Tatsumi E, Nishinaka T, Taenaka Y, Nakata M, Takano H. Prolonged nonpulsatile left heart bypass diminishes vascular contractility. *Int J Artif Organs* 1999;22(7):492-8.
89. Mavroudis C. To pulse or not to pulse. *Ann Thorac Surg* 1978;25(3):259-71.
90. Jaffrin M, Reul H. Blood pumps and extracorporeal circuits. In: Verdonck P, Verhoeven R, Rieu R, Pelissier R, eds. *Cardiovascular fluid dynamics, principles and clinical applications*. Marseille, 1994;5.3-5.
91. Cudkovicz L. *The human bronchial circulation in health and disease*. Baltimore: Williams & Wilkins; 1968.
92. Anstadt MP, Tedder M, Hegde SS, Perez-Tamayo RA, Crain BJ, Khian Ha VL, et al. Pulsatile versus nonpulsatile reperfusion improves cerebral blood flow after cardiac arrest. *Ann Thorac Surg* 1993;56(3):453-61.
93. Henze T, Stephan H, Sonntag H. Cerebral dysfunction following extracorporeal circulation for aortocoronary bypass surgery: No differences in neuropsychological outcome after pulsatile versus nonpulsatile flow. *Thorac Cardiovasc Surg* 1990;38(2):65-8.

94. Onoe M, Mori A, Watarida S, Sugita T, Shiraishi S, Nojima T, et al. The effect of pulsatile perfusion on cerebral blood flow during profound hypothermia with total circulatory arrest. *J Thorac Cardiovasc Surg* 1994;108(1):119-25.
95. Sezai A, Shiono M, Orime Y, Nakata K, Hata M, Nemoto M, et al. Comparison studies of major organ microcirculations under pulsatile and non-pulsatile assisted circulations. *Artif Organs* 1996;20(2):139-42.
96. Kashiwazaki S. Effects of artificial circulation by pulsatile and non-pulsatile flow on brain tissues. *Ann Thorac Cardiovasc Surg* 2000;6(6):389-96.
97. Hindman B. Cerebral physiology during cardiopulmonary bypass: Pulsatile versus nonpulsatile flow. *Adv Pharmacol* 1994;31:607-16.
98. Nishinaka T, Tatsumi E, Nishimura T, Taenaka Y, Imada K, Takano H, et al. Effects of reduced pulse pressure to the cerebral metabolism during prolonged nonpulsatile left heart bypass. *Artif Organs* 2000;24(8):676-9.
99. Sezai A, Shiono M, Orime Y, Nakata K, Hata M, Yamada H, et al. Renal circulation and cellular metabolism during left ventricular assisted circulation: Comparison study of pulsatile and non-pulsatile assists. *Artif Organs* 1997;21(7):830-5.
100. Sezai A, Shiono M, Orime Y, Nakata K, Hata M, Iida M, et al. Major organ function under mechanical support: Comparative studies of pulsatile and nonpulsatile circulation. *Artif Organs* 1999;23(3):280-5.
101. Kihara S, Litwak K, Nichols L, Litwak P, Kameneva M, Wu Z, et al. Smooth muscle cell hypertrophy of renal cortex arteries with chronic continuous flow left ventricular assist. *Ann Thorac Surg* 2003;75(1):178-83.
102. Fukae K, Tominaga R, Tokunaga S, Kawachi Y, Imaizumi T, Yasui H. The effects of pulsatile systemic perfusion on renal sympatic nerve activity in anesthetized dogs. *J Thorac Cardiovasc Surg* 1996;111:478-84.
103. Saito S, Westaby S, Piggott D, Katsumata T, Dudnikov S, Robson D, et al. Reliable long-term non-pulsatile circulatory support without anticoagulation. *Eur J Cardiothorac Surg* 2001;19(5):678-83.
104. Saito S, Westaby S, Piggot D, Dudnikov S, Robson D, Catarino P, et al. End-organ function during chronic nonpulsatile circulation. *Ann Thorac Surg* 2002;74(4):1080-5.
105. Yada I, Golding L, Harasaki H, Jacobs G, Koike S, Yozu R, et al. Physiopathological studies of nonpulsatile blood flow in chronic models. *Trans Am Soc Artif Intern Organs* 1983;29:520-5.
106. Taenaka Y, Tatsumi E, Nakamura H, Nakatani T, Yagura A, Sekii H, et al. Physiologic reactions of awake animals to an immediate switch from a pulsatile to non-pulsatile systemic circulation. *ASAIO Trans* 1990;36:M541-M4.
107. Kojima R, Nosé Y. Rhythmical fluctuation of arterial pressure after implantation of cardiac prosthesis. *Artif Organs* 1994;18(9):621-6.
108. Fukamachi K, Tominaga R, Harasaki H, Smith W, Golding L. Effect of respiration on arterial pressure wave in calves with non-pulsatile biventricular bypass. *ASAIO J* 1994;40(4):981-5.
109. Yambe T, Nitta S, Sonobe T, Naganuma S, Kakinuma Y, Kobayashi S, et al. Origin of the rhythmical fluctuations in the animal without a natural heartbeat. *Artif Organs* 1993;17:1017-21.
110. Frazier OH, Myers TJ, Westaby S, Gregoric ID. Clinical experience with an implantable, intracardiac, continuous flow circulatory support device: Physiologic implications and their relationship to patient selection. *Ann Thorac Surg* 2004;77(1):133-42.

111. Frazier OH, Myers TJ, Westaby S, Gregoric ID. Use of the jarvik 2000 left ventricular assist system as a bridge to heart transplantation or as destination therapy for patients with chronic heart failure. *Ann Surg* 2003;237(5):631-6.
112. Letsou GV, Myers TJ, Gregoric ID, Delgado R, Shah N, Robertson K, et al. Continuous axial-flow left ventricular assist device (jarvik 2000) maintains kidney and liver perfusion for up to 6 months. *Ann Thorac Surg* 2003;76(4):1167-70.
113. Frazier OH, Shah NA, Myers TJ, Robertson KD, Gregoric ID, Delgado R. Use of the flowmaker (jarvik 2000) left ventricular assist device for destination therapy and bridging to transplantation. *Cardiology* 2004;101(1-3):111-6.
114. Losert U, Glogar D, Mayr H, Mohl W, Ogris E, Stohr H, et al. Regional myocardial blood flow during nonpulsatile left ventricular bypass in calves. *Trans Am Soc Artif Intern Organs* 1982;28:86-92.
115. Golding LR, Jacobs G, Murakami T, Takatani S, Valdes F, Harasaki H, et al. Chronic nonpulsatile blood flow in an alive, awake animal 34-day survival. *Trans Am Soc Artif Intern Organs* 1980;26:251-5.
116. Potapov EV, Loebe M, Nasser BA, Sinawski H, Koster A, Kuppe H, et al. Pulsatile flow in patients with a novel nonpulsatile implantable ventricular assist device. *Circulation* 2000;102(19 Suppl 3):III183-7.
117. Wieselthaler GM, Schima H, Lassnigg AM, Dworschak M, Pacher R, Grimm M, et al. Lessons learned from the first clinical implants of the debakey ventricular assist device axial pump: A single center report. *Ann Thorac Surg* 2001;71(3 Suppl):S139-43; discussion S44-6.
118. Qian K, Zeng P, Ru W, Yuan H. Axial reciprocation of rotating impeller: A novel approach to preventing thrombosis in centrifugal pump. *ASAIO J* 2002;48(5):562-4.
119. Rosenfeldt F, Ostberg B, Tcherkas D, Pastoriza-Pinol J, Southwell J. A novel valveless rotary pump for cardiac assist. *Artif Organs* 1997;21(5):420-5.
120. Monties J, Trinkl J, Mesana T, Havlik P, Demunck J. Cora valveless pulsatile rotary pump: New design and control. *Ann Thorac Surg* 1996;61(1):463-8.
121. Meyns B, Nishimura Y, Racz R, Jashari R, Flameng W. Organ perfusion with hemopump device assistance with and without intraaortic balloon pumping. *J Thorac Cardiovasc Surg* 1997;114(2):243-53.
122. Reddy R, Goldstein A, Pacella J, Cattivera G, Clark R, Magovern G. End organ function with prolonged nonpulsatile circulatory support. *ASAIO J* 1995;41(3):M547-M51.
123. Altieri F, Berson A, Borovetz H, Butler K, Byrd G, Ciarkowski AA, et al. Long-term mechanical circulatory support system reliability recommendation. *ASAIO J* 1998;44:108-14.
124. Frank O. Die grundform des arteriellen pulses erste abhandlung: Mathematische analyse. *Z Biol* 1899;37:483-526.
125. Stergiopoulos N, Westerhof BE, Westerhof N. Total arterial inertance as the fourth element of the windkessel model. *Am J Physiol* 1999;276:H81-H8.
126. Westerhof N, Elzinga G, Sipkema P. An artificial arterial system for pumping hearts. *J Appl Physiol* 1971;31(5):776-81.
127. Broemser P, Ranke F. Ueber die messung des schlagvolumens des herzens auf unblutigen weg. *Z. Biol.* 1930;90:467-507.
128. Westerhof N. Analog studies of human systemic arterial hemodynamics. Philadelphia, PA: University of Pennsylvania; 1968.
129. Donovan FM, Jr. Design of a hydraulic analog of the circulatory system for evaluating artificial hearts. *Biomater Med Devices Artif Organs* 1975;3(4):439-49.

130. Brighton JA. Mock circulatory system for testing lva assist artificial hearts. Interim Report: National Institute of Health, National Heart Lung Institute; 1975 Februari 17.
131. Rosenberg G, Winfred MP, Landis DL, Pierce WS. Design and evaluation of the pennsylvania state university mock circulatory system. *ASAIO journal* 1981;April/Jue:41-9.
132. Knierbein B, Reul H, Eilers R, Lange M, Kaufmann R, Rau G. Compact mock loop of the systemic and pulmonary circulation for blood pump testing. *Int J Artif Organs* 1992;15(1):40-8.
133. Ferrari G, De Lazzari C, Kozarski M, Clemente F, Gorczynska K, Mimmo R, et al. A hybrid mock circulatory system: Testing a prototype under physiologic and pathological conditions. *Asaio J* 2002;48(5):487-94.
134. Sharp MK, Dharmalingham RK. Development of a hydraulic model of the human systemic circulation. *Asaio J* 1999;45(6):535-40.
135. Ferrari G, De Lazzari C, Mimmo R, Tosti G, Ambrosi D, Gorczynska K. A computer controlled mock circulatory system for mono- and biventricular assist device testing. *Int J Artif Organs* 1998;21(1):26-36.
136. Segers P, Dubois F, De Wachter D, Verdonck P. Role and relevancy of a cardiovascular simulator. *CVE* 1998;3(1):48-56.
137. Segers P. Biomechanische modellering van het arterieel systeem voor de niet-invasieve bepaling van de arteriële compliantie. Gent: Universiteit Gent; 1997.
138. Westerhof N, Bosman F, De Vries CJ, Noordergraaf A. Analog studies of the human systemic arterial tree. *J Biomechanics* 1969;2:121-43.
139. Reul H, van Son JA, Steinseifer U, Schmitz B, Schmidt A, Schmitz C, et al. In vitro comparison of bileaflet aortic heart valve prostheses. St. Jude medical, carbomedics, modified edwards-duromedics, and sorin-bicarbon valves. *J Thorac Cardiovasc Surg* 1993;106(3):412-20.
140. Schichl K, Affeld K. A computer controlled versatile pulse duplicator for precision testing of artificial heart valves. *Int J Artif Organs* 1993;16(10):722-8.
141. Schima H, Baumgartner H, Spitaler F, Kuhn P, Wolner E. A modular mock circulation for hydromechanical studies on valves, stenoses, vascular grafts and cardiac assist devices. *Int J Artif Organs* 1992;15(7):417-21.
142. Woodard JC, Rock SM, Portner PM. A sophisticated electromechanical ventricular simulator for ventricular assist system testing. *ASAIO Trans* 1991;37(3):M210-1.
143. Baloa LA, Boston JR, Antaki JF. Elastance-based control of a mock circulatory system. *Ann Biomed Eng* 2001;29(3):244-51.
144. Barbaro V, Boccanera G, Daniele C, Grigioni M, Palombo A. Approaching comparability and results of pulsatile flow in vitro testing of prosthetic heart valves. *J Med Eng Technol* 1995;19(4):115-8.
145. Verdonck P, Kleven A, Verhoeven R, Angelsen B, Vandenbogaerde J. Computer-controlled in vitro model of the human left heart. *Med Biol Eng Comput* 1992;30(6):656-9.
146. Ingels NB, Jr., Daughters GT, Nikolic SD, DeAnda A, Moon MR, Bolger AF, et al. Left ventricular diastolic suction with zero left atrial pressure in open-chest dogs. *Am J Physiol* 1996;270(4 Pt 2):H1217-24.
147. Burkhoff D, Sugiura S, Yue DT, Sagawa K. Contractility-dependent curvilinearity of end-systolic pressure-volume relations. *Am J Physiol* 1987;252(6 Pt 2):H1218-27.
148. Segers P, Stergiopulos N, Westerhof N. Quantification of the contribution of cardiac and arterial remodeling to hypertension. *Hypertension* 2000;36(5):760-5.

149. Stergiopoulos N, Meister JJ, Westerhof N. Determinants of stroke volume and systolic and diastolic aortic pressure. *Am J Physiol* 1996;270(6 Pt 2):H2050-9.
150. Segers P, Steendijk P, Stergiopoulos N, Westerhof N. Predicting systolic and diastolic aortic pressure and stroke volume in the intact sheep. *J Biomechanics* 2001;34(1):41-50.
151. Maughan WL, Shoukas AA, Sagawa K, Weisfeldt ML. Instantaneous pressure-volume relationship of the canine right ventricle. *Circ Res* 1979;44(3):309-15.
152. Sagawa K. The end-systolic pressure-volume relation of the ventricle: Definition, modifications and clinical use. *Circulation* 1981;63(6):1223-7.
153. Thomas JD, Zhou J, Greenberg N, Bibawy G, McCarthy PM, Vandervoort PM. Physical and physiological determinants of pulmonary venous flow: Numerical analysis. *Am J Physiol* 1997;272(5 Pt 2):H2453-65.
154. Clark JW, Pruett RC, Baldrige DL, Srinivasan R, Bourland HM, Cole JS, et al. Functional model for the characterisation of the ventricular mechanics of the human subject. *Med Biol Eng Comput* 1977;15(4):335-48.
155. Vollkron M, Schima H, Huber L, Wieselthaler G. Interaction of the cardiovascular system with an implanted rotary assist device: Simulation study with a refined computer model. *Artif Organs* 2002;26(4):349-59.
156. Sun Y. Modeling the dynamic interaction between left ventricle and intra-aortic balloon pump. *Am J Physiol* 1991;261(4 Pt 2):H1300-11.
157. Santamore WP, Meier GD, Bove AA. Effects of hemodynamic alterations on wall motion in the canine right ventricle. *Am J Physiol* 1979;236(2):H254-62.
158. Grignola JC, Pontet J, Vallarino M, Gines F. The characteristics proper of the cardiac cycle phases of the right ventricle. *Rev Esp Cardiol* 1999;52(1):37-42.
159. Hunter WC, Janicki JS, Weber KT, Noordergraaf A. Systolic mechanical properties of the left ventricle. Effects of volume and contractile state. *Circ Res* 1983;52(3):319-27.
160. Campbell KB, Ringo JA, Knowlen GG, Kirkpatrick RD, Schmidt SL. Validation of optional elastance-resistance left ventricle pump models. *Am J Physiol* 1986;251(2 Pt 2):H382-97.
161. Shroff SG, Janicki JS, Weber KT. Left ventricular systolic dynamics in terms of its chamber mechanical properties. *Am J Physiol* 1983;245(1):H110-24.
162. Grignola JC, Ginés F. Left ventricle-like mechanical properties of the right ventricle due to an acute afterload increase. 2003.
163. Palladino JL, Rabbany SY, Mulier JP, Noordergraaf A. A perspective on myocardial contractility. *Technol Health Care* 1997;5(1-2):135-44.
164. Sharp MK, Pantalos GM, Minich L, Tani LY, McGough EC, Hawkins JA. Aortic input impedance in infants and children. *J Appl Physiol* 2000;88(6):2227-39.
165. Lambermont B, Gerard P, Detry O, Kolh P, Potty P, Defraigne JO, et al. Comparison between three- and four-element windkessel models to characterize vascular properties of pulmonary circulation. *Arch Physiol Biochem* 1997;105(7):625-32.
166. Toy S, Melbin J, Noordergraaf A. Reduced models of arterial systems. *IEEE transactions on biomedical engineering* 1985;32(2):174-6.
167. Matsumoto T. Study of parameters for evaluation of the effect of assist pump on the natural heart [PhD dissertation]. Sapporo: Hokkaido University; 1987.
168. Taylor MG. An approach to an analysis of the arterial pulse wave. I. Oscillations in an attenuating line. *Phys Med Biol* 1957;1(3):258-69.

169. Fogliardi R, Burattini R, Campbell KB. Identification and physiological relevance of an exponentially tapered tube model of canine descending aortic circulation. *Med Eng Phys* 1997;19(3):201-11.
170. Burattini R, Gnudi G. Computer identification of models for the arterial tree input impedance: Comparison between two new simple models and first experimental results. *Med Biol Eng Comput* 1982;20(2):134-44.
171. Burattini R, Knowlen GG, Campbell KB. Two arterial effective reflecting sites may appear as one to the heart. *Circ Res* 1991;68(1):85-99.
172. Shroff SG, Berger DS, Korcarz C, Lang RM, Marcus RH, Miller DE. Physiological relevance of t-tube model parameters with emphasis on arterial compliances. *Am J Physiol* 1995;269(1 Pt 2):H365-74.
173. Avolio AP. Multi-branched model of the human arterial system. *Med Biol Eng Comput* 1980;18(6):709-18.
174. Zhou J, Armstrong GP, Medvedev AL, Smith WA, Golding LA, Thomas JD. Numeric modeling of the cardiovascular system with a left ventricular assist device. *Asaio J* 1999;45(1):83-9.
175. Giridharan GA, Skliar M, Olsen DB, Pantalos GM. Modeling and control of a brushless dc axial flow ventricular assist device. *Asaio J* 2002;48(3):272-89.
176. Yu YC, Boston JR, Simaan MA, Miller PJ, Antaki JF. Pressure-volume relationship of a pulsatile blood pump for ventricular assist device development. *Asaio J* 2001;47(3):293-301.
177. Wolff MR, de Tombe PP, Harasawa Y, Burkhoff D, Bier S, Hunter WC, et al. Alterations in left ventricular mechanics, energetics, and contractile reserve in experimental heart failure. *Circ Res* 1992;70(3):516-29.
178. Kass DA, Maughan WL. From 'emax' to pressure-volume relations: A broader view. *Circulation* 1988;77(6):1203-12.
179. Nishida T, Meyns B, Zietkiewicz M, Perek B, Xia Z, Goebel C, et al. The effect of sudden failure of a rotary blood pump on left ventricular performance in normal and failing hearts. *Artif Organs* 2000;24(11):893-8.
180. Ishida Y, Meisner JS, Tsujioka K, Gallo JI, Yorán C, Frater RW, et al. Left ventricular filling dynamics: Influence of left ventricular relaxation and left atrial pressure. *Circulation* 1986;74(1):187-96.
181. Sun Y, Sjöberg BJ, Ask P, Loyd D, Wranne B. Mathematical model that characterizes transmitral and pulmonary venous flow velocity patterns. *Am J Physiol* 1995;268(1 Pt 2):H476-89.
182. Alexander J, Jr., Sunagawa K, Chang N, Sagawa K. Instantaneous pressure-volume relation of the ejecting canine left atrium. *Circ Res* 1987;61(2):209-19.
183. Teichholz L, Kreulen T, Herman M, Gorlin R. Problems in echocardiographic volume determinations: Echocardiographic-angiographic correlations in the presence of absence of asynergy. *Am J Cardiol* 1976;37(1):7-11.
184. Yin FC. Ventricular wall stress. *Circ Res* 1981;49(4):829-42.
185. Olsen DB. Rotary blood pumps: A new horizon. *Artif Organs* 1999;23(8):695-6.
186. Westaby S, Banning AP, Jarvik R, Frazier OH, Pigott DW, Jin XY, et al. First permanent implant of the jarvik 2000 heart. *The Lancet* 2000;356(9233):900-3.
187. Vandenberghe S, Segers P, Meyns B, Verdonck P. Hydrodynamic characterisation of ventricular assist devices. *Int J Artif Organs* 2001;24(7):470-7.

188. Suga H. External mechanical work from relaxing ventricle. *Am J Physiol* 1979;236(3):H494-7.
189. Ishihara H, Yokota M, Sobue T, Saito H. Relation between ventriculoarterial coupling and myocardial energetics in patients with idiopathic dilated cardiomyopathy. *J Am Coll Cardiol* 1994;23(2):406-16.
190. Burkhoff D, Sagawa K. Ventricular efficiency predicted by an analytical model. *Am J Physiol* 1986;250(6 Pt 2):R1021-7.
191. Sunagawa K, Maughan WL, Sagawa K. Optimal arterial resistance for the maximal stroke work studied in isolated canine left ventricle. *Circ Res* 1985;56(4):586-95.
192. Kelly RP, Ting CT, Yang TM, Liu CP, Maughan WL, Chang MS, et al. Effective arterial elastance as index of arterial vascular load in humans. *Circulation* 1992;86(2):513-21.
193. Antonatos PG, Foussas SG, Nanas SN, Karamoussalis DG, Theocharis AG, Anthopoulos LP, et al. Effect of acute changes in aortic pressure on the coronary reserve. *Cardiovasc Res* 1991;25(12):995-1001.
194. Vandenberghe S, Segers P, Meyns B, Verdonck PR. Effect of rotary blood pump failure on left ventricular energetics assessed by mathematical modeling. *Artif. Organs* 2002;26(12):1032-9.
195. Takaoka H, Takeuchi M, Odake M, Yokoyama M. Assessment of myocardial oxygen consumption (vo₂) and systolic pressure- volume area (pva) in human hearts. *Eur Heart J* 1992;13 Suppl E:85-90.
196. Linneweber J, Nonaka K, Takano T, Kawahito S, Schulte-Eistrup S, Motomura T, et al. Hemodynamic exercise response in calves with an implantable biventricular centrifugal blood pump. *Artif Organs* 2001;25(12):1018-21.
197. Tayama E, Niimi Y, Takami Y, Ohashi Y, Ohtsuka G, Glueck JA, et al. Hemolysis test of a centrifugal pump in a pulsatile mode: The effect of pulse rate and rpm variance. *Artif Organs* 1997;21(12):1284-7.
198. Wang SS, Chu SH, Chou NK, Qian KX. The pulsatile impeller pump for left ventricular assist. *Artif Organs* 1996;20(12):1310-3.
199. Gobel C, Arvand A, Rau G, Reul H, Meyns B, Flameng W, et al. A new rotary blood pump for versatile extracorporeal circulation: The deltastream. *Perfusion* 2002;17(5):373-82.
200. Undar A, Lodge AJ, Daggett CW, Runge TM, Ungerleider RM, Calhoun JH. The type of aortic cannula and membrane oxygenator affect the pulsatile waveform morphology produced by a neonate-infant cardiopulmonary bypass system in vivo. *Artif Organs* 1998;22(8):681-6.
201. Kono A, Maughan WL, Sunagawa K, Hamilton K, Sagawa K, Weisfeldt ML. The use of left ventricular end-ejection pressure and peak pressure in the estimation of the end-systolic pressure-volume relationship. *Circulation* 1984;70(6):1057-65.
202. Mihaylov D, Verkerke GJ, Blanksma PK, Elstrodt J, De Jong ED, Rakhorst G. Evaluation of the optimal driving mode during left ventricular assist with pulsatile catheter pump in calves. *Artif Organs* 1999;23(12):1117-22.
203. Shiiya N, Zelinsky R, Deleuze PH, Loisanse DY. Changes in hemodynamics and coronary blood flow during left ventricular assistance with the hemopump. *Ann Thorac Surg* 1992;53(6):1074-9.
204. Vandenberghe S, Nishida T, Segers P, Meyns B, Verdonck P. The impact of pump speed and inlet cannulation site on left ventricular unloading with a rotary blood pump. *Artif Organs* 2004;in press.

205. Loebe M, Kaufmann F, Hetzer R. Extracorporeal support: The berlin heart. In: Goldstein D, Oz M, eds. *Cardiac assist devices*. Armonk: Futura Publishing Company, 2000;275-87.
206. Jett G, Lazzara R. Extracorporeal support: The abiomed bvs 5000. In: Goldstein D, Oz M, eds. *Cardiac assist devices*. Armonk: Futura Publishing Company, 2000;235-50.
207. Pennington D, Oaks T. Extracorporeal support: The thoratec device. In: Goldstein D, Oz M, eds. *Cardiac assist devices*. Armonk: Futura Publishing Company, 2000;251-62.
208. Agati S, Bruschi G, Russo C, Colombo T, Lanfranconi M, Vitali E. First successful italian clinical experience with debakey vad. *J Heart Lung Transplant* 2001;20(8):914-7.
209. Cooley DA. Initial clinical experience with the jarvik 2000 implantable axial-flow left ventricular assist system. *Circulation* 2002;105(24):2808-9.
210. Kucukaksu DS, Sener E, Undar A, Noon GP, Tasdemir O, Frazier OH, et al. First turkish experience with the micromed debakey vad. *Tex Heart Inst J* 2003;30(2):114-20.
211. Westaby S, Banning AP, Saito S, Pigott DW, Jin XY, Catarino PA, et al. Circulatory support for long-term treatment of heart failure - experience with an intraventricular continuous flow pump. *Circulation* 2002;105(22):2588-91.
212. Meyns B, Siess T, Nishimura Y, Racz R, Reul H, Rau G, et al. Miniaturized implantable rotary blood pump in atrial-aortic position supports and unloads the failing heart. *Cardiovascular Surgery* 1998;6(3):288-95.
213. Steendijk P, Staal E, Jukema JW, Baan J. Hypertonic saline method accurately determines parallel conductance for dual-field conductance catheter. *Am J Physiol Heart Circ Physiol* 2001;281(2):H755-63.
214. Cohen DJ, Kress DC, Swanson DK, DeBoer LW, Berkoff HA. Effect of cannulation site on the primary determinants of myocardial oxygen consumption during left heart bypass. *J Surg Res* 1989;47(2):159-65.
215. Sethia B, Martin W, Wheatley DJ. The effects of left atrial and left-ventricular cannulation on left-ventricular function. *Int. J. Artif. Organs* 1985;8(6):331-4.
216. Kono S, Nishimura K, Nishina T, Yuasa S, Ueyama K, Hamada C, et al. Autosynchronized systolic unloading during left ventricular assist with a centrifugal pump. *J. Thorac. Cardiovasc. Surg.* 2003;125(2):353-60.
217. Pennock JL, Pae WE, Pierce WS, Waldhausen JA. Reduction of myocardial infarct size - comparison between left atrial and left-ventricular bypass. *Circulation* 1979;59(2):275-9.
218. Mihaylov D. Development of the puca pump - a trans-arterial ventricular assist device. Groningen: Rijksuniversiteit Groningen; 2000.
219. Swanson WM, Clark RE. A simple cardiovascular system simulator: Design and performance. *J Bioeng* 1977;1(2):135-45.
220. Patel DJ, Defreitas FM, Fry DL. Hydraulic input impedance to aorta and pulmonary artery in dogs. *J Appl Physiol* 1963;18:134-40.
221. Stergiopoulos N, Meister JJ, Westerhof N. Simple and accurate way for estimating total and segmental arterial compliance: The pulse pressure method. *Ann Biomed Eng* 1994;22(4):392-7.
222. Liu Z, Brin KP, Yin FC. Estimation of total arterial compliance: An improved method and evaluation of current methods. *Am J Physiol* 1986;251(3 Pt 2):H588-600.
223. Simon AC, Safar ME, Levenson JA, London GM, Levy BI, Chau NP. An evaluation of large arteries compliance in man. *Am J Physiol* 1979;237(5):H550-4.
224. Segers P, Brimiouille S, Stergiopoulos N, Westerhof N, Naeije R, Maggiorini M, et al. Pulmonary arterial compliance in dogs and pigs: The three-element windkessel model revisited. *Am J Physiol* 1999;277(2 Pt 2):H725-31.

225. Segers P, Verdonck P, Deryck Y, Brimiouille S, Naeije R, Carlier S, et al. Pulse pressure method and the area method for the estimation of total arterial compliance in dogs: Sensitivity to wave reflection intensity. *Ann Biomed Eng* 1999;27(4):480-5.
226. Patel D, Greenfield J, Austen W, Morrow A, Fry D. Pressure-flow relationships in the ascending aorta and femoral artery of man. *J Appl Physiol* 1965;20:459-63.
227. Kantrowitz A, Tjonneland S, Freed PS, Phillips SJ, Butner AN, Sherman JL, Jr. Initial clinical experience with intraaortic balloon pumping in cardiogenic shock. *Jama* 1968;203(2):113-8.
228. Scholz KH, Tebbe U, Chemnitiu M, Kreuzer H, Schroder T, Hering JP, et al. Transfemoral placement of the left ventricular assist device "hemopump" during mechanical resuscitation. *Thorac Cardiovasc Surg* 1990;38(2):69-72.
229. Meyns BP, Nishimura Y, Jashari R, Racz R, Leunens VH, Flameng WJ. Ascending versus descending aortic balloon pumping: Organ and myocardial perfusion during ischemia. *Ann Thorac Surg* 2000;70(4):1264-9.
230. Rakhorst G, van Loon JP, Elstrodt J, van der Plaats A, Verkerke GJ. Measuring pump performance. *Med Device Technol* 2001;12(4):18-20.
231. Zwart H. Complete left heart bypass without thoracotomy: An experimental study in dogs. Amsterdam; 1966.
232. Hoepfer MM, Maier R, Tongers J, Niedermeyer J, Hohlfeld JM, Hamm M, et al. Determination of cardiac output by the fick method, thermodilution, and acetylene rebreathing in pulmonary hypertension. *Am J Respir Crit Care Med* 1999;160(2):535-41.
233. Linde C, Gadler F, Edner M, Nordlander R, Rosenqvist M, Ryden L. Results of atrioventricular synchronous pacing with optimized delay in patients with severe congestive heart failure. *Am J Cardiol* 1995;75(14):919-23.
234. Wade OL, Bishop JM. *Cardiac output and regional blood flow*. London: Blackwell; 1962.
235. Mihaylov D, Kik C, Elstrodt J, Verkerke GJ, Blanksma PK, Rakhorst G. Development of a new introduction technique for the pulsatile catheter pump. *Artif Organs* 1997;21(5):425-7.
236. Hoeft A, Sonntag H, Stephan H, Kettler D. Validation of myocardial oxygen demand indices in patients awake and during anesthesia. *Anesthesiology* 1991;75(1):49-56.
237. Reitan JA, Martucci RW, Levine NA. A computer evaluation of the ratio of the diastolic pressure-time index to the time-tension index from three arterial sites in dogs. *J Clin Monit* 1986;2(2):95-9.
238. Nichols WW, Pepine CJ. Ventricular/vascular interaction in health and heart failure. *Compr Ther* 1992;18(7):12-9.
239. Vandenberghe S, Van Loon JP, Segers P, Rakhorst G, Verdonck P. In vitro evaluation of the puca ii intra-arterial lvad. *Int J Artif Organs* 2003;26(8):743-52.
240. Antaki JF, Liu Y, Wu ZJ, Diegel P, Long J. Cannula design can reduce regurgitant flow during vad stoppage: When a check valve is not a check valve. *ASAIO journal* 2001;47:127.
241. Frazier OH, Myers TJ, Gregoric ID, Khan T, Delgado R, Croitoru M, et al. Initial clinical experience with the jarvik 2000 implantable axial-flow left ventricular assist system. *Circulation* 2002;105(24):2855-60.
242. Rakhorst G, Verkerke GJ, Hensens AG, de Muinck ED, Blanksma PK, Pillon M, et al. In vitro evaluation of the influence of pulsatile intraventricular pumping on ventricular pressure patterns. *Artif Organs* 1994;18(7):494-9.
243. Verkerke GJ, Geertsema AA, Mihaylov D, Blanksma PK, Rakhorst G. Numerical simulation of the influence of a left ventricular assist device on the cardiovascular system. *Int J Artif Organs* 2000;23(11):765-73.

244. Mihaylov D, Rakhorst G, van der Plaats A, van Loon JF, Hummel MM, Elstrodt J, et al. In vivo and in vitro experience with the puca-ii, a single-valved pulsatile catheter-pump. *Int J Artif Organs* 2000;23(10):697-702.
245. Ursino M. A mathematical model of the carotid baroregulation in pulsating conditions. *IEEE Trans Biomed Eng* 1999;46(4):382-92.
246. Ursino M. Interaction between carotid baroregulation and the pulsating heart: A mathematical model. *Am J Physiol* 1998;275(5 Pt 2):H1733-47.
247. Clément F, Médigue C, Monti A, Sorine M. The cardiovascular system and its short-term control: Modeling and signal analysis. In: Riethmuller M, Corieri P, eds. *Biological fluid dynamics*. Rhode Saint Genèse: von Karman Institute, 2003;1-52.
248. Raines JK, Jaffrin MY, Shapiro AH. A computer simulation of arterial dynamics in the human leg. *J Biomech* 1974;7(1):77-91.
249. Taher MF, Cecchini AB, Allen MA, Gobran SR, Gorman RC, Guthrie BL, et al. Baroreceptor responses derived from a fundamental concept. *Ann Biomed Eng* 1988;16(5):429-43.
250. Xu L, Fu M. Computer modeling of interactions of an electric motor, circulatory system, and rotary blood pump. *Asaio J* 2000;46(5):604-11.
251. O'Leary DS, Pantalos GM, Sharp MK. Feedback control of mean aortic pressure in a dynamic model of the cardiovascular system. *ASAIO journal* 1999;45:587-94.
252. Johnson A, Dooly C. Exercise physiology. In: Bronzino J, ed. *Biomedical engineering handbook*. Boca Raton: CRC Press Inc., 1995;391-410.
253. Nichols W, O'Rourke M. *Mcdonald's blood flow in arteries: Theoretical, experimental, and clinical principles*. 4th ed. London: Edward Arnold; 1998.
254. Ferrari G, Nicoletti A, De Lazzari C, Clemente F, Tosti G, Guaragno M, et al. A physical model of the human systemic arterial tree. *Int J Artif Organs* 2000;23(9):647-57.
255. Smith AM. A model circulatory system for use in undergraduate physiology laboratories. *Am J Physiol* 1999;277(12):S92-S9.
256. Yoshizawa M, Iemura S, Abe K, Kakinuma Y, Akiho H, Yambe T, et al. Parameter optimization approach to estimation of emax under cardiac assistance. In: Akustu T, Koyanagi H, eds. *Heart replacement - artificial heart 6*. Tokyo: Springer-Verlag, 1997;378-81.
257. Suga H, Sagawa K, Demer L. Determinants of instantaneous pressure in canine left ventricle. Time and volume specification. *Circ Res* 1980;46(2):256-63.
258. Shroff SG, Janicki JS, Weber KT. Evidence and quantitation of left ventricular systolic resistance. *Am J Physiol* 1985;249(2 Pt 2):H358-70.
259. Campbell KB, Kirkpatrick RD, Knowlen GG, Ringo JA. Late-systolic pumping properties of the left ventricle. Deviation from elastance-resistance behavior. *Circ Res* 1990;66(1):218-33.

No animals were harmed for the purpose of this research. The reported sheep experiments (chapter IV) were performed earlier at the KULeuven and the obtained data were not fully explored at the time. The calve experiment (chapter VI) was part of a surgical training program.

May this be a plea for the more efficient use of available animal data and the exchange of previously acquired (and published) data between research groups. This work should also be an encouragement for the use of alternative modeling methods when possible.